PROPERTIES OF MINIMALLY DOUBLED FERMIONS

Dissertation zur Erlangung des Grades
"Doktor der Naturwissenschaften"

vorgelegt am Fachbereich
Physik, Mathematik und Informatik
der Johannes Gutenberg-Universität in Mainz

JOHANNES GUTENBERG
UNIVERSITÄT MAINZ

Johannes Heinrich Weber
geboren in Groß-Gerau

Mainz, den 13. März 2015

Abstract

The majority of quark actions in lattice QCD encounter difficulties with chiral symmetry and its spontaneous symmetry breaking, which is realised only in compliance with the Nielsen-Ninomiya No-Go theorem. Minimally doubled fermions are a category of discretisations of strictly local chiral fermions which reproduce two degenerate quark flavours in the continuum limit. The Dirac operator complies with the No-Go theorem by having two poles at different points in the Brillouin zone. Their alignment implies that hypercubic symmetry is explicitly broken at finite lattice spacing.

Boriçi-Creutz and Karsten-Wilczek (KW) fermions are two different variants of minimally doubled fermions, which are studied in perturbation theory. Renormalisation properties are studied and three counterterms, which arise due to explicit loss of hypercubic symmetry, are determined perturbatively. Inclusion of counterterms removes the anisotropy from self-energy and vacuum polarisation at one-loop level. Corrections to local bilinears are calculated and chiral symmetry is tested. Vector and axial symmetry currents are derived and their conservation is verified.

Numerical simulations of KW fermions in the quenched approximation are used to determine non-perturbative renormalisation criteria. The relevant fermionic counterterm is tuned using two complementary approaches. First, the action's anisotropy is reflected in an anisotropic pseudoscalar mass. The minimum of the mass anisotropy defines the tuned action. Second, some hadronic correlation functions have oscillating contributions. Restoration of the tree-level frequency spectrum is used as complementary condition, which agrees within errors. Due to lack of a numerically robust non-perturbative condition, the marginal fermionic counterterm is fixed to the estimate from perturbation theory.

The hadron spectrum is studied with a properly tuned KW action. As the spontaneously broken chiral symmetry $\mathrm{SU}(2)_A$ is reduced to $\mathrm{U}(1)_A$ due to the fermion action, only one pseudoscalar meson is a (Pseudo-) Goldstone boson at finite cutoff. The pseudoscalar channel is studied and Goldstone boson-like behaviour including quenched chiral logarithms is observed, which agrees with phenomenological predictions. A second channel using γ^0 instead of γ^5 is studied. Its ground state scales with the bare quark mass like a (Pseudo-) Goldstone boson, but retains a residual mass in the chiral limit, which vanishes as $\mathcal{O}(a^2)$ in the continuum limit. This strongly indicates that the γ^0 channel contains a pseudoscalar meson which is affected by lattice artifacts. These simulations in the chiral regime indicate that KW fermions are not affected by exceptional configurations.

The first numerical study of KW fermions is a cornerstone for future applications. Simulations using dynamical KW fermions and including missing quark-disconnected contributions will overcome present deficiencies. Vector mesons and nucleons are the next milestones in a study of the hadron spectrum.

Zusammenfassung

Die Mehrheit der Quarkwirkungen in Gitter QCD leidet an Problemen mit chiraler Symmetrie und deren spontaner Brechung, die nur gemäß des Nielsen-Ninomiya Theorems realisiert wird. Minimal verdoppelte Fermionen sind eine Kategorie von Diskretisierungen strikt lokaler, chiraler Fermionen, die im Kontinuumslimes zwei entartete Quark Flavours reproduzieren. Der Dirac Operator erfüllt das Theorem, da er zwei Polstellen an ungleichen Punkten der Brillouin-Zone hat. Diese Anordnung zieht explizite Brechung der hyperkubische Symmetrie bei endlichem Gitterabstand nach sich.

Boriçi-Creutz und Karsten-Wilczek (KW) Fermionen sind zwei Varianten, die in Störungstheorie untersucht werden. Aufgrund expliziter hyperkubischer Symmetriebrechung erfordert Renormierung drei Counterterme, die perturbativ bestimmt werden. Mittels der Counterterme wird die Anisotropie aus Selbst-Energie und Vakuum-Polarisation auf Ein-Schleifen Niveau entfernt. Korrekturen zu bilinearen Operatoren werden berechnet und chirale Symmetrie überprüft. Vektorielle und axiale Symmetrieströme werden hergeleitet und deren Erhaltung verifiziert.

Numerische Simulation von KW Fermionen in Quenched Approximation dienen der Bestimmung nicht-perturbativer Renormierungsbedingungen. Der relevante fermionische Counterterm wird mit zwei komplementären Ansätzen justiert. Erstens spiegelt sich die Anisotropie der Wirkung in einer Anisotropie der pseudoskalaren Masse wider. Das Minimum der Massenanisotropie definiert die kalibrierte Wirkung. Zweitens haben manche hadronische Korrelatoren oszillierende Anteile. Wiederherstellung des Tree-level Frequenzspektrums ist eine komplementäre Bedingung, die innerhalb der Fehler übereinstimmt. Mangels einer numerisch robusten, nicht-perturbativen Bedingung wird der marginale fermionische Counterterm auf die Vorhersage der Störungstheorie fixiert.

Das Hadronenspektrum wird mit einer korrekt eingestellten KW Wirkung untersucht. Da die spontan gebrochene chirale Symmetrie $SU(2)_A$ durch die Fermionwirkung zu $U(1)_A$ reduziert ist, ist nur eines der pseudoskalaren Mesonen bei endlichem Cutoff ein (Pseudo-) Goldstone Boson. In der Untersuchung des pseudoskalaren Kanals wird Goldstone Boson-artiges Verhalten einschließlich Quenched Chiral Logarithms im Einklang mit phänomenologischen Vorhersagen beobachtet. Ein zweiter Kanal mit γ^0 anstelle von γ^5 wird untersucht. Dessen Grundzustand skaliert mit der nackten Quarkmasse wie ein (Pseudo-) Goldstone Boson, aber behält eine residuale Masse im chiralen Limes, welche wie $\mathcal{O}(a^2)$ im Kontinuumslimes verschwindet. Dies ist ein starkes Indiz, dass der γ^0 Kanal ein von Gitterartefakten betroffenes pseudoskalares Meson enthält. Diese Simulationen im chiralen Regime zeigen, dass KW Fermionen nicht von Exceptional Configurations betroffen sind.

Die erste numerische Studie von KW Fermionen ist Grundlage zukünftiger Anwendungen. Überwindung derzeitiger Unzulänglichkeiten erfordert Simulationen mit dynamischen KW Fermionen unter Berücksichtigung fehlender Quark-disconnected Beiträge. Vektormesonen und Nukleonen sind die nächsten Meilensteine der Untersuchung des Hadronenspektrums.

概略

格子上における量子色力学のクォーク作用の多くはカイラル対称性を保持することが困難であり、Nielsen-二宮の定理にある通り，制限が加わることが知られている。Minimally doubled fermions(MDF)は，局在するカイラル・フェルミ粒子を離散化することによって、連続極限における縮退のフレーバー数が2となるように定式化されている。 ブリュアン領域において二つのゼロ点が存在するならば、そのようなディラック演算子は上記の定理を満たす。 有限の格子間隔の場合には，四次元の格子対称性の破れが上記のゼロ点の方向性の結果となる。

Boriçi-Creutz, 及び, Karsten-Wilczek(KW)フェルミオンは，二種類の異なるMDFであり，本研究では，これらのMDFを摂動論を用いて検証する。 四次元の格子対称性の破れにより，繰り込みは３つの，異方性を持ったcounter term (CT) によって特徴付けられる。 また，これらのCTは摂動論によって求まる。 このCTを取り込むことによって，自己エネルギーと真空偏極の異方性は１-ループのオーダーで取り除かれる。 また，双一次の演算子の１-ループ補正を計算することによってカイラル対称性を検討する。 さらに，ベクトル対称性，及び，軸性ベクトル対称性のカレントを導出し，これらを通して保存則を確認する。

クェンチ近似を用いた数値シミュレーションによって，KWフェルミオンの非摂動的な繰り込み条件の設定を行う。 フェルミ作用の三次元のCTは，以下の２つの要素から構成される手法によって計算される。 第一に，遷移行列の異方性が擬スカラーの質量の異方性に映し出されることから，質量における異方性の最小値によって，作用を定義することができる。 次に，異なる極を含むハドロン相関関数が振動する成分を持つにことに注目する。 この振動成分の周波数スペクトルを再現するための条件を求めることができ，この条件によって再現されたスペクトルは，元の振動に誤算の範囲で一致することが確認できる。 また，四次元格子上のCTを数値的に評価するための必要条件を特定するために，前述の摂動論による予測を使用する。

上記の繰り込み条件によって改良されたKW作用を用いて，ハドロン・スペクトルの研究を行う。 自発的に破れるカイラル対称性は，格子上におけるフェルミオンの定式化によりSU(2)$_A$ が破れ,U(1)$_A$だけが残る。このことから，有限の格子間隔の場合には,擬スカラー中間子のうちの一つのみが南部ボソンの役割を担う。 擬スカラー・チャンネルには，このような現象論的な予測に従う，クェンチ・カイラル対数を含んだ南部ボソンとの対応が見られる。 次に，γ^5 の代わりγ^0 を用いるチャンネルの研究を行う。 本チャンネルにおける基底状態の質量スペクトラムは南部ボソンと類似しているが，有限の格子間隔による寄与がカイラル極限に残ったとしても，連続極限においては$\mathcal{O}(a^2)$ で消滅することが示される。 このことから，γ^0 チャンネルの基底状態は,量子エラーの影響を受けている擬スカラーであるということが結論付けられる。

本研究におけるMDFの数値的な検証は，今後のMDF研究の礎になるであろう。 一方で，現在までの数値計算には不十分な点が残る。今後の進展として，MDFによって定式化された動的フェルミオンの導入，及び, quark-disconnected 図の計算は欠かせないと考える。 また，ベクトル中間子と核子は，更なるハドロン・スペクトル研究の目標である。

Contents

Introduction

The recent discovery [1] of a Higgs boson at CERN, which is at the level of present knowledge not dissimilar to the Higgs boson of the Standard Model (SM) [76,138,157], strongly supports the SM as the appropriate theory of particle physics at the energy scales, which are nowadays accessible in experimental observations. The Nobel prize of physics 2013 was awarded for the theoretical suggestion of the Higgs mechanism [11,55,86,92] of spontaneous breakdown of the electroweak SU(2) symmetry as the origin of a non-vanishing vacuum expectation value (VEV) of a Higgs field. It requires the existence of at least one scalar Higgs boson as a particle, contributes longitudinal polarisation degrees of freedom to the weak gauge bosons and generates the mass of all elementary particles through Yukawa couplings between massless, bare fields and a Higgs field with its non-vanishing VEV. Whereas the non-trivial electroweak vacuum structure of the Higgs field sets the scale of elementary particle masses in the SM through its VEV, it is not the dominant contribution to the mass of the visible universe. Instead the internal structure of baryons, bound states of strongly interacting elementary fields, is responsible for the overwhelming majority of this mass. The constituent quark masses, which are due to the Higgs mechanism, contribute only about 2% to the proton's total mass. The mass of hydrogen is completely dominated by the proton mass, which exceeds the electron mass (due to the Higgs mechanism) by nearly a factor 2000. Thus, the mass of the visible universe, which mainly consists of hydrogen and helium atoms, is almost entirely due to the strong interactions. Hence, the mass and structure of the visible universe cannot be understood without a thorough comprehension of the strong interactions.

Since the advent of particle accelerators in the late 1940's and early 1950's, experimental observations of a multitude of previously unknown particles necessitated a rethinking of subatomic physics in general and of the strong interactions in particular. The previously known particle spectrum contained protons, electrons and photons, which were readily accessible in many atomic systems already in the 1920's, as well as neutrons [40], positrons [50], muons [6,7] and, as postulated particles, Pauli's neutrino [128] and Yukawa's meson [164]. The muon was considered as a candidate for the meson, since its mass agreed with the postulated meson mass within a factor of two. Elec-

tric charge and isospin [90] were considered as the charges of elementary quanta. With the experimental discovery of pions and kaons in 1947 [108, 137], the pion fit into the isospin picture as Yukawa's meson. However, kaon decays indicated new physics as their time scales greatly exceeded those of pion-nucleon reactions. A new quantum number called strangeness [127] was introduced, which is violated in weak decays. As more and more additional hadrons (the 'particle zoo') were discovered in new particle accelerator facilities, theoretical models of hadrons could not keep up with the speed of discovery. In the meantime, the development of Quantum Electrodynamics (QED) [53, 54, 58–60, 140, 141, 146] as the quantised U(1) gauge theory of the photon and the electron advanced very quickly. With high precision calculations such as the Lamb shift in the spectrum of hydrogen [22, 107], QED was already an established theory, while the model of the strong interactions was still in its infancy.

Experimental pion-nucleon scattering data did not match the prediciton of a renormalisable, pseudoscalar pion-nucleon coupling, which predicted large s-wave contributions [8, 9, 51]. Instead, the energy dependence of pion-nucleon interactions was in good agreement with gradient-coupling models in which low-energy pions decouple from the nucleons and from other pions, since their coupling is proportional to their 4-momenta. The shift symmetry of these soft pions led to an interpretation of the pion as an almost massless (Pseudo-) Goldstone boson of a spontaneously broken chiral symmetry of the strong interactions [79, 117]. An explicit, soft breaking of the chiral symmetry was considered the source of the finite pion mass. However, the nature of the fundamental chiral fermions was still obscure. Detailed studies of weak pion decays [77, 78] revealed a relation between the axial charge of the neutron in beta decay and the pion-nucleon coupling constant from the gradient-coupling model, which was coined the Goldberger-Treiman relation. It is understood in terms of the *Partially Conserved Axial Current* (PCAC) hypothesis [69]. Axial currents do not preserve the vacuum of the strong interactions, but instead serve as interpolating operators for pseudoscalar meson fields and create one-particle states. The same axial currents participate in the *V-A-coupling* of the weak interactions and mediate the weak decay of the neutron. Application of axial current operators on external particle wave-functions successfully procured amplitudes involving soft pions from amplitudes without them through the use of *chiral Ward identities* [156]. This current algebra was successfully applied to a variety of strong processes, even though the fundamental carriers of chiral charge were still missing.

Gell-Mann and Ne'eman introduced an approximate global SU(3) symmetry of the hadron spectrum [66, 118] as *the eightfold way.* Hadrons with equal space-time quantum numbers J^{PC} and similar masses were considered as an SU(3) multiplet. Isospin and strangeness quantum numbers were united in a group-theoretical sense. The eightfold way described the known particle spectrum with great success, but predicted new states [67]. Though the existence of Delta baryons with spin-3/2 had been known since 1952 [10, 28], a spin-3/2 baryon decuplet implied the existence of a new baryon with strangeness $S = -3$, which would have to be a long-lived state with a unique decay sig-

nature via three weak decays. This Omega baryon Ω^- was discovered only in 1964 [17] after its earlier prediction in the eightfold way. Hypothetical fermionic constituents were suggested by Gell-Mann [68, 70] as the origin of the *flavour* SU(3) symmetry. As part of a spin-3/2 baryon decuplet, three states at the decuplet's corners (Δ^{++}, Δ^-, Ω^-) must have fully-symmetric spin and flavour wave functions of all constituents. However, as fermions, they must have a totally antisymmetric wave function. This implies antisymmetry in a new quantum number of the constituents, which was called *colour*.

These hypothetised fundamental carriers of flavour SU(3) and colour SU(3) quantum numbers were referred to as *quarks* [68]. Whereas deep inelastic electron scattering on nucleons indeed revealed point-like constituents [23] inside of the nucleons, quarks could not be isolated in a detector. Fritzsch, Gell-Mann and Leutwyler suggested [61] that the quarks' colour charge is coupled to an octet of *gluons*, fictitious neutral gauge bosons in the adjoint representation of the colour gauge group with dynamics of a Yang-Mills field [163]. Their theory of the strong interactions had already reached its modern form except for the number of flavours. However, a mechanism of colour confinement for quarks and gluons, which simultaneously allowed for Bjorken scaling [23], was still lacking. With the proof of asymptotic freedom by Gross, Politzer and Wilczek [81–83, 131] using perturbation theory and Wilson's demonstration of a colour confinement mechanism on a space-time lattice in the strong coupling limit [160], the theory of quarks and gluons quickly started to gain acceptance. It is nowadays included in the Standard Model as Quantum Chromodynamics (QCD), a quantised SU(3) gauge theory, and covers the interactions of eight gauge fields, massless vector bosons called gluons, amongst each other and with six species of quarks, which are massive spin-1/2 fields. The six species are labelled as flavours *up*, *down*, *strange*, *charm*, *bottom* and *top*. They are identical copies which differ only in their masses and their electroweak couplings[1].

QCD can be studied successfully in the framework of perturbation theory only in the high energy regime. The running coupling is small at high four-momentum transfer, since the colour anti-screening effect of the self-interacting gluon field is lessened at short distances, and quarks and gluons are asymptotically free. In stark contrast, quarks and gluons or coloured composita thereof cannot exist as almost free particles at lower energies due to a linearly rising colour potential, which is the root of confinement. Potentials in general and the quark potential in particular are non-perturbative effects. Any perturbation series with a finite number of terms inevitably fails to bring forth such a potential. Since gluons are fields in the adjoint representation and quarks are fields in the fundamental representation of the colour gauge group SU(3), only composita which belong to the trivial representation can exist as stable *hadrons* at the hadronic scale. Mesons with one valence quark-antiquark pair ($|q\bar{q}\rangle$) and baryons with three totally colour-antisymmetric valence quarks ($|qqq\rangle$) are the only hadrons for which experimental evidence exists. Even though they are allowed by the gauge symmetry of QCD, glueballs without any valence quarks (e.g. $|gg\rangle$ or $|ggg\rangle$) as well as exotic meson-like states (e.g. $|q\bar{q}g\rangle$ or $|q\bar{q}q\bar{q}\rangle$) and

---

[1]Whereas flavour eigenstates of the strong interactions have definite mass and electric charge, weak interactions couple to quarks in a different basis. This is the origin of the CKM matrix [30, 105].

pentaquarks ($|qqqq\bar{q}\rangle$) still lack experimental evidence[2].
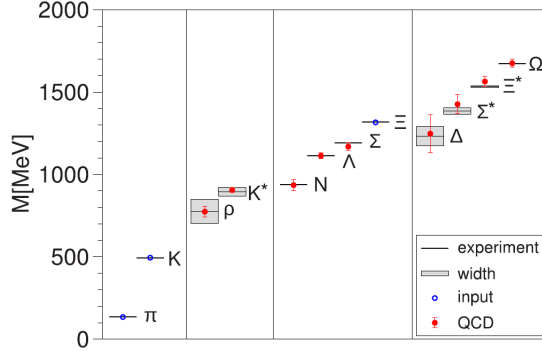
Figure 1: Ab initio calculations with lattice QCD reproduce the experimental light hadron spectrum within errors. The figure is taken from [52].

Any approach aimed at understanding the spectrum of QCD with ab initio calculations must necessarily involve non-perturbative methods. Observables are calculated without the need for a perturbation series with the path integral (cf. section 1.1.2), which can be evaluated numerically in computer simulations. An estimate of the path integral based on a representative subset of configuration space with controlled statistical errors is obtained using importance sampling, where configurations are weighted with the classical action on a discretised Euclidean space-time. The lattice spacing serves as a non-perturbative cutoff, which removes ultraviolet divergences. This is the strategy of lattice QCD, which has attained remarkable success in the description of the strong interactions that is evident in figure 1. Nevertheless, a shortcoming which is intrinsically connected to the lattice regularisation is the intricacy of the implementation of chiral symmetry [120, 121]. Wilson fermions [160], which had been used in the calculations of [52], explicitly break chiral symmetry at finite cutoff. Though Ginsparg-Wilson fermions [72] retain a chiral symmetry for one single quark species at finite lattice spacing, their Dirac operators lack ultralocality and turn out as numerically costly. Staggered fermions [144], which retain an ultralocal, non-singlet chiral symmetry, include four mass-degenerate species of quarks. Simulations with dynamical staggered fermions make use of a rooting procedure, which reduces the number of mass-degenerate sea quark species to one or two. Though the root of a determinant is mathematically well-defined, rooting a quantum field theory with non-singlet properties may lead to pathologies and fail to reproduce QCD in the continuum limit. This rooting procedure is subject of ongoing and controversial discussions (cf. [44]). Minimally doubled fermions [98] are a type of lattice fermions with two mass-degenerate species and an ultralocal, non-singlet chiral symmetry. Since the Dirac operator is ultracolal, numerical application of these lattice fermions is supposedly similarly simple and fast as Wilson fermions. If the species are interpreted as an isospin doublet of light quarks, such actions may provide a compromise between the theoretical cleanliness of Ginsparg-Wilson fermions and the numerical efficiency of Wilson fermions.

---

[2]The charmonium spectrum contains X, Y and Z states [14, 41] that cannot be explained as $|q\bar{q}\rangle$ states, but their detailed nature is still unclear. They are candidates for $|q\bar{q}g\rangle$- or $|q\bar{q}q\bar{q}\rangle$-states.

The study of *properties of minimally doubled fermions* is the subject of this thesis. Among the different kinds of minimally doubled fermions know at present, Karsten-Wilczek [98, 159] and Boriçi-Creutz fermions [27, 46] are studied within this thesis using various different approaches. Since these actions explicitly break the hypercubic lattice symmetry at finite lattice spacing, there is a risk that these theories fail to reproduce an isotropic continuum theory due to operator mixing if these anisotropic effects are not properly accounted for by renormalisation. Therefore, the main focus of this thesis lies on renormalisation of minimally doubled fermion actions.

Chapter 1 outlines foundations of continuum and lattice QCD. Wilson and Ginsparg-Wilson fermions are juxtaposed with minimally doubled fermions. Results from other research groups concerning minimally doubled fermions are touched. Chapter 2 covers analytical investigations of minimally doubled fermions using lattice perturbation theory [35–38]. The fermionic self-energy and the fermionic contribution to the vacuum polarisation are calculated and their anisotropies are removed using the counterterms of the theory. Renormalisation factors of fermionic bilinears are calculated and the symmetry currents of the theory are derived. Chapter 3 contains analytical studies of the structure of minimally doubled fermions in the naïve continuum limit. A formal decomposition of the spinors into a pair of fields suggests the existence of oscillating contributions in some correlation functions. Later on, it is concluded from $CP\Theta$ symmetry of Karsten-Wilczek fermions in the quenched approximation that correlation functions with the same charge conjugation eigenstates at source and sink are invariant under time reflection. Chapter 4 encompasses numerical studies of Karsten-Wilczek fermions in the quenched approximation [155]. Foreseeable difficulties for numerical simulations are discussed and an overview of the setup of simulations is given. Methods for dealing with a lack of symmetry under time reflection are discussed. No signature for this broken reflection symmetry is observed in data. Next, two independent approaches to non-perturbative tuning of the relevant counterterm's coefficient are discussed in detail. The first approach, which minimises the anisotropy that is observed in the mass of the pseudoscalar ground state, is scrutinised with regard to its various systematical uncertainties, which are dominated by finite size effects and the chiral extrapolation. The second approach restores the frequency spectrum of an oscillating ratio of correlation functions to its tree-level form. These oscillations are related to fermion doubling in a comparison with naïve and Wilson fermions and systematical uncertainties of the approach are examined. The numerical part is concluded with an investigation of the scaling behaviour of the ground states of two different channels using the non-perturbatively tuned theory. The ground state of the γ^5 channel scales like a (Pseudo-) Goldstone boson including quenched chiral logarithms at finite cutoff. Since the ground state of the γ^0 channel scales like a (Pseudo-) Goldstone boson up to $\mathcal{O}(a^2)$-corrections, it is identified as a pseudoscalar that is massive in the chiral limit due to lattice artefacts. The study with pseudoscalar masses below $300\,\mathrm{MeV}$ shows that Karsten-Wilczek fermions are not affected by exceptional configurations. Finally, chapter 5 summarises the results and provides an outlook to future applications of minimally doubled fermions.

Foundations

1.1 QCD in the continuum

The topic of this section is a brief review of QCD as a quantised field theory of the strong interactions. The first focus lies on the fields of QCD and the structure of its action. The symmetries of QCD are discussed in the absence of electroweak interactions. The second focus lies on the quantisation of the QCD action within the path integral formalism as it had been conceived by Feynman [57] and on renormalisation. In general, this part follows mainly [130]. The treatment of chiral symmetry follows [139]. Notational conventions are guided by [65].

1.1.1 The QCD action and its symmetries

The fields and the action of QCD

QCD is a quantised SU(3) gauge theory which includes massive matter fields called quarks and massless gauge fields called gluons. The quarks are described by Dirac four-spinors in the fundamental representation of the gauge group,

$$\psi_\alpha^{a,(f)}(x), \quad \bar\psi_\alpha^{a,(f)}(x), \tag{1.1}$$

which carry spinor indices α, colour indices a and flavour indices (f) as defined in the appendix (A.2). The spinor field $\psi^{(f)}(x)$ has twelve independent components at each point x, which are represented by anti-commuting Grassmann numbers due to their compliance with Fermi statistics. The $\psi^{(f)}(x)$ can be interpreted as a component of a six-dimensional vector $\psi(x)$ in flavour space. The adjoint spinor field is defined by $\bar\psi = \psi^\dagger \gamma^0$, where γ^0 is the Dirac matrix associated with time (cf. appendix A.4). In the path integral approach to quantisation, $\bar\psi$ and ψ are treated as independent degrees of freedom.

The gluons are described by four-vector fields in the gauge group's adjoint representation,

$$A_\mu^{ab}(x) \equiv A_\mu^c(x) T_c^{ab}, \tag{1.2}$$

which carry space-time indices μ and colour indices a, b as defined in the appendix (A.2). The gluon fields $A_\mu^{ab}(x)$, which are 3×3-matrices can be expressed through eight hermitian fields $A_\mu^c(x)$ using the eight generators T_c of the gauge group SU(3) as in eq. (1.2). In total, the gluon field A has 32 components at each space-time point x. Since it is a massless spin-1 vector field, only sixteen components are independent.

The action of QCD is a functional of the fields ψ, $\bar\psi$ and A. The action functional has a piece which depends only on the gluon field, which is called gluon action $S^g[A]$, pure gauge action or Yang-Mills action, which reads

$$S^{\mathrm{g}}[A] = \int\limits_{\mathbb{M}^4} \frac{1}{4g_0^2} F^{\mu\nu,ab}(x) F_{\nu\mu}^{ba}(x) \; d^4x, \tag{1.3}$$

and a piece which involves quark and gauge fields, which is called quark action or fermion action $S^f[\psi, \bar\psi, A]$,

$$S^{\mathrm{f}}[\psi, \bar\psi, A] = \sum_{(f)} \int\limits_{\mathbb{M}^4} \bar\psi_\alpha^{a,(f)}(x) \left(i\gamma_{\alpha\beta}^\mu D_\mu^{ab} - m_0^{(f)} \delta^{ab} \delta\alpha\beta \right) \psi_\beta^{b,(f)}(x) \; d^4x. \tag{1.4}$$

Among the seven parameters of the QCD action, there is one bare coupling constant g_0 and six bare quark masses $m_0^{(f)}$. The coupling g_0 of QCD cannot be defined for on-shell quantities like the coupling e of QED, since QCD is a confining theory and its charge carriers, quarks and gluons, cannot be observed in an asymptotic state under on-shell conditions. This is why the coupling of QCD must be defined with methods of the renormalisation group (cf. section 1.1.2). The six masses fall apart into a set of light masses and another set of heavy masses (cf. table 1.1). QCD has a natural scale, Λ^{QCD}, which is a function of its seven parameters. Typical four-momenta of states of the QCD spectrum are of the order of Λ^{QCD}, which is about 200 MeV. The strange quark mass m_s is considered as light in some applications and as heavy in others, since it compares with Λ^{QCD} within a factor of two. The up and down quark masses, m_u and m_d, however, are always considered as light. Since the quark action is explicitly written as a sum of different flavours, the following discussion is exactly equal for all flavours. A concise notation for one flavour reads

$$S^{\mathrm{QCD}}[\psi, \bar\psi, A] = \int\limits_{\mathbb{M}^4} \bar\psi(x) \left(i\gamma^\mu D_\mu - m_0 \right) \psi(x) + \frac{1}{2g_0^2} \mathrm{Tr} \left(F^{\mu\nu}(x) F_{\mu\nu}(x) \right) \; d^4x \tag{1.5}$$

and has to be interpreted in the sense of eqs. (1.3) and (1.4). The kinetic term of the quark action contains Dirac matrices γ^μ (cf. appendix A.4.2) and the covariant derivative,

$$D_\mu^{ab} \psi_\alpha^b(x) \equiv \left(\delta^{ab} \partial_\mu + i A_\mu^{ab}(x) \right) \psi_\alpha^b(x), \tag{1.6}$$

Light quarks			
f	$m^{(f)}$ (exp.) [MeV]	$m^{(f)}$ (th.) [MeV]	e.m. charge [e]
u	$2.3^{+0.7}_{-0.5}$	2.16 ± 0.11	$+2/3$
d	$4.8^{+0.5}_{-0.3}$	$4.68 \pm 0.14 \pm 0.07$	$-1/3$
s	95 ± 5	$93.8 \pm 1.5 \pm 1.9$	$-1/3$
Heavy quarks			
f	$m^{(f)}$ (exp.) [GeV]		e.m. charge [e]
c	1.275 ± 0.025		$+2/3$
b	4.18 ± 0.03		$-1/3$
t	$173.07 \pm 0.52 \pm 0.72$		$+2/3$

Table 1.1: Quarks are separated by Λ^{QCD} into light flavours ($m^{(f)} \lesssim \Lambda^{QCD}$) and heavy flavours ($m^{(f)} \gtrsim \Lambda^{QCD}$). Quark masses are taken from [20] and [13].

which couples quark and gluon fields. The covariant derivative implicitly depends on the space-time point x through the gauge field $A_\mu(x)$. The commutator of two covariant derivatives at the same space-time point x gives rise to the field strength tensor $F_{\mu\nu}(x)$,

$$F_{\mu\nu}^{ab}(x) \equiv -i\left[D_\mu^{ac}, D_\nu^{cb}\right] \equiv \partial_\mu A_\nu^{ab}(x) - \partial_\nu A_\mu^{ab}(x) + i\left[A_\mu^{ac}(x), A_\nu^{cb}(x)\right]. \tag{1.7}$$

The field strength tensor $F_{\mu\nu}$, which is a 3×3-matrix just like the gauge field A_μ can be rewritten in a vector notation with hermitian fields $F_{\mu\nu}^c$ multiplied by the generators of the gauge group SU(3).

Gauge symmetry in QCD

The QCD action is invariant under local gauge transformations $\Omega(x) = e^{i\omega^c(x)T_c}$, which are fully parameterised by eight real parameters $\omega^c(x)$, since the gauge group SU(3) is an eight-dimensional compact Lie group. Gauge transformations are simultaneously applied to all fields which lie in non-trivial representations of SU(3),

$$
\begin{aligned}
\psi_\alpha^a(x) &\overset{\Omega(x)}{\to} \Omega^{ab}(x)\psi_\alpha^b(x), \\
\bar{\psi}_\alpha^a(x) &\overset{\Omega(x)}{\to} \bar{\psi}_\alpha^b(x)(\Omega^{ab})^\dagger(x), \\
F_{\mu\nu}^{ab}(x) &\overset{\Omega(x)}{\to} \Omega^{ac}(x)F_{\mu\nu}^{cd}(x)(\Omega^{bd})^\dagger(x).
\end{aligned}
\tag{1.8}
$$

The invariance of the quark action in eq. (1.4) is achieved by the covariant derivative of the fermion field, which transforms like the fermion field itself in eq. (1.6). This is due to the nontrivial behaviour of the gauge field $A_\mu(x)$ under gauge transformations:

$$D_\mu^{ab}\psi_\alpha^b(x) \overset{\Omega(x)}{\to} \Omega^{ab}(x)D_\mu^{bc}\psi_\alpha^c(x), \tag{1.9}$$

$$A_\mu^{ab}(x) \overset{\Omega(x)}{\to} \Omega^{ac}(x)A_\mu^{cd}(x)(\Omega^{bd})^\dagger(x) + i\left(\partial_\mu\Omega^{ac}(x)\right)(\Omega^{bc})^\dagger(x) = A_\mu^{ab}(x) + D_\mu^{ab}\omega^{bc}(x). \tag{1.10}$$

The covariant derivative is related to the concept of parallel transport in the framework of differential geometry. Space-time $\mathbb{M}^4$ and the gauge group SU(3) form a vector bundle

in the sense that each space-time point x is vested with its own copy of SU(3). Therefore, fields which belong to non-trivial representations of the gauge group at different points transform differently under gauge transformations. A gauge transporter $U(x, x + a\hat{e}_\mu)$ is introduced, which compensates for different copies of SU(3) at base points x and $x + a\hat{e}_\mu$. A sensible derivative of a field $\psi(x)$ is thus defined in the limit of vanishing distance a,

$$
\begin{aligned}
D_\mu^{bc} \psi^c(x) &\overset{!}{=} \lim_{a \to 0} \frac{1}{a} \left\{ U^{bc}(x, x + a\hat{e}_\mu)\psi^c(x + a\hat{e}_\mu) - \psi^b(x) \right\} \\
&= \lim_{a \to 0} U^{bc}(x, x + a\hat{e}_\mu) \frac{1}{a} \left\{ \psi^c(x + a\hat{e}_\mu) - \psi^c(x) \right\} + \lim_{a \to 0} \frac{1}{a} \left\{ U^{bc}(x, x + a\hat{e}_\mu) - \delta^{bc} \right\} \psi^c(x) \\
&= \left(\delta^{bc} \partial_\mu + [\partial_\mu U(x', x)]_{x'=x}^{bc} \right) \psi^c(x),
\end{aligned}
\tag{1.11}
$$

where $U^{bc}(x, x) = \delta^{bc}$ was used. A comparison with eq. (1.6) reveals

$$
[\partial_\mu U(x', x)]_{x'=x}^{bc} = iA_\mu^{bc}(x), \quad U(x, x + a\hat{e}_\mu) = 1 + ia\hat{e}_\mu A_\mu^c(x)T_c + \mathcal{O}(a^2) \equiv U_\mu(x). \tag{1.12}
$$

The gauge field A_μ is the connection of the covariant derivative. The gauge transporter is generalised to arbitrary differentiable paths $\mathcal{C}$ and the parallel transporter reads

$$
U(x, y) = \exp\left(i \int_x^y T_c \sum_{\mu=0}^3 A_\mu^c ds_\mu \right), \tag{1.13}
$$

which is a Wilson line between the points x and y.

Discrete symmetries of QCD

Besides its gauge symmetry, the QCD action retains its structure under three individual discrete symmetry transformations, which are charge conjugation (often referred to as C symmetry), parity transformation (P) and time reversal (often referred to as Θ symmetry). Parity and time reversal are global symmetries, since the transformations connect fields with different space-time arguments. Parity is defined with a unitary operator acting on fields and space-time points,

$$
\begin{aligned}
(x_0, \mathbf{x}) &\overset{P}{\to} (x_0, -\mathbf{x}), \\
\psi(x_0, \mathbf{x}) &\overset{P}{\to} \gamma_0 \, \psi(x_0, -\mathbf{x}), \\
\bar{\psi}(x_0, \mathbf{x}) &\overset{P}{\to} \bar{\psi}(x_0, -\mathbf{x}) \, \gamma_0, \\
(A_0(x_0, \mathbf{x}), \mathbf{A}(x_0, \mathbf{x})) &\overset{P}{\to} (A_0(x_0, -\mathbf{x}), -\mathbf{A}(x_0, \mathbf{x})),
\end{aligned}
\tag{1.14}
$$

whereas time reversal must be defined with an anti-unitary operator, which enacts complex conjugation on all c-numbers and operators alongside its operation on fields and space-time points,

$$
\begin{aligned}
(x_0, \mathbf{x}) &\overset{\Theta}{\to} (-x_0, \mathbf{x}), \\
\psi(x_0, \mathbf{x}) &\overset{\Theta}{\to} \gamma_1 \gamma_3 \, \psi(-x_0, \mathbf{x}), \\
\bar{\psi}(x_0, \mathbf{x}) &\overset{\Theta}{\to} -\bar{\psi}(x_0, -\mathbf{x}) \, \gamma_1 \gamma_3, \\
(A_0(x_0, \mathbf{x}), \mathbf{A}(x_0, \mathbf{x})) &\overset{\Theta}{\to} -(-A_0(-x_0, \mathbf{x}), \mathbf{A}(-x_0, \mathbf{x})).
\end{aligned}
\tag{1.15}
$$

Lastly, charge conjugation replaces particles by antiparticles and vice versa. Since space-time points are unaltered, charge conjugation can be locally defined with the charge conjugation matrix C of eq. (A.33),

$$
\begin{aligned}
\psi(x_0, \mathbf{x}) &\overset{C}{\to} C\,\bar{\psi}^T(x_0, \mathbf{x}), \\
\bar{\psi}(x_0, \mathbf{x}) &\overset{C}{\to} -\psi^T(x_0, \mathbf{x})\,C, \\
(A_0(x_0, \mathbf{x}), \mathbf{A}(x_0, \mathbf{x})) &\overset{C}{\to} -\left(A_0(x_0, \mathbf{x}), \mathbf{A}(x_0, \mathbf{x})\right).
\end{aligned} \tag{1.16}
$$

The product $CP\Theta$ leaves the structure of any field theory invariant, since the action is scalar and must necessarily be invariant under space-time transformations.

Approximate chiral symmetry in QCD

Nevertheless, the QCD action has additional symmetries, some of which are only approximately realised. These approximate symmetries can be identified, when the quarks are sufficiently lighter and external four-momenta are sufficiently smaller than Λ^{QCD}. On the one hand, small external four-momenta in QCD processes as well as the light quark masses can be treated as a perturbation to a theory with vanishing external four-momenta and quark masses. On the other hand, heavy quark states are strongly suppressed as they are produced only far off shell in processes with low external four-momenta and hence do not contribute to asymptotic states. As a result, QCD processes with small external four-momenta can be described by an effective theory of interactions between hadronic states consisting of the light flavours only, whereas the heavy degrees of freedom are integrated out. The a priori unknown effective coupling constants and the symmetry of interactions of such an effective theory are determined by QCD.

Right-handed and left-handed components of the $N_f = 3$ light quark fields $\psi^{(f)}$ are defined using the chirality projectors of eq. (A.31),

$$
\psi_{R,L}^{(f)}(x) = P_{R,L}\psi^{(f)}(x), \quad \bar{\psi}_{R,L}^{(f)}(x) = \bar{\psi}^{(f)}(x)P_{L,R}. \tag{1.17}
$$

In the chiral limit, where light quark masses are set to zero, left- and right-handed quarks decouple in the chiral quark action,

$$
S^{\text{ch.}}[\psi, \bar{\psi}, A] = \sum_{f=1}^{N_f} \int_{\mathbb{R}^4} \bar{\psi}_R^{(f)}(x)\,(i\gamma^\mu D_\mu)\,\psi_R^{(f)}(x) + \bar{\psi}_L^{(f)}(x)\,(i\gamma^\mu D_\mu)\,\psi_L^{(f)}(x)\ d^4x. \tag{1.18}
$$

The action is invariant under two individual sets of global symmetry transformations for right-handed or left-handed quarks,

$$
\begin{aligned}
\psi_{R,L}^{\prime(g)}(x) &= \exp\left(-i\sum_{j=1}^{8}\Theta_{R,L}^j T_j^{gf}\right)e^{-i\Theta_{R,L}}\psi_{R,L}^{(f)}(x), \\
\bar{\psi}_{R,L}^{\prime(g)}(x) &= \bar{\psi}_{R,L}^{(f)}(x)\exp\left(i\sum_{j=1}^{8}\Theta_{R,L}^j T_j^{fg}\right)e^{i\Theta_{R,L}},
\end{aligned} \tag{1.19}
$$

where the T_j are the generators of a flavour symmetry group SU(3) (cf. appendix A.3). The independent transformations of right-handed and left-handed fields can be equivalently represented by vector and axial transformations, which simultaneously transform right-handed and left-handed fields with $\Theta_V^j = (\Theta_R^j + \Theta_L^j)/2$, $\Theta_A^j = (\Theta_R^j - \Theta_L^j)/2$ and $\Theta_V = (\Theta_R + \Theta_L)/2$. The action of the axial transformation on the flavour group's three-vectors includes the chirality matrix γ_5,

$$
\begin{aligned}
\psi'^{(g)}(x) &= \exp\left(-i\sum_{j=1}^{8}\Theta_A^j T_j^{gf}\gamma_5\right)\psi^{(f)}(x), \\
\bar{\psi}'^{(g)}(x) &= \bar{\psi}^{(f)}(x)\exp\left(-i\sum_{j=1}^{8}\Theta_A^j T_j^{fg}\gamma_5\right),
\end{aligned}
\tag{1.20}
$$

and leaves the chiral quark action invariant. This flavoured axial symmetry SU(3)$_A$ is spontaneously broken in QCD and the axial charge operators do not annihilate the vacuum. Instead, when applied to the vacuum state, they create massless pseudoscalar bosons, which have the same quantum numbers as the axial charge operators. These are the (Pseudo-) Goldstone bosons of QCD. In this idealised case, pions, kaons and the eta meson are massless and fully degenerate in all interactions.

These axial transformations cease to be symmetry transformations in the presence of light quark masses. Therefore, the spontaneously broken axial symmetry is explicitly broken by the light quark masses and the (Pseudo-) Goldstone bosons acquire small masses, while their degeneracies are partially lifted. In the spectrum of QCD, they can be identified as the light pseudoscalar meson octet. In a limiting case with degenerate up and down quark masses, $m_u = m_d = m_{ud} < m_s$, isospin is realised as a symmetry and pions are fully degenerate and considerably lighter than the kaons. In the real world, isospin symmetry is broken by the finite mass difference of up and down quarks as well as their different electroweak charges. The presence of light quark masses reduces the flavoured vector symmetries as well. The singlet vector transformation is preserved as a symmetry transformation for arbitrary quark masses and is connected to baryon number conservation. For degenerate light quarks, all flavoured vector symmetries are preserved and the perfect flavour symmetry of the eightfold way of Gell-Mann and Ne'eman is realised. The divergences of the axial symmetry currents are proportional to products of pseudoscalar quark bilinears and combinations of quark masses in the form which was realised in the PCAC relation.

1.1.2 Quantisation of QCD with the path integral approach

The path integral

The path integral approach to quantisation as it had been suggested by Feynman [57] expresses quantum mechanical amplitudes, such as the time evolution operator $U(x_i, t_i; x_f, t_f)$ between states x_i and x_f, as a functional integral of the observables weighted with the

classical action over all possible paths between initial and final points:

$$\langle U(x_i, t_i; x_f, t_f) \rangle = \int\limits_{x(t_i)=x_i}^{x(t_f)=x_f} \mathcal{D}x(t) e^{iS[x(t)]}. \tag{1.21}$$

Paths in the neighbourhood of the classical solution $x_{cl}(t)$ dominate the path integral and produce small quantum corrections, whereas outlying paths are suppressed by strong cancellations. The path integral is generalised to quantum field theories (QFTs), where observables are functionals of elementary field variables. The path integral of QCD reads

$$\langle \mathcal{O} \rangle = \frac{1}{Z} \int \mathcal{D}\bar{\psi}\mathcal{D}\psi\mathcal{D}A \ \mathcal{O}[\psi, \bar{\psi}, A] \ e^{iS^{QCD}[\psi, \bar{\psi}, A]}, \tag{1.22}$$

where $Z = \langle 1 \rangle$ is a constant and $S^{QCD}[\psi, \bar{\psi}, A]$ is defined in eq. (1.5). However, there are two obstacles which must be overcome before the path integral of QCD can be evaluated.

Firstly, due to gauge invariance, the integration overcounts gauge field configurations, which are connected by gauge transformations. The naïve gluon propagator,

$$\left(\partial^2 g_{\mu\nu} - \partial_\mu \partial_\nu \right) D_g^{\nu\rho, ab}(x-y) \stackrel{!}{=} i\delta_\mu^\rho \delta^{(4)}(x-y)\delta^{ab}, \tag{1.23}$$

has no solution for gauge fields, which are connected to vanishing A by the gauge transformations of eq. (1.10) and thus consist only of a derivative of a scalar function. These physically equivalent configurations must be culled by an ingenious gauge-fixing procedure, which has been developed by Fadeev and Popov [56]. An arbitrary gauge-fixing parameter ξ is introduced, which modifies the gluon propagator,

$$\left(\partial^2 g_{\mu\nu} - \left(1 - \frac{1}{\xi} \right) \partial_\mu \partial_\nu \right) D_g^{\nu\rho, ab}(x-y) \stackrel{!}{=} i\delta_\mu^\rho \delta^{(4)}(x-y)\delta^{ab}, \tag{1.24}$$

and unphysical degrees of freedom, which are called Faddeev-Popov ghosts, are coupled to the gluon field and cancel the contributions from unphysical polarisations of gauge bosons. Since physical observables are naturally gauge invariant, any effects due to particular choices of the gauge-fixing parameter ξ or contributions of unphysical gauge field or ghost degrees of freedom cancel completely in any observables. Secondly, non-perturbative evaluation of the path integral of QCD must be restricted to an evaluation of its kernel on a relatively small number of representative gauge field configurations due to technical reasons. Following the idea of importance sampling, a small but representative ensemble of configurations which yields a good estimate of the full path integral is required. Hence, the majority of configuration must belong to the neighbourhood of the classical path. However, an explicit bias which generally rejects outlying configurations is not acceptable. Gauge field configurations can be produced with Monte-Carlo methods and their vicinity to the classical path is determined from the numerical value of the action. Yet, because a complex exponential $e^{iS^{QCD}}$ is not a valid weight factor

that would have to be real, importance sampling cannot be applied straightforwardly.

Both of these obstacles are lifted simultaneously by the approach of Lattice QCD, which uses the analytic continuation of the QCD action of eq. (1.5) on a discretised Euclidean space-time (cf. appendix A.4). The discretised space-time requires another representation of the gauge fields in terms of the gauge transporters of eq. (1.12), which are integrated with the gauge-invariant Haar measure. Thus, the Haar measure dispenses with gauge-fixing. The exponential factor changes into $e^{-S_E^{QCD}}$, which is a real, suitable weight factor for importance sampling. Lattice QCD is addressed in section 1.2.

Renormalisation

The seven parameters of the QCD action, the bare coupling g_0 and the six bare masses $m_0^{(f)}$, as well as the field variables ψ, $\bar{\psi}$ and A are subject to renormalisation in the quantised theory. The quantities in the action are defined in the absence of interactions, whereas the physical fields naturally include any interaction effects in full. Quantum corrections, which are diagrammatically represented by loops in a perturbative approach, lead to finite and divergent contributions beyond the bare quantities. These corrections are absorbed into coefficients of counterterms at any given renormalisation scale M, where the physical values of the parameters of the theory are known. In a so-called renormalisable quantum field theory, a finite number of counterterms is sufficient for the complete absorption of all quantum corrections into their coefficients. The same coefficients are repeatedly modified at each order in a perturbative expansion. In an effective field theory, absorption requires an infinite number of counterterms. However, if the quantum corrections are computed in a well-defined perturbative expansion, the number of counterterms which are required for absorbing divergences at each order of the perturbation theory is still finite and divergences can be removed order by order.

Due to the requirement of renormalisation, the coupling constant g of the interactions which are the origin of the quantum corrections receives quantum corrections itself. These quantum corrections to the coupling constant g are determined by the Callan-Symanzik β function of QCD,

$$\beta(g) \equiv M \frac{\partial g}{\partial M}, \tag{1.25}$$

which describes the dependence of the coupling constant g on changes of the renormalisation scale M. In that sense the coupling constant is actually a running coupling parameter. In the case of QED, a renormalisation scale M is chosen as the physical scale of on shell electrons, which can propagate as asymptotic states. Therefore, the classical electron mass and electric charge can be used in the renormalisation procedure.

On the contrary, due to the colour confinement property of QCD, neither the quarks in the fundamental representation nor the gluons in the adjoint representation of the gauge group can propagate as asymptotic states into a detector. However, they can behave

as almost free particles when they carry very high four-momenta. The beta function of QCD (in the chiral limit) reads

$$\beta(g) = -\frac{g^3}{(4\pi)^2}\left(\beta_0 + \frac{g^2}{(4\pi)^2}\beta_1\right) + \mathcal{O}(g^7), \tag{1.26}$$

$$\beta_0 = \left(\frac{11}{3}C(G) - \frac{4}{3}N_f C(R)\right), \tag{1.27}$$

$$\beta_1 = \left(\frac{34}{3}C^2(G) - N_f C(R)\left(\frac{20}{3}C(G) + 4C_2(R)\right)\right), \tag{1.28}$$

where the Casimir operators of the adjoint and fundamental representations, $C(G)$, $C(R)$ and $C_2(R)$, are defined in appendix A.3. N_f is the number of massless quark flavours in the theory. If $N_f < (11/4)\,C(G)/C(R) = 16.5$, the coefficient β_0 is positive and the β-function has negative curvature in g. Therefore, there is a high four-momentum scale, where the coupling strength vanishes and quarks and gluons behave as free particles. This property is aymptotic freedom of QCD, which was discovered by Gross, Politzer and Wilczek [81–83, 131]. Asymptotic freedom is the reason why the coupling constant of QCD can be measured at the electroweak scale. The world average of measurements of the coupling is given in the particle data book [20] as

$$\alpha_s(M_Z^2) \equiv \frac{g^2(M_Z^2)}{4\pi} = 0.1184 \pm 0.0007, \tag{1.29}$$

which must be evolved with renormalisation group methods to the scale of interest.

1.2   Lattice QCD

This part follows mostly [65]. It includes a brief introduction to Lattice QCD (LQCD) as a discretisation of an analytic continuation of the continuum action of eq. (1.5) to Euclidean space-time as it had been conceived for the first time by Wilson [160]. The gluon action is discretised as the Wilson plaquette action and Wilson fermions are introduced as the standard case of lattice fermions, which is compared in section 1.3 with minimally doubled fermion actions. A lattice realisation of chiral symmetry according to the Ginsparg-Wilson equation [72] employing Ginsparg-Wilson fermions with an Overlap operator [119] is presented for contrasting juxtaposition.

1.2.1   Discretisation of QCD on a Euclidean space-time

The analytic continuation of the QCD action from Minkowski space-time to Euclidean space-time is rather straightforward. The Osterwalder-Schrader approach [124, 126] is used for the Wick rotation[1] (cf. appendix A.4). Wick rotation is applied to eq. (1.5) and

---

[1]The terminology is taken over from [149, 153].

produces an overall factor i,

$$S_M^{QCD}[\psi^M, \bar\psi^M, A^M] = iS_E^{QCD}[\psi^E, \bar\psi^E, A^E], \tag{1.30}$$

which multiplies the Euclidean QCD action (without Euclidean indexing),

$$S^{QCD}[\psi, \bar\psi, A] = \int_{\mathbb{R}^4} \bar\psi(x)\left(\gamma^\mu D_\mu + m_0\right)\psi(x) - \frac{1}{4}\mathrm{Tr}\left(F_{\mu\nu}(x)F_{\mu\nu}(x)\right)\ d^4x. \tag{1.31}$$

Euclidean space-time is discretised according to appendix A.4.3 using eqs. (A.38) and (A.39). The lattice spacing a, the intrinsic length scale of the discretised theory, is treated as a small quantity and its inverse serves as a cutoff removing UV divergences. The limit $a \to 0$ of tree-level quantities is called the *naïve continuum limit*. However, since interactions mix terms of different powers in the lattice spacing a, an appropriate renormalisation prescription is required in the determination of the continuum limit.

Fermion fields are defined on the lattice sites labelled by n. Partial derivatives cannot be defined on a lattice and have to be discretised as finite differences. Two naïve versions,

$$\nabla_\mu\psi_n = \frac{1}{a}\left(\psi_{n+\hat e_\mu} - \psi_n\right) = \partial_\mu\psi(x) - \frac{a}{2}\psi(x) + \mathcal{O}(a^2), \tag{1.32}$$

$$\nabla_\mu^*\psi_n = \frac{1}{a}\left(\psi_n - \psi_{n-\hat e_\mu}\right) = \partial_\mu\psi(x) + \frac{a}{2}\psi(x) + \mathcal{O}(a^2), \tag{1.33}$$

are combined to a symmetrised form[2] with reduced discretisation errors,

$$\frac{1}{2}(\nabla_\mu + \nabla_\mu^*)\psi_n = \frac{1}{2a}\left(\psi_{n+\hat e_\mu} - \psi_{n-\hat e_\mu}\right) = \partial_\mu\psi(x) + \mathcal{O}(a^2). \tag{1.34}$$

As fermion fields in the kinetic term sit on neighbouring sites, they transform differently under gauge transformations. A gauge-invariant kinetic term uses gauge links U_n^μ,

$$U_n^\mu \equiv U^\mu(an, a(n + \hat e_\mu)) = e^{iaA^\mu(a(n+\hat e_\mu/2))} = e^{iaA_{n+\hat e_\mu/2}^\mu}, \tag{1.35}$$

which are the Euclidean analogue of the parallel transporters of eq. (1.12). Since gauge transporters U_n^μ instead of the connection $A_{n+\hat e_\mu/2}^\mu$ are the field variables in LQCD, eq. (1.35) defines the connection in LQCD. Gauge links U_n^μ are defined by the end sites n and $n + \hat e_\mu$ which they connect. The particular definition of the site label of the connection, which is exactly in the middle between the ends of the gauge link, simplifies calculations in lattice perturbation theory in section 2. Thus, the symmetrically discretised covariant derivative reads

$$D^\mu[U]\psi_n = \frac{1}{2a}\left(U_n^\mu\psi_{n+\hat e_\mu} - U_{n-\hat e_\mu}^{\mu\dagger}\psi_{n-\hat e_\mu}\right) = \left(\partial^\mu + iA^\mu(x)\right)\psi(x) + \mathcal{O}(a^2) = D^\mu\psi(x) + \mathcal{O}(a^2) \tag{1.36}$$

and is conveniently expressed as a matrix with two site indices,

$$D_{n,m}^\mu[U] = \frac{1}{2a}\left(U_n^\mu\delta_{n+\hat e_\mu,m} - U_{n-\hat e_\mu}^{\mu\dagger}\delta_{n-\hat e_\mu,m}\right). \tag{1.37}$$

---

[2]Only the symmetrised form has the desired hermiticity properties.

The contraction of the discretised covariant derivative $D_{n,m}^\mu[U]$ with Dirac matrices γ^μ,

$$D_{n,m}^N = \sum_{\mu=0}^{3} \gamma^\mu D_{n,m}^\mu[U],$$
(1.38)

is referred to as the naïve Dirac operator and implicitly depends on the local gauge fields U. It is a remarkable feature of the naïve Dirac operator that it connects only fields on even with fields on odd sites as defined in eq. (A.40), which is inherited by many other discretised Dirac operators. It is employed in the naïve fermion action with mass m_0,

$$S^N[\psi, \bar\psi, U] = a^4 \sum_{n,m \in \Lambda} \bar\psi_n \left(D_{n,m}^N + m_0 \delta_{n,m} \right) \psi_m.$$
(1.39)

However, the action of eq. (1.39) is not well-suited for simulations of QCD due to the so-called doubling problem, which is covered in section 1.2.3.

Since the field strength tensor $F_{\mu\nu}(x)$ is defined through explicit use of derivatives, discretisation of the gauge action of eq. (1.3) requires a lattice representation of the field strength tensor that uses only finite differences. Any chain of neighbouring gauge links is a discretised expression for a Wilson line. If the Wilson line returns to its origin in a so-called Wilson loop, it becomes a gauge-invariant object. The smallest possible Wilson loop in the μ-ν plane is the so-called plaquette $U_n^{\mu\nu}$, which can be expanded in the gauge fields A using eq. (1.35),

$$\begin{aligned}
U_n^{\mu\nu} =& U_n^\mu U_{n+\hat e_\mu}^\nu U_{n+\hat e_\nu}^{\mu\dagger} U_n^{\nu\dagger} & (1.40) \\
=& e^{iaA_{n+\hat e_\mu/2}^\mu} \, e^{iaA_{n+\hat e_\mu+\hat e_\nu/2}^\nu} \, e^{-iaA_{n+\hat e_\nu+\hat e_\mu/2}^\mu} \, e^{-iaA_{n+\hat e_\nu/2}^\nu} \\
=& e^{ia^2 (\nabla^\mu A_{n+\hat e_\nu/2}^\nu - \nabla^\nu A_{n+\hat e_\mu/2}^\mu + i \left[A_{n+\hat e_\nu+\hat e_\mu/2}^\mu, A_{n+\hat e_\nu/2}^\nu \right])} + \mathcal O(a^3) \\
=& e^{ia^2 F^{\mu\nu}(x)} + \mathcal O(a^3), & (1.41)
\end{aligned}$$

until it yields the exponentiated field strength tensor up to higher orders in the lattice spacing. Hence, the plaquette as an exponentiated multiple of a discretised version of the field strength tensor is used in the so-called plaquette action,

$$S^p[U] = \sum_{n \in \Lambda} \sum_{\mu < \nu} \frac{2}{g_0^2} \mathrm{Re}\,\mathrm{Tr}(1 - U_n^{\mu\nu}),$$
(1.42)

which was originally conceived by Wilson [160]. The inverse coupling constant is usually abbreviated as

$$\beta = \frac{6}{g_0^2},$$
(1.43)

and is non-analytically related the lattice spacing a. The product of lattice spacing and length of the time direction plays the role of an inverse temperature $a N_0 = 1/(k_B T)$.

16

1.2.2 Symmetries of Lattice QCD

Most symmetries of the Minkowski space-time QCD action are carried over to the Euclidean QCD action, though some symmetries are replaced by a counterpart. The symmetry under transformations with elements of the proper orthochronous Lorentz group $\mathcal{L}_+^\uparrow$ together with the spatial rotation group SO(3) are substituted by an SO(4) symmetry, since Euclidean time is fully equivalent to any spatial direction. The naïve discretisation procedure breaks the rotation group SO(4) down to the hypercubic group W_4. The symmetry transformations of eqs. (1.14) and (1.16), parity P and charge conjugation C, fully carry over to Euclidean space-time. Due to the full equivalence of the four directions of Euclidean space-time, the parity transformation can be generalised to reflections P_μ, which leave only the $\hat{e}_\mu$ direction invariant,

$$
\begin{aligned}
x_\nu &\overset{P_\mu}{\to} P_\mu x_\nu \equiv (-1)^{1-\delta_{\mu\nu}} x_\nu, \\
\psi(x) &\overset{P_\mu}{\to} \gamma^\mu \psi(P_\mu x), \\
\bar{\psi}(x) &\overset{P_\mu}{\to} \bar{\psi}(P_\mu x)\, \gamma^\mu, \\
A_\lambda(x) &\overset{P_\mu}{\to} (-1)^{1-\delta_{\mu\lambda}} A_\lambda(P_\mu x).
\end{aligned}
\tag{1.44}
$$

Hermiticity of the Minkowski space-time quark action is not carried over to Euclidean space-time in the OS approach for Euclidean field theories [124, 126]. Nevertheless, γ^5 hermiticity of the Dirac operator,

$$
\gamma^5 D^\dagger \gamma^5 = D,
\tag{1.45}
$$

is a property of Euclidean Dirac operators that are analytic continuations of hermitian Dirac operators on Minkowski space-time. The product $Q = \gamma^5 D$ is a hermitian Dirac operator if D is γ^5 hermitian.

Time reflection Θ of the Euclidean space-time QCD action is realised with three successive generalised parity transformations with cyclical spatial indices, e.g. $P_1 P_2 P_3$. The reflection is generalised to reflection of the single $\hat{e}_\mu$ direction in Euclidean space-time,

$$
\begin{aligned}
x_\nu &\overset{\Theta_\mu}{\to} \Theta_\mu x_\nu \equiv (-1)^{\delta_{\mu\nu}} x_\nu, \\
\psi(x) &\overset{\Theta_\mu}{\to} \gamma^\mu \gamma^5 \psi(\Theta_\mu x), \\
\bar{\psi}(x) &\overset{\Theta_\mu}{\to} \bar{\psi}(\Theta_\mu x)\, \gamma^5 \gamma^\mu, \\
A^\nu(x) &\overset{\Theta_\mu}{\to} \delta^{\mu\nu} A^\nu(\Theta_\mu x).
\end{aligned}
\tag{1.46}
$$

In a discretised theory, time-reflection can be performed with two different methods. Either one temporal site index is fixed and the lattice is reflected at this hyperplane, which is called site-reflection. Or the invariant hyperplane is chosen in the middle of a link between two neighbouring temporal hyperplanes, which is called link-reflection. If either site- or link-reflection is a symmetry of the discretised theory, the continuum limit satisfies Θ symmetry. The condition, whether the Minkowski space-time QFT, which

is obtained from any Euclidean space-time QFT by the analytic continuation back to Minkowski space-time with an inverse Wick rotation, satisfies Θ symmetry or not has been covered by Osterwalder et al. [125, 126]. The associated Minkowski space-time QFT satisfies Θ symmetry, if any correlation function, which depends only on fields at positive times (defined with either site- or link reflection) is necessarily positive.

1.2.3   Doubling problem and No-Go theorem

The naïvely discretised fermion action of eq. (1.39) contains spurious fermionic degrees of freedom, which are called doublers. This property is apparent in the momentum space representation of the naïve fermion action in the free theory with trivial gauge fields,

$$S^N[\psi, \bar\psi] = \frac{1}{|\Lambda|} \sum_{k \in \widetilde{\Lambda}} \bar\psi(k) \left(\frac{i}{a} \sum_{\mu=0}^{3} \gamma^\mu \sin(ak_\mu) + m_0 \right) \psi(k), \qquad (1.47)$$

where $|\Lambda|$ is defined in appendix A.4.3. On the one hand, the naïve Dirac operator's chiral limit $D^N(k) = \frac{i}{a}\gamma^\mu \sin(ak_\mu)$ vanishes, if all four-momentum components satisfy

$$k_\mu = n_\mu \frac{\pi}{a}, \;\; n_\mu = \{0, 1\}. \qquad (1.48)$$

In a four-dimensional lattice, each dimension contributes a factor two for a total of sixteen poles of $D^N(k)$. On the other hand, the continuum Dirac operator $D(k) = i\gamma^\mu k_\mu$ has only one pole, if all momentum components vanish. Because each pole represents a real and degenerate fermion species[3], the naïvely discretised Dirac operator has fifteen spurious species compared to the Dirac operator of QCD on a space-time continuum. The degeneracy is due to invariance of the action of eq. (1.39) under any products ($\mu \in \{0, 1, 2, 3\}$) of the following unitary symmetry transformations:

$$\psi_n \to \chi_n = T_n^\mu \psi_n, \quad \bar\psi_n \to \bar\chi_n = \bar\psi_n (T_n^\mu)^{-1}, \quad T_n^\mu = (-1)^{n_\mu} Q^\mu, \quad Q^\mu = \gamma^\mu \gamma^5. \quad (1.49)$$

These are the spin factors (cf. eq. (2.10) in [99]) that reflect the symmetry between the sixteen species. Since the number of zero modes of the naïve Dirac operator is doubled for every space-time direction, these spurious degrees of freedom are called doublers and their presence is known as the doubling problem. Appropriate modification of the naïve Dirac action solves the doubling problem.

However, Nielsen and Ninomiya presented a No-Go theorem [121], which identified limitations to such modifications. According to Niedermayer [120], there is a limitation that no Dirac operator can simultaneously satisfy

    (a) $D_{n,m}$ is local   (bounded by $Ce^{-\gamma|n-m|}$)
    (b) $D(p) = i\gamma^\mu p_\mu + \mathcal{O}(ap^2)$ for $p \ll \pi/a$
    (c) $D(p)$ is invertible for $p \neq 0$ (has no massless doublers)
    (d) $\gamma^5 D + D\gamma^5 = 0$ (chiral symmetry)

---

[3]Since these poles differ by local spin factors [99], lattice fermions are called species in the following.

In brief, ultralocal lattice discretisations of the Dirac operator cannot have an odd number of chiral fermions without failing to reproduce the continuum Dirac operator in the naïve continuum limit. Therefore, any modification of the naïve Dirac operator must lack at least one of these properties. First, Wilson's discretisation of the quark action, which explicitly sacrifices the chiral symmetry is discussed. Second, the Ginsparg-Wilson relation [72], as a possible non-ultralocal realisation of chiral symmetry on a space-time lattice, and Neuberger's overlap operator [119] as an example of Ginsparg-Wilson fermions are covered. Finally[4], minimally doubled fermions of the types suggested by Karsten [98] and Wilczek [159] as well as the types suggested by Creutz [45] and Borici [26] are introduced. The presence of exactly two chiral zero modes inevitably breaks the hypercubic symmetry of the space-time lattice.

1.2.4 Wilson fermions

Wilson's solution [160] to the doubling problem adds to the naïve Dirac operator of eq. (1.38) an addititional operator, that constitutes the Wilson term,

$$D_{n,m}^W = \mathbf{1} \sum_{\mu=0}^{3} \frac{r}{2a} \left(2\delta_{n,m} - \left(U_n^\mu \delta_{n+\hat{e}_\mu, m} + U_{n-\hat{e}_\mu}^{\mu\dagger} \delta_{n-\hat{e}_\mu, m} \right) \right), \tag{1.50}$$

which trivially vanishes in the naïve continuum limit. In the free theory with trivial gauge fields, it can be expressed through

$$D^W \psi_n = -\frac{ar}{2} \mathbf{1} \sum_{\mu=0}^{3} \nabla_\mu \nabla_\mu^* \psi_n = -\frac{r}{2} \mathbf{1} \sum_{\mu=0}^{3} \left(\nabla_\mu - \nabla_\mu^* \right) \psi_n, \tag{1.51}$$

which shows that it is a discretised form of a d'Alembertian operator. The momentum space representation of the Wilson term in the free theory,

$$D^W(k) = \mathbf{1} \sum_{\mu=0}^{3} \frac{r}{a} \left(1 - \cos\left(ak_\mu \right) \right), \tag{1.52}$$

formally resembles a four-momentum dependent mass term. It vanishes at $k = (0, 0, 0, 0)$, which corresponds to the continuum Dirac operator's pole. All spurious fermion modes acquire *mass terms* that diverge in the continuum limit. Due to this infinite mass, the doublers decouple from the dynamics of the continuum fermion. The Wilson term, however, explicitly breaks chiral symmetry:

$$(D^N + D^W)\gamma^5 + \gamma^5(D^N + D^W) = 2\gamma^5 D^W. \tag{1.53}$$

If the lattice spacing a is sufficiently small, cutoff effects due to the Wilson term break chiral symmetry softly like the quark masses. Then cutoff effects can be treated as

---

[4]This is by no means exhaustive, e.g. staggered fermions are a third type of lattice fermions with a large number of different subtypes.

a perturbation to chiral symmetry and the spectrum of QCD can be recovered in the continuum limit. Otherwise, the spontaneous breakdown of chiral symmetry due to QCD cannot be studied numerically. Subtle properties of QCD due to the broken chiral symmetry might be obscured in studies with Wilson fermions.

1.2.5 Ginsparg-Wilson fermions

In 1981, Ginsparg and Wilson [72] suggested a discretised form of chiral symmetry as

$$D^{GW}\gamma^5 + \gamma^5 D^{GW} = a D^{GW}\gamma^5 D^{GW}, \tag{1.54}$$

which is known as the Ginsparg-Wilson equation. Eq. (1.54) requires that any Ginsparg-Wilson Dirac operator D^{GW} has non-vanishing contributions for arbitrarily separated lattice sites. Locality in the usual sense (ultralocality) is therefore sacrificed in these Dirac operators. However, an infinitesimal chiral transformation of the quark fields with

$$\psi' = e^{i\alpha\gamma^5(\mathbf{1} - \frac{a}{2}D^{GW})}\psi, \quad \bar{\psi}' = \bar{\psi}e^{i\alpha(\mathbf{1} - \frac{a}{2}D^{GW})\gamma^5} \tag{1.55}$$

leaves a Ginsparg-Wilson quark action invariant,

$$L[\psi', \bar{\psi}'] = \bar{\psi}'D^{GW}\psi' = \bar{\psi}D^{GW}\psi = L[\psi, \bar{\psi}]. \tag{1.56}$$

Lattice chirality projectors are defined with a non-local Ginsparg-Wilson chirality matrix,

$$\hat{\gamma}^5 = \gamma^5(\mathbf{1} - aD^{GW}), \quad \hat{P}_R = \frac{\mathbf{1} + \hat{\gamma}^5}{2}, \quad \hat{P}_L = \frac{\mathbf{1} - \hat{\gamma}^5}{2} \tag{1.57}$$

and Ginsparg-Wilson fermions with a finite quark mass are obtained with

$$D^{GW,m} = \omega D^{GW} + m\mathbf{1}, \quad \omega = 1 - \frac{am}{2}. \tag{1.58}$$

For a long time, no Dirac operator that qualified as a Ginsparg-Wilson Dirac operator D^{GW} was discovered until the 1990s. Kaplan [97] suggested domain wall fermions, Hasenfratz et al. [89] suggested perfect actions and Neuberger [119] suggested the overlap operator, which all qualify as Ginsparg-Wilson fermions. The overlap operator reads

$$D^{ov} = \frac{1}{a}\left(\mathbf{1} + \gamma^5 \operatorname{sign}(Q)\right) = \frac{1}{a}\left(\mathbf{1} + \frac{\gamma^5 Q}{\sqrt{Q^2}}\right), \tag{1.59}$$

where Q is the overlap kernel, which can be any undoubled hermitian Dirac operator with real eigenvalues such as $Q = \gamma^5(D^N + D^W)$. Due to the presence of the sign function, the overlap Dirac operator is not a sparse matrix in space-time even with a sparse kernel matrix Q. It must be approximated with considerable numerical effort and is computationally quite expensive. Nevertheless, it is shown by Hernandez et al. [91] that the magnitude of components of the Ginsparg-Wilson Dirac operator decreases at least exponentially with the distance between sites,

$$\left|(D_{n,m}^{GW})_{\alpha\beta}^{\bar{a}\bar{b}}\right| \leq C \exp\left(-\gamma\|n - m\|\right). \tag{1.60}$$

As the coefficients C and γ are independent of the gauge configuration and the lattice spacing a, the exponential fall-off shrinks to zero and a local field theory is recovered in the continuum limit. In that sense, the non-locality of the overlap operator can be considered as only a technical problem of calculations.

1.3 Minimally doubled fermions

Minimally doubled fermions are another type of discretised fermion actions, which have explicit ultralocal chiral symmetry. An additional ultralocal operator D^{md} that anticommutes with the standard chirality matrix γ^5 is added to the naïve fermion action. D^{md} reduces the number of poles of the lattice Dirac operator to two. Since these poles are located at different points on a line through the Brillouin zone, their displacement explicitly necessitates a reduction of the hypercubic symmetry of the naïve Dirac operator. Their different momentum support implies that they acquire different spin factors. Chiral fermions in the continuum limit can be defined as linear combinations of fields on neighbouring sites [159]. These two fermions show sensitivity to fluctuations of local gauge fields which may lift the degeneracy between both at finite lattice spacing. This is the analogue of taste-splitting and taste-breaking for staggered fermions [24, 104]. Two different types of minimally doubled fermions, Karsten-Wilczek [98, 159] and Boriçi-Creutz fermions [26, 27, 45, 46] are covered in more detail. Other types of minimally doubled fermions such as twisted ordering fermions [116] and generalisations of Karsten-Wilcek and Boriçi-Creutz types [32–34] are not covered here.

1.3.1 Karsten-Wilczek fermions

Karsten-Wilczek fermions were suggested in response to the No-Go theorem of Nielsen and Ninomiya [121] by Karsten [98] as a strictly local, chiral Dirac operator with the minimal number of chiral fermion species. The additional term vanishes only at the two temporal doublers and hence lessens the degeneracy and removes fourteen spurious fermions. Wilczek generalised the action further through the Wilczek parameter (called ζ throughout this thesis) and suggested a gluonic counterterm [159]. Pernici studied the action with the Karsten-Wilczek term in the $\hat{e}_1$ direction [129]. He suggested to consider the two fermion species as two flavours of QCD, constructed the transfer matrix and discussed fermionic counterterms. Moreover, he showed that the free action has a different species symmetry than the naïve action. In the wake of the minimally doubled fermion revival by Creutz [45] and Boriçi [26], Bedaque et al. [18] revisited the symmetries of the Karsten-Wilczek action. A study of the perturbative renormalisation of Karsten-Wilczek fermions at one-loop level [35, 36, 38] independently derived its counterterm structure in perturbation theory (cf. section 2). Tiburzi [145] studied the spin-flavour structure and the axial anomaly with Karsten-Wilczek fermions and Creutz suggested an approach to flavours of minimally doubled fermions using point-split fields [47]. Later, Misumi

21

et al. studied the index theorem [48] with Karsten-Wilczek fermions, their spin-flavour representation [101] and an interpretation as fermions with flavoured chemical potential [114, 115]. The additional operator of the Karsten-Wilczek term reads

$$D_{n,m}^{KW} = \sum_{\mu \neq \underline{\alpha}} \frac{i\zeta}{2a} \gamma^{\underline{\alpha}} \left(2\delta_{n,m} - \left(U_n^\mu \delta_{n+\hat{e}_\mu,m} + U_{n-\hat{e}_\mu}^{\mu\dagger} \delta_{n-\hat{e}_\mu,m} \right) \right), \qquad (1.61)$$

and is added to the naïve Dirac operator of eq. (1.38) to form the full Karsten-Wilczek operator. $\hat{e}_{\underline{\alpha}}$ is the unit vector along the alignment of the Karsten-Wilczek term and can be any one of the four Euclidean directions. The additional operator breaks the hypercubic group W_4 down to the cubic subgroup W_3, which excludes the $\hat{e}_{\underline{\alpha}}$ direction. Any combination of permutations of axes and reflections P_μ within the orthogonal complement of the $\hat{e}_{\underline{\alpha}}$ direction ($\mu \neq \underline{\alpha}$) is a symmetry of the Karsten-Wilczek action. However, neither the operators $\Theta_{\underline{\alpha}}$ for $n_{\underline{\alpha}}$ reflection of the $\hat{e}_{\underline{\alpha}}$ direction nor C for charge conjugation are symmetry operators of the Karsten-Wilczek action, since neither leaves the Karsten-Wilczek operator form-invariant. Nevertheless, the combination $\Theta_{\underline{\alpha}}C = C\Theta_{\underline{\alpha}}$ leaves the Karsten-Wilczek action form-invariant. Therefore, the product $CP\Theta$ is a symmetry of the Karsten-Wilczek action for any choice of $\underline{\alpha}$. The two doublers are located on the $\underline{\alpha}$ axis,

$$k_{\underline{\alpha}} = n_{\underline{\alpha}} \frac{\pi}{a}, \; n_{\underline{\alpha}} = \{0,1\}; \; k_\mu = 0, \; \mu \neq \underline{\alpha}. \qquad (1.62)$$

The mechanism which removes the spurious doublers is evident in the free momentum space Karsten-Wilczek action,

$$S^{KW}[\psi, \bar{\psi}] = \frac{1}{|\Lambda|} \sum_{k \in \widetilde{\Lambda}} \bar{\psi}(k) \left(\frac{i}{a} \sum_{\mu=0}^{3} \left\{ \gamma^\mu \sin(ak_\mu) + \zeta(1 - \delta_{\mu\underline{\alpha}})\gamma^{\underline{\alpha}}(1 - \cos(ak_\mu)) \right\} + m_0 \right) \psi(k).$$
$$(1.63)$$

The magnitude of the Karsten-Wilczek term exceeds the magnitude of the $\gamma^{\underline{\alpha}}$-component of the naïve kinetic term, if the Wilczek parameter satisfies $|\zeta| > 1/2$ at any of the spurious doublers $k_\mu = \pi/a$, $\mu \neq \underline{\alpha}$,

$$|\zeta|(1 - \cos(ak_\mu)) = 2|\zeta| > 1 \geq |\sin(ak_{\underline{\alpha}})|. \qquad (1.64)$$

Thus, the massless Dirac equation $(D^N(k) + D^{KW}(k))\psi(k) = 0$ has no solution, if any of the four-momentum components is non-zero except $k_{\underline{\alpha}}$. This leads to Pernici's symmetry transformation between mirror fermions [129],

$$\psi_n \to (-1)^{n_{\underline{\alpha}}} \psi_{R_{\underline{\alpha}} n}, \quad \bar{\psi}_n \to \bar{\psi}_{R_{\underline{\alpha}} n} (-1)^{n_{\underline{\alpha}}}, \quad R_\mu n_\nu = (1 - 2\delta_{\mu\nu}) n_\nu, \qquad (1.65)$$

which can be understood as a combination of $n_{\underline{\alpha}}$ reflection $\Theta_{\underline{\alpha}}$ of eq. (1.46) and the unitary operator $T_n^{\underline{\alpha}}$ of eq. (1.49). Thus, the combination of any two of the three operators C, $\Theta_{\underline{\alpha}}$ and $T_n^{\underline{\alpha}}$ leaves the Karsten-Wilczek action form-invariant. The Karsten-Wilczek action requires three counterterms [18,36,38,129], which are the only further relevant and

marginal operators in the operator product expansion, which comply with the Karsten-Wilczek term's symmetry. The two fermionic counterterm operators read

$$D^3_{n,m} = c^{KW}(g_0)\ \frac{i}{a}\gamma^{\underline{\alpha}}\delta_{n,m}, \tag{1.66}$$

$$D^4_{n,m} = d^{KW}(g_0)\ \gamma^{\underline{\alpha}}D^{\underline{\alpha}}_{n,m}[U], \tag{1.67}$$

where $D^{\underline{\alpha}}_{n,m}[U]$ is the $\underline{\alpha}$ component of the usual lattice covariant derivative of eq. (1.37). It amounts to a renormalisation of the fermionic speed of light in the $\hat{e}_{\underline{\alpha}}$ direction. The gluonic counterterm is due to a carryover of the anisotropy to the gauge fields and reads

$$S^{4p}[U] = \sum_{n\in\Lambda}\sum_{\mu\neq\underline{\alpha}} d^{KW}_P(g_0)\frac{\beta}{3}\mathrm{Re}\,\mathrm{Tr}(1 - U^{\mu\underline{\alpha}}_n). \tag{1.68}$$

It amounts to a renormalisation of the gluonic speed of light in the $\hat{e}_{\underline{\alpha}}$ direction. The dimension three counterterm has the same symmetry ($C\Theta_{\underline{\alpha}}$ instead of C and $\Theta_{\underline{\alpha}}$ individually) as the Karsten-Wilczek term. However, both dimension four counterterms are form-invariant under charge conjugation, any n_μ reflection (P_μ or Θ_μ) and the unitary operators ($T^{\underline{\alpha}}_n$). Thus, the full Karsten-Wilczek action has three counterterms,

$$S^f[\psi,\bar{\psi},U] = a^4\sum_{n,m\in\Lambda}\bar{\psi}_n\left(D^N_{n,m} + D^{KW}_{n,m} + D^3_{n,m} + D^4_{n,m} + m_0\delta_{n,m}\right)\psi_m, \tag{1.69}$$

$$S^g[U] = \sum_{n\in\Lambda}\sum_{\mu<\nu}\frac{\beta}{3}\mathrm{Re}\,\mathrm{Tr}(1 - U^{\mu\nu}_n)\left(1 + d^{KW}_P(g_0)\delta_{\mu\underline{\alpha}}\right), \tag{1.70}$$

with a priori unknown coefficients $c^{KW}(g_0)$, $d^{KW}(g_0)$ and $d^{KW}_P(g_0)$, which depend on the parameters of the theory (in the chiral limit only g_0 and ζ). These counterterm coefficients[5] must be tuned in order to restore isotropy to the continuum limit.

1.3.2 Boriçi-Creutz fermions

Boriçi-Creutz fermions were suggested by Creutz [45] as a four-dimensional generalisation of graphene. Graphene layers of single atom thickness had been extracted for the first time by Geim and Novoselov in 2004 [95] and they demonstrated that electrons in graphene propagate as a two-dimensional gas of massless Dirac fermions [122]. Boriçi placed these four-dimensional graphene actions on orthogonal lattices [26]. Bedaque et al. studied symmetries of these actions [18], introduced an iso-doublet notation and pointed out the non-singlet structure of the Boriçi-Creutz operator. They demonstrated that Boriçi-Creutz actions on totally symmetric hyperdiamond lattices do not reproduce the correct continuum limit [19]. Cichy et al. [42] studied cutoff effects of Boriçi-Creutz fermions at tree level and Boriçi found scaling behaviour of pseudoscalar masses with Boriçi-Creutz fermions consistent with predictions of chiral perturbation theory [27]. Misumi and Kimura [102, 103] studied hyperdiamond lattices of different

---

[5]The label ^{KW} of the coefficients and the coupling dependence are usually omitted in the following.

dimensionalities and demonstrated that minimal doubling and hyperdiamond structure are compatible only in two dimensions. One-loop renormalisation properties were determined in perturbative studies of Boriçi-Creutz fermions [35–38]. The spin-flavour representation of Boriçi-Creutz fermions was covered in [101]. The additional operator is

$$D_{n,m}^{BC} = \sum_\mu \frac{i\zeta}{2a} (\Gamma - \gamma^\mu) \left(\left(U_n^\mu \delta_{n+\hat{e}_\mu,m} + U_{n-\hat{e}_\mu}^{\mu\dagger} \delta_{n-\hat{e}_\mu,m} \right) - 2\delta_{n,m} \right), \qquad (1.71)$$

and its fermionic bilinear is the Boriçi-Creutz term with parameter[6] $\zeta = \pm 1$ and where

$$\Gamma \equiv \frac{1}{2} \sum_{\nu=0}^{3} \gamma^\nu. \qquad (1.72)$$

The additional operator is added to the naïve Dirac operator of eq. (1.38) to form the full Boriçi-Creutz operator. A transformed set of Dirac matrices,

$$\gamma^{\mu\prime} \equiv \Gamma\gamma^\mu\Gamma = \Gamma - \gamma^\mu, \qquad (1.73)$$

allows for a convenient notation of the additional operator,

$$D_{n,m}^{BC} = \sum_\mu \frac{i\zeta}{2a} \gamma^{\mu\prime} \left(U_n^\mu \delta_{n+\hat{e}_\mu,m} + U_{n-\hat{e}_\mu}^{\mu\dagger} \delta_{n-\hat{e}_\mu,m} \right) - \frac{i\zeta}{a} 2\Gamma\delta_{n,m}. \qquad (1.74)$$

The symmetry of the Boriçi-Creutz action has been studied by Creutz [46]. The residual W_3 cubic symmetry of the Boriçi-Creutz action can be made transparent most easily using a real, self-inverse and symmetric matrix,

$$A = \frac{\zeta}{2} \begin{pmatrix} +1 & +1 & +1 & +1 \\ +1 & -1 & +1 & -1 \\ +1 & +1 & -1 & -1 \\ +1 & -1 & -1 & +1 \end{pmatrix} = A^{-1} = A^T = A^*, \qquad (1.75)$$

which transforms the site basis $\hat{e}_\mu$ to a new orthonormal basis $\hat{f}_\nu$ ($\hat{f}$ basis),

$$\hat{f}_\nu = A_{\nu\mu}\hat{e}_\mu, \quad \hat{e}_\mu = A_{\mu\nu}\hat{f}_\nu. \qquad (1.76)$$

The Dirac matrices in the $\hat{f}$ basis are linear combinations of the old Dirac matrices,

$$\Gamma^\nu = A^{\nu\mu}\gamma^\mu, \quad \gamma^\mu = A^{\mu\nu}\Gamma^\nu, \quad \text{in particular} \quad \zeta\Gamma \equiv \Gamma^0. \qquad (1.77)$$

The naïve Dirac operator is form-invariant under the coordinate transformation to the $\hat{f}$ basis and the additional operator written in the $\hat{f}$ basis reads

$$D_{n,m}^{BC} = -\sum_{\nu,\mu} \frac{i}{2a} \Gamma^\nu A^{\nu\mu} \left(U_n^\mu \delta_{n+\hat{e}_\mu,m} + U_{n-\hat{e}_\mu}^{\mu\dagger} \delta_{n-\hat{e}_\mu,m} \right) \qquad (1.78)$$

$$+ \sum_\mu \frac{i}{a} \Gamma^0 A^{0\mu} \left(U_n^\mu \delta_{n+\hat{e}_\mu,m} + U_{n-\hat{e}_\mu}^{\mu\dagger} \delta_{n-\hat{e}_\mu,m} \right) + \frac{i}{a} 2\Gamma^0\delta_{n,m}, \qquad (1.79)$$

---

[6]Some authors (e.g. [101]) use a generalised Boriçi-Creutz action with arbitrary values of ζ. A brief discussion why these actions are not considered here is presented at the end of this section.

where the residual cubic symmetry of the linear span

$$\text{span}(V) = \left\{ \sum_{i=1}^{3} \lambda_i \hat{f}_i \mid \hat{f}_1, \hat{f}_2, \hat{f}_3 \right\} \tag{1.80}$$

is evident in eq. (1.78). However, any reflection of the $\hat{f}_0$ direction changes the sign of the last term in eq. (1.79). Moreover, a simultaneous reflection of all directions $(P\Theta = P_f\Theta_f)$ changes the overall sign of the additional operator of eq. (1.71). Because charge conjugation induces a sign change in the additional operator as well, the Boriçi-Creutz action satisfies $CP\Theta$ symmetry. The two doublers are aligned on the $\hat{f}_0$-axis,

$$k_0 = n_0 \frac{\pi}{a}, \ n_0 = \{0, 1\}; \ k_\nu = 0, \ \nu \neq 0. \tag{1.81}$$

Whereas this looks very much alike eq. (1.62), the length of one period on the axes in the $\hat{f}$ basis is $4\pi/a$ instead of $2\pi/a$. Hence, the Boriçi-Creutz term in eq. (1.71) and the Karsten-Wilczek term in eq. (1.61) are not exactly rotated analogues. Only even sites in the site basis $\hat{e}_\mu$ are mapped on points with integer labels in the $\hat{f}$ basis $\hat{f}_\nu$. Odd sites in the site basis are mapped on points with half-integer labels in the $\hat{f}$ basis and vice versa. In terms of the site basis $\hat{e}_\mu$, the doublers are located at

$$k_\mu = n\zeta \frac{\pi}{2a} \ \forall \mu, \ n = \{0, 1\}, \tag{1.82}$$

where all components are equal. The mechanism, which removes the spurious doublers is covered in great detail by Creutz [46]. Among the two pieces of the additional operator, the first is unitarily equivalent to the naïve Dirac operator with shifted four-momentum,

$$\frac{i\zeta}{a} \gamma^{\mu\prime} \cos(ak_\mu) = \Gamma\left(\frac{i}{a}\gamma^\mu \sin\left(ak_\mu + \zeta\frac{\pi}{2}\right)\right)\Gamma, \tag{1.83}$$

and vanishes at four-momenta that maximize the naïve Dirac operator. The second piece is a constant

$$-\frac{i\zeta}{a}2\Gamma = -\frac{i}{a}\sum_\mu \gamma^\mu \zeta = -\frac{i\zeta}{a}\sum_\mu \gamma^{\mu\prime} \tag{1.84}$$

that cancels the with the first piece exactly at the continuum pole of the naïve Dirac operator $(k_\mu = 0 \ \forall \ \mu)$, whereas it cancels with the naïve Dirac operator exactly a single pole of the first piece of the additional operator of the Boriçi-Creutz term $(k_\mu = \zeta\pi/(2a) \ \forall \ \mu)$. Any other pole of either operator is only incompletely cancelled by the second piece and does not persist as a pole of the full Boriçi-Creutz operator. Therefore, minimal doubling is achieved and the free momentum space Boriçi-Creutz action reads

$$S^{BC}[\psi, \bar{\psi}] = \frac{1}{|\Lambda|} \sum_{k \in \widetilde{\Lambda}} \bar{\psi}(k) \left(\frac{i}{a} \sum_{\mu=0}^{3} \{\gamma^\mu \sin(ak_\mu) + \zeta\gamma^{\mu\prime}(\cos(ak_\mu))\} + \left\{m_0 - \frac{i\zeta}{a}2\Gamma\right\}\right)\psi(k). \tag{1.85}$$

The Boriçi-Creutz action requires three counterterms [18, 35–38], which are the only further relevant and marginal operators in the operator product expansion that comply with the Boriçi-Creutz term's symmetry. The two fermionic counterterm operators read

$$D^3_{n,m} = c^{BC}(g_0) \, \frac{i}{a} \Gamma \delta_{n,m}, \tag{1.86}$$

$$D^4_{n,m} = d^{BC}(g_0) \, \frac{1}{2} \Gamma \sum_{\mu=0}^{3} D^\mu_{n,m}[U], \tag{1.87}$$

where $D^\mu_{n,m}[U]$ are the μ-components of the usual lattice covariant derivative of eq. (1.37). The dimension four counterterm can be understood as the $\Gamma^0 D^0_{n,m}[U]$ component of the naïve Dirac operator in the $\hat{f}$ basis. The gluonic counterterm is due to a carryover of the anisotropy to the gauge fields and reads

$$S^{4p}[U] = \sum_{n\in\Lambda} \sum_{\mu,\nu,\rho=0}^{3} d^{BC}_P(g_0) \left(\widehat{F}^{\mu\rho}_n \widehat{F}^{\rho\nu}_n \right), \tag{1.88}$$

where $\widehat{F}^{\mu\rho}_n$ is some lattice discretisation of the gluon field strength tensor. In the $\hat{f}$-basis, the term takes a form which clearly underscores the analogy to eq. (1.68),

$$S^{4p}[U] = \sum_{n\in\Lambda} \sum_{\rho=1}^{3} d^{BC}_P(g_0) \frac{1}{4} \left(\widehat{F}^{0\rho}_n \widehat{F}^{\rho 0}_n \right). \tag{1.89}$$

The dimension four counterterms amount to different renormalisation of the speed of light for fermions and gluons in the $\hat{f}_0$-direction. The dimension three counterterm has the same $CP\Theta$ symmetry as the additional term of eq. (1.71). However, both dimension four counterterms are additionally form-invariant under charge conjugation as well as any n_μ reflection (P_μ or Θ_μ). The full Boriçi-Creutz action contains its three counterterms,

$$S^f[\psi, \bar{\psi}, U] = a^4 \sum_{n,m\in\Lambda} \bar{\psi}_n \left(D^N_{n,m} + D^{BC}_{n,m} + D^3_{n,m} + D^4_{n,m} + m_0 \delta_{n,m} \right) \psi_m, \tag{1.90}$$

$$S^g[U] = \sum_{n\in\Lambda} \sum_{\mu<\nu} \frac{\beta}{3} \mathrm{Re\,Tr}(1 - U^{\mu\nu}_n) + \sum_{\rho=0}^{3} 2d^{BC}_P(g_0) \left(\widehat{F}^{\mu\rho}_n \widehat{F}^{\rho\nu}_n \right), \tag{1.91}$$

with a priori unknown coefficients $c^{BC}(g_0)$, $d^{BC}(g_0)$ and $d^{BC}_P(g_0)$, which depend on the parameters of the theory g_0. These counterterm coefficients[7] must be tuned in order to restore isotropy to the continuum limit. The additional operator could be generalised [101] with $\zeta \neq \pm 1$, if the dimension-four counterterm were included with a changed coefficient,

$$D^{4,mod}_{n,m} = \left(d^{BC}(g_0) + 2(|\zeta| - 1) \right) \frac{1}{2} \Gamma \sum_{\mu=0}^{3} D^\mu_{n,m}[U]. \tag{1.92}$$

---

[7]The label ^{BC} of the coefficients and the coupling dependence are usually omitted in the following.

The action would maintain minimal doubling with the same zero modes as in eq. (1.82). However, eq. (1.92) changes the naïve continuum limit of the Dirac operator, which is

$$\lim_{a \to 0} D^{mod}(p) = \lim_{a \to 0} D^N(p) + D^{4,mod}(p) = i \sum_\mu \left(\gamma^\mu + (|\zeta| - 1)\Gamma \right) p_\mu. \qquad (1.93)$$

Hence, the naïve continuum limit of the modified Boriçi-Creutz actions fails to agree with the correct continuum action $i \sum_\mu \gamma^\mu p_\mu$ unless $|\zeta| = 1$. This is why these modified actions are not given any further consideration here.

Perturbative studies

Though the objective of LQCD is to study QCD in the non-perturbative regime, Lattice Perturbation Theory (LPT) is an important tool. Here, LPT studies are applied to determine renormalisation properties of minimally doubled fermions. Their counterterms are a manifestiation of the anisotropy and their coefficients are calculated at one-loop level. It is shown how isotropy is restored to the continuum limit in perturbation theory up to $\mathcal{O}(g_0^4)$ corrections through application of counterterms. However, only coefficients of counterterms in the continuum limit are known at one-loop level. If there are different lattice operators with the same continuum limit, a one-loop LPT calculation cannot necessarily discern which counterterm operator is favourable at finite cutoff. This is important if counterterm operators include lattice derivatives such as eqs. (1.67) and (1.87), as one-loop calculations are ignorant of their discretisation[1]. Nevertheless, the dependence of one-loop coefficients on tree-level parameters (such as ζ) restricts possible choices of lattice counterterm operators. LPT calculations demonstrate the renormalisability of minimally doubled fermions (cf. sections 2.3.1 and 2.3.3). LPT substantiates the statements [18, 145] that the axial symmetry current of minimally doubled fermions is conserved in the perturbative regime for arbitrary gauge coupling. Vector and axial symmetry currents, which are derived with chiral Ward-Takahashi identities have renormalisation factors equal to one, since contributions from proper vertex renormalisation and legs cancel exactly (cf. section 2.3.2).

The chapter starts with a discussion of general technical aspects of LPT is section 2.1, which are taken from [31]. The next section 2.2 covers propagators and vertices of minimally doubled fermions, which were already presented in [35–38]. The calculation of one-loop corrections is then covered in more detail in section 2.3. Finally, the concept of boosted perturbation theory (BPT) [110] is introduced and the perturbative estimates from BPT for non-perturbative coefficients are presented in section 2.4. Lastly, results of perturbative studies are summarised as interim findings (I) in section 2.5.

---

[1]Two-loop coefficients explicitly discriminate between these choices, since counterterms have to be included in loop calculations up to $\mathcal{O}(g_0^4)$.

2.1 Technical aspects of lattice perturbation theory

LPT has been covered in great detail by Capitani in [31]. This section covers only those concepts from chapters 15 and 18 of [31], which are necessary in the following. These are the power counting theorem of Reisz [133–136], the subtraction scheme for divergent integrals from Kawai et al. [100] and basic bosonic integrals, which were first studied by Caracciolo et al. [39].

2.1.1 The power counting theorem of Reisz

Any LPT integral I with L loops has a generic structure ([31], p. 208, eq. (15.1))

$$I = \int\limits_{-\pi/a}^{+\pi/a} \frac{d^4k_1}{(2\pi)^4} \cdots \int\limits_{-\pi/a}^{+\pi/a} \frac{d^4k_L}{(2\pi)^4} \frac{V(k,q;m,a)}{C(k,q;m,a)}, \tag{2.1}$$

where k_j are internal loop four-momenta, q_j are external four-momenta, m represents masses of all particles on internal lines and a is the lattice spacing. The denominator is written as a product of denominators of individual propagators ([31], p. 208, eq. (15.2)),

$$C(k,q;m,a) = \prod_{i=1}^{L} C_i(l_i;m,a), \tag{2.2}$$

with line momenta $l_i(k,q)$, which can be expressed as linear combinations of internal four-momenta k_j and external four-momenta q_j. The numerator and denominator have to satisfy a set of conditions (V1,V2, C1,C2,C3 and L1,L2 in [31]). C3 is quoted here verbatim ([31], p. 209, eq. (15.7)), because it is not satisfied in LPT calculations with minimally doubled fermions without additional precautions:

"(C3) There exist positive constants a_0 and A such that

$$|C_i(l_i;m,a)| \geq A(\hat{l}_i^2 + m_i^2) \tag{2.3}$$

for all $a \leq a_0$ and all l_i's."

The variable $\hat{l}$ on the right hand side of eq. (2.3) is defined as

$$\hat{l}_\mu \equiv \frac{2}{a}\sin\left(\frac{al_\mu}{2}\right). \tag{2.4}$$

Lattice integrals at finite a are necessarily finite in the ultraviolet (UV) region. Instead, their divergence is entirely in the infrared (IR). Evaluation of any LPT integral requires knowledge of its superficial degree of divergence ([31], p. 209, eq. (15.12)). The superficial degree of divergence $\deg V$ of a numerator V is defined as

$$V(\lambda k,q;m,\lambda a) \overset{\lambda \to \infty}{=} K\lambda^{\deg V} + \mathcal{O}(\lambda^{\deg V - 1}), \tag{2.5}$$

where $K \neq 0$. With an analogous definition of $\deg C$ for the denominator, the full superficial degree of divergence is given by

$$\deg I = 4L + \deg V - \deg C. \tag{2.6}$$

In the one-loop calculations of section 2.3, chiral fermions are assumed. A common mass parameter is introduced in all denominators as a mass regularisation in the infrared.

2.1.2 Subtraction scheme for lattice integrals

One-loop integrals I, which are calculated in section 2.3 depend on one or two external four-momenta p and q, where the latter case applies within this thesis only to quadratically divergent contributions to the vacuum polarisation with $p = q$. The subtraction scheme is demonstrated here for integrals with only one external four-momentum p,

$$I = \int\limits_{-\pi/a}^{\pi/a} \frac{d^4 k}{(2\pi)^2} \mathcal{I}(k, p), \tag{2.7}$$

which are representative of logarithmically or linearly divergent contributions to the fermionic self-energy. Following the scheme introduced by Kawai et al. [100], the divergent integral is artificially split into two pieces J and $I - J$, where

$$J = \int\limits_{-\pi/a}^{\pi/a} \frac{d^4 k}{(2\pi)^2} \mathcal{I}(k, 0) + \sum_{\mu=0}^{3} \left[p_\mu \int\limits_{-\pi/a}^{\pi/a} \frac{d^4 k}{(2\pi)^2} \left. \frac{\partial \mathcal{I}(k, p)}{\partial p_\mu} \right|_{p=0} \right] \tag{2.8}$$

is obtained as a Taylor expansion of I up to first order in the external four-momentum p. Thus, external particles are assumed as belonging to the neighbourhood of the standard pole $k_\mu = 0 \; \forall \; \mu$. All integrands in J are evaluated for vanishing external four-momenta and in the chiral limit, which greatly simplifies the calculation. Renormalisation of the quark mass is calculated from a Taylor expansion in the bare mass, where integrals are evaluated in the chiral limit. However, even for IR-finite cases of the original integral I, both integrals J and $I - J$ are IR-divergent and require an intermediate IR-regularisation scheme. The second piece, $I - J$, is UV-finite and is evaluated in the limit $a \to 0$. The first piece J can be simplified further with subtractions of well-known basic integrals $\widetilde{J}$, which share the same IR divergence. Hence, the difference $J - \widetilde{J}$ is IR-finite. The lattice spacing a is absorbed by rescaling the integration momentum,

$$ak \to k', \tag{2.9}$$

and the integral itself is transformed into a pure number multiplying a power of the lattice spacing a. The subtracted IR divergence is obtained from basic bosonic integrals $\widetilde{J}$, which are known at very high precision. The basic integrals that are used in the

presented calculations are expressed with the notation of eq. (2.4) as

$$\mathcal{B}(1) \equiv \int\limits_{-\pi/a}^{\pi/a} \frac{d^4k}{(2\pi)^4} \frac{1}{\sum_\mu \hat{k}_\mu^2} = \frac{1}{a^2} Z_0, \tag{2.10}$$

$$\mathcal{B}(1;1,1) \equiv \int\limits_{-\pi/a}^{\pi/a} \frac{d^4k}{(2\pi)^4} \frac{\hat{k}_{\underline{\mu}}^2 \hat{k}_{\underline{\nu}}^2}{\sum_\lambda \hat{k}_\lambda^2} = 4a^2 Z_1, \tag{2.11}$$

$$\mathcal{B}(2) \equiv \int\limits_{-\pi/a}^{\pi/a} \frac{d^4k}{(2\pi)^4} \frac{1}{\left(\sum_\mu \hat{k}_\mu^2 + M^2\right)^2} = \frac{1}{16\pi^2}\left(-\log{(aM)^2}) - \gamma_E + F_0\right). \tag{2.12}$$

The Euler-Mascheroni constant γ_E also appears in continuum loop integrals,

$$\gamma_E = 0.57721566490153286. \tag{2.13}$$

These basic integrals are taken from [31], p. 254, eqs. (18.23), (18.24) and (18.26). Other bosonic integrals are defined in [31], p. 254, eq. (18.15) using eq. (2.4) as

$$\mathcal{B}(p; n_0, n_1, n_2, n_3) = \int\limits_{-\pi/a}^{\pi/a} \frac{d^4k}{(2\pi)^4} \frac{\hat{k}_0^{2n_0} \hat{k}_1^{2n_1} \hat{k}_2^{2n_2} \hat{k}_3^{2n_3}}{\left(\sum_\mu \hat{k}_\mu^2 + M^2\right)^p} \tag{2.14}$$

and satisfy recursion relations, which are summarised in appendix B.1.

Basic bosonic constants	
Z_0	0.154933390231060214084837208
Z_1	0.107781313539874001343391550
F_0	4.369225233874758

Table 2.1: Numerical values of basic bosonic constants in LPT are taken from [31], p. 254., Table 2. These constants are defined in eqs. (2.10), (2.11) and (2.12).

2.1.3 Numerical integration and finite volume effects

The remaining lattice integrals $J - \widetilde{J}$ are evaluated with discrete summation methods for periodic analytic functions taken from [111]. Integrals I of analytic periodic functions $f(k)$ are estimated as

$$I = \int \frac{d^4k}{(2\pi)^4} f(k) = \frac{1}{N^4} \sum_{\mu=0}^{3} \sum_{n_\mu=1}^{N} f(2\pi \frac{n}{N}) + \mathcal{O}(e^{-\epsilon N}) \equiv I(N) + \mathcal{O}(e^{-\epsilon N}), \tag{2.15}$$

where ϵ is given by the absolute value of the singularity of the integrand which is closest to the real axis (eqs. (5.42)-(5.44) in chapter 5.3 of [111]). The convergence of the integrals

is accelerated by changing the integration variable according to (eqs. (5.46)-(5.51) in chapter 5.3 of [111]) as

$$k = k' - \alpha \sin{(k')}, \quad 0 \le \alpha < 1, \tag{2.16}$$

which moves the singularity away from the real axis. The integrand takes the new form

$$\hat{f}(k') = (1 - \alpha \cos{k'})f(k(k')) \tag{2.17}$$

and the summation is replaced by

$$I = \frac{1}{N^4} \sum_{\mu=0}^{3} \sum_{n_\mu=1}^{N} \hat{f}(2\pi \frac{n}{N}) + \mathcal{O}(e^{-\hat{\epsilon}N}) \equiv \hat{I}(N) + \mathcal{O}(e^{-\hat{\epsilon}N}), \tag{2.18}$$

where $\hat{\epsilon} = \mathcal{O}(1)$. The summation is performed for various discretisations of the Brillouin zone with different N. According to eq. (6.5) in chapter 6 of [111], the finite volume effects for lattice one-loop diagrams with engineering dimension δ in the absence of external momenta and masses take the form

$$D(f) \sim a^{\delta-4}[A + B \log(1/N)] + (aN)^{\delta-4} \sum_{m=0}^{\infty} a_m (1/N)^m. \tag{2.19}$$

Therefore, multiple $\hat{I}(N)$ with large, but similar N are extrapolated to $N \to \infty$ with

$$\hat{I}(N) = I_\infty + \frac{dI}{N^2}. \tag{2.20}$$

2.2 Propagators and vertices

Propagators and vertices for Karsten-Wilczek and Boriçi-Creutz fermions have been already presented in [35–38]. Their properties are covered in detail in the next two sections. Propagators and vertices are derived from the exponentiated action in the path integral with variational methods in the limit of weak coupling g_0. Since perturbative expressions are lengthy, the following abbreviations are used:

$$\begin{aligned} s_p^\mu &\equiv \sin{(ap_\mu)} \\ c_p^\mu &\equiv \cos{(ap_\mu)} \\ \hat{s}_p^\mu &\equiv 2\sin{(ap_\mu/2)} \\ \hat{c}_p^\mu &\equiv 2\cos{(ap_\mu/2)} \end{aligned} \tag{2.21}$$

When the Euclidean index is omitted in terms within parentheses that include any of the expressions defined in eq. (2.21), their index is to be understood as being summed over (e.g. $(\hat{s}_p) \equiv \sum_\mu (\hat{s}_p^\mu)$, $(\hat{s}_p \hat{s}_p \hat{c}_p) \equiv \sum_\mu (\hat{s}_p^\mu \hat{s}_p^\mu \hat{c}_p^\mu)$). Summations, which are restricted to

all but the $\hat{e}_\alpha$ direction (e.g. $(\hat{s}_p \hat{c}_p)_\perp \equiv \sum_{\mu \neq \underline{\alpha}} (\hat{s}_p^\mu \hat{c}_p^\mu)$) are abbreviated with an additional lower index "$\perp$". For a similar purpose, the abbreviation $\varrho^{\mu\nu}$ is introduced:

$$\varrho^{\mu\nu} \equiv 1 - \delta^{\mu\nu}. \tag{2.22}$$

The propagator is obtained as the inverse of the free momentum space Dirac operator,

$$S(p; m, a) = \frac{D^\dagger(p; m, a)}{D(p; m, a) D^\dagger(p; m, a)}. \tag{2.23}$$

The vertices must be derived from a variation of the connection A^μ instead of the gauge links U^μ, which are related by eq. (1.35). Moreover, the coupling constant must be extracted from the definition of the connection as $A^\mu = g_0 \mathcal{A}^\mu$. Since one-loop corrections are of order $\mathcal{O}(g_0^2)$, the gauge links have to be expanded up to order $\mathcal{O}(g_0^2)$,

$$U_n^\mu = 1 + i a g_0 \mathcal{A}_{n + \hat{e}_\mu / 2}^\mu - \frac{a^2 g_0^2}{2!} \mathcal{A}_{n + \hat{e}_\mu / 2}^\mu \mathcal{A}_{n + \hat{e}_\mu / 2}^\mu + \mathcal{O}(g_0^3) \tag{2.24}$$

which generates vertices of fermions with two gluons that produce tadpole diagrams of LPT, which do not have counterparts in continuum QCD. Each gluon field $\mathcal{A}_{n + \hat{e}_\mu / 2}^\mu$ is expressed through its Fourier transform $\mathcal{A}^\mu(k)$. The gluon propagator is taken from [31], p. 144, eq. (5.62). It is obtained from an expansion of the plaquette action and requires use of the Fadeev-Popov procedure [15]. Once a gauge has been fixed using a gauge fixing parameter ξ, the gluon propagator reads

$$G_{\mu\nu}^{ab}(p; M, a) \equiv \delta^{ab} G_{\mu\nu}(p; M, a), \quad G_{\mu\nu}(p; M, a) \equiv \frac{\delta^{\mu\nu} - (1 - \xi) \frac{\hat{s}_p^\mu \hat{s}_p^\nu}{(\hat{s}_p)^2 + (aM)^2}}{(\hat{s}_p)^2 + (aM)^2}, \tag{2.25}$$

where a mass parameter M is included only for the purpose of mass regularisation. The overall denominator is referred to as the gluon denominator $D^g(p; M, a) = (\hat{s}_p)^2 + (aM)^2$.

2.2.1 Karsten-Wilczek fermions

The fermion propagator for Karsten-Wilczek fermions is obtained by inverting the free Dirac operator in eq. (1.63). It reads

$$S(p; \zeta, m_0, a) = a \frac{-i(\gamma \cdot s_p) - i \frac{\zeta}{2} \gamma^\alpha (\hat{s}_p)_\perp^2 + a m_0}{(s_p)^2 + \frac{\zeta^2}{4} \left((\hat{s}_p)_\perp^2 \right)^2 + (a m_0)^2 + \zeta s_p^\alpha (\hat{s}_p)_\perp^2} \tag{2.26}$$

and is multiplied by a Kronecker symbol δ^{bc} in SU(3) space. Its denominator, which is later referred to as $D(p; \zeta, m_0, a)$, vanishes at both doublers of eq. (1.62), which clearly violates condition C3 of eq. (2.3). Whether or not the second doubler generates an IR divergence depends on properties of the other contributions to the loop integral. The propagator has the correct continuum limit $S(p; \zeta, m_0, 0) = (\sum_\mu i \gamma^\mu p_\mu + m_0)^{-1}$ in the neighbourhood of its first doubler and can be interpreted as a quark propagator in the limit $a \to 0$. In the neighbourhood of the second doubler, the four-momentum p must be expanded around the pole in line with [99, 145] as

$$p_\mu = \frac{\pi}{a} \delta^{\mu\underline{\alpha}} + q_\mu. \tag{2.27}$$

33

Expansion of the propagator yields

$$S(q + \frac{\pi}{a}\hat{e}_{\underline{\alpha}}; \zeta, m_0, a) = a \frac{-i \sum_\mu \left(\gamma^\mu s_q^\mu (1 - 2\delta^{\mu\underline{\alpha}}) \right) - i\zeta\gamma^{\underline{\alpha}}(\hat{s}_q)^2_\perp + am_0}{(s_q)^2 + \frac{\zeta^2}{4}\left((\hat{s}_q)^2_\perp\right)^2 + (am_0)^2 - \zeta s_q^{\underline{\alpha}}(\hat{s}_q)^2_\perp} \tag{2.28}$$

which does not match a free quark in the limit $a \to 0$:

$$\lim_{a \to 0} S(q + \frac{\pi}{a}\hat{e}_{\underline{\alpha}}; \zeta, m_0, a) = \left(\sum_\mu i\gamma^\mu q_\mu (1 - 2\delta^{\mu\underline{\alpha}}) + m_0 \right)^{-1}. \tag{2.29}$$

If the poles correspond to degenerate quarks in the limit $a \to 0$, they must be related by a unitary transformation like eq. (1.49 for naïve fermions). It is defined as

$$\lim_{q \to 0} \chi(q) \equiv \mathcal{Q}\psi(q + \frac{\pi}{a}\hat{e}_{\underline{\alpha}}), \quad \lim_{q \to 0} \bar{\chi}(q) \equiv \bar{\psi}(q + \frac{\pi}{a}\hat{e}_{\underline{\alpha}})\mathcal{Q}^\dagger. \tag{2.30}$$

with matrices $\mathcal{Q}$ and $\mathcal{Q}^\dagger$. Thus, the propagator is transformed by left and right multiplication with their inverse matrices. $\mathcal{Q}$ and $\mathcal{Q}^\dagger$ equal $Q^{\underline{\alpha}}$ of eq. (1.49) up to phase factors,

$$\mathcal{Q} = e^{i\vartheta} i\gamma^{\underline{\alpha}}\gamma^5, \quad \mathcal{Q}^\dagger = e^{-i\vartheta} i\gamma^{\underline{\alpha}}\gamma^5 = \mathcal{Q}^{-1}, \tag{2.31}$$

and bring the continuum limit of the shifted propagator in the neighbourhood of the second pole to the original form in the neighbourhood of the first pole. The phase ϑ of the matrix $\mathcal{Q}$ is unrestricted and taken as zero for convenience. The propagator is called $S_\chi(q; \zeta, m_0, a)$ after four-momentum shift and unitary transformation reads

$$S_\chi(q; \zeta, m_0, a) \equiv \mathcal{Q}^\dagger S(q + \frac{\pi}{a}\hat{e}_{\underline{\alpha}}; \zeta, m_0, a)\mathcal{Q} = a \frac{-i(\gamma \cdot s_q) + i\zeta\gamma^{\underline{\alpha}}(\hat{s}_q)^2_\perp + am_0}{(s_q)^2 + \frac{\zeta^2}{4}\left((\hat{s}_q)^2_\perp\right)^2 + (am_0)^2 - \zeta s_q^{\underline{\alpha}}(\hat{s}_q)^2_\perp}, \tag{2.32}$$

which satisfies

$$S_\chi(p; \zeta, m_0, a) = S(p; -\zeta, m_0, a). \tag{2.33}$$

Since the Karsten-Wilczek term of eq. (1.61) changes its sign under charge conjugation C, transforming the fermions with $(-1)^{n_{\underline{\alpha}}}\mathcal{Q}C$ (with arbitrary phase ϑ) and gauge fields with C is a local symmetry. The propagator always (with the exception of the limit $a \to 0$) includes both doublers, though $S(p; \zeta, m_0, a)$ and $S_\chi(p; \zeta, m_0, a)$ differ by $\mathcal{O}(a)$ effects. Since left and right multiplication of the chirality matrix γ^5 with matrices $\mathcal{Q}$ and $\mathcal{Q}^\dagger$ changes its sign as $\mathcal{Q}^\dagger\gamma^5\mathcal{Q} = -\gamma^5$, the two doublers always correspond to fermion modes with opposite chirality in compliance with the No-Go theorem of Nielsen and Ninomiya [121]. The fermion-fermion-gluon vertex reads

$$V_1^\mu(p, q; \zeta, a) = -i\frac{g_0}{2} \left(\gamma^\mu \hat{c}_{p+q}^\mu + \zeta\gamma^{\underline{\alpha}}\varrho^{\underline{\alpha}\mu}\hat{s}_{p+q}^\mu \right) \tag{2.34}$$

and is multiplied by an SU(3) generator $(T^d)^{bc}$, where d is the gluon's colour index and b and c are the fermions' colour indices. The fermion-fermion-gluon-gluon vertex reads

$$V_2^{\mu\nu}(p, q; \zeta, a) = ia\frac{g_0^2}{4}\delta^{\mu\nu} \left(\gamma^\mu \hat{s}_{p+q}^\mu - \zeta\gamma^{\underline{\alpha}}\varrho^{\underline{\alpha}\mu}\hat{c}_{p+q}^\mu \right) \tag{2.35}$$

and is multiplied by an anticommutator of two SU(3) generators (cf. eq. (A.10)),

$$\left\{T^d, T^e\right\}^{bc} = \left(\frac{1}{3}\delta^{de}\delta^{bc} + d^{def}(T^f)^{bc}\right), \tag{2.36}$$

where d and e are colour indices of the two emitted gluons. b and c are colour indices of the fermion fields. The four-momentum p is attributed to an incoming fermion field and q is attributed to an outgoing fermion field in both vertices.

2.2.2 Boriçi-Creutz fermions

Propagators and vertices for Boriçi-Creutz fermions are obtained like those for Karsten-Wilczek fermions. In particular, the SU(3) structure is identical to the previous case and is therefore not repeated here. The fermion propagator is derived by inverting the free momentum space Boriçi-Creutz Dirac operator of eq. (1.85) and reads

$$S(p; \zeta, m_0, a) = a\frac{N(p; \zeta, m_0, a)}{D(p; \zeta, m_0, a)}, \tag{2.37}$$

with

$$N(p; \zeta, m_0, a) = -i\sum_\mu \left(\gamma^\mu s_p^\mu - \frac{\zeta}{2}\gamma^{\mu\prime}(\hat{s}_p^\mu)^2\right) + am_0, \tag{2.38}$$

$$D(p; \zeta, m_0, a) = (s_p)^2 + \zeta^2 \left((c_p)^2 - 2(c_p) + 4\right) - \zeta\left(2(s_p) + 2(s_p c_p) - (s_p)(c_p)\right) + (am_0)^2. \tag{2.39}$$

Its denominator $D(p; \zeta, m_0, a)$ vanishes at both doublers of eq. (1.82) and thus violates condition C3 of eq. (2.3). Whether or not the second doubler generates an IR divergence depends on properties of the other contributions to the loop integral. The propagator has the correct continuum limit $S(p; \zeta, m_0, 0) = (\sum_\mu i\gamma^\mu p_\mu + m_0)^{-1}$ in the neighbourhood of its first doubler and can be interpreted as a quark propagator in the limit $a \to 0$. In line with the considerations of [18, 99], the four-momentum p must be expanded around the pole in the neighbourhood of the second doubler as

$$p_\mu = \zeta\frac{\pi}{2a} + q_\mu. \tag{2.40}$$

Expansion of the propagator yields

$$S(q + \frac{\pi}{2a}; \zeta, m_0, a) = a\frac{N'(q; \zeta, m_0, a)}{D'(q; \zeta, m_0, a)} \tag{2.41}$$

with

$$N'(q; \zeta, m_0, a) = -i\sum_\mu \left(\gamma^\mu \zeta c_q^\mu - \zeta\gamma^{\mu\prime}(1 + \zeta s_q^\mu)\right) + am_0$$

$$D'(q; \zeta, m_0, a) = (\zeta c_q)^2 + \zeta^2 \left((\zeta s_q)^2 + 2\zeta(s_q) + 4\right) - \zeta^2 \left(2(c_q) - 2(c_q\zeta s_q) + (c_q)(\zeta s_q)\right) + (am_0)^2$$
$$= \zeta^4(s_q)^2 + \zeta^2 \left((c_q)^2 - 2(c_q) + 4\right) + \zeta^3 \left(2(s_q) + 2(s_q c_q) - (s_q)(c_q)\right) + (am_0)^2. \tag{2.42}$$

Eq. (2.41) does not match a free quark in the limit $a \to 0$:

$$\lim_{a \to 0} S(q + \zeta \frac{\pi}{2a}; \zeta, m_0, a) = \frac{i\zeta^2 \sum_\mu \gamma^{\mu'} q_\mu + m_0}{\zeta^4 \sum_\mu q_\mu^2 + m_0^2}. \tag{2.43}$$

If the poles correspond to degenerate quarks in the limit $a \to 0$, a unitary transformation similar to eq. (1.49 for naïve fermions) must relate the fields. With a similar notation but different matrices $\mathcal{Q}$ and $\mathcal{Q}^\dagger$ that are fixed in eq. (2.45), it is defined as

$$\lim_{q \to 0} \chi(q) \equiv \lim_{q \to 0} \mathcal{Q}\psi(q + \zeta \frac{\pi}{2a}), \quad \lim_{q \to 0} \bar{\chi}(q) \equiv \lim_{q \to 0} \bar{\psi}(q + \zeta \frac{\pi}{2a})\mathcal{Q}^\dagger. \tag{2.44}$$

Therefore, the propagator is transformed by left and right multiplication with the inverse matrices. The shifted propagator of eq. (2.43) can be transformed into a free quark propagator only if $\zeta^2 = 1$. Left and right multiplication of the propagator with

$$\mathcal{Q} = e^{i\vartheta} i\Gamma\gamma^5, \quad \mathcal{Q}^\dagger = e^{-i\vartheta} i\Gamma\gamma^5 = \mathcal{Q}^{-1} \tag{2.45}$$

bring the continuum limit of the shifted propagator in the neighbourhood of the second pole to the original form in the neighbourhood of the first pole. The phase ϑ of the matrix $\mathcal{Q}$ is unrestricted and taken as zero for convenience. The propagator is called $S_\chi(q; \zeta, m_0, a)$ after four-momentum shift and unitary transformation reads

$$S_2(q; \zeta, m_0, a) \equiv \mathcal{Q}^\dagger S(q + \frac{\pi}{2a}; \zeta, m_0, a)\mathcal{Q} \tag{2.46}$$

$$= \frac{a\left(-i\sum_\mu \left(\zeta^2 \gamma^\mu s_q^\mu - \frac{\zeta}{2}\gamma^{\mu'}(\hat{s}_q^\mu)^2\right) + am_0\right)}{\zeta^4 (s_q)^2 + \zeta^2 \left((c_q)^2 - 2(c_q) + 4\right) + \zeta^3 \left(2(s_q) + 2(s_q c_q) - (s_q)(c_q)\right) + (am_0)^2},$$

which satisfies

$$S_\chi(p; \pm 1, m_0, a) = S(p; \mp 1, m_0, a), \tag{2.47}$$

which strongly resembles the corresponding relation for Karsten-Wilczek fermions of eq. (2.33). Moreover, as the Boriçi-Creutz term changes its sign under charge conjugation C, transforming fermion fields with $i^{-n_\Sigma}\mathcal{Q}C$ and $i^{n_\Sigma}\mathcal{Q}C$ (with arbitrary phase ϑ) and gauge fields with C is a local symmetry, where n_Σ is defined in eq. (A.40). The propagator always (with the exception of the limit $a \to 0$) includes both doublers, though $S(p; \zeta, m_0, a)$ and $S\chi(p; \zeta, m_0, a)$ differ by $\mathcal{O}(a)$ effects, which has been already pointed out by Bedaque et al. [18]. Since left and right multiplication of the chirality matrix γ^5 with matrices $\mathcal{Q}$ and $\mathcal{Q}^\dagger$ changes its sign as $\mathcal{Q}^\dagger \gamma^5 \mathcal{Q} = -\gamma^5$, the two doublers always describe fermion modes with opposite chirality in compliance with the No-Go theorem of Nielsen and Ninomiya [121]. The fermion-fermion-gluon vertex reads

$$V_1^\mu(p, q; \zeta, a) = -i\frac{g_0}{2}\left(\gamma^\mu \hat{c}_{p+q}^\mu - \zeta\gamma^{\mu'}\hat{s}_{p+q}^\mu\right) \tag{2.48}$$

and the fermion-fermion-gluon-gluon vertex reads

$$V_2^{\mu\nu}(p, q; \zeta, a) = ia\frac{g_0^2}{4}\delta^{\mu\nu}\left(\gamma^\mu \hat{s}_{p+q}^\mu + \zeta\gamma^{\mu'}\hat{c}_{p+q}^\mu\right), \tag{2.49}$$

where fermionic four-momenta represent incoming fermions and the colour structure is the same as in the previous case (cf. text below eqs. (2.34 and 2.35)).

36

2.3 One-loop corrections

After relevant technical aspects are summarised in section 2.1 and necessary propagators and vertices are derived in section 2.2, the calculation of one-loop corrections for minimally doubled fermions is covered. Fermionic self-energy and the fermionic contribution to the vacuum polarisation are discussed in detail.

2.3.1 Fermionic self-energy

Figure 2.1: The 1-loop contribution to the fermionic self-energy consists of a sunset (left) and a tadpole (right) diagram.

The fermionic self-energy is calculated from the sum of the sunset diagram (left side of figure 2.1) and the tadpole diagram (right side of figure 2.1),

$$I^{ad}(p; \zeta, m_0, a) = I_s^0(p; \zeta, m_0, a) \cdot C_s^{ad} + I_t^0(p; \zeta, m_0, a) \cdot C_t^{ad}. \qquad (2.50)$$

The sunset diagram[2] involves colour indices $a, b, c, d \in \{1, 2, 3\}$ and $e, f \in \{1, \dots, 8\}$ as

$$I_s^0(p; \zeta, m_0, a) \cdot C_s^{ad} = \int_{-\pi/a}^{+\pi/a} \frac{d^4 k}{(2\pi)^4} \sum_{\mu, \nu = 0}^{3} V_1^\mu(p, k) S(k; \zeta, m_0, a) V_1^\nu(k, p)$$

$$\times \sum_{b, c; e, f} (T^e)^{ab} G_{\mu\nu}^{ef}(p - k; 0, a) \delta^{bc} (T^f)^{cd} \qquad (2.51)$$

The tadpole diagram includes a symmetry factor $1/2$,

$$I_t^0(p; \zeta, m_0, a) \cdot C_t^{ad} = \frac{1}{2} \int_{-\pi/a}^{+\pi/a} \frac{d^4 k}{(2\pi)^4} \sum_{\mu, \nu = 0}^{3} V_2^{\mu\nu}(p, p) \sum_{b, c} \left(\frac{1}{3} \delta^{bc} \delta^{ad} + \sum_e d^{bce} (T^e)^{ad} \right) G_{\mu\nu}^{bc}(k; 0, a),$$

$$(2.52)$$

---

[2]Since the gluon propagator of eq. (2.25) is isotropic and relatively simple compared to fermion propagators of eqs. (2.26) and (2.37), the momentum difference $p - k$ is assigned to the gluon propagator.

and involves colour indices $a, d \in \{1, 2, 3\}$ and $b, c, e \in \{1, \ldots, 8\}$. The SU(3) structure is independent of the discretisation and collapses to $C_F \delta^{ad}$ after using eq. (A.12),

$$C_s^{ad} = \sum_{b,c=1}^{3} \sum_{e,f=1}^{8} (T^e)^{ab} \delta^{ef} \delta^{bc} (T^f)^{cd} = \sum_{e=1}^{8} (T^e T^e)^{ad} \qquad = C_F \delta^{ad}, \qquad (2.53)$$

$$C_t^{ad} = \sum_{b,c} \frac{1}{2} \left(\frac{1}{3} \delta^{bc} \delta^{ad} + \sum_{b,c} d^{bce} (T^e)^{ad} \right) = \frac{1}{6} \sum_{e=1}^{8} \delta^{ad} \qquad = C_F \delta^{ad}, \qquad (2.54)$$

which is included into the integrals $I_{s,t}(p; \zeta, m_0, a) = C_F I_{s,t}^0(p; \zeta, m_0, a)$ as

$$I_s(p; \zeta, m_0, a) = C_F \int \frac{d^4 k}{(2\pi)^4} \sum_{\mu,\nu} V_1^\mu(p, -k) S(k; \zeta, m_0, a) V_1^\nu(k, -p) G_{\mu\nu}(p - k; 0, a),$$

$$(2.55)$$

$$I_t(p; \zeta, 0, a) = C_F \int \frac{d^4 k}{(2\pi)^4} \sum_{\mu,\nu} V_2^{\mu\nu}(p, p) G_{\mu\nu}(k; 0, a) \equiv I_t(p; \zeta, a). \qquad (2.56)$$

Tadpole diagram

Without internal fermions in the tadpole diagram, there is no problem with condition C3 of eq. (2.3). Mass regularisation is not required, since the superficial degree of divergence is negative, deg $I_t = -1$. Any ξ dependence of a power divergence must cancel exactly with the sunset diagram. For Karsten-Wilczek fermions, the tadpole diagram reads

$$I_t(p; \zeta, a) = ia^3 \frac{g_0^2 C_F}{4} \int \frac{d^4 k}{(2\pi)^4} \sum_{\mu,\nu} \delta^{\mu\nu} \left(\frac{\left(\gamma^\mu \hat{s}_{2p}^\mu - \zeta \gamma^{\underline{\alpha}} \varrho^{\alpha\mu} \hat{c}_{2p}^\mu \right)}{\left(\hat{s}_k \right)^2} \right.$$

$$\left. - (1 - \xi)(\hat{s}_k^\mu \hat{s}_k^\nu) \frac{\left(\gamma^\mu \hat{s}_{2p}^\mu - \zeta \gamma^{\underline{\alpha}} \varrho^{\alpha\mu} \hat{c}_{2p}^\mu \right)}{\left(\hat{s}_k \right)^2 \left(\hat{s}_k \right)^2} \right), \qquad (2.57)$$

which is simplified algebraically to (terms that vanish for $a \to 0$ have been dropped)

$$I_t(p; \zeta, a) = ia \frac{g_0^2 C_F}{2} \left(a\gamma \cdot p - 3\zeta \gamma^{\underline{\alpha}} \right) \left(1 - \frac{(1 - \xi)}{4} \right) \int \frac{d^4 k}{(2\pi)^4} \frac{1}{\left(\hat{s}_k \right)^2}. \qquad (2.58)$$

The loop integral is identical to eq. (2.10) and the tadpole contribution reads

$$I_t(p; \zeta, a) = \frac{g_0^2 C_F Z_0}{2} \left(1 - \frac{(1 - \xi)}{4} \right) \left(i\gamma \cdot p - i \frac{3\zeta}{a} \gamma^{\underline{\alpha}} \right). \qquad (2.59)$$

For Boriçi-Creutz fermions, the tadpole diagram reads

$$I_t(p; \zeta, a) = ia^3 \frac{g_0^2 C_F}{4} \int \frac{d^4 k}{(2\pi)^4} \sum_{\mu,\nu} (\delta^{\mu\nu}) \left(\frac{\left(\gamma^\mu \hat{s}_{2p}^\mu + \zeta \gamma^{\mu\prime} \hat{c}_{2p}^\mu \right)}{\left(\hat{s}_k \right)^2} \right.$$

$$\left. - (1 - \xi)(\hat{s}_k^\mu \hat{s}_k^\nu) \frac{\left(\gamma^\mu \hat{s}_{2p}^\mu + \zeta \gamma^{\mu\prime} \hat{c}_{2p}^\mu \right)}{\left(\hat{s}_k \right)^2 \left(\hat{s}_k \right)^2} \right), \qquad (2.60)$$

which is simplified algebraically to (terms that vanish for $a \to 0$ have been dropped)

$$I_t(p; \zeta, a) = ia\frac{g_0^2 C_F}{2}\left(a\gamma \cdot p + 2\zeta\Gamma\right)\left(1 - \frac{(1-\xi)}{4}\right)\int \frac{d^4k}{(2\pi)^4}\frac{1}{(\hat{s}_k)^2}. \tag{2.61}$$

Again, the loop integral is identical to eq. (2.10) and the tadpole contribution reads

$$I_t(p; \zeta, a) = \frac{g_0^2 C_F Z_0}{2}\left(1 - \frac{(1-\xi)}{4}\right)\left(i\gamma \cdot p + i\frac{2\zeta}{a}\Gamma\right). \tag{2.62}$$

Sunset diagram

The integral $I_s(p; \zeta, m_0, a)$ of the sunset diagram is split into two pieces, the lattice integral $J(p, m_0; \zeta, M, a)$, and the continuum integral $I_s(p; \zeta, m_0, a) - J(p, m_0; \zeta, M, a)$. The external momenta p and the mass m_0 are treated as small and the integral $J(p, m_0; \zeta, M, a)$ is subjected to a Taylor expansion in p and m_0,

$$J(p, m_0; \zeta, M, a) = \sum_\chi i\gamma^\chi J_3^\chi(\zeta, a) + \sum_{\chi, \theta} i\gamma^\chi p_\theta J_4^{\theta\chi}(\zeta, M, a) + m_0 J_m(\zeta, M, a) \tag{2.63}$$

$$J_3^\chi(\zeta, 0, a) = \int\sum \text{tr}\left\{\gamma^\chi V_1^\mu(0, k)S(k; \zeta, 0, a)V_1^\nu(k, 0)G_{\mu\nu}(-k; 0, a)\right\}, \tag{2.64}$$

$$J_4^{\theta\chi}(\zeta, M, a) = \int\sum \text{tr}\left\{\gamma^\chi \frac{\partial\left\{V_1^\mu(p, k)S(k; \zeta, 0, a)V_1^\nu(k, p)G_{\mu\nu}(p - k; 0, a)\right\}}{\partial p_\theta}\right\}_{p=0}, \tag{2.65}$$

$$J_m(\zeta, M, a) = m_0\int\sum \text{tr}\left\{\frac{\partial\left\{V_1^\mu(0, k)S(k; \zeta, m_0, a)V_1^\nu(k, 0)G_{\mu\nu}(-k; 0, a)\right\}}{\partial m_0}\right\}_{m_0=0}. \tag{2.66}$$

Each self-energy integral in eqs. (2.64), (2.65) and (2.66) is integrated and summed as

$$\int\sum \text{tr}\left(\ldots\right) \equiv \int\limits_{-\pi/a}^{+\pi/a}\frac{d^4k}{(2\pi)^4}\sum_{\mu, \nu}\frac{1}{4}\text{tr}\left(\ldots\right). \tag{2.67}$$

$J_4^{\theta\chi}(\zeta, M, a)$ and $J_m(\zeta, M, a)$ are regularised in the IR with a small mass term M^2 in each denominator. The indices θ of the Taylor expansion in p and χ of the projection to Dirac matrices may differ, since the anisotropy of the fermion action allows for the persistence of complicated combinations of indices in the continuum limit.

Karsten-Wilczek fermions

For Karsten-Wilczek fermions, the power divergent integral $J_3(\zeta, a)$ reads

$$J_3(\zeta, a) = \sum_\chi i\gamma^\chi J_3^\chi(\zeta, a),$$

$$J_3^\chi(\zeta, a) = a^3\frac{g_0^2 C_F}{4}\int\sum \text{tr}\left\{\gamma^\chi\left(\gamma^\mu \hat{c}_k^\mu + \zeta\gamma^{\underline{\alpha}}\varrho^{\alpha\mu}\hat{s}_k^\mu\right)\left((\gamma \cdot s_k) + \frac{\zeta}{2}\gamma_{\underline{\alpha}}(\hat{s}_k)_\perp^2\right)\right.$$

$$\left. \times\, (\gamma^\nu \hat{c}_k^\nu + \zeta\gamma^{\underline{\alpha}}\varrho^{\alpha\nu}\hat{s}_k^\nu)\right\}\frac{\delta^{\mu\nu} - (1-\xi)\frac{\hat{s}_{-k}^\mu \hat{s}_{-k}^\nu}{D^g(-k; 0, a)}}{D^{KW}(k; \zeta, 0, a)D^g(-k; 0, a)}. \tag{2.68}$$

The fermion propagator has two separate divergences at the poles of eq. (1.62). However, the gluon denominator vanishes only at the standard pole. Thus, the superficial degree of divergence is deg $I_1 = -1$ at the first pole. Since deg $I_2 = 1$ at the second pole, it does not contribute to the divergence of the integral. Even though condition C3 of eq. (2.3) is not met by all propagators, there is no extra divergence and the power counting theorem of Reisz is applicable. Due to the negative degree of divergence, IR regularisation is not needed. The integral of eq. (2.68) is split into a Feynman gauge part ($\mathcal{J}_0 = J_3^\chi|_{\xi=1}$) and a gauge fixing part ($\mathcal{J}_1 = (\xi - 1)(\partial J_3^\chi/\partial\xi)$), which is the rest of eq. (2.68). Numerators N_0 of $\mathcal{J}_0$ and N_1 of $\mathcal{J}_1$ are simplified algebraically to eqs. (B.7) and (B.8). Since only $k_{\underline{\alpha}}$ contributes to the denominator as an odd power, odd powers of other Euclidean components of k in the numerators N_0 and N_1 are integrated to zero. Hence, symmetry restricts the power divergence to the $\gamma^{\underline{\alpha}}$-component. Numerators collapse to

$$N_0 = \delta^{\chi\underline{\alpha}}\left\{ \left(s_k^{\underline{\alpha}} + \frac{\zeta}{2}(\hat{s}_k)_\perp^2\right)\left((\hat{c}_k^{\underline{\alpha}})^2 - (\hat{c}_k)_\perp^2 + \zeta^2(\hat{s}_k)_\perp^2\right) + 4\zeta(s_k)_\perp^2\right\}, \qquad (2.69)$$

$$N_1 = \delta^{\chi\underline{\alpha}}\left\{ s_k^{\underline{\alpha}}\left(4(s_k)^2 + 3\zeta^2\left((\hat{s}_k)_\perp^2\right)^2\right) + \zeta(\hat{s}_k)_\perp^2\left(4\left(s_k^{\underline{\alpha}}\right)^2 + 2(s_k)^2 + \frac{\zeta^2}{2}\left((\hat{s}_k)_\perp^2\right)^2\right)\right\}. \qquad (2.70)$$

It is noteworthy that the numerators contain only terms which are even in $k^{\underline{\alpha}}$ and odd in ζ and vice versa, whereas the denominators add even powers of $k^{\underline{\alpha}}$ and ζ to odd powers of both. Thus, the overall contribution from J_3^χ to c_{1L} is necessarily an odd function[3] of ζ. The final form of the power divergent integral $J_3^\chi(\zeta, a)$ reads

$$J_3^\chi(\zeta, a) = ia^3\frac{g_0^2 C_F}{4}\delta^{\chi\underline{\alpha}}\int\frac{d^4k}{(2\pi)^4}\frac{N_0 - (1-\xi)\frac{N_1}{D^g(-k;0,1)}}{D^{KW}(k;\zeta,0,1)D^g(-k;0,1)}. \qquad (2.71)$$

It is evaluated numerically for $\zeta = +1$ after rescaling (cf. eq. (2.9)) and yields

$$J_3(+1, a) = \frac{i}{a}\gamma^{\underline{\alpha}}\frac{g_0^2 C_F}{16\pi^2}\left(7.166866 - 9.17479(1-\xi)\right). \qquad (2.72)$$

Mass renormalisation is due to the integral $J_m(\zeta, M, a)$ of eq. (2.66), which reads

$$J_{m_0}(m_0; \zeta, M, a) = m_0 J_m(\zeta, M, a),$$

$$J_m(\zeta, M, a) = a^4\frac{g_0^2 C_F}{4}\int\sum\mathrm{tr}\left\{(\gamma^\mu\hat{c}_k^\mu + \zeta\gamma^{\underline{\alpha}}\varrho^{\underline{\alpha}\mu}\hat{s}_k^\mu)(\gamma^\nu\hat{c}_k^\nu + \zeta\gamma^{\underline{\alpha}}\varrho^{\underline{\alpha}\nu}\hat{s}_k^\nu)\right\}$$

$$\times\frac{\delta^{\mu\nu} - (1-\xi)\frac{\hat{s}_{-k}^\mu\hat{s}_{-k}^\nu}{D^g(-k;M,a)}}{D^{KW}(k;\zeta,M,a)D^g(-k;M,a)} \qquad (2.73)$$

for Karsten-Wilczek fermions. The fermion propagator has two separate divergences at the poles of eq. (1.62). However, the gluon denominator vanishes only at the standard

---

[3]The contribution to c_{1L} from the tadpole in eq. (2.59) is directly proportional to ζ.

40

pole. Thus, the superficial degree of divergence is deg $I_1 = 0$ at the first pole. Since deg $I_2 = 2$ at the second pole, it does not contribute to the logarithmic divergence of the integral. Though the condition C3 of eq. (2.3) is not met by all propagators, there is no extra divergence and the power counting theorem of Reisz is applicable. Eq. (2.73) is split into Feynman gauge ($\mathcal{J}_2 = J_m|_{\xi=1}$) and gauge fixing ($\mathcal{J}_3 = (\xi - 1)(\partial J_m/\partial \xi)$) parts. Numerators N_2 of $\mathcal{J}_2$ and N_3 of $\mathcal{J}_3$ are simplified algebraically to

$$N_2 = (\hat{c}_k)^2 + \zeta^2 (\hat{s}_k)_\perp^2 \tag{2.74}$$

$$N_3 = 4(s_k)^2 + \zeta^2 \left((\hat{s}_k)_\perp^2\right)^2 + 4\zeta s_k^\alpha (\hat{s}_k)_\perp^2. \tag{2.75}$$

Since N_2 and N_3 contain only terms which are even in k and ζ or odd in k^α and ζ, the one-loop coefficient Σ_2 of the mass renormalisation is an even function of ζ. Thus, the lattice contribution to mass renormalisation reads

$$J_m(\zeta, M, a) = a^4 \frac{g_0^2 C_F}{4} \int \frac{d^4 k}{(2\pi)^4} \frac{N_2 - (1-\xi)\frac{N_3}{D^g(-k;M,a)}}{D^{KW}(k;\zeta,M,a)D^g(-k;M,a)} \tag{2.76}$$

and would still be IR-divergent without M^2 in the denominator. The IR regulator is removed from $J_m(\zeta, M, a)$ by subtracting base integrals $\widetilde{J}_m(M, a)$ such as eq. (2.12) with appropriate prefactors. The difference $J_m(\zeta, M, a) - \widetilde{J}_m(M, a)$ is IR-finite for any M^2 by construction. It is evaluated for $\zeta = +1$ after rescaling (cf. eq. (2.9)) and removing the IR regulator,

$$J_m(+1, 0, a) - \widetilde{J}_m(0, a) = \frac{g_0^2 C_F}{16\pi^2}(-1.200712). \tag{2.77}$$

Next, the IR regularised base integrals with the necessary prefactors,

$$\begin{aligned}\widetilde{J}_m(M, a) &\equiv g_0^2 C_F \cdot 4\left(\mathcal{B}(2) - (1-\xi)\mathcal{B}(3;1)\right) \\ &= g_0^2 C_F \left(-15.168038 + 4\log(aM)^2 + (1-\xi)\left(3.292010 - \log(aM)^2\right)\right),\end{aligned} \tag{2.78}$$

are added to the finite integral to obtain the complete IR regularised lattice integral,

$$\begin{aligned}J_{m_0}(m_0; +1, M, a) = m_0 \frac{g_0^2 C_F}{16\pi^2}\Big\{&4\log(aM)^2 - 16.36875 \\ &+ (1-\xi)\left(-\log(aM)^2 + 3.292010\right)\Big\}.\end{aligned} \tag{2.79}$$

Lastly, wavefunction renormalisation is the most laborious part of the self-energy's calculation. It is due to the integral $J_4(p; \zeta, M, a)$ of eq. (2.65), which reads

$$J_4(p; \zeta, M, a) = \sum_{\theta,\chi} i\gamma^\chi p_\theta J_4^{\theta\chi}(\zeta, M, a),$$

$$J_4^{\theta\chi}(\zeta, M, a) = a^4 \frac{g_0^2 C_F}{4} \int \frac{d^4 k}{(2\pi)^4}\left\{\left(\frac{N_4}{D_4} + \frac{N_5}{D_5}\right) - (1-\xi)\left(\frac{N_6 + N_7}{D_5} + \frac{N_8}{D_6}\right)\right\} \tag{2.80}$$

for Karsten-Wilczek fermions. Denominators D_4 - D_6 and numerators N_4 - N_8 are shown in appendix B.2.1 in eqs. (B.9) - (B.16). Since any pieces of the algebraically simplified numerators of eqs. (B.17) - (B.21) contain only terms which are either even in k and ζ or odd in both, one-loop coefficients Σ_1 and d_{1L} that are obtained from $J_4^{\theta\chi}(\zeta, M, a)$ are even functions[4] of ζ. Since odd momenta in the denominator are restricted to $k^{\underline{\alpha}}$, any odd powers of momenta k^θ and k^χ contribute only to the integral if the indices θ and χ are matched with each other or with $\underline{\alpha}$. This last stage of algebraic simplification of the numerators requires equality of the indices θ and χ:

$$N_4 = -\delta^{\theta\chi}\left\{(s_k^\theta)^2\left[2 - \zeta^2\left(\delta^{\theta\underline{\alpha}} - \varrho^{\theta\underline{\alpha}}(1 + (\hat{s}_k)_\perp^2)\right)\right] - \zeta s_k^{\underline{\alpha}}\left[\varrho^{\theta\underline{\alpha}}(\hat{c}_k^\theta)^2 - \delta^{\theta\underline{\alpha}}(\hat{s}_k)_\perp^2\right]\right\}, \qquad (2.81)$$

$$N_5 = -\delta^{\theta\chi}\left\{2(s_k^\theta)^2\left[(\hat{c}_k)^2 - 2(\hat{c}_k^\theta)^2 - \zeta^2\delta^{\theta\underline{\alpha}}(\hat{s}_k)_\perp^2\right]\right.$$
$$\left. + \zeta s_k^{\underline{\alpha}}\left[8(s_k^\theta)^2 + \delta^{\theta\underline{\alpha}}\left(8\left((s_k)_\perp^2 - (s_k^{\underline{\alpha}})^2\right) + (\hat{s}_k)_\perp^2\left((\hat{c}_k^{\underline{\alpha}})^2 - (\hat{c}_k)_\perp^2 + \zeta^2((\hat{s})_\perp^2)\right)\right)\right]\right\}, \qquad (2.82)$$

$$N_6 = -\delta^{\theta\chi}\left\{2(\hat{s}_k^\theta)^2\left[(s_k)^2 - \zeta^2(\hat{s}_k)_\perp^2\left(\varrho^{\theta\underline{\alpha}} - \frac{(\hat{s}_k)_\perp^2}{2}\right)\right] + \zeta s_k^{\underline{\alpha}}(\hat{s}_k)_\perp^2\left[3(\hat{s}_k^\theta)^2 - \zeta^2\delta^{\theta\underline{\alpha}}(\hat{s}_k)_\perp^2\right]\right\}, \qquad (2.83)$$

$$N_7 = -\delta^{\theta\chi}\left\{2\left[(\hat{c}_k^\theta)^2\left((s_k)^2 + \zeta^2((\hat{s}_k)_\perp^2)^2\right) + \left(2 - \delta^{\theta\underline{\alpha}}\right)\zeta^2(s_k^\theta)^2(\hat{s})_\perp^2\right] + 2\zeta s_k^{\underline{\alpha}}(\hat{c}_k^\theta)^2(\hat{s}_k)_\perp^2\right\}, \quad (2.84)$$

$$N_8 = -\delta^{\theta\chi}4\left\{(s_k^\theta)^2\left[4(s)^2 + \zeta^2\left(2\delta^{\theta\underline{\alpha}} + 1\right)((\hat{s}_k)_\perp^2)^2\right] + \zeta s_k^{\underline{\alpha}}(\hat{s}_k)_\perp^2\left[4(s_k^\theta)^2 + \delta^{\theta\underline{\alpha}}\frac{8 - \zeta^2((\hat{s}_k)_\perp^2)^2}{4}\right]\right\}. \qquad (2.85)$$

After the simplified numerators are obtained, the superficial degree of divergence is calculated as deg $I_1 = 0$ at the first pole. Since deg $I_2 = 2$ at the second pole, it does not contribute to the divergence of the integral. Though condition C3 of eq. (2.3) is not fulfilled by all propagators, there is no extra divergence and the power counting theorem of Reisz is applicable. Since ratios N_4/D_4 and N_6/D_5 are due to discretisation effects, they do not contribute to the superficial degree of divergence. Moreover, any structure proportional to $\delta^{\theta\underline{\alpha}}$ or $\varrho^{\theta\underline{\alpha}}$ is either multiplied by ζ^2 or by $\zeta s_k^{\underline{\alpha}}$. The latter must combine with $\zeta s_k^{\underline{\alpha}}$ in the fermionic denominator. Hence, the coefficient d_{1L} of the anisotropic dimension-four counterterm is entirely due to even powers of ζ. The integral $J_4^{\theta\chi}(\zeta, M, a)$ has three divergent pieces, which require IR regularisation with a mass M^2 in all denominators. The IR regulator is removed from $J_4^{\chi\theta}(\zeta, M, a)$ by subtracting base integrals $\widetilde{J}_4^{\chi\theta}(M, a)$ of the form of eq. (2.14) with appropriate prefactors. The difference $J_4^{\chi\theta}(\zeta, M, a) - \widetilde{J}_4^{\chi\theta}(M, a)$ is IR-finite for any M^2 by construction. It is evaluated for $\zeta = +1$ after rescaling (cf. eq. (2.9)) and removing the IR regulator,

$$J_4^{\theta\chi}(+1, 0, a) - \widetilde{J}_4^{\theta\chi}(0, a) = \frac{g_0^2 C_F}{16\pi^2}\delta^{\theta\chi}\left(2.29985 - 0.12554\,\delta^{\theta\underline{\alpha}} + (1 - \xi)\,(2.558262)\right). \qquad (2.86)$$

---

[4]The 1-loop contribution to Σ_1 from the tadpole diagram is independent of ζ. Since Σ_1 receives a contribution from a continuum integral without any ζ dependence, it cannot be an odd function of ζ.

Next, the IR regularised base integrals with the necessary prefactors,

$$
\begin{aligned}
\widetilde{J}_4^{\theta\chi}(M,a) =\ & g_0^2 C_F \delta^{\theta\chi} \cdot 4 \left(\mathcal{B}(3,1) + (1-\xi)\cdot 2\left(\mathcal{B}(3,1) - \mathcal{B}(4,2) - 3\mathcal{B}(3,1,1)\right)\right) \\
=\ & \frac{g_0^2 C_F}{16\pi^2} \left(\log{(aM)^2} - 3.292010 + (1-\xi)\left(-\log{(aM)^2} + 3.62534\right)\right),
\end{aligned}
\tag{2.87}
$$

are added to the finite integral to obtain the complete IR regularised lattice integral,

$$
\begin{aligned}
J_4(p;+1,M,a) = \sum_\theta i\gamma^\theta p_\theta \frac{g_0^2 C_F}{16\pi^2} \Big\{ & \log{(aM)^2} - 0.99216 - 0.12554\,\delta^{\theta\underline{\alpha}} \\
& + (1-\xi)\left(-\log{(aM)^2} + 6.350272\right) \Big\}.
\end{aligned}
\tag{2.88}
$$

Boriçi-Creutz fermions

The preceding procedure for Karsten-Wilczek fermions is closely mirrored for Boriçi-Creutz fermions. Since technical details are very similar, individual steps are not repeated here. The superficial degree of divergence is the same for both discretisations. The second divergence of the fermion propagator violates condition C3 of eq. (2.3) without violating the power counting theorem of Reisz due to the presence of the gluon propagator. Mass renormalisation is applied and the subtracted integrals $\widetilde{J}_m(M,a)$ of eq. (2.78) and $\widetilde{J}_4^{\theta\chi}(M,a)$ of eq. (2.87) are identical. For Boriçi-Creutz fermions, the power divergent integral $J_3^\chi(\zeta,a)$ reads

$$
J_3(\zeta,a) = \sum_\chi i\gamma^\chi J_3^\chi(\zeta,a),
$$

$$
\begin{aligned}
J_3^\chi(\zeta,a) = i a^3 \frac{g_0^2 C_F}{4} \int \sum \mathrm{tr}\ \Big\{ & \gamma^\chi \left(\gamma^\mu \hat{c}_k^\mu - \zeta\gamma^{\mu\prime}\hat{s}_k^\mu\right) \sum_\lambda \left(\gamma_\lambda s_p^\lambda - \zeta\gamma_\lambda'(1-c_p^\lambda)\right) \\
& \times \left(\gamma^\nu \hat{c}_k^\nu - \zeta\gamma^{\nu\prime}\hat{s}_k^\nu\right) \Big\} \frac{\delta^{\mu\nu} - (1-\xi)\frac{\hat{s}_{-k}^\mu \hat{s}_{-k}^\nu}{D^g(-k;0,a)}}{D^{BC}(k;\zeta,0,a)D^g(-k;0,a)}.
\end{aligned}
\tag{2.89}
$$

The algebra is presented in appendix B.2.2. $\zeta = +1$ is fixed and $J_3^\chi(+1,a)$ reads

$$
J_3(+1,a) = \frac{i}{a} \sum_\chi \left(\frac{1}{2}\gamma^\chi\right) \frac{g_0^2 C_F}{16\pi^2} \left(5.07558 + 6.11653(1-\xi)\right).
\tag{2.90}
$$

Due to the different anisotropic Dirac structure, there is no Kronecker symbol for Euclidean indices here. The combination $\sum_\chi \left(\frac{1}{2}\gamma^\chi\right) = \Gamma$ is the matrix of eq. (1.72). Mass renormalisation is calculated from $J_{m_0}(m_0;\zeta,M,a)$ of eq. (2.66) in the same way as for Karsten-Wilczek fermions. For Boriçi-Creutz fermions, the integral reads

$$
J_m(\zeta,M,a) = a^4 \frac{g_0^2 C_F}{4} \int \sum \mathrm{tr}\ \left\{(\gamma^\mu \hat{c}_k^\mu - \zeta\gamma^{\mu\prime}\hat{s}_k^\mu)(\gamma^\nu \hat{c}_k^\nu - \zeta\gamma^{\nu\prime}\hat{s}_k^\nu)\right\} \frac{\delta^{\mu\nu} - (1-\xi)\frac{\hat{s}_{-k}^\mu \hat{s}_{-k}^\nu}{D^g(-k;M,a)}}{D^{BC}(k;\zeta,M,a)D^g(-k;M,a)}.
\tag{2.91}
$$

43

The algebra is shown in appendix B.2.2. $\zeta = +1$ is fixed and $J_{m_0}(m_0; +1, M, a)$ reads

$$
\begin{aligned}
J_{m_0}(m_0; +1, M, a) = & m_0 \frac{g_0^2 C_F}{16\pi^2} \Big\{ 4 \log{(aM)^2} - 21.48729 \\
& + (1 - \xi) \Big(-\log{(aM)^2} + 3.292010 \Big) \Big\}.
\end{aligned} \tag{2.92}
$$

Wavefunction renormalisation is due to the integral $J_4(p; \zeta, M, a)$ of eq. (2.65), which is again the hardest part of the self-energy's calculation. The integral $J_4(p; \zeta, M, a)$ reads

$$
J_4(p; \zeta, M, a) = \sum_{\theta, \chi} i\gamma^\chi p_\theta J_4^{\theta\chi}(\zeta, M, a),
$$

$$
J_4^{\theta\chi}(\zeta, M, a) = ia^4 \frac{g_0^2 C_F}{4} \int \frac{d^4 k}{(2\pi)^4} \Big\{ \Big(\frac{N_4}{D_4} + \frac{N_5}{D_5} \Big) - (1 - \xi) \Big(\frac{N_6 + N_7}{D_5} + \frac{N_8}{D_6} \Big) \Big\} \tag{2.93}
$$

for Boriçi-Creutz fermions, where denominators D_4 - D_6 and numerators N_4 - N_8 are presented in appendix B.2.2 in eqs. (B.28) - (B.35). The algebra, which is even more tedious than for Karsten-Wilczek fermions is also shown in appendix B.2.2. $\zeta = +1$ is fixed and $J_4(p; +1, M, a)$ reads

$$
\begin{aligned}
J_4(p; +1, M, a) = & \sum_{\theta\chi} i\gamma^\chi p_\theta \frac{g_0^2 C_F}{16\pi^2} \Big(\delta^{\theta\chi} \Big\{ \log{(aM)^2} - 3.42642 \Big\} + \frac{1}{2} \cdot 1.52766 \\
& + \delta^{\theta\chi}(1 - \xi) \Big(-\log{(aM)^2} + 6.350272 \Big) \Big\}.
\end{aligned} \tag{2.94}
$$

Continuum integral

The continuum integral $I(p; \zeta, m_0, 0) - J(p, m_0; \zeta, M, 0)$ is independent of discretisations:

$$
K(p, m_0; M) = I(p; 0, m_0, 0) - \lim_{M^2 \to 0} J(p, m_0; 0, M, 0). \tag{2.95}
$$

Even though $K(p, m_0; M)$ is already UV finite and IR regularised, it is easily evaluated using dimensional regularisation. The associated additional scale $\mathcal{M}$ cancels between I and J. The external four-momentum p contributes only in the gluon propagator,

$$
G_{\mu\nu}(p - k; 0) = \frac{1}{(p - k)^2 + M^2} \Big(\delta^{\mu\nu} - (1 - \xi) \Big(\frac{(p - k)^\mu (p - k)^\nu}{(p - k)^2} \Big) \Big), \tag{2.96}
$$

and the continuum integral reads

$$
\begin{aligned}
K(p, m_0; M) = & -g_0^2 C_F \Bigg(\int\limits_{-\infty}^{+\infty} \frac{d^d k}{(2\pi)^d} \mathcal{M}^{4-d} \sum_{\mu, \nu} \Big(\gamma^\mu \frac{\sum_\lambda -i\gamma^\lambda k_\lambda + m_0}{k^2} \gamma^\nu \Big) G_{\mu\nu}(p - k) \\
& + \int\limits_{-\infty}^{+\infty} \frac{d^d k}{(2\pi)^d} \mathcal{M}^{4-d} \sum_{\mu, \nu} \Big(\gamma^\mu \frac{\sum_\lambda -i\gamma^\lambda k_\lambda}{k^2 + M^2} \gamma^\nu \Big) \sum_\theta p_\theta \Big(\frac{\partial G_{\mu\nu}(p - k; M)}{\partial p_\theta} \Big)_{p=0} \\
& + \int\limits_{-\infty}^{+\infty} \frac{d^d k}{(2\pi)^d} \mathcal{M}^{4-d} \sum_{\mu, \nu} \Big(\gamma^\mu \frac{m_0}{k^2 + M^2} \gamma^\nu \Big) G_{\mu\nu}(k; M) \Bigg).
\end{aligned} \tag{2.97}
$$

$K(p, m_0; M)$ is evaluated to

$$K(p, m_0; M) = \frac{g_0^2 C_F}{16\pi^2} \left\{ i\gamma \cdot p \left(\log \frac{p^2}{M^2} - 2 - (1 - \xi) \left(\log \frac{p^2}{M^2} - \frac{5}{3} \right) \right) \right.$$

$$\left. + m_0 \left(4 \left(\log \left(\frac{p^2}{M^2} \right) - 2 \right) - (1 - \xi) \left(\log \left(\frac{p^2}{M^2} \right) - \frac{5}{2} \right) \right) \right\}. \qquad (2.98)$$

Full self-energy

With the calculation of the continuum integral, all pieces of the LPT self-energy calculation are completed. The full fermionic self-energy of Karsten-Wilczek fermions is the sum of eqs. (2.59), (2.72), (2.79), (2.88) and (2.98) and reads

$$\Sigma(p, m_0) = i\gamma \cdot p \Sigma_1(p) + m_0 \Sigma_2(p) + \frac{i}{a} \gamma^{\underline{\alpha}} c_{1L}(g_0) + i\gamma^{\underline{\alpha}} p_{\underline{\alpha}} d_{1L}(g_0), \qquad (2.99)$$

where the one-loop coefficients are given by

$$\Sigma_1(p) = \frac{g_0^2 C_F}{16\pi^2} \left\{ \log{(ap)^2} + 9.24089 + (1 - \xi) \left(-\log{(ap)^2} + 4.792010 \right) \right\}, \qquad (2.100)$$

$$\Sigma_2(p) = \frac{g_0^2 C_F}{16\pi^2} \left\{ 4\log{(ap)^2} - 24.36875 + (1 - \xi) \left(-\log{(ap)^2} + 5.792010 \right) \right\}, \qquad (2.101)$$

$$c_{1L}(g_0) = \frac{g_0^2 C_F}{16\pi^2} \cdot (-29.53228), \qquad (2.102)$$

$$d_{1L}(g_0) = \frac{g_0^2 C_F}{16\pi^2} \cdot (-0.12554). \qquad (2.103)$$

With the inclusion of fermionic counterterms of eqs. (1.66) and (1.67), the one-loop propagator for Karsten-Wilczek fermions reads

$$\frac{1}{i\not{p} + m_0} + \frac{1}{i\not{p} + m_0} \left\{ i\not{p}\Sigma_1 + m_0\Sigma_2 + \frac{i}{a}\gamma^{\underline{\alpha}}(c_{1L} - c) + i\gamma^{\underline{\alpha}}p_{\underline{\alpha}}(d_{1L} - d) \right\} \frac{1}{i\not{p} + m_0}$$

$$= \frac{1}{i\not{p}(1 - \Sigma_1) + m_0(1 - \Sigma_2) + \frac{i}{a}\gamma^{\underline{\alpha}}(c - c_{1L}) + i\gamma^{\underline{\alpha}}p_{\underline{\alpha}}(d - d_{1L})}. \qquad (2.104)$$

Once the coefficients of the counterterms are set to

$$c(g_0) = c_{1L}(g_0) + \mathcal{O}(g_0^4), \qquad (2.105)$$

$$d(g_0) = d_{1L}(g_0) + \mathcal{O}(g_0^4), \qquad (2.106)$$

the anisotropy is completely removed from the renormalised propagator at one-loop level,

$$\Sigma(p, m_0) = \frac{Z_2}{i\not{p} + Z_m m_0}, \qquad (2.107)$$

45

which has standard form. Wavefunction (Z_2) and mass (Z_m) renormalisation factors are

$$Z_2 = (1 - \Sigma_1)^{-1}, \tag{2.108}$$

$$Z_m = 1 - (\Sigma_2 - \Sigma_1). \tag{2.109}$$

The full fermionic self-energy of Boriçi-Creutz fermions has different anisotropic terms but an analogous structure,

$$\Sigma(p, m_0) = i\gamma \cdot p\, \Sigma_1(p) + m_0 \Sigma_2(p) + \frac{i}{a}\Gamma c_{1L}(g_0) + i\Gamma \sum_\mu p_\mu d_{1L}(g_0), \tag{2.110}$$

where the one-loop coefficients are given by

$$\Sigma_1(p) = \frac{g_0^2 C_F}{16\pi^2}\left\{ \log (ap)^2 + 6.80663 + (1 - \xi)\left(-\log (ap)^2 + 4.792010\right)\right\}, \tag{2.111}$$

$$\Sigma_2(p) = \frac{g_0^2 C_F}{16\pi^2}\left\{ 4\log (ap)^2 - 29.48729 + (1 - \xi)\left(-\log (ap)^2 + 5.792010\right)\right\}, \tag{2.112}$$

$$c_{1L}(g_0) = \frac{g_0^2 C_F}{16\pi^2} \cdot (+29.54170), \tag{2.113}$$

$$d_{1L}(g_0) = \frac{g_0^2 C_F}{16\pi^2} \cdot (+1.52766). \tag{2.114}$$

Once fermionic counterterms of eqs. (1.86) and (1.87) with coefficients

$$c(g_0) = c_{1L}(g_0) + \mathcal{O}(g_0^4), \tag{2.115}$$

$$d(g_0) = d_{1L}(g_0) + \mathcal{O}(g_0^4) \tag{2.116}$$

are included, the Boriçi-Creutz fermion propagator recovers its isotropy and takes the standard form of eq. (2.107) with Z_2 and Z_m given by eqs. (2.108) and (2.109) using coefficients Σ_1 and Σ_2 of eqs. (2.111) and (2.112).

Both fermionic self-energies share the same gauge-fixing contributions proportional to $(1 - \xi)$. This is necessarily true for all lattice fermions due to gauge invariance. As a consequence, the anisotropic terms proportional to $(1 - \xi)$ must invariably cancel between tadpole and sunset diagrams. Coefficients of dimension-three counterterms are very similar but have different sign. This seems natural since the on-site pieces of Karsten-Wilczek term in eq. (1.61) and of Boriçi-Creutz term in eq. (1.71) have opposite sign. In contrast, the smallness of the coefficient of the dimension four counterterm of the Karsten-Wilczek action is not thoroughly understood at present.

2.3.2 Local bilinears and symmetry currents

Renormalisation factors for local fermionic bilinears are required for many applications. They are computed by evaluating the vertex diagram (a) of figure 2.2 and adding the self-energy contribution for the legs of figure 2.3. Because both fermion actions preserve chiral
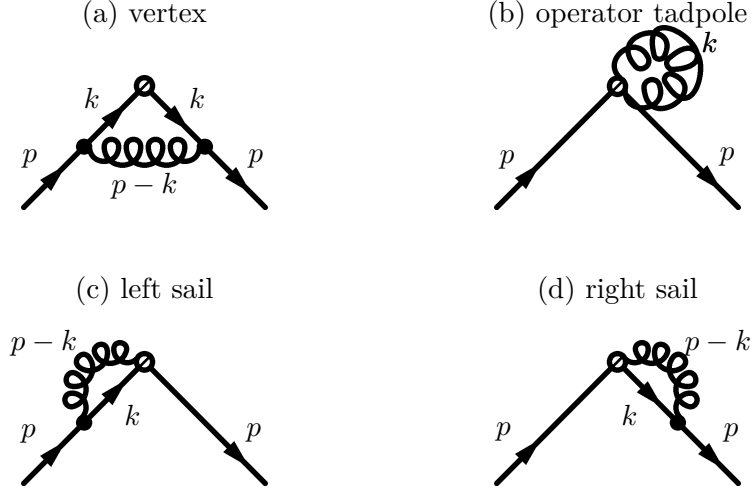
Figure 2.2: Four diagrams are required for the proper vertex renormalisation of the symmetry currents. Merely the vertex diagram (a) is suffcient for local bilinears.

symmetry, they each have identical scalar and pseudoscalar renormalisation factors. Moreover, vector and axial-vector renormalisation factors are identical due to chiral symmetry for each action. These local currents undergo anisotropic mixing, which is not absorbed by the counterterms of their actions. The tensor current, however, does not have anisotropic contributions. One-loop results for local currents are presented as a summary. Symmetry currents are covered in more detail. They are constructed using infinitesimal vector and axial transformations, which yield point-split current operators. In the chiral limit, the point-split axial-vector current is conserved as well. The symmetry currents further require contributions from two sails ((c) and (d)) and from the operator tadpole (b) of figure 2.2. The sum of these proper contributions exactly cancels the self-energy contribution from the legs of figure 2.3. Therefore, the renormalisation constant is exactly one before any counterterms are included.

Karsten-Wilczek fermions

Vertex corrections for insertion of scalar or pseudoscalar densities are equal: $\Lambda_P = \Lambda_S \gamma^5$. The vertex correction of the scalar density equals $-\Sigma_2(p)$ of eq. (2.101) and reads

$$\Lambda_S = \frac{g_0^2 C_F}{16\pi^2} \left(-4 \log (ap)^2 + 24.36875 + (1 - \xi) \left(\log (ap)^2 - 5.792010 \right) \right) \qquad (2.117)$$

Thus, the renormalisation factor of the pseudoscalar density,

$$Z_P = 1 - (\Lambda_P + \Sigma_1), \qquad (2.118)$$

is the inverse of the mass renormalisation factor Z_m of eq. (2.109). Local vector and axial currents undergo anisotropic renormalisation. The vertex correction to the local

47

(e) left leg sunset

(f) left leg tadpole

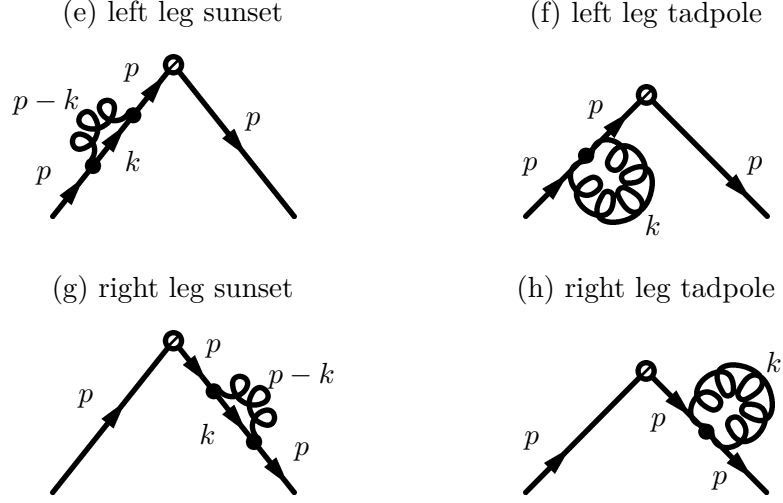(g) right leg sunset

(h) right leg tadpole

Figure 2.3: Renormalisation of the legs contributes four further diagrams to the renormalisation of local bilinears and symmetry currents.

vector current reads

$$\Lambda_V^\mu = \frac{g_0^2 C_F}{16\pi^2} \cdot \gamma^\mu \left(-\log\left(ap\right)^2 + 10.44610 - 2.88914 \cdot \delta^{\mu\underline{\alpha}} + (1-\xi)\left(\log\left(ap\right)^2 - 4.792010\right) \right) \tag{2.119}$$

and the vertex correction to the axial current is obtained as $\Lambda_A^\mu = \Lambda_V^\mu \gamma^5$. Finally, the tensor current does not undergo anisotropic renormalisation and reads

$$\Lambda_T^{\mu\nu} = \frac{g_0^2 C_F}{16\pi^2} \sigma^{\mu\nu} \left(4.17551 + (1-\xi)\left(L - 3.792010\right) \right). \tag{2.120}$$

Symmetry currents are constructed by applying infinitesimal vector and axial transformations to the fermion fields in the action,

$$\begin{array}{llll} \delta_V \psi_n &=& i\alpha_n^V \psi_n, & \delta_V \bar\psi_n &=& -i\alpha_n^V \bar\psi_n, \\ \delta_A \psi_n &=& i\alpha_n^A \gamma^5 \psi_n, & \delta_A \bar\psi_n &=& +i\alpha_n^A \bar\psi_n \gamma^5, \end{array} \tag{2.121}$$

which yield point-split symmetry currents

$$V_n^\mu = \bar\psi_n \frac{\gamma^\mu(1 + d\delta^{\mu\underline\alpha}) - i\zeta\gamma^{\underline\alpha}\varrho^{\alpha\mu}}{2} U_n^\mu \psi_{n+\hat e_\mu} + \bar\psi_{n+\hat e_\mu} \frac{\gamma^\mu(1 + d\delta^{\mu\underline\alpha}) + i\zeta\gamma^{\underline\alpha}\varrho^{\alpha\mu}}{2} U_n^{\mu\dagger} \psi_n, \tag{2.122}$$

$$A_n^\mu = \bar\psi_n \frac{\gamma^\mu(1 + d\delta^{\mu\underline\alpha}) - i\zeta\gamma^{\underline\alpha}\varrho^{\alpha\mu}}{2} \gamma^5 U_n^\mu \psi_{n+\hat e_\mu} + \bar\psi_{n+\hat e_\mu} \frac{\gamma^\mu(1 + d\delta^{\mu\underline\alpha}) + i\zeta\gamma^{\underline\alpha}\varrho^{\alpha\mu}}{2} \gamma^5 U_n^{\mu\dagger} \psi_n. \tag{2.123}$$

Whereas the vector transformation $\delta_V \psi_n$ commutes with the matrices $\mathcal{Q}$ and $\mathcal{Q}^\dagger$ of eq. (2.31), the axial transformation anticommutes with $\mathcal{Q}$ and $\mathcal{Q}^\dagger$,

$$\gamma^5 \mathcal{Q} = -\mathcal{Q}\gamma^5, \quad \mathcal{Q}^\dagger \gamma^5 = -\gamma^5 \mathcal{Q}^\dagger. \tag{2.124}$$

48

The axial transformation produces a current which has opposite sign for both doublers [5]. Only the vector symmetry current of eq. (2.122) is covered in detail here, since the axial current of eq. (2.123), which is a symmetry current in the chiral limit, is treated identically. Evaluation of the vertex correction, the two sails and the operator tadpole of figure 2.2 yields the proper one-loop contribution to the vector symmetry current

$$\frac{g_0^2 C_F}{16\pi^2} \gamma^\mu \left(-\log(ap)^2 - 9.24089 + 0.12554 \cdot \delta^{\mu\underline{\alpha}} + (1 - \xi)\left(\log(ap)^2 - 4.79201\right)\right), \tag{2.125}$$

if the counterterm's contribution in eq. (2.122) is excluded. Using Σ_1 and d_{1L} of eqs. (2.100) and (2.103), this proper contribution is expressed as

$$\gamma^\mu(-\Sigma_1(p) - d_{1L}(g_0)\delta^{\mu\underline{\alpha}}). \tag{2.126}$$

Since the self-energy contribution from the legs not only includes the wavefunction renormalisation $Z_2 = (1 - \Sigma_1)^{-1}$, but also the anisotropic contribution from d_{1L}, the full renormalisation factor amounts to

$$\gamma^\mu(-\Sigma_1 - d_{1L}\delta^{\mu\underline{\alpha}} + (1 - \Sigma_1)^{-1} + d_{1L}\delta^{\mu\underline{\alpha}}) = \gamma^\mu \cdot 1 \tag{2.127}$$

and supports the claim of current conservation. In particular, the vector symmetry current is conserved even before inclusion of counterterms. Hence it cannot be used as a device for tuning the coefficient d in contradiction to previous conclusions [36]. In particular, the Ward identity is satisfied only if the point-split symmetry current is used instead of the local axial current.

Boriçi-Creutz fermions

Vertex corrections for insertion of scalar or pseudoscalar densities are equal: $\Lambda_P = \Lambda_S \gamma^5$. The vertex correction of the scalar density equals $-\Sigma_2(p)$ of eq. (2.112) and reads

$$\Lambda_S = \frac{g_0^2 C_F}{16\pi^2}\left(-4\log(ap)^2 + 29.48729 + (1 - \xi)\left(\log(ap)^2 - 5.792010\right)\right). \tag{2.128}$$

Local vector and axial currents undergo anisotropic renormalisation. The vertex correction to the local vector current reads

$$\begin{aligned}\Lambda_V^\mu &= \frac{g_0^2 C_F}{16\pi^2} \cdot \sum_\nu \gamma^\nu \left(\delta^{\mu\nu}\left(-\log(ap)^2 + 9.54612\right) - \frac{1}{2} \cdot 0.10037 \right.\\ &\quad + \left. \delta^{\mu\nu}(1 - \xi)\left(\log(ap)^2 - 4.792010\right)\right)\end{aligned} \tag{2.129}$$

---

[5]The axial current is interpreted as an isovector current unrelated to the axial anomaly in [145]. There, an explicit expression for the isosinglet axial current is presented and the Abelian axial anomaly for Karsten-Wilczek fermions in two dimensions is derived from it perturbatively.

and the vertex correction to the axial current is $\Lambda_A^\mu = \Lambda_V^\mu \gamma^5$. Lastly, the tensor current does not undergo anisotropic renormalisation and reads

$$\Lambda_T^{\mu\nu} = \frac{g_0^2 C_F}{16\pi^2} \sigma^{\mu\nu} \left(2.16548 + (1-\xi)\left(L - 3.792010\right)\right). \tag{2.130}$$

Symmetry currents which are constructed using transformations of eq. (2.121) read

$$V_n^\mu = \bar{\psi}_n \frac{\gamma^\mu + d^{BC}\Gamma + i\gamma^{\mu'}}{2} U_n^\mu \psi_{n+\hat{e}_\mu} + \bar{\psi}_{n+\hat{e}_\mu} \frac{\gamma^\mu + d^{BC}\Gamma - i\gamma^{\mu'}}{2} U_n^{\mu\dagger} \psi_n, \tag{2.131}$$

$$A_n^\mu = \bar{\psi}_n \frac{\gamma^\mu + d^{BC}\Gamma + i\gamma^{\mu'}}{2} \gamma^5 U_n^\mu \psi_{n+\hat{e}_\mu} + \bar{\psi}_{n+\hat{e}_\mu} \frac{\gamma^\mu + d^{BC}\Gamma - i\gamma^{\mu'}}{2} \gamma^5 U_n^{\mu\dagger} \psi_n. \tag{2.132}$$

Analogously to the case for Karsten-Wilczek fermions ineq. (2.124), the axial transformation anticommutes with the matrices of eq. (2.45). Again, only the vector symmetry current is covered in detail. The axial current, which is conserved in the chiral limit, is treated equally. Evaluation of the vertex correction, the sails and the operator tadpole of figure 2.2 yields the proper one-loop contribution to the vector symmetry current

$$\frac{g_0^2 C_F}{16\pi^2} \sum_\nu \gamma^\nu \left\{ -\delta^{\mu\nu}\left(\log(ap)^2 + 6.80664\right) - \frac{1}{2} \cdot 1.52766 + \delta^{\mu\nu}(1-\xi)\left(\log(ap)^2 - 4.79201\right) \right\}, \tag{2.133}$$

if the counterterm's contribution in eq. (2.131) is excluded. This proper contribution is expressed using Σ_1 and d_{1L} of eqs. (2.111) and (2.114) and yields

$$\sum_\nu \gamma^\nu \left(-\delta^{\mu\nu}\Sigma_1(p) - \frac{1}{2} \cdot d_{1L}(g_0)\right), \tag{2.134}$$

which combines with the self-energy contribution from the legs to

$$\sum_\nu \gamma^\nu \left(-\delta^{\mu\nu}\Sigma_1 - \frac{1}{2} \cdot d_{1L} + \delta^{\mu\nu}(1-\Sigma_1)^{-1} + \frac{1}{2} \cdot d_{1L}\delta^{\mu\alpha}\right) = \gamma^\mu \cdot 1. \tag{2.135}$$

Hence, the vector symmetry current is conserved even before inclusion of counterterms and the Ward identity is satisfied only if the point-split symmetry current is used instead of the local axial current.

2.3.3 Fermionic contribution to the vacuum polarisation

Since Karsten-Wilczek and Boriçi-Creutz fermions break hypercubic symmetry, it must be expected that fermion loops communicate this anisotropy to quantities that are isotropic at tree level. First and foremost, the validity of the Ward-Takahashi identity has to be confirmed, because the tensor structure of the vacuum polarisation tensor is modified in an anisotropic theory. The fermionic contribution to the vacuum polarisation, which is simply referred to as "the vacuum polarisation" here for brevity's sake, reveals the extent of induced anisotropy. The gluonic dimension four counterterm is used to restore isotropy to its continuum limit. The bubble diagram (left side of figure 2.4)

Figure 2.4: The one-loop fermionic contribution to the vacuum polarisation consists of a bubble (left) and a tadpole (right) diagram, the latter of which cancels the quadratic power divergence of the former.

of the vacuum polarisation introduces a new aspect, which has not been encountered in the preceding LPT calculations. Due to the fact that all internal lines are fermion propagators, both poles of the fermion propagator contribute on equal footing. Hence, a naïve approach to the bubble diagram does not satisfy condition C3 of eq. (2.3) for the applicability of the power counting theorem of Reisz.

The vacuum polarisation is calculated from the sum of the bubble diagram and the tadpole diagram (right side of figure 2.4),

$$I^{ad\,\theta\chi}(p;\zeta,a) = I_b^{0\,\theta\chi}(p;\zeta,a) \cdot C_b^{ad} + I_t^{0\,\theta\chi}(p;\zeta,a) \cdot C_t^{ad}, \tag{2.136}$$

where space-time parts of bubble and tadpole diagrams are given by

$$I_b^{0\,\theta\chi}(p;\zeta,a) = - \int\limits_{-\pi/a}^{+\pi/a} \frac{d^4k}{(2\pi)^4} \mathrm{tr}\left\{ V_1^\theta(k,p+k)S(p+k;\zeta,0,a)V_1^\chi(p+k,k)S(k;\zeta,0,a) \right\}, \tag{2.137}$$

$$I_t^{0\,\theta\chi}(p;\zeta,a) = - \int\limits_{-\pi/a}^{+\pi/a} \frac{d^4k}{(2\pi)^4} \mathrm{tr}\left\{ V_2^{\theta\chi}(k,k)S(k;\zeta,0,a) \right\}. \tag{2.138}$$

Both integrals contain an overall factor (-1) due to having *one closed fermion loop*. The symmetry factor $1/2$ of the tadpole diagram is allotted to C_t^{ad}. The SU(3) structure is independent of the discretisation and collapses to $C_2\,\delta^{a,d}$ using eq. (A.11),

$$I_{b,c}^{ad} = \sum_{b,c,e,f=1}^{3} (T^a)^{fb}\delta^{bc}(T^d)^{ce}\delta^{ef} = \mathrm{tr}(T^aT^d) = C_2\delta^{ad}, \tag{2.139}$$

$$I_{t,c}^{ad} = \frac{1}{2}\sum_{b,c}\delta^{bc}\left(\frac{1}{3}\delta^{bc}\delta^{ad} + \sum_{b,c}d^{bce}(T^e)^{ad} \right) = \frac{1}{2}\delta^{ad} = C_2\delta^{ad}. \tag{2.140}$$

51

which is included in the integrals $I_{b,t}^{\theta\chi}(p;\zeta,a) \equiv C_2 I_{b,t}^{0\,\theta\chi}(p;\zeta,a)$ as

$$
I_b^{\theta\chi}(p;\zeta,a) = -C_2 \int\limits_{-\pi/a}^{+\pi/a} \frac{d^4k}{(2\pi)^4} \mathrm{tr}\left\{ V_1^\theta(k,p+k) S(p+k;\zeta,0,a) V_1^\chi(p+k,k) S(k;\zeta,0,a) \right\},
$$

(2.141)

$$
I_t^{\theta\chi}(p;\zeta,a) = -C_2 \int\limits_{-\pi/a}^{+\pi/a} \frac{d^4k}{(2\pi)^4} \mathrm{tr}\left\{ V_2^{\theta\chi}(k,k) S(k;\zeta,0,a) \right\} \equiv I_t^{\theta\chi}(\zeta,a).
$$

(2.142)

Tadpole diagram

The tadpole diagram of eq. (2.142) is independent of the external four-momentum and yields a constant, which – by virtue of its mass dimension – must be a quadratic power divergence. Hence, the superficial degree of divergence of the tadpole diagram is negative, $\deg I_t = -2$, IR regularisation is not required and there is no problem with condition C3 of eq. (2.3). For Karsten-Wilczek fermions, the tadpole diagram reads

$$
I_t^{\theta\chi}(\zeta,a) = -\delta^{\theta\chi} a^2 \frac{g_0^2 C_2}{4} \int \frac{d^4k}{(2\pi)^4} \mathrm{tr}\left\{ \left(\gamma^\theta \hat{s}_{2k}^\theta - \zeta\gamma^{\underline{\alpha}} \varrho^{\theta\underline{\alpha}} \hat{c}_{2k}^\theta \right) \frac{(\gamma\cdot s_k) + \frac{\zeta}{2}\gamma^{\underline{\alpha}}(\hat{s}_k)_\perp^2}{D^{KW}(k;\zeta,0,a)} \right\},
$$

(2.143)

which is simplified algebraically to

$$
I_t^{\theta\chi}(\zeta,a) = -\delta^{\theta\chi} a^2 g_0^2 C_2 \int \frac{d^4k}{(2\pi)^4} \frac{2(s_k^\theta)^2 + \zeta^2(\hat{s}_k)_\perp^2 (c_k)_\perp + 2\zeta s_k^{\underline{\alpha}}[\delta^{\theta\underline{\alpha}} - \varrho^{\theta\underline{\alpha}}(c_k)_\perp]}{D^{KW}(k;\zeta,0,a)}.
$$

(2.144)

Because the odd power in $\zeta s_k^{\underline{\alpha}}$ in the numerator must combine with the odd power of $\zeta s_k^{\underline{\alpha}}$ in the denominator or be trivially integrated to zero, the integral is an even function of ζ. After setting $\zeta = +1$ and rescaling (cf. eq. (2.9)), the integral is evaluated to

$$
I_t^{\theta\chi}(+1,a) = \delta^{\theta\chi} \frac{g_0^2 C_2}{a^2} \left(-36.31464 \cdot \varrho^{\theta\underline{\alpha}} + 7.12931 \cdot \delta^{\theta\underline{\alpha}} \right).
$$

(2.145)

For Boriçi-Creutz fermions, the tadpole diagram reads

$$
I_t^{\theta\chi}(\zeta,a) = -\delta^{\theta\chi} a^2 \frac{g_0^2 C_2}{4} \int \frac{d^4k}{(2\pi)^4} \sum_\mu \mathrm{tr}\left\{ \frac{\left(\gamma^\theta \hat{s}_{k+k}^\theta + \zeta\gamma^{\theta\prime} \hat{c}_{k+k}^\theta \right) \left(\gamma^\mu s_k^\mu - \zeta\gamma^{\mu\prime} \frac{1}{2}(\hat{s}_k^\mu)^2 \right)}{D^{BC}(k;\zeta,0,a)} \right\},
$$

(2.146)

which is simplified algebraically to

$$
I_t^{\theta\chi}(\zeta,a) = -\delta^{\theta\chi} a^2 g_0^2 C_2 \int \frac{d^4k}{(2\pi)^4} \frac{2\big[(s_k^\theta)^2 + \zeta^2\left((c_k) - (c_k)^2\right)\big] + 6\zeta(s_k)}{D^{BC}(k;\zeta,0,a)}.
$$

(2.147)

52

Since the odd power in $\zeta(s_k)$ in the numerator must combine with the odd power of $\zeta(s_k)$ in the denominator or be trivially integrated to zero, the integral is an even function of ζ. After setting $\zeta = +1$ and rescaling (cf. eq. (2.9)), the integral is evaluated to

$$I_t^{\theta\chi}(+1, a) = \delta^{\theta\chi} \frac{g_0^2 C_2}{a^2} \cdot (-73.71980) \,. \tag{2.148}$$

Bubble diagram

The integral $I_b^{\theta\chi}(p; \zeta, a)$ of the bubble diagram is split into two pieces, the lattice integral $J^{\theta\chi}(p; \zeta, M, a)$, and the continuum integral $I_b^{\theta\chi}(p; \zeta, a) - J^{\theta\chi}(p; \zeta, M, a)$. The external four-momentum p is treated as small and the integral $J^{\theta\chi}(p; \zeta, M, a)$ is subjected to a Taylor expansion in p up to second order,

$$J^{\theta\chi}(p; \zeta, a) = J_2^{\theta\chi}(\zeta, a) + \sum_{\eta, \xi} p_\eta p_\xi J_{\eta\xi}^{\theta\chi}(\zeta, M, a) \tag{2.149}$$

$$J_2^{\theta\chi}(\zeta, a) = -\int \mathrm{tr} \left\{ V_1^\theta(k, k) S(k; \zeta, 0, a) V_1^\chi(k, k) S(k; \zeta, 0, a) \right\} , \tag{2.150}$$

$$J_{\eta\xi}^{\theta\chi}(\zeta, M, a) = -\frac{1}{2} \int \mathrm{tr} \left\{ \frac{\partial^2 \left\{ V_1^\theta(k, p+k) S(p+k; \zeta, M, a) V_1^\chi(p+k, k) S(k; \zeta, M, a) \right\}}{\partial p_\eta \partial p_\xi} \right\}_{p=0} , \tag{2.151}$$

where each of the vacuum polarisation integrals in eqs. (2.150 and 2.151 is integrated as

$$\int \mathrm{tr} \, (\dots) \equiv \int\limits_{-\pi/a}^{+\pi/a} \frac{d^4 k}{(2\pi)^4} \mathrm{tr} \, (\dots) \tag{2.152}$$

and where $J_{\eta\xi}^{\theta\chi}(\zeta, M, a)$ is IR regularised with a small mass term M^2 in every denominator. The indices η and ξ of the Taylor expansion in p do not necessarily have to match indices θ and χ of the vertices, since the anisotropy of the fermion action allows for the persistence of various combinations of indices in the continuum limit.

Karsten-Wilczek fermions

For Karsten-Wilczek fermions, the power divergent integral $J_2^{\theta\chi}(\zeta, a)$ reads

$$J_2^{\theta\chi}(\zeta, a) = -a^2 \frac{g_0^2 C_2}{4} \int \mathrm{tr} \left\{ \left(\gamma^\theta \hat{c}_{2k}^\theta + \zeta \gamma^{\underline{\alpha}} \varrho^{\theta\underline{\alpha}} \hat{s}_{2k}^\theta \right) \frac{(\gamma \cdot s_k) + \frac{\zeta}{2} \gamma_{\underline{\alpha}} (\hat{s}_k)_\perp^2}{D^{KW}(k; \zeta, 0, a)} \right.$$
$$\left. \times \left(\gamma^\chi \hat{c}_{2k}^\chi + \zeta \gamma^{\underline{\alpha}} \varrho^{\theta\underline{\alpha}} \hat{s}_{2k}^\chi \right) \frac{(\gamma \cdot s_k) + \frac{\zeta}{2} \gamma_{\underline{\alpha}} (\hat{s}_k)_\perp^2}{D^{KW}(k; \zeta, 0, a)} \right\}. \tag{2.153}$$

The part of the numerator, which is non-vanishing upon integration,

$$N_0 = \delta^{\theta\chi} \left\{ 2(s_k^\theta)^2 - 4(s_k)^2(c_k^\theta)^2 - 4\zeta s_k^{\underline{\alpha}} \left[(1 - 2\delta^{\theta\underline{\alpha}})(\hat{s}_k)_\perp^2(c_k^\theta)^2 - \varrho^{\theta\underline{\alpha}}(s_k^\theta)^2(4c_k^\theta + \zeta^2((\hat{s}_k)_\perp^2)^2) \right] \right.$$
$$\left. - \zeta^2 \left[(1 - 2\delta^{\theta\underline{\alpha}})((\hat{s}_k)_\perp^2)^2(c_k^\theta)^2 - \varrho^{\theta\underline{\alpha}}(s_k^\theta)^2(4((s_k^{\underline{\alpha}})^2 - (s_k)_\perp^2) + \zeta^2((\hat{s}_k)_\perp^2)^2) \right] \right\}, \tag{2.154}$$

53

has been simplified algebraically by taking into account that only $k^{\underline{\alpha}}$ contributes as an odd power in the denominator. Therefore, the integral $J_2(\zeta, a)$ is reduced to

$$J_2^{\theta\chi}(\zeta, a) = -\delta^{\theta\chi} a^2 g_0^2 C_2 \int \frac{d^4 k}{(2\pi)^4} \frac{N_0}{(D^{KW}(k; \zeta, 0, a))^2}. \tag{2.155}$$

Odd powers in $\zeta s_k^{\underline{\alpha}}$ in the numerator must combine with odd powers of $\zeta s_k^{\underline{\alpha}}$ in the denominator and the integral turns out to be an even function of ζ. The power divergent integral is evaluated after setting $\zeta = +1$ and rescaling (cf. eq. (2.9)) and exactly cancels the power divergent tadpole contribution of eq. (2.145):

$$J_2^{\theta\chi}(+1, a) = \delta^{\theta\chi} \frac{g_0^2 C_2}{a^2} \left(36.31464 \cdot \varrho^{\theta\underline{\alpha}} - 7.12931 \cdot \delta^{\theta\underline{\alpha}} \right). \tag{2.156}$$

The integral $J_{\eta\xi}^{\theta\chi}(\zeta, M, a)$ of eq. (2.151) is far too cumbersome for explicit presentation. Due to the exclusive presence of two fermion propagators, it is IR divergent at both poles and has to be regularised at both in order to satisfy condition C3 of eq. (2.3). A simple method to obtain both IR divergences is to calculate the standard IR divergence[6] from the continuum integral $J_{\eta\xi}^{\theta\chi}(M, 0)$, replace all loop momenta as $k^\mu \to \hat{s}_k^\mu$ and finally add a second standard IR divergence that is shifted from the second pole to the first. The continuum integral $J_{\eta\xi}^{\theta\chi}(\zeta, M, 0)$ reads

$$J_{\eta\xi}^{\theta\chi}(M, 0) = \frac{g_0^2 C_2}{2} \int\limits_{-\infty}^{+\infty} \frac{d^d k}{(2\pi)^d} \text{tr} \left\{ \gamma^\theta \left\{ \frac{\partial^2 S(p+k; 0, M, 0)}{\partial p_\eta \partial p_\xi} \right\}_{p=0} \gamma^\chi S(k; 0, M, 0) \right\}$$

$$= -g_0^2 C_2 \, 4 \int\limits_{-\infty}^{+\infty} \frac{d^d k}{(2\pi)^d} \left\{ \frac{\left[\delta^{\theta\chi} \delta^{\eta\xi} k^2 - (\delta^{\eta\chi} \delta^{\theta\xi} + \delta^{\eta\theta} \delta^{\chi\xi})((k^\theta)^2 + (k^\chi)^2) \right]}{(k^2 + M^2)^3} \right.$$

$$\left. - 4 \frac{\left[\delta^{\theta\chi} \delta^{\eta\xi} (k^\eta)^2 (k^2 - 2(k^\theta)^2) - 2(\delta^{\eta\chi} \delta^{\theta\xi} + \delta^{\eta\theta} \delta^{\chi\xi})((k^\theta)^2 (k^\chi)^2) \right]}{(k^2 + M^2)^4} \right\}. \tag{2.157}$$

It is transformed into a lattice integral for the first divergence without any obstacles,

$$\widetilde{J}_{1\,\eta\xi}^{\theta\chi}(M, a) = -4 \, g_0^2 C_2 a^4 \int\limits_{-\pi/a}^{+\pi/a} \frac{d^d k}{(2\pi)^d} \left\{ \frac{\left[\delta^{\theta\chi} \delta^{\eta\xi} (\hat{s}_k)^2 - (\delta^{\eta\chi} \delta^{\theta\xi} + \delta^{\eta\theta} \delta^{\chi\xi})((\hat{s}_k^\theta)^2 + (\hat{s}_k^\chi)^2) \right]}{((\hat{s}_k)^2 + (aM)^2)^3} \right.$$

$$\left. - 4 \frac{\left[\delta^{\theta\chi} \delta^{\eta\xi} (\hat{s}_k^\eta)^2 ((\hat{s}_k)^2 - 2(\hat{s}_k^\theta)^2) - 2(\delta^{\eta\chi} \delta^{\theta\xi} + \delta^{\eta\theta} \delta^{\chi\xi})((\hat{s}_k^\theta)^2 (\hat{s}_k^\chi)^2) \right]}{((\hat{s}_k)^2 + (aM)^2)^4} \right\}$$

$$= 4 \, g_0^2 C_2 \left\{ 4 \delta^{\theta\chi} \delta^{\eta\xi} \left[\mathcal{B}(3, 1) - (1 - 2\delta^{\eta\theta}) \mathcal{B}(4, 2) - (1 + 2\delta^{\eta\theta}) \mathcal{B}(4, 1, 1) \right] \right.$$

$$\left. - 2(\delta^{\eta\chi} \delta^{\theta\xi} + \delta^{\eta\theta} \delta^{\chi\xi}) \left[\mathcal{B}(3, 1) - 4\delta^{\theta\chi} \mathcal{B}(4, 2) - 4(1 - \delta^{\theta\chi}) \mathcal{B}(4, 1, 1) \right] \right\}. \tag{2.158}$$

---

[6]If the lattice divergence is automatically constructed from the lattice integral, it may pick up extra finite terms due to discretisation effects. These extra terms are due to higher derivatives of trigonometric function of external four-momenta. They are included in the regularised lattice integral (cf. eq. (2.162)).

The second divergence is obtained by a shift $k^{\underline{\alpha}} \to k^{\underline{\alpha}} - \pi/a$, which transforms the trigonometric functions as

$$(\hat{s}_k^\theta)^2 \to (\hat{t}_k^\theta)^2, \quad (\hat{t}_k^\theta)^2 \equiv (\hat{s}_k^\theta)^2 + 2\delta^{\theta\underline{\alpha}}(2 - (\hat{s}_k^{\underline{\alpha}})^2), \quad (\hat{t}_k)^2 \equiv (\hat{s}_k)^2 + 2(2 - (\hat{s}_k^{\underline{\alpha}})^2). \quad (2.159)$$

Thus, the second divergence reads

$$\widetilde{J}_{2\,\eta\xi}^{\theta\chi}(M,a) = \widetilde{J}_{1\,\eta\xi}^{\theta\chi}(M,a)\bigg|_{\hat{s}_k \to \hat{t}_k}, \quad (2.160)$$

which is numerically identical to eq. (2.158) after integration. The tensor components[7] of each divergence $\widetilde{J}_{j\,\eta\xi}^{\theta\chi}(M,a)$ are invariant under interchanges of θ and χ and interchanges of η and ξ. Non-vanishing tensor components are evaluated to

$$
\begin{aligned}
\widetilde{J}_{j\,\theta\chi}^{\theta\chi}(M,a) &= +16g_0^2 C_2(\mathcal{B}(3,1) - 4\mathcal{B}(4,1,1)) &&= +4.13588 - \tfrac{4}{3}\log{(aM)^2}, \\
\widetilde{J}_{j\,\theta\theta}^{\eta\eta}(M,a) &= -16g_0^2 C_2(\mathcal{B}(3,1) - \mathcal{B}(4,2) - \mathcal{B}(4,1,1)) &&= -5.84941 + \tfrac{4}{3}\log{(aM)^2}.
\end{aligned}
$$
$$(2.161)$$

After subtraction of the divergences $\widetilde{J}_{j\,\eta\xi}^{\theta\chi}(M,a)$, the lattice integral is automatically IR finite by construction. The regulator is removed and loop momenta are rescaled (cf. eq. (2.9)). For $\zeta = +1$, the integral evaluates to

$$
\begin{aligned}
J_{\eta\xi}^{\theta\chi}(+1,0,a) - \sum_{j=1}^{2}\widetilde{J}_{j\,\eta\xi}^{\theta\chi}(0,a) &= \delta^{\theta\chi}\delta^{\eta\xi}\Big\{-2.51804 - \frac{4}{3}\Big\} + (\delta^{\eta\chi}\delta^{\theta\xi} + \delta^{\eta\theta}\delta^{\chi\xi})\Big\{\frac{+7.2785}{2}\Big\} \\
&+ \Big[2\delta^{\theta\chi}\delta^{\eta\xi}(\delta^{\theta\underline{\alpha}} + \delta^{\eta\underline{\alpha}}) - (\delta^{\eta\chi}\delta^{\theta\xi} + \delta^{\eta\theta}\delta^{\chi\xi})(\delta^{\theta\underline{\alpha}} + \delta^{\chi\underline{\alpha}})\Big]\frac{12.69766}{4}.
\end{aligned}
$$
$$(2.162)$$

After adding the divergences $\widetilde{J}_{j\,\eta\xi}^{\theta\chi}(M,a)$ of eq. (2.161) and including external momenta p_η and p_ξ, the lattice integral finally yields

$$
\begin{aligned}
J^{\theta\chi} &= \Big(p^\theta p^\chi - \delta^{\theta\chi}p^2\Big)\frac{g_0^2 C_2}{16\pi^2}\Big(-\frac{8}{3}\log{(aM)^2} + 15.55024\Big) \\
&- \Big(p^\theta p^\chi(\delta^{\theta\underline{\alpha}} + \delta^{\chi\underline{\alpha}}) - \delta^{\theta\chi}(p^2\delta^{\theta\underline{\alpha}}\delta^{\chi\underline{\alpha}} + (p^{\underline{\alpha}})^2)\Big)\frac{g_0^2 C_2}{16\pi^2}\cdot 12.69766, \quad (2.163)
\end{aligned}
$$

where it is noted explicitly that the term $-8/3\log{(aM)^2}$ is due to subtraction of IR divergences for both poles. The Ward identity is satisfied despite the anisotropic contribution.

---

[7]Other tensor components of the divergences are integrated to 0 once symmetries between different Euclidean components of loop momenta in the numerator have been exploited.

Boriçi-Creutz fermions

Boriçi-Creutz fermions mirror the strategy for Karsten-Wilczek fermions. The power divergent integral $J_2^{\theta\chi}(\zeta, a)$ reads

$$
J_2^{\theta\chi}(\zeta, a) = - a^2 \frac{g_0^2 C_2}{4} \int \mathrm{tr} \left\{ \left(\gamma^\theta \hat{c}_{2k}^\theta - \zeta \gamma^{\theta\prime} \hat{s}_{2k}^\theta \right) \frac{\left(\sum_\mu \left(\gamma_\mu s_k^\mu - \zeta \gamma_\mu'(1 - c_k^\mu) \right) \right)}{D^{BC}(k; \zeta, 0, a)} \right.
$$
$$
\left. \times \left(\gamma^\chi \hat{c}_{2k}^\chi - \zeta \gamma^{\chi\prime} \hat{s}_{2k}^\chi \right) \frac{\left(\sum_\nu \left(\gamma_\nu s_k^\nu - \zeta \gamma_\nu'(1 - c_k^\nu) \right) \right)}{D^{KBC}(k; \zeta, 0, a)} \right\}
\tag{2.164}
$$

and is evaluated directly for $\zeta = +1$ after rescaling (cf. eq. (2.9)) as

$$
J_2^{\theta\chi}(\zeta, a) = \delta^{\theta\chi} \frac{g_0^2 C_2}{a^2} \cdot (73.71980),
\tag{2.165}
$$

which precisely cancels the tadpole's power divergence of eq. (2.148). The second divergence of $J_{\eta\xi}^{\theta\chi}(\zeta, M, a)$ is obtained with a shift $k^\mu \to k^\mu - \pi/(2a) \; \forall \mu$ between the two poles, which transforms the trigonometric functions as

$$
(\hat{s}_k^\theta)^2 \to (\hat{t}_k^\theta)^2, \quad (\hat{t}_k^\theta)^2 \equiv 2(1 - s_k^\theta), \quad (\hat{t}_k)^2 \equiv 2(4 - (s_k)).
\tag{2.166}
$$

After subtraction of the divergences $\widetilde{J}_{j\,\eta\xi}^{\theta\chi}(M, a)$, the lattice integral is automatically IR finite by construction. The regulator is removed and loop momenta are rescaled (cf. eq. (2.9)). For $\zeta = +1$, the integral evaluates to

$$
J_{\eta\xi}^{\theta\chi}(0, a) - \sum_{j=1}^{2} \widetilde{J}_{j\,\eta\xi}^{\theta\chi}(0, a) = \delta^{\theta\chi} \delta^{\eta\xi} \left\{ -4.38389 - \frac{4}{3} \right\} + (\delta^{\eta\chi} \delta^{\theta\xi} + \delta^{\eta\theta} \delta^{\chi\xi}) \left\{ \frac{+9.1443}{2} \right\}
$$
$$
+ \left[\delta^{\theta\chi} + \delta^{\eta\xi} - (\delta^{\eta\chi} + \delta^{\theta\xi} + \delta^{\eta\theta} + \delta^{\chi\xi}) \right] \cdot 0.9094.
\tag{2.167}
$$

After adding the divergences $\widetilde{J}_{j\,\eta\xi}^{\theta\chi}(M, a)$ of eq. (2.161) and including external momenta p_η and p_ξ, the lattice integral finally yields

$$
J^{\theta\chi} = \left(p^\theta p^\chi - \delta^{\theta\chi} p^2 \right) \frac{g_0^2 C_2}{16\pi^2} \left(-\frac{8}{3} \log (aM)^2 + 19.2349 \right)
$$
$$
- \left((p^\theta + p^\chi) \left(\sum_\lambda p^\lambda \right) - p^2 - \delta^{\theta\chi} \left(\sum_\lambda p^\lambda \right)^2 \right) \frac{g_0^2 C_2}{16\pi^2} \cdot 0.9094,
\tag{2.168}
$$

where it is noted explicitly that the term $-8/3 \log (aM)^2$ is due to subtraction of IR divergences for both poles. The Ward identity is satisfied despite the anisotropic contribution.

Continuum integral

Evaluation of the continuum integral mirrors section 2.3.1. However, the limit $a \to 0$ for small p in $I^{\theta\chi}(p; \zeta, 0) - J^{\theta\chi}(p; \zeta, M, 0)$ contains propagators with only one single fermion

mode each and thus corresponds to a one-flavour theory. Hence, the continuum integral requires an extra factor 2 for the two flavours,

$$K^{\theta\chi}(p;M) = 2(I^{\theta\chi}(p;0,0) - \lim_{M^2\to0} J^{\theta\chi}(p;0,M,0)). \tag{2.169}$$

$K^{\theta\chi}(p;M)$ is evaluated using dimensional regularisation even though it is already UV finite and IR regularised. Cancellation of the presence of the IR regulator of eqs. (2.163) and (2.168) would fail without the flavour factor 2. The additional dimensional regulator cancels between $I^{\theta\chi}(p;0,0)$ and $J^{\theta\chi}(p;0,M,0)$ and the integral reads

$$K^{\theta\chi}(p;M) = + g_0^2 C_2 \left(\int_{-\infty}^{+\infty} \frac{d^dk}{(2\pi)^d} \mathcal{M}^{4-d} \mathrm{tr}\left\{ \gamma^\theta S(p+k;0,0,0)\gamma^\chi S(k;0,0,0) \right\} \right.$$

$$\left. - \frac{1}{2}\sum_{\eta,\xi} p^\eta p^\xi \mathrm{tr}\left\{ \gamma^\theta \left\{ \frac{\partial^2 S(p+k;0,M,0)}{\partial p_\eta \partial p_\xi} \right\}_{p=0} \gamma^\chi S(k;0,M,0) \right\} \right). \tag{2.170}$$

The power divergence of the zeroth order of the Taylor expansion vanishes in dimensional regularisation in the limit of vanishing IR regulator M. The integral evaluates to

$$K(p;M) = \left(p^\theta p^\chi - \delta^{\theta\chi} p^2 \right) \frac{g_0^2 C_2}{16\pi^2} \cdot 2 \cdot \left\{ -\frac{4}{3}\log\frac{p^2}{M^2} + \frac{20}{9} \right\}. \tag{2.171}$$

Full fermionic contribution to the vacuum polarisation

The sum of eqs. (2.145), (2.156), (2.163) and (2.171) completes the full fermionic contribution to the vacuum polarisation for Karsten-Wilczek fermions and reads

$$I^{\theta\chi}(p) = \left(p^\theta p^\chi - \delta^{\theta\chi} p^2 \right) \Pi(p^2) + A^{\theta\chi}(p)\widetilde{\Pi}(g_0), \tag{2.172}$$

where

$$\Pi(p^2) = \frac{g_0^2 C_2}{16\pi^2} \left(-\frac{8}{3}\log(ap)^2 + 19.99468 \right) \tag{2.173}$$

$$A^{\theta\chi}(p) = p^\theta p^\chi(\delta^{\theta\underline{\alpha}} + \delta^{\chi\underline{\alpha}}) - \delta^{\theta\chi}(p^2\delta^{\theta\underline{\alpha}}\delta^{\chi\underline{\alpha}} + (p^{\underline{\alpha}})^2) \tag{2.174}$$

$$\widetilde{\Pi}(g_0) = -\frac{g_0^2 C_2}{16\pi^2} \cdot 12.69766. \tag{2.175}$$

Even before inclusion of counterterms, the Ward identity is satisfied:

$$\sum_\theta p_\theta I^{\theta\chi}(p) = \sum_\chi p_\chi I^{\theta\chi}(p) = 0. \tag{2.176}$$

Using $\mathcal{Q}$ from eq. (2.31), the anisotropic term $A^{\theta\chi}(p)$ is expressed as

$$A^{\theta\chi}(p) = \frac{1}{4}\left(\frac{1}{2}[\mathcal{Q},\slashed{p}]\left(\{\gamma^\theta,\slashed{p}\}[\gamma^\chi,\mathcal{Q}] + \{\gamma^\chi,\slashed{p}\}[\gamma^\theta,\mathcal{Q}]\right) - p^2[\mathcal{Q},\gamma^\theta][\gamma^\chi,\mathcal{Q}] - \delta^{\theta\chi}[\mathcal{Q},\slashed{p}][\slashed{p},\mathcal{Q}] \right) \tag{2.177}$$

In the presence of the anisotropic term of eq. (2.174), the tree-level tensor structure cannot be recoverd in the full one-loop gluon propagator. Once the anisotropic term has been removed by tuning the gluonic counterterm of eq. (1.68) using eq. (2.175),

$$d_P(g_0) = -\frac{g_0^2 C_2}{16\pi^2} \cdot 12.69766 + \mathcal{O}(g_0^4), \tag{2.178}$$

the one-loop gluon propagator takes the standard form

$$\Gamma^{\mu\nu}(p) = Z_3 \frac{\delta^{\mu\nu} - (1 - \xi(1 + \Pi(p^2)))\frac{p^\mu p^\nu}{p^2}}{p^2} \tag{2.179}$$

and the charge renormalisation factor Z_3 is obtained as

$$Z_3 = (1 - \Pi(0))^{-1}. \tag{2.180}$$

The sum of eqs. (2.148), (2.165), (2.168) and (2.171) completes the full fermionic contribution to the vacuum polarisation for Boriçi-Creutz fermions eq. (2.172) with

$$\Pi(p^2) = \frac{g_0^2 C_2}{16\pi^2} \left(-\frac{8}{3} \log(ap)^2 + 23.6793 \right) \tag{2.181}$$

$$A^{\theta\chi}(p) = (p^\theta + p^\chi) \left(\sum_\lambda p^\lambda \right) - p^2 - \delta^{\theta\chi} \left(\sum_\lambda p^\lambda \right)^2 \tag{2.182}$$

$$\widetilde{\Pi}(g_0) = -\frac{g_0^2 C_2}{16\pi^2} \cdot 0.9094 \tag{2.183}$$

Again, the Ward identity of eq. (2.176) is satisfied before inclusion of counterterms and the anisotropic term is expressed through the Dirac structure of eq. (2.177) using $\mathcal{Q}$ from eq. (2.45). The anisotropy must be removed at one-loop level by tuning the gluonic counterterm of eq. (1.88) using eq. (2.183),

$$d_P(g_0) = -\frac{g_0^2 C_2}{16\pi^2} \cdot 0.9094 + \mathcal{O}(g_0^4) \tag{2.184}$$

in order to have the charge renormalisation factor of eq. (2.180) and the one-loop gluon propagator of eq. (2.179) take their standard forms.

Whether there is any deeper meaning to the Dirac structure of eq. (2.177) is not fully understood at present. However, the presence of two matrices $\mathcal{Q}$ seems to indicate that the anisotropic contribution is due to fermion loops which receive contributions from the propagation of different fermion species.

2.4   Boosted perturbation theory

Boosted perturbation theory (BPT) has been suggested by Lepage and Mackenzie [110] as a means to extend the validity of perturbative calculations into the non-perturbative regime. Non-perturbative effects are estimated with the average plaquette value,

$$U_0 = \sqrt[4]{\frac{1}{|\Lambda|} \sum_{n \in \Lambda} \sum_{\mu < \nu} U_n^{\mu\nu}}, \tag{2.185}$$

which is included in a boosted coupling constant (also called Parisi's coupling),

$$g_P^2 = g_0^2 / U_0^4, \tag{2.186}$$

which replaces g_0 in one-loop quantities. Predictions from BPT often serve as good starting points for non-perturbative studies. In the case of minimally doubled fermions, coefficients of the anisotropic counterterms have to be tuned non-perturbatively. Estimates from BPT are used to pin down a region of interest where anisotropic effects are expected to be mild compared with the untuned theory. BPT predictions are listed in table 2.2.

Karsten-Wilczek fermions							
β	U_0^4	c_{1L}	c_{BPT}	d_{1L}	d_{BPT}	$d_{P,1L}$	$d_{P,BPT}$
5.8	0.567	-0.258	-0.454	-0.00110	-0.00193	-0.0924	-0.163
6.0	0.594	-0.249	-0.420	-0.00106	-0.00179	-0.0893	-0.150
6.2	0.614	-0.241	-0.393	-0.00103	-0.00167	-0.0865	-0.141
Boriçi-Creutz fermions							
β	U_0^4	c_{1L}	c_{BPT}	d_{1L}	d_{BPT}	$d_{P,1L}$	$d_{P,BPT}$
5.8	0.567	$+0.258$	$+0.455$	$+0.0133$	$+0.0235$	-0.00298	-0.00525
6.0	0.594	$+0.249$	$+0.420$	$+0.0129$	$+0.0217$	-0.00288	-0.00485
6.2	0.614	$+0.241$	$+0.393$	$+0.0125$	$+0.0203$	-0.00279	-0.00454

Table 2.2: Boosted one-loop coefficients serve as starting point for non-perturbative renormalisation. Numerical values for U_0^4 are due to [16].

2.5   Interim findings (I)

With the completion of perturbative studies at one-loop level, it is demonstrated that Karsten-Wilczek and Boriçi-Creutz actions are renormalisable quantum field theories. Due to their anisotropies, each action requires three counterterms. Even though the actions' anisotropies are different, their counterterms are exact analogues.

Both fermionic counterterms are required for recovery of isotropy of the fermion propagator. Once these counterterms are included with appropriate one-loop coefficients, the

continuum limit of the fermion propagator takes the standard form of a one-flavour quark propagator. An exchange of the two doublers by a shift of the fermion's four-momentum from one pole to the other and application of the matrices $\mathcal{Q}$ and $\mathcal{Q}^\dagger$ (of eqs. (2.31) or (2.45)) in the sense of the unitary transformation in eq. (1.49) changes the sign of the Karsten-Wilczek (or Boriçi-Creutz) term. The coefficient $c(g_0)$ of the dimension-three counterterm inherits this sign, whereas the other coeffcients of the self-energy – Z_2, Z_m and $d(g_0)$ – are unchanged by this transformation. This verifies that the discretised forms of the counterterm operators presented in section 1.3 are appropriate choices for the actions over the full range of fermionic four-momenta. It is noteworthy that the coefficients of the relevant counterterms for both actions are almost equal in magnitude.

The fermionic contribution to the vacuum polarisation is anisotropic before inclusion of the gluonic counterterm, which recovers the gluon propagator's isotropy at one-loop level. Nevertheless, the Ward identity is satisfied even without counterterms and power divergences cancel between bubble and tadpole diagrams. Since all internal lines correspond to fermion propagators, both poles contribute on equal footing to the diagram and the logarithmic divergence indicates a two-flavour theory. The coefficient $d_P(g_0)$ of the anisotropic term is finite and even under the analogue of eq. (1.49).

Lastly, interacting minimally doubled fermions retain their chiral symmetry, which is reflected by the equality of renormalisation factors of local scalar and pseudoscalar densities as well as vector and axial vector currents, even though the latter undergo anisotropic renormalisation that necessitates additional counterterms. The tensor current is isotropic. Minimally doubled fermions have two symmetry currents involving only fields at neighbouring sites. This vector current and axial current both satisfy chiral Ward identities. Such an ultralocal axial symmetry current is not available for the majority of fermion discretisations. The PCAC relation is satisfied at one-loop level only if the axial symmetry current is used.

For a theory of two quark flavours, the presence of a single, conserved axial symmetry current implies there is only one (Pseudo-) Goldstone boson in the chiral limit. Thus, the spectrum must include two states which fail to be (Pseudo-) Goldstone bosons at finite lattice spacing, but become degenerate with the (Pseudo-) Goldstone boson in the continuum limit. Hence, a lattice artefacts contributes to their masses, which is the analogue of taste-breaking for staggered fermions [24, 104]. Of course, a third kind of pseudoscalar boson must have the role of the pseudoscalar singlet and retain a non-vanishing mass even in the continuum limit. Numerical simulations in chapter 4 aim at identifying at least one of the would-be (Pseudo-) Goldstone bosons.

Structure and symmetry

Perturbative studies of minimally doubled fermions reproduce standard behaviour of quarks in the continuum limit once three counterterms are included. At one loop, the propagator resembles the one-flavour expression, though the vacuum polarisation's logarithmic divergence implies a two-flavour theory. It seems as if minimally doubled fermions within purely fermionic loops resemble staggered fermions rather than Wilson fermions. Before embarking on an extensive numerical study, analytical methods are used to explore the limit $a \to 0$ of Karsten-Wilczek fermions by means of an expansion in the lattice spacing a. The focus of section 3.1 is on a formal decomposition of Karsten-Wilczek fermions in terms of a pair of fields with different momentum support. This decomposition suggests additional oscillating contribution in some correlation functions – as is known for the case of staggered fermions (e.g. [5]) – but with a frequency that depends on the coefficients of the counterterms. The focus of section 3.2 is on the interdependence of charge conjugation and Euclidean reflections for minimally doubled fermions, which is due to the $CP\Theta$ symmetry of their actions. It is shown that observables in the quenched approximation with definite charge conjugation quantum number are automatically symmetric under the broken reflection symmetry . A short summary of interim findings is presented in section 3.3.

3.1 Decomposition into a pair of fields

The aim of this section is to analyse Karsten-Wilczek fermions with an action that includes counterterms with arbitrary coefficients. This study in the naïve continuum limit ($a \to 0$) reveals a dependence of correlation functions on mismatched counterterm coefficients, which is valuable for defining non-perturbative tuning schemes. The relevant operator of eq. (1.67) diverges as a is taken to zero. Hence, its arbitrary coefficient has to be dealt with by a local field transformation before any expansion in a can be attempted.

This is covered in section 3.1.1. A transformation along these lines was suggested for the first time by Pernici [129]. However, the coefficient of the divergent operator persistently modifies the boundary conditions. This was noted for the first time in [18]. The new approach within this thesis is keeping the operator with a coefficient that is required for cancellation of power divergences while absorbing the *mismatch* of its coefficient into a field transformation. Next, in section 3.1.2, the spinor fields of the free theory are related to a pair of fields, each having a different momentum support. The decomposition into this pair of *components*, which must be defined with support on multiple lattice sites, follows ideas concerning a *flavour interpretation*[1] that has been applied to staggered fermions [80, 147] for a long time and to minimally doubled fermions [18, 101, 145] as well. The requirement that both components satisfy the same field equations in limit $a \to 0$ fixes their mixture and recovers the matrices of eq. (2.31). Later on, this definition of components is generalised to interacting fields in section 3.1.3. Before support on different lattice sites can be defined, any mismatch of the divergent operator's coefficient must be shifted into local phase factors. It turns out that these phase factors for both components must be related by complex conjugation due to the components' non-trivial mixture that is observed in the free theory as well. Lastly, the decomposition is plugged into interpolating operators that are used in the construction of mesonic correlation functions in section 3.1.4. These correlation functions contain sixteen different pieces due to 2^4 possible combinations of components, which can be sorted into five sets with different properties. Whereas two sets yield non-oscillating contributions with J^{PC} that is expected for the interpolating operator, two other sets yield oscillating contributions with different Dirac structure and different J^{PC}. The oscillation's frequency depends on the mismatch of the divergent operator's coefficient. The last set with eight contributions must vanish due to symmetry violation.

3.1.1 Absorption of a coefficient into a local field transformation

The full Karsten-Wilczek fermion action has been introduced in eq. (1.69) as

$$S^f[\psi, \bar{\psi}, U] = a^4 \sum_{n,m \in \Lambda} \bar{\psi}_n \left(D_{n,m}^N + D_{n,m}^{KW} + D_{n,m}^3 + D_{n,m}^4 + m_0 \delta_{n,m} \right) \psi_m, \qquad (3.1)$$

which involves both fermionic counterterms. In the following, the case is considered where the counterterms' coefficients c and d do not match the tuned values $c(g_0)$ and $d(g_0)$ required for restoring the tree-level form to the propagator. This would be the case if either the counterterms were included in the free theory or if the coefficients were improperly tuned in the interacting theory. Hence, expressions for the coefficients read in these cases

$$c = c(g_0) + \delta c, \ d = d(g_0) + \delta d \ : \quad c(g_0), d(g_0) = \mathcal{O}(g_0^2); \ \delta c, \delta d = \mathcal{O}(1). \qquad (3.2)$$

---

[1]It is not *a priori* clear whether or not a flavour interpretation is eventually adequate for minimally doubled fermions. Hence, the pair of components is only a formal tool without flavour interpretation.

On the one hand, the mismatches δc and δd do not depend on the gauge coupling g_0 and δc causes a uncancelled divergence of the theory in the limit $a \to 0$. On the other hand, the quantities $c(g_0)$ and $d(g_0)$ are necessary for a cancellation of interaction effects that would also diverge for $a \to 0$. Thus, the contribution proportional to δc from the relevant operator $D^3_{n,m}$ of eq. (1.66) must be removed. The mismatch δc is absorbed into modified boundary conditions by a local field transformation of spinor fields

$$\psi_n = e^{-i\varphi n_{\underline{\alpha}}}\psi^c_n, \qquad \bar\psi_n = \bar\psi^c_n e^{+i\varphi n_{\underline{\alpha}}}. \tag{3.3}$$

The phase φ is fixed later in order to remove the mismatch δc in the divergent term. The gluon action is obviously invariant under the transformation of eq. (3.3). The fermion action is rewritten in terms of the transformed fields ψ^c and $\bar\psi^c$ as

$$S^f[\psi^c, \bar\psi^c, U] = a^4 \sum_{n,m\in\Lambda} \bar\psi^c_n e^{+i\varphi n_{\underline{\alpha}}} \left(D^N_{n,m} + D^{KW}_{n,m} + D^3_{n,m} + D^4_{n,m} + m_0\delta_{n,m} \right) e^{-i\varphi m_{\underline{\alpha}}}\psi^c_m$$

$$= a^4 \sum_{n,m\in\Lambda} \bar\psi^c_n \Big(\sum_{\mu\neq\underline{\alpha}} \gamma^\mu D^\mu_{n,m}[U] + D^{KW}_{n,m} + D^3_{n,m} + m_0\delta_{n,m}$$

$$+ e^{+i\varphi n_{\underline{\alpha}}} \left\{ \gamma^{\underline{\alpha}} D^{\underline{\alpha}}_{n,m}[U] + D^4_{n,m} \right\} e^{-i\varphi m_{\underline{\alpha}}} \Big)\psi^c_m. \tag{3.4}$$

Both operators in the lower line of eq. (3.4) have the structure of the $\hat{e}_{\underline{\alpha}}$ component of the lattice covariant derivative of eq. (1.37). This term is abbreviated as

$$\{\mathcal{D}\psi\}_n = \tfrac{1+d}{2a} \left(U^{\underline{\alpha}}_n e^{-i\varphi(n_{\underline{\alpha}}+1)}\psi^c_{n+\hat{e}_{\underline{\alpha}}} - U^{\underline{\alpha}\dagger}_{n-\hat{e}_{\underline{\alpha}}} e^{-i\varphi(n_{\underline{\alpha}}-1)}\psi^c_{n-\hat{e}_{\underline{\alpha}}} \right)$$

and satisfies a lattice product rule for sufficiently small values of a and φ,

$$\{\mathcal{D}\psi\}_n = (1+d)e^{-i\varphi n_{\underline{\alpha}}} \left(D^{\underline{\alpha}}_{n,m}[U]\psi^c_m - i\tfrac{\varphi}{2a} \left\{ U^{\underline{\alpha}}_n\psi^c_{n+\hat{e}_{\underline{\alpha}}} + U^{\underline{\alpha}\dagger}_{n-\hat{e}_{\underline{\alpha}}}\psi^c_{n-\hat{e}_{\underline{\alpha}}} \right\} + \mathcal{O}(\varphi^2) \right)$$

$$= (1+d)e^{-i\varphi n_{\underline{\alpha}}} \left(D^{\underline{\alpha}}_{n,m}[U]\psi^c_m - 2i\tfrac{\varphi}{2a}\psi^c_n + \mathcal{O}(a, \varphi^2) \right)$$

$$= e^{-i\frac{\varphi}{a}an_{\alpha}} \left\{ (1+d)D^{\underline{\alpha}}_{n,m}[U] - i\frac{(1+d)\varphi}{a}\delta_{n,m} \right\}\psi^c_m + \mathcal{O}(a, \varphi^2). \tag{3.5}$$

When the lattice product rule of eq. (3.5) is plugged into the fermion action of eq. (3.4), the last remaining phase factors cancel and the action up to effects of $\mathcal{O}(a, \varphi^2)$ reads

$$S^f[\psi^c, \bar\psi^c, U] = a^4 \sum_{n,m\in\Lambda} \bar\psi^c_n \left(D^N_{n,m} + D^{KW}_{n,m} + i\tfrac{c-(1+d)\varphi}{a}\gamma^{\underline{\alpha}}\delta_{n,m} + D^4_{n,m} + m_0\delta_{n,m} \right)\psi^c_m, \tag{3.6}$$

where $D^3_{n,m}$ and the second term of eq. (3.5) have been combined. After the phase φ is fixed to

$$\varphi = \frac{\delta c}{1+d}, \tag{3.7}$$

the mismatch δc of the relevant counterterm's coefficient appears exclusively in the combination of eq. (3.7) in the boundary conditions of the fermion fields ψ^c and $\bar\psi^c$ up to corrections of $\mathcal{O}(a, \varphi^2)$. The remaining coefficient $c(g_0)$ of the divergent operator exactly cancels power divergent interaction effects. Hence, fields with extended support on multiple sites can be constructed from ψ^c and $\bar\psi^c$.

3.1.2 Decomposition in the free theory

Decomposition of spinor fields into components that differ in chirality and spin due to having different momentum support has been in use for various types of lattice fermions for a long time (e.g. [80,99,147]). Decomposition for minimally doubled fermions featured first in [18, 145] and is generalised in the following. Components ϕ and χ of spinors ψ for Karsten-Wilczek fermions are defined by a summation of the full lattice using *decomposition kernels* g^ϕ and g^χ that restrict the components' momentum support as

$$
\begin{aligned}
\psi_n &= \sum_{k\in\Lambda} g^\phi_{n,k}\phi_k + (-1)^{n_\alpha}\mathcal{Q}g^\chi_{n,k}\chi_k \\
\bar\psi_n &= \sum_{k\in\Lambda} \bar\phi_k(g^\phi_{n,k})^\dagger + (-1)^{n_\alpha}\bar\chi_k\bar{\mathcal{Q}}(g^\chi_{n,k})^\dagger
\end{aligned} \tag{3.8}
$$

The symbols $\mathcal{Q}$ and $\bar{\mathcal{Q}}$ represent a priori unknown matrices that allow for mixtures of two components with different spin and chirality into the same original spinor fields. Because the matrices later turn out to be the same objects as in eq. (2.31), the same symbols $\mathcal{Q}$ and $\bar{\mathcal{Q}}$ are used here as well. The alternating factor $(-1)^{n_\alpha}$ accounts for momentum support at different poles in the Brillouin zone according to eq. (1.62). The only required properties of decomposition kernels here are a reasonably fast decrease for increasing distance $|n-k|$ and a Kronecker symbol $\delta_{n,k}$ in the limit $a \to 0$,

$$
g^\phi_{n,k} = \delta_{n,k} + \mathcal{O}(a), \qquad g^\chi_{n,k} = \delta_{n,k} + \mathcal{O}(a). \tag{3.9}
$$

This decomposition is a generalisation of the decomposition in [145] with more general decomposition kernels. The field components ϕ and χ do not necessarily have a simple relation to the physical flavours of the theory (cf. the discussion in section 2 of [80]). Combinations of matrices and factors $(-1)^{n_\alpha}$ are wrapped up into a concise notation as

$$
\mathcal{R}_n = (-1)^{n_\alpha}\,\mathcal{Q}, \qquad \bar{\mathcal{R}}_n = (-1)^{n_\alpha}\,\bar{\mathcal{Q}}. \tag{3.10}
$$

The decomposition of eq. (3.8) is plugged into the Karsten-Wilczek fermion action of eq. (3.1) neglecting counterterms and interactions initially. Hence, the action reads

$$
S^f[\phi,\bar\phi,\chi,\bar\chi] = a^4 \sum_{k,l\in\Lambda} \mathcal{L}^{\bar\phi\phi}[\phi_l,\bar\phi_k] + \mathcal{L}^{\bar\chi\chi}[\chi_l,\bar\chi_k] + \mathcal{L}^{\bar\phi\chi}[\chi_l,\bar\phi_k] + \mathcal{L}^{\bar\chi\phi}[\phi_l,\bar\chi_k], \tag{3.11}
$$

$$
\mathcal{L}^{\bar\phi\phi}[\phi_l,\bar\phi_k] = \sum_{n,m\in\Lambda} \bar\phi_k(g^\phi_{n,k})^\dagger \left(D^N_{n,m} + D^{KW}_{n,m} + m_0\delta_{n,m}\right) g^\phi_{m,l}\phi_l, \tag{3.12}
$$

$$
\mathcal{L}^{\bar\chi\chi}[\chi_l,\bar\chi_k] = \sum_{n,m\in\Lambda} \bar\chi_k(g^\chi_{n,k})^\dagger\bar{\mathcal{R}}_n \left(D^N_{n,m} + D^{KW}_{n,m} + m_0\delta_{n,m}\right) \mathcal{R}_m g^\chi_{m,l}\chi_l, \tag{3.13}
$$

$$
\mathcal{L}^{\bar\phi\chi}[\chi_l,\bar\phi_k] = \sum_{n,m\in\Lambda} \bar\phi_k(g^\phi_{n,k})^\dagger \left(D^N_{n,m} + D^{KW}_{n,m} + m_0\delta_{n,m}\right) \mathcal{R}_m g^\chi_{m,l}\chi_l, \tag{3.14}
$$

$$
\mathcal{L}^{\bar\chi\phi}[\phi_l,\bar\chi_k] = \sum_{n,m\in\Lambda} \bar\chi_k(g^\chi_{n,k})^\dagger\bar{\mathcal{R}}_n \left(D^N_{n,m} + D^{KW}_{n,m} + m_0\delta_{n,m}\right) g^\phi_{m,l}\phi_l. \tag{3.15}
$$

Next, decomposition kernels are treated as part of the Dirac kernels for field components. Thus, the Dirac kernel $K_{k,l}^{\bar{\chi},\chi}$ in the Lagrangian $\mathcal{L}^{\bar{\chi}\chi}[\chi_l, \bar{\chi}_k] = \bar{\chi}_k K_{k,l}^{\bar{\chi},\chi} \chi_l$ of eq. (3.13) reads

$$
K_{k,l}^{\bar{\chi},\chi} = \sum_{n \in \Lambda} (g_{n,k}^\chi)^\dagger \Big(\sum_{\mu \neq \underline{\alpha}} \frac{1}{2a} \bar{\mathcal{R}}_n \gamma^\mu \mathcal{R}_n \big\{ g_{n+\hat{e}_\mu,l}^\chi - g_{n-\hat{e}_\mu,l}^\chi \big\} + m_0 \bar{\mathcal{R}}_n \mathcal{R}_n g_{n,l}^\chi
$$
$$
+ \frac{1}{2a} \big\{ \bar{\mathcal{R}}_n \gamma^{\underline{\alpha}} \mathcal{R}_{n+\underline{\hat{\alpha}}} g_{n+\hat{e}_{\underline{\alpha}},l}^\chi - \bar{\mathcal{R}}_n \gamma^{\underline{\alpha}} \mathcal{R}_{n-\underline{\hat{\alpha}}} g_{n-\hat{e}_{\underline{\alpha}},l}^\chi \big\}
$$
$$
+ \frac{i\zeta}{2a} \bar{\mathcal{R}}_n \gamma^{\underline{\alpha}} \mathcal{R}_n \sum_{\mu \neq \underline{\alpha}} \big\{ g_{n+\hat{e}_\mu,l}^\chi + g_{n-\hat{e}_\mu,l}^\chi - 2g_{n,l}^\chi \big\} \Big). \tag{3.16}
$$

The structure of the lattice derivatives in the $\hat{e}_{\underline{\alpha}}$ direction simplifies, because

$$
\bar{\mathcal{R}}_n \mathcal{M} \mathcal{R}_{n\pm\underline{\hat{\alpha}}} = -\bar{\mathcal{R}}_n \mathcal{M} \mathcal{R}_n = -\bar{\mathcal{Q}} \mathcal{M} \mathcal{Q} \tag{3.17}
$$

is valid for arbitrary matrices $\mathcal{M}$. Hence, the Dirac kernel $K_{k,l}^{\bar{\chi},\chi}$ reads

$$
K_{k,l}^{\bar{\chi},\chi} = \sum_{n \in \Lambda} (g_{n,k}^\chi)^\dagger \Big(\sum_{\mu \neq \underline{\alpha}} \frac{1}{2a} (\bar{\mathcal{Q}} \gamma^\mu \mathcal{Q}) \big\{ g_{n+\hat{e}_\mu,l}^\chi - g_{n-\hat{e}_\mu,l}^\chi \big\} + m_0 (\bar{\mathcal{Q}} \mathcal{Q}) g_{n,l}^\chi
$$
$$
- \frac{1}{2a} (\bar{\mathcal{Q}} \gamma^{\underline{\alpha}} \mathcal{Q}) \big\{ g_{n+\hat{e}_{\underline{\alpha}},l}^\chi - g_{n-\hat{e}_{\underline{\alpha}},l}^\chi \big\}
$$
$$
+ \frac{i\zeta}{2a} (\bar{\mathcal{Q}} \gamma^{\underline{\alpha}} \mathcal{Q}) \sum_{\mu \neq \underline{\alpha}} \big\{ g_{n+\hat{e}_\mu,l}^\chi + g_{n-\hat{e}_\mu,l}^\chi - 2g_{n,l}^\chi \big\} \Big). \tag{3.18}
$$

Components ϕ and χ satisfy the same field equations in the limit $a \to 0$ if and only if the Dirac kernels of Lagrangians $\mathcal{L}^{\bar{\phi}\phi}[\phi_l, \bar{\phi}_k]$ and $\mathcal{L}^{\bar{\chi}\chi}[\chi_l, \bar{\chi}_k]$ take the same form in the limit $a \to 0$. As the limit $a \to 0$ of the decomposition kernels is taken, this implies three conditions for the matrices $\mathcal{Q}$ and $\bar{\mathcal{Q}}$:

$$
\left\{
\begin{array}{rll}
(\bar{\mathcal{Q}} \mathcal{Q}) = & 1 & \text{equality of the mass term} \\
(\bar{\mathcal{Q}} \gamma^\mu \mathcal{Q}) = & \gamma^\mu & \text{equality of the perpendicular kinetic term} \\
(\bar{\mathcal{Q}} \gamma^{\underline{\alpha}} \mathcal{Q}) = & -\gamma^{\underline{\alpha}} & \text{equality of the parallel kinetic term}
\end{array}
\right\}. \tag{3.19}
$$

It is evident that the set of conditions requires that $\mathcal{Q}$ and $\bar{\mathcal{Q}}$ equal the matrices of eq. (2.31) up to choices of the arbitrary phase ϑ. Because the Karsten-Wilczek term is the leading order correction to the naïve continuum limit of the Karsten-Wilczek Dirac operator and has opposite sign in the kernels $K_{k,l}^{\bar{\phi},\phi}$ and $K_{k,l}^{\bar{\chi},\chi}$, the components satisfy field equations that differ at finite lattice spacing a by the sign of the Karsten-Wilczek term's contribution. This is the coordinate space analogue to eq. (2.33). Component-mixing Lagrangians $\mathcal{L}^{\bar{\phi}\chi}[\chi_l, \bar{\phi}_k]$ and $\mathcal{L}^{\bar{\chi}\phi}[\phi_l, \bar{\chi}_k]$ of eqs. (3.14) and (3.15) have Dirac kernels $K_{k,l}^{\bar{\phi},\chi}$

and $K^{\bar{\chi},\phi}_{k,l}$ which read

$$
\begin{aligned}
K^{\bar{\phi},\chi}_{k,l} = \sum_{n\in\Lambda} e^{i(\frac{\pi}{2}+\vartheta)}(-1)^{n_{\underline{\alpha}}}(g^{\phi}_{n,k})^{\dagger} \Big(&\sum_{\mu,\nu,\lambda} \frac{1}{4a}(-i\Sigma^{\lambda\nu}\epsilon^{\nu\lambda\mu\underline{\alpha}})\big\{g^{\chi}_{n+\hat{e}_{\mu},l} - g^{\chi}_{n-\hat{e}_{\mu},l}\big\} \\
&+ \frac{1}{2a}\gamma^5\big\{g^{\chi}_{n+\hat{e}_{\underline{\alpha}},l} - g^{\chi}_{n-\hat{e}_{\underline{\alpha}},l}\big\} + m_0\gamma^{\underline{\alpha}}\gamma^5 g^{\chi}_{n,l} \\
&+ \frac{i\zeta}{2a}\gamma^5 \sum_{\mu\neq\underline{\alpha}} \big\{g^{\chi}_{n+\hat{e}_{\mu},l} + g^{\chi}_{n-\hat{e}_{\mu},l} - 2g^{\chi}_{n,l}\big\}\Big), \quad (3.20)
\end{aligned}
$$

$$
\begin{aligned}
K^{\bar{\chi},\phi}_{k,l} = \sum_{n\in\Lambda} e^{i(\frac{\pi}{2}-\vartheta)}(-1)^{n_{\underline{\alpha}}}(g^{\chi}_{n,k})^{\dagger} \Big(&\sum_{\mu,\nu,\lambda} \frac{1}{4a}(-i\Sigma^{\lambda\nu}\epsilon^{\nu\lambda\mu\underline{\alpha}})\big\{g^{\phi}_{n+\hat{e}_{\mu},l} - g^{\phi}_{n-\hat{e}_{\mu},l}\big\} \\
&+ \frac{1}{2a}\gamma^5\big\{g^{\phi}_{n+\hat{e}_{\underline{\alpha}},l} - g^{\phi}_{n-\hat{e}_{\underline{\alpha}},l}\big\} + m_0\gamma^{\underline{\alpha}}\gamma^5 g^{\phi}_{n,l} \\
&- \frac{i\zeta}{2a}\gamma^5 \sum_{\mu\neq\underline{\alpha}} \big\{g^{\phi}_{n+\hat{e}_{\mu},l} + g^{\phi}_{n-\hat{e}_{\mu},l} - 2g^{\phi}_{n,l}\big\}\Big). \quad (3.21)
\end{aligned}
$$

The role of these terms in the limit $a \to 0$ is clarified by a Fourier transform of the component fields to momentum space. Hereby, the limit $a \to 0$ of decomposition kernels g^{ϕ} and g^{χ} is taken according to eq. (3.9). The component-mixing piece of the action up to corrections of $\mathcal{O}(a)$ reads

$$
\begin{aligned}
S' = &\ e^{i(\frac{\pi}{2}+\vartheta)} \int \frac{d^4q}{(2\pi)^4} \bar{\phi}(q + \frac{\pi}{a}\hat{e}_{\underline{\alpha}}) \Big\{\gamma^5 q^{\underline{\alpha}} + m_0\gamma^{\underline{\alpha}}\gamma^5 - \frac{i}{2}\Sigma^{\lambda\nu}\epsilon^{\nu\lambda\mu\underline{\alpha}}q^{\mu}\Big\} \chi(q) \\
&+ e^{i(\frac{\pi}{2}-\vartheta)} \int \frac{d^4q}{(2\pi)^4} \bar{\chi}(q + \frac{\pi}{a}\hat{e}_{\underline{\alpha}}) \Big\{\gamma^5 q^{\underline{\alpha}} + m_0\gamma^{\underline{\alpha}}\gamma^5 - \frac{i}{2}\Sigma^{\lambda\nu}\epsilon^{\nu\lambda\mu\underline{\alpha}}q^{\mu}\Big\} \phi(q) + \mathcal{O}(a). \\
&\hspace{11cm} (3.22)
\end{aligned}
$$

If either component has small four-momentum q in the vicinity of the pole $q^2 = 0$, the four-momentum $q + \pi/a\,\hat{e}_{\underline{\alpha}}$ of the other component in eq. (3.22) is inevitably near the pole at the cutoff. Thus, both components decouple in the limit $a \to 0$ of the free theory. This result has been discussed already by Pernici [129]. Moreover, decomposition kernels g^{ϕ} and g^{χ} can be defined on non-overlapping regions of the Brillouin zone enforcing $|q_{\underline{\alpha}}| \leq \pi/(2a)$ for component momenta. This definition manifestly prohibits mixing of components without four-momentum exchange. Tiburzi applied this scheme in a calculation of the chiral anomaly for Karsten-Wilczek fermions [145]. Putting everything together, the simplified free Lagrangians for the components read

$$
S^f[\phi,\bar{\phi},\chi,\bar{\chi}] = a^4 \sum_{k,l\in\Lambda} \mathcal{L}^{\bar{\phi}\phi}[\phi_l,\bar{\phi}_k] + \mathcal{L}^{\bar{\chi}\chi}[\chi_l,\bar{\chi}_k] + \mathcal{L}^{\bar{\phi}\chi}[\chi_l,\bar{\phi}_k] + \mathcal{L}^{\bar{\chi}\phi}[\phi_l,\bar{\chi}_k] \quad (3.23)
$$

$$\mathcal{L}^{\bar{\phi}\phi}[\phi_l, \bar{\phi}_k] = \sum_{n,m \in \Lambda} \bar{\phi}_k (g_{n,k}^\phi)^\dagger \left(D_{n,m}^N + D_{n,m}^{KW} + m_0 \delta_{n,m} \right) g_{m,l}^\phi \phi_l, \tag{3.24}$$

$$\mathcal{L}^{\bar{\chi}\chi}[\chi_l, \bar{\chi}_k] = \sum_{n,m \in \Lambda} \bar{\chi}_k (g_{n,k}^\chi)^\dagger \left(D_{n,m}^N - D_{n,m}^{KW} + m_0 \delta_{n,m} \right) g_{m,l}^\chi \chi_l, \tag{3.25}$$

$$\mathcal{L}^{\bar{\phi}\chi}[\chi_l, \bar{\phi}_k] = \sum_{n,m \in \Lambda} \bar{\phi}_k (-1)^{n_{\underline{\alpha}}} (g_{n,k}^\phi)^\dagger \left(D_{n,m}^N + D_{n,m}^{KW} + m_0 \delta_{n,m} \right) \mathcal{Q} g_{m,l}^\chi \chi_l, \tag{3.26}$$

$$\mathcal{L}^{\bar{\chi}\phi}[\phi_l, \bar{\chi}_k] = \sum_{n,m \in \Lambda} \bar{\chi}_k (-1)^{n_{\underline{\alpha}}} (g_{n,k}^\chi)^\dagger \left(D_{n,m}^N - D_{n,m}^{KW} + m_0 \delta_{n,m} \right) \bar{\mathcal{Q}} g_{m,l}^\phi \phi_l. \tag{3.27}$$

It is made explicit how the Karsten-Wilczek term distinguishes between both components and how they decouple in the limit $a \to 0$ of the free theory. The component-mixing terms contain alternating factors $(-1)^{n_{\underline{\alpha}}}$ that do not cancel because of contributions from different regions of the Brillouin zone. This phenomenon is well-known from staggered fermions [80].

3.1.3 Absorption of the coefficient into component fields

The preceding derivation in section 3.1.2 defines field components for free Karsten-Wilczek fermions. In the limit $a \to 0$, they satisfy the same field equations and decouple. Nevertheless, the Karsten-Wilczek term contributes differently to their field equations at finite lattice spacing. It seems plausible that components can still be defined for sufficiently weak interactions. Such ideas have been extensively discussed for the case of staggered fermions in [80]. However, local gauge invariance requires generalisation of the previous definition of components using decomposition kernels $g^\phi[U]$ and $g^\chi[U]$ as

$$\begin{aligned} \psi_n &= \sum_{k \in \Lambda} e^{-i\varphi^\phi n_{\underline{\alpha}}} g_{n,k}^\phi[U] \phi_k + (-e^{-i\varphi^\chi})^{n_{\underline{\alpha}}} \mathcal{Q} g_{n,k}^\chi[U] \chi_k \\ \bar{\psi}_n &= \sum_{k \in \Lambda} \bar{\phi}_k (g_{n,k}^\phi[U])^\dagger e^{i\varphi^\phi n_{\underline{\alpha}}} + (-e^{i\varphi^\chi})^{n_{\underline{\alpha}}} \bar{\chi}_k \bar{\mathcal{Q}} (g_{n,k}^\chi[U])^\dagger \end{aligned}. \tag{3.28}$$

Smooth transition from interacting to free theory without counterterms requires

$$\lim_{c,d,g_0 \to 0} \varphi^\phi = \lim_{c,d,g_0 \to 0} \varphi^\chi = 0. \tag{3.29}$$

Gauge invariance of component bilinears requires that the decomposition kernels $g_{n,k}^\phi[U]$ and $g_{n,k}^\chi[U]$ include parallel transport. This can be achieved by a definition as products of the free theory's decomposition kernels $g_{n,k}^\phi$ and $g_{n,k}^\chi$ and Wilson lines[2] between sites n and k. The concise notation of eq. (3.10) is generalised by including phase factors

---

[2]In [145], Tiburzi defines components of the free Karsten-Wilczek action ($\underline{\alpha} = 0$) with extended support in the $\hat{e}_0$ direction ("energy smearing"). In this case, parallel transport of the component fields can be achieved by the path-ordered products of gauge links U^0 between n and k (the shortest possible Wilson line). There is no simple shortest Wilson line if the components' support is not restricted to a single axis. This is necessarily the case for Boriçi-Creutz fermions, where the components are spread out along the hypercube's diagonal. In such a case, a scheme must either define a single path or the average of multiple paths for parallel transport (cf. similar ideas in [152]).

$e^{\pm i\varphi^\chi}$ into matrices $\mathcal{R}_n^{\varphi^\chi}$ and $\bar{\mathcal{R}}_n^{\varphi^\chi}$ and phase factors $e^{\pm i\varphi^\phi}$ into scalar factors $r_n^{\varphi^\phi}$ and $\bar{r}_n^{\varphi^\phi}$. These new abbreviations read

$$\left\{ \begin{array}{llll} \mathcal{R}_n^{\varphi^\chi} = & (-e^{-i\varphi^\chi})^{n_{\underline{\alpha}}}\, \mathcal{Q}, & \bar{\mathcal{R}}_n^{\varphi^\chi} = & (-e^{+i\varphi^\chi})^{n_{\underline{\alpha}}}\, \bar{\mathcal{Q}} \\ r_n^{\varphi^\phi} = & (+e^{-i\varphi^\phi})^{n_{\underline{\alpha}}}, & \bar{r}_n^{\varphi^\phi} = & (+e^{+i\varphi^\phi})^{n_{\underline{\alpha}}} \end{array} \right\}. \tag{3.30}$$

The decomposition of eq. (3.28) is plugged into the Karsten-Wilczek fermion action of eq. (3.1) for the interacting theory as it is done for the free theory in eq. (3.11). The fermion action is decomposed into the sum of four Lagrangians,

$$S^f[\phi,\bar{\phi},\chi,\bar{\chi},U] = a^4 \sum_{k,l\in\Lambda} \mathcal{L}^{\bar{\phi}\phi}[\phi_l,\bar{\phi}_k,U] + \mathcal{L}^{\bar{\chi}\chi}[\chi_l,\bar{\chi}_k,U] + \mathcal{L}^{\bar{\phi}\chi}[\chi_l,\bar{\phi}_k,U] + \mathcal{L}^{\bar{\chi}\phi}[\phi_l,\bar{\chi}_k,U], \tag{3.31}$$

$$\mathcal{L}^{\bar{\phi}\phi}[\phi_l,\bar{\phi}_k,U] = \sum_{n,m} \bar{\phi}_k (g_{n,k}^\phi[U])^\dagger \bar{r}_n^{\varphi^\phi} \left(D_{n,m}^N + D_{n,m}^{KW} + D_{n,m}^3 + D_{n,m}^4 + m_0\delta_{n,m}\right) r_m^{\varphi^\phi} g_{m,l}^\phi[U]\phi_l, \tag{3.32}$$

$$\mathcal{L}^{\bar{\chi}\chi}[\chi_l,\bar{\chi}_k,U] = \sum_{n,m} \bar{\chi}_k (g_{n,k}^\chi[U])^\dagger \bar{\mathcal{R}}_n^{\varphi^\chi} \left(D_{n,m}^N + D_{n,m}^{KW} + D_{n,m}^3 + D_{n,m}^4 + m_0\delta_{n,m}\right) \mathcal{R}_m^{\varphi^\chi} g_{m,l}^\chi[U]\chi_l, \tag{3.33}$$

$$\mathcal{L}^{\bar{\phi}\chi}[\chi_l,\bar{\phi}_k,U] = \sum_{n,m} \bar{\phi}_k (g_{n,k}^\phi[U])^\dagger \bar{r}_n^{\varphi^\phi} \left(D_{n,m}^N + D_{n,m}^{KW} + D_{n,m}^3 + D_{n,m}^4 + m_0\delta_{n,m}\right) \mathcal{R}_m^{\varphi^\chi} g_{m,l}^\chi[U]\chi_l, \tag{3.34}$$

$$\mathcal{L}^{\bar{\chi}\phi}[\phi_l,\bar{\chi}_k,U] = \sum_{n,m} \bar{\chi}_k (g_{n,k}^\chi[U])^\dagger \bar{\mathcal{R}}_n^{\varphi^\chi} \left(D_{n,m}^N + D_{n,m}^{KW} + D_{n,m}^3 + D_{n,m}^4 + m_0\delta_{n,m}\right) r_m^{\varphi^\phi} g_{m,l}^\phi[U]\phi_l. \tag{3.35}$$

Dirac kernels (e.g. $\mathcal{K}_{k,l}^{\bar{\chi},\chi}$) of the Lagrangians are defined analogously to the free theory in section 3.1.2. The analogue of eq. (3.17) in the interacting theory is

$$\bar{\mathcal{R}}_n^{\varphi^\chi} \mathcal{M} \mathcal{R}_{n\pm\hat{\underline{\alpha}}}^{\varphi^\chi} = -e^{\mp i\varphi^\chi} \bar{\mathcal{R}}_n^{\varphi^\chi} \mathcal{M} \mathcal{R}_n^{\varphi^\chi} = -e^{\mp i\varphi^\chi} \bar{\mathcal{Q}}\mathcal{M}\mathcal{Q}, \quad \bar{r}_n^{\varphi^\phi} \mathcal{M} r_{n\pm\hat{\underline{\alpha}}}^{\varphi^\phi} = +e^{\mp i\varphi^\phi}\mathcal{M}. \tag{3.36}$$

Hence, parallel kinetic terms of both Dirac kernels $\mathcal{K}_{k,l}^{\bar{\phi},\phi}$ and $\mathcal{K}_{k,l}^{\bar{\chi},\chi}$ include phase factors like those which feature in eq. (3.4),

$$K_{k,l}^{\bar{\phi},\phi} = \sum_{n\in\Lambda} (g_{n,k}^\phi[U])^\dagger \left(+\sum_{\mu\neq\underline{\alpha}} \frac{1}{2a}\gamma^\mu \left\{ U_n^\mu g_{n+\hat{e}_\mu,l}^\phi[U] - U_{n-\hat{e}_\mu}^{\mu\dagger} g_{n-\hat{e}_\mu,l}^\phi[U] \right\} + m_0 g_{n,l}^\phi \right.$$
$$\left. + \gamma^{\underline{\alpha}} \left[\frac{1+d}{2a} \left\{ e^{-i\varphi^\phi} U_n^{\underline{\alpha}} g_{n+\hat{e}_{\underline{\alpha}},l}^\phi[U] - e^{+i\varphi^\phi} U_{n-\hat{e}_{\underline{\alpha}}}^{\underline{\alpha}\dagger} g_{n-\hat{e}_{\underline{\alpha}},l}^\phi[U] \right\} + i\frac{c}{a} g_{n,l}^\phi[U] \right] \right.$$
$$\left. + \frac{i\zeta}{2a}\gamma^{\underline{\alpha}} \sum_{\mu\neq\underline{\alpha}} \left\{ U_n^\mu g_{n+\hat{e}_\mu,l}^\chi[U] + U_{n-\hat{e}_\mu}^{\mu\dagger} g_{n-\hat{e}_\mu,l}^\chi[U] - 2g_{n,l}^\chi[U] \right\} \right),$$

$$K_{k,l}^{\bar{\chi},\chi} = \sum_{n\in\Lambda} (g_{n,k}^\chi[U])^\dagger \left(+\sum_{\mu\neq\underline{\alpha}} \frac{1}{2a}\bar{\mathcal{Q}}\gamma^\mu\mathcal{Q} \left\{ U_n^\mu g_{n+\hat{e}_\mu,l}^\chi[U] - U_{n-\hat{e}_\mu}^{\mu\dagger} g_{n-\hat{e}_\mu,l}^\chi[U] \right\} + m_0\bar{\mathcal{Q}}\mathcal{Q}g_{n,l}^\chi[U] \right.$$
$$\left. - \bar{\mathcal{Q}}\gamma^{\underline{\alpha}}\mathcal{Q} \left[\frac{1+d}{2a} \left\{ e^{-i\varphi^\chi} U_n^{\underline{\alpha}} g_{n+\hat{e}_{\underline{\alpha}},l}^\chi[U] - e^{+i\varphi^\chi} U_{n-\hat{e}_{\underline{\alpha}}}^{\underline{\alpha}\dagger} g_{n-\hat{e}_{\underline{\alpha}},l}^\chi[U] \right\} - i\frac{c}{a} g_{n,l}^\chi[U] \right] \right.$$
$$\left. + \frac{i\zeta}{2a}\bar{\mathcal{Q}}\gamma^{\underline{\alpha}}\mathcal{Q} \sum_{\mu\neq\underline{\alpha}} \left\{ U_n^\mu g_{n+\hat{e}_\mu,l}^\chi[U] + U_{n-\hat{e}_\mu}^{\mu\dagger} g_{n-\hat{e}_\mu,l}^\chi[U] - 2g_{n,l}^\chi[U] \right\} \right).$$

The lattice product rule of eq. (3.5) applies and yields up to $\mathcal{O}(a, \varphi^2)$

$$\frac{1+d}{2a}\left\{e^{-i\varphi^\phi}U_{\underline{n}}^{\alpha}g_{n+\hat{e}_{\underline{\alpha}},l}^{\phi}[U] - e^{+i\varphi^\phi}U_{n-\hat{e}_{\underline{\alpha}}}^{\alpha\dagger}g_{n-\hat{e}_{\underline{\alpha}},l}^{\phi}[U]\right\} + i\frac{c}{a}g_{n,l}^{\phi}[U]$$

$$= \{1+d\}D_{n,m}^{\alpha}g_{m,l}^{\phi}[U] + i\frac{c-(1+d)\varphi^\phi}{a}g_{n,l}^{\phi}[U], \tag{3.37}$$

$$\frac{1+d}{2a}\left\{e^{-i\varphi^\chi}U_{\underline{n}}^{\alpha}g_{n+\hat{e}_{\underline{\alpha}},l}^{\chi}[U] - e^{+i\varphi^\chi}U_{n-\hat{e}_{\underline{\alpha}}}^{\alpha\dagger}g_{n-\hat{e}_{\underline{\alpha}},l}^{\chi}[U]\right\} - i\frac{c}{a}g_{n,l}^{\chi}[U]$$

$$= \{1+d\}D_{n,m}^{\alpha}g_{m,l}^{\chi}[U] - i\frac{c+(1+d)\varphi^\chi}{a}g_{n,l}^{\chi}[U]. \tag{3.38}$$

Unmatched divergent operators in eqs. (3.37) and (3.38) must cancel before a expansion in a can be attempted. A divergence due to a mismatch of coefficients as in eq. (3.2) cancels if the phases φ^ϕ and φ^χ satisfy two different conditions,

$$\varphi^\phi = \frac{\delta c}{1+d}, \qquad \varphi^\chi = -\frac{\delta c}{1+d}. \tag{3.39}$$

This implies $\varphi \equiv \varphi^\phi = -\varphi^\chi$. Because $\delta c \overset{c,d,g_0\to0}{\to} 0$, these phases satisfy the requirement of eq. (3.29) for a smooth transition to the free theory. The opposite sign of phases for both components has been already pointed out in [129]. The difference is not surprising in the light of section 2.3.1, since c is an odd function of the Wilczek parameter ζ. Hence, it affects the Dirac field χ of the second component with momentum support near $p = \pi/a\hat{e}_{\underline{\alpha}}$ as $-c$. The first component ϕ with momentum support near $p = 0$ is treated like the spinor field ψ^c that was discussed in section 3.1.1. The phase factors $\pm e^{\mp i\varphi}$ can be interpreted as plane wave terms of a Fourier transform that ensure that each pole corresponds to a component with vanishing four-momentum. If the conditions of eq. (3.39) are met, the mismatched divergent operator ($\propto \delta c$) is removed from the Dirac kernels $\mathcal{K}_{k,l}^{\bar{\phi},\phi}$ and $\mathcal{K}_{k,l}^{\bar{\chi},\chi}$. The remainder of the counterterm operator ($\propto c(g_0)$) exactly cancels the divergences due to interaction effects. The condition for the matrices $\mathcal{Q}$ and $\bar{\mathcal{Q}}$ in the interacting theory remains the same as in eq. (3.19).

Though the mismatched coefficient δc of the divergent operator ceases to appear explicitly in the Lagrangians $\mathcal{L}^{\bar{\phi}\phi}[\phi_l, \bar{\phi}_k, U]$ and $\mathcal{L}^{\bar{\chi}\chi}[\chi_l, \bar{\chi}_k, U]$, it persists in the components' boundary conditions due to their definition in eq. (3.28). Nevertheless, the component-mixing Lagrangians $\mathcal{L}^{\bar{\phi}\chi}[\chi_l, \bar{\phi}_k, U]$ and $\mathcal{L}^{\bar{\chi}\phi}[\phi_l, \bar{\chi}_k, U]$ of eqs. (3.34) and (3.35) retain its explicit appearance. Their Dirac kernels $K_{k,l}^{\bar{\phi},\chi}$ and $K_{k,l}^{\bar{\chi},\phi}$ explictly depend on the mismatched coefficient δc through phases φ^ϕ and φ^χ, which fail to cancel in

$$K_{k,l}^{\bar{\phi},\chi} = \sum_{n\in\Lambda} e^{i(\frac{\pi}{2}+\vartheta)}(-e^{+i(\varphi^\phi-\varphi^\chi)})^{n_{\underline{\alpha}}}(g_{n,k}^{\phi}[U])^\dagger\Big(+\frac{1+d}{2a}\gamma^5\left\{U_{\underline{n}}^{\alpha}g_{n+\hat{e}_{\underline{\alpha}},l}^{\chi}[U] - U_{n-\hat{e}_{\underline{\alpha}}}^{\alpha\dagger}g_{n-\hat{e}_{\underline{\alpha}},l}^{\chi}[U]\right\}$$

$$+ \sum_{\mu,\nu,\lambda}\frac{1}{4a}(-i\Sigma^{\lambda\nu}\epsilon^{\nu\lambda\mu\underline{\alpha}})\left\{U_n^\mu g_{n+\hat{e}_\mu,l}^{\chi}[U] - U_{n-\hat{e}_\mu}^{\mu\dagger}g_{n-\hat{e}_\mu,l}^{\chi}[U]\right\} + m_0\gamma^\alpha\gamma^5 g_{n,l}^{\chi}[U]$$

$$+ \frac{i\zeta}{2a}\gamma^5\sum_{\mu\neq\underline{\alpha}}\left\{U_n^\mu g_{n+\hat{e}_\mu,l}^{\chi}[U] + U_{n-\hat{e}_\mu}^{\mu\dagger}g_{n-\hat{e}_\mu,l}^{\chi}[U] - 2g_{n,l}^{\chi}[U]\right\} + i\gamma^5\frac{c+(1+d)\varphi^\chi}{a}g_{n,l}^{\chi}[U]\Big),$$

$$\tag{3.40}$$

$$K^{\bar{\chi},\phi}_{k,l} = \sum_{n\in\Lambda} e^{i(\frac{\pi}{2}-\vartheta)}(-e^{-i(\varphi^\phi-\varphi^\chi)})^{n_{\underline{\alpha}}}(g^\chi_{n,k}[U])^\dagger\Big(+\frac{1+d}{2a}\gamma^5\Big\{U^{\underline{\alpha}}_n g^\phi_{n+\hat{e}_{\underline{\alpha}},l}[U] - U^{\underline{\alpha}\dagger}_{n-\hat{e}_{\underline{\alpha}}}g^\phi_{n-\hat{e}_{\underline{\alpha}},l}[U]\Big\}$$

$$+\sum_{\mu,\nu,\lambda}\frac{1}{4a}(-i\Sigma^{\lambda\nu}\epsilon^{\nu\lambda\mu\underline{\alpha}})\Big\{U^\mu_n g^\phi_{n+\hat{e}_\mu,l}[U] - U^{\mu\dagger}_{n-\hat{e}_\mu}g^\phi_{n-\hat{e}_\mu,l}[U]\Big\} + m_0\gamma^{\underline{\alpha}}\gamma^5 g^\phi_{n,l}[U]$$

$$-\frac{i\zeta}{2a}\gamma^5\sum_{\mu\neq\underline{\alpha}}\Big\{U^\mu_n g^\phi_{n+\hat{e}_\mu,l}[U] + U^{\mu\dagger}_{n-\hat{e}_\mu}g^\phi_{n-\hat{e}_\mu[U],l} - 2g^\phi_{n,l}[U]\Big\} - i\gamma^5\frac{c-(1+d)\varphi^\phi}{a}g^\phi_{n,l}[U]\Big).$$

$$(3.41)$$

The mismatched divergent operators ($\propto \delta c$) in the last terms in each of eqs. (3.40) and (3.41) cancel if the phases φ^ϕ and φ^χ are fixed according to eq. (3.39). However, there are remaining overall phase factors ξ_n and ξ_n^*, which are defined as

$$\xi_n \equiv (-e^{i(\varphi^\phi-\varphi^\chi)})^{n_{\underline{\alpha}}} = (-e^{i(2\varphi)})^{n_{\underline{\alpha}}} = (-e^{i(2\delta c)/(1+d)})^{n_{\underline{\alpha}}}. \qquad (3.42)$$

These phase factors bear witness that a mismatch δc affects the components of interacting fields not only at the boundary, but is presumably visible in component-mixing terms even in the bulk of the lattice. The signature of this mismatch shows in oscillating correlation functions that are considered in the next section 3.1.4. This section is closed with a summary of the simplified Lagrangians for components of interacting fields:

$$S^f[\phi,\bar{\phi},\chi,\bar{\chi}] = a^4\sum_{k,l}\mathcal{L}^{\bar{\phi}\phi}[\phi_l,\bar{\phi}_k,U] + \mathcal{L}^{\bar{\chi}\chi}[\chi_l,\bar{\chi}_k,U] + \mathcal{L}^{\bar{\phi}\chi}[\chi_l,\bar{\phi}_k,U] + \mathcal{L}^{\bar{\chi}\phi}[\phi_l,\bar{\chi}_k,U], \quad (3.43)$$

$$\mathcal{L}^{\bar{\phi}\phi}[\phi_l,\bar{\phi}_k,U] = \sum_{n,m}\bar{\phi}_k(g^\phi_{n,k}[U])^\dagger\left[D^N_{n,m}+D^{KW}_{n,m}+D^4_{n,m}+(m_0+i\frac{c(g_0)}{a}\gamma^{\underline{\alpha}})\delta_{n,m}\right]g^\phi_{m,l}[U]\phi_l,$$

$$(3.44)$$

$$\mathcal{L}^{\bar{\chi}\chi}[\chi_l,\bar{\chi}_k,U] = \sum_{n,m}\bar{\chi}_k(g^\chi_{n,k}[U])^\dagger\left[D^N_{n,m}-D^{KW}_{n,m}+D^4_{n,m}+(m_0-i\frac{c(g_0)}{a}\gamma^{\underline{\alpha}})\delta_{n,m}\right]g^\chi_{m,l}[U]\chi_l,$$

$$(3.45)$$

$$\mathcal{L}^{\bar{\phi}\chi}[\chi_l,\bar{\phi}_k,U] = \sum_{n,m}\bar{\phi}_k(g^\phi_{n,k}[U])^\dagger\xi_n\left[D^N_{n,m}+D^{KW}_{n,m}+D^4_{n,m}+(m_0+i\frac{c(g_0)}{a}\gamma^{\underline{\alpha}})\delta_{n,m}\right]\mathcal{Q}g^\chi_{m,l}[U]\chi_l,$$

$$(3.46)$$

$$\mathcal{L}^{\bar{\chi}\phi}[\phi_l,\bar{\chi}_k,U] = \sum_{n,m}\bar{\chi}_k(g^\chi_{n,k}[U])^\dagger\xi_n^*\left[D^N_{n,m}-D^{KW}_{n,m}+D^4_{n,m}+(m_0-i\frac{c(g_0)}{a}\gamma^{\underline{\alpha}})\delta_{n,m}\right]\bar{\mathcal{Q}}g^\phi_{m,l}[U]\phi_l.$$

$$(3.47)$$

There is no explicit appearance of a mismatch δc in the relevant counterterm's coefficient up to $\mathcal{O}(a,\delta c^2)$ in the single-component Lagrangians of eqs. (3.44) and (3.45), though it modifies their non-trivial boundary conditions. However, the component-mixing Lagrangians of eqs. (3.46) and (3.47) retain an explicit dependence on δc through phase factors ξ_n and ξ_n^* which manifest the mismatch even in the bulk of the lattice.

3.1.4 Components in correlation functions

Next, decomposition into a pair of fields as defined in eq. (3.28) is applied to hadronic correlation functions. A typical mesonic two-point correlation function is the expectation value (denoted by $\langle \ldots \rangle_U$) of the product of two interpolating operators, which are fermionic bilinears with matrices $\mathcal{M}$ or $\mathcal{N}$. This mesonic correlation function

$$\mathcal{C}_{\mathcal{M},\mathcal{N}}(t) = \langle \sum_{n \in \Lambda_t^0} -\mathrm{tr}(O_{\mathcal{N}}(t)\bar{O}_{\mathcal{M}}(0)) \rangle_U = \langle \sum_{n \in \Lambda_t^0} -\mathrm{tr}(\bar{\psi}_n \mathcal{N}^\dagger \psi_n \bar{\psi}_0 \mathcal{M} \psi_0) \rangle_U \qquad (3.48)$$

has a connected and a quark-disconnected contribution, which are obtained from different Wick contractions of the fields. Only the former is discussed in detail in the following. As spinor fields are expressed through components fields, abbreviations from eqs. (3.30) are employed extensively. The decomposed interpolating operators read

$$\bar{O}_{\mathcal{M}}(0) = \left\{ \bar{\phi}_k (g_{0,k}^\phi[U])^\dagger \bar{r}_0^\varphi + \bar{\chi}_k (g_{0,k}^\chi[U])^\dagger \bar{\mathcal{R}}_0^{-\varphi} \right\} \mathcal{M} \left\{ r_0^\varphi (g_{0,l}^\phi[U])\phi_l + \mathcal{R}_0^{-\varphi}(g_{0,l}^\chi[U])\chi_l \right\}, \qquad (3.49)$$

$$O_{\mathcal{N}}(t) = \left\{ \bar{\phi}_v (g_{n,v}^\phi[U])^\dagger \bar{r}_n^\varphi + \bar{\chi}_v (g_{n,v}^\chi[U])^\dagger \bar{\mathcal{R}}_n^{-\varphi} \right\} \mathcal{N} \left\{ r_n^\varphi (g_{n,w}^\phi[U])\phi_w + \mathcal{R}_n^{-\varphi}(g_{n,w}^\chi[U])\chi_w \right\}. \qquad (3.50)$$

The Lagrangians of eqs. (3.44), ..., (3.47) are used in Wick contractions of the components. It is necessary to mention at this stage that transitions between the components are possible (at least through four-momentum exchanges in the interacting theory). It is understood that reference to a particular component on a fermion line is meaningful only at their endpoints. The correlation function is expressed through propagators of the components and split into sixteen pieces. Among these, twelve pieces require an odd number of transitions between different components on at least one of the fermion lines. They are arranged into three sets, which are denoted as the third, fourth and fifth set in the ensuing discussion. The remaining four pieces with an even number of transitions between components on each fermion line belong to two sets with fundamentally different properties. The two pieces of the first set, which have at each endpoint the same component on both fermion lines, exactly mirror two contributions from usual single-flavour theories (e.g. Wilson fermions) and read

$$\mathcal{C}_{\mathcal{M},\mathcal{N}}^{\phi\bar{\phi}\phi\bar{\phi}}(t) = \langle \sum_{n \in \Lambda_t^0} \mathrm{tr}\left(S_{w,k}^{\phi\bar{\phi}}(g_{0,k}^\phi[U])^\dagger \mathcal{M}(g_{0,l}^\phi[U]) S_{l,v}^{\phi\bar{\phi}}(g_{n,v}^\phi[U])^\dagger \mathcal{N}(g_{n,w}^\phi[U]) \right) \rangle_U, \qquad (3.51)$$

$$\mathcal{C}_{\mathcal{M},\mathcal{N}}^{\chi\bar{\chi}\chi\bar{\chi}}(t) = \langle \sum_{n \in \Lambda_t^0} \mathrm{tr}\left(S_{w,k}^{\chi\bar{\chi}}(g_{0,k}^\chi[U])^\dagger \bar{\mathcal{Q}}\mathcal{M}\mathcal{Q}(g_{0,l}^\chi[U]) S_{l,v}^{\chi\bar{\chi}}(g_{n,v}^\chi[U])^\dagger \bar{\mathcal{Q}}\mathcal{N}\mathcal{Q}(g_{n,w}^\chi[U]) \right) \rangle_U. \qquad (3.52)$$

Dirac matrices for the second component can differ at most by a factor (-1), since

$$\bar{\mathcal{Q}}\mathcal{M}\mathcal{Q} = \pm\mathcal{M}, \quad \left\{ \begin{array}{ll} + : & \mathbf{1}, i\gamma^{\underline{\alpha}}\gamma^5, \gamma^\mu, \Sigma^{\nu\lambda} \quad \forall\, \mu, \nu, \lambda \neq \underline{\alpha} \\ - : & \gamma^5, \gamma^{\underline{\alpha}}, i\gamma^\mu\gamma^5, \Sigma^{\underline{\alpha}\mu} \quad \forall\, \mu \neq \underline{\alpha} \end{array} \right\}. \qquad (3.53)$$

Thus, $\mathcal{C}_{\mathcal{M},\mathcal{N}}^{\phi\bar{\phi}\phi\bar{\phi}}(t)$ and $\mathcal{C}_{\mathcal{M},\mathcal{N}}^{\chi\bar{\chi}\chi\bar{\chi}}(t)$ are structurally identical. Quark-disconnected contributions to the processes of the first set are postponed until discussion of the third set.

The two pieces of the second set have the same component at both endpoints of each fermion line, but different components on both fermion lines at each endpoint. They exhibit oscillating phase factors ξ_n and ξ_n^* that were defined in eq. (3.42) and read

$$\mathcal{C}_{\mathcal{M},\mathcal{N}}^{\phi\bar{\phi}\chi\bar{\chi}}(t) = \langle \sum_{n\in\Lambda_t^0} \xi_n^* \text{tr}\left(S_{w,k}^{\phi\bar{\phi}}(g_{0,k}^\phi[U])^\dagger \mathcal{M}\mathcal{Q}(g_{0,l}^\chi[U])S_{l,v}^{\chi\bar{\chi}}(g_{n,v}^\phi[U])^\dagger \bar{\mathcal{Q}}\mathcal{N}(g_{n,w}^\phi[U])\right)\rangle_U, \quad (3.54)$$

$$\mathcal{C}_{\mathcal{M},\mathcal{N}}^{\chi\bar{\chi}\phi\bar{\phi}}(t) = \langle \sum_{n\in\Lambda_t^0} \xi_n \text{tr}\left(S_{w,k}^{\chi\bar{\chi}}(g_{0,k}^\chi[U])^\dagger \bar{\mathcal{Q}}\mathcal{M}(g_{0,l}^\phi[U])S_{l,v}^{\phi\bar{\phi}}(g_{n,v}^\phi[U])^\dagger \mathcal{N}\mathcal{Q}(g_{n,w}^\chi[U])\right)\rangle_U. \quad (3.55)$$

These Dirac matrices are obviously different from those in eqs. (3.51) and (3.52). Therefore, the two sets overlap with $q\bar{q}$ states that have different J^{PC}. Matrix relations between matrices for both sets are listed in table 3.1. On the one hand, in the case $\underline{\alpha} = 0$, the $\hat{e}_{\underline{\alpha}}$ direction is parallel to the time direction. Thus, the two sets of component bilinears have different parity eigenvalues. Oscillating factors ξ_n and ξ_n^* are not summed over for $\underline{\alpha} = 0$ and an oscillation along the time direction persists. On the other hand, in the case $\underline{\alpha} \neq 0$, the $\hat{e}_{\underline{\alpha}}$ direction is perpendicular to the time direction. Hence, the two sets of component field bilinears have different spin. Oscillating factors ξ_n and ξ_n^* are summed over for $\underline{\alpha} \neq 0$ and strong cancellations that lead to suppression of component field bilinears from the second set are expected.

$\mathcal{M}$	$\mathbf{1}$	γ^5	γ^μ	$\Sigma^{\underline{\alpha}\mu}$
$\mathcal{M}\mathcal{Q}$	$i\gamma^{\underline{\alpha}}\gamma^5$	$-i\gamma^{\underline{\alpha}}$	$\frac{1}{2}\Sigma^{\nu\lambda}\epsilon^{\lambda\nu\mu\underline{\alpha}}$	$\gamma^\mu\gamma^5$
$\bar{\mathcal{Q}}\mathcal{M}$	$i\gamma^{\underline{\alpha}}\gamma^5$	$+i\gamma^{\underline{\alpha}}$	$\frac{1}{2}\Sigma^{\nu\lambda}\epsilon^{\lambda\nu\mu\underline{\alpha}}$	$-\gamma^\mu\gamma^5$

Table 3.1: Dirac matrices for both sets of components field bilinears with even numbers of transitions on each fermion line yield different quantum numbers for both sets.

In the end, the twelve remaining pieces with at least one fermion line with an odd number of transitions between the components fall into three different sets, which are denoted as third, fourth and fifth set in the following. Typical representatives of these sets are

$$\mathcal{C}_{\mathcal{M},\mathcal{N}}^{\phi\bar{\chi}\chi\bar{\phi}}(t) = \langle \sum_{n\in\Lambda_t^0} \text{tr}\left(S_{w,k}^{\phi\bar{\chi}}(g_{0,k}^\chi[U])^\dagger \bar{\mathcal{Q}}\mathcal{M}\mathcal{Q}(g_{0,l}^\chi[U])S_{l,v}^{\chi\bar{\phi}}(g_{n,v}^\phi[U])^\dagger \mathcal{N}(g_{n,w}^\phi[U])\right)\rangle_U, \quad (3.56)$$

$$\mathcal{C}_{\mathcal{M},\mathcal{N}}^{\chi\bar{\phi}\chi\bar{\phi}}(t) = \langle \sum_{n\in\Lambda_t^0} \xi_n \text{tr}\left(S_{w,k}^{\chi\bar{\phi}}(g_{0,k}^\phi[U])^\dagger \mathcal{M}\mathcal{Q}(g_{0,l}^\chi[U])S_{l,v}^{\chi\bar{\phi}}(g_{n,v}^\phi[U])^\dagger \mathcal{N}\mathcal{Q}(g_{n,w}^\chi[U])\right)\rangle_U, \quad (3.57)$$

$$\mathcal{C}_{\mathcal{M},\mathcal{N}}^{\chi\bar{\chi}\chi\bar{\phi}}(t) = \langle \sum_{n\in\Lambda_t^0} \xi_n \text{tr}\left(S_{w,k}^{\chi\bar{\chi}}(g_{0,k}^\chi[U])^\dagger \bar{\mathcal{Q}}\mathcal{M}\mathcal{Q}(g_{0,l}^\chi[U])S_{l,v}^{\chi\bar{\phi}}(g_{n,v}^\phi[U])^\dagger \mathcal{N}\mathcal{Q}(g_{n,w}^\chi[U])\right)\rangle_U.$$

$$(3.58)$$

The first representative of the third set is $\mathcal{C}_{\mathcal{M},\mathcal{N}}^{\phi\bar{\chi}\chi\bar{\phi}}(t)$ of eq. (3.56). It is a connected contribution to a process, which has the same component on both fermion lines at each endpoint, but different components at each endpoint of each of the fermion lines. Thus, there must be an odd number of transitions between the components on each of the fermion lines, which sets the process apart from the first set. A pictorial representation

of such a process is given by the diagram in the left part of figure 3.1. Crosses represent either two- or three-point insertions such as transitions between the components or interaction vertices with gauge fields and hatched circles represent the coupling of component fields to external meson fields. The second piece of the third set is $\mathcal{C}_{\mathcal{M},\mathcal{N}}^{\chi\bar{\phi}\phi\bar{\chi}}(t)$ and requires exactly analogous treatment. Processes such as those described in eq. (3.56) are usually realised only in quark-disconnected contributions (right diagram in figure 3.1). The doubled curly line indicates interaction with non-perturbative gauge fields or exchange of at least three gluons, since such processes are OZI suppressed [94, 123, 165]. The leading contribution is $\mathcal{O}(a^2)$ if the components satisfy the same field equations in the continuum limit. Here, the quark-disconnected contributions to these processes involve only even numbers of transitions between the components on each fermion line and also exist for undoubled fermion fields (such as Wilson fermions). Moreover, quark-disconnected contributions to processes of the first set are analogous to quark-disconnected contributions to processes of the third set with the exception that the components on all fermion lines at all endpoints are the same. Hence, if oddness of the number of transitions between components on both fermions lines is used as the criterion for classification, these quark-disconnected contributions all belong to the first set.
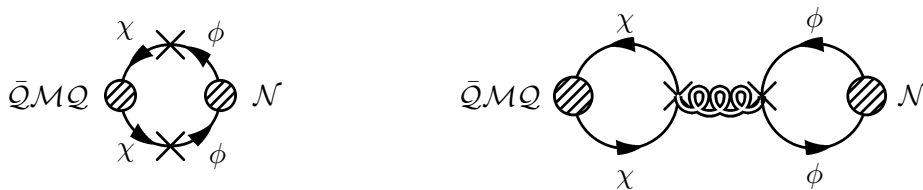
Figure 3.1: Left: The third set are connected contributions to processes that involve different components at both endpoints. Right: The same structure occurs in quark-disconnected diagrams. The notation is explained in the text.

It must be pointed out as a caveat that these diagrams serve only as a guide to the eyes and must not be understood as equivalent to a mathematical formula (in the sense of a Feynman diagram). This caveat holds for the entirety of diagrams in figures 3.1, 3.2 and 3.3. First, assignment of any single component to a fermion line is meaningful only for asymptotically free fields at its endpoints, since there can be arbitrary numbers (though odd for the third set) of transitions between the components. Second, fermion lines for the components have decomposition kernels at their endpoints, which depend on local gauge fields appearing in parallel transports. Hence, perturbative treatment in the weak coupling regime must also include perturbative expansion of the decomposition kernels (which are not yet specified at this level of the discussion) before components can be considered as asymptotically free.

The first representative of the fourth set is $\mathcal{C}_{\mathcal{M},\mathcal{N}}^{\chi\bar{\phi}\chi\bar{\phi}}(t)$ of eq. (3.57). It is a connected contribution to a process, which has different components at each endpoint of each of

Figure 3.2: Left: The fourth set are connected contributions to processes that involve different components at both endpoints of each fermion line and on both fermion lines at each endpoints. Right: The same structure occurs in quark-disconnected diagrams as well. The notation is explained in the text.

the fermion lines and also different components on each fermion line at each endpoint. Hence, there must be an odd number of transitions between the components on each of the fermion lines, which sets the process apart from the second set. A pictorial representation of such a process is given by the diagram in the left part of figure 3.2, which may be understood in the sense of the aforementioned caveat as a guide to the eyes. The same process also receives a quark-disconnected contribution, which is depicted in the right diagram of figure 3.2. An analogous piece $\mathcal{C}_{\mathcal{M},\mathcal{N}}^{\phi\bar{\chi}\phi\bar{\chi}}(t)$ and a quark disconnected contribution to the same process exist as well. Furthermore, there are two quark-disconnected diagrams contributing to the processes of eqs. (3.54) and (3.55). These contributions also involve an odd number of transitions between components on each fermion line. This is why these quark-disconnected contributions are considered as part of the fourth set. Neither of these diagrams is found in a theory of undoubled fermion fields. In order to obtain the correct continuum limit, the entirety of diagrams contributing to processes of the fourth set must either cancel mutually or vanish individually in the continuum limit.

Figure 3.3: The fifth set requires an odd number of transitions between the components on fermion lines. Since symmetries are violated, the sum of all contributions must vanish.

The first representative of the fifth set is $\mathcal{C}_{\mathcal{M},\mathcal{N}}^{\chi\bar{\chi}\chi\bar{\phi}}(t)$ of eq. (3.58). It is a connected contribution to a process, which has equal components on both fermion lines at one endpoint and different components on both fermion lines at the other endpoint. Thus, there must be an odd number of transitions between the components on one of the fermion lines and an even number of transitions between the components on the other fermion line. The

74

total number of transitions between the components is odd for the fifth set. This sets it apart from the other four sets, where the total number of transitions has always been even. A pictorial representation of such a process is given by the diagram in the left part of figure 3.3. Quark-disconnected contributions to the same kind of process exist as well and are depicted in the right diagram in figure 3.3. In the sense of the aforementioned caveat, these diagrams must not be considered as more than a guide to the eyes. In total, there are eight processes in the fifth set. Since source and sink interpolating operators are multiplied by an odd number of matrices $\mathcal{Q}$ and $\bar{\mathcal{Q}}$, the component bilinears (assuming $\mathcal{M} = \mathcal{N}$) accumulate an odd power of γ^5. Due to these contributions, either parity for $\underline{\alpha} = 0$ or spin for $\underline{\alpha} \neq 0$ would not be conserved. However, since either quantum number is conserved in the respective theory of minimally doubled fermions, the entirety of diagrams contributing to processes of the fifth set must cancel mutually or vanish individually on each gauge configuration.

In summary, decomposition of interpolating operators suggests five sets of contributions. The first set represents contributions that would also be observed for undoubled fermion actions. Moreover, the component bilinears have the same Dirac structure and J^{PC} as the original interpolating operators. Contributions from the first set do not include oscillating terms. The third set contributes only one kind of process that may interfere with processes of the first set. Nevertheless, there are no oscillating terms due to the third set and it matches the first set's Dirac structure. There are no additional processes that arise exclusively due to the third set. The second set represents contributions that would only be observed for undoubled fermion actions if both fermion lines would be assigned to different quark flavours. As an example, this kind of contribution is observed with Wilson fermions if one fermion line is considered as an *up* quark and the other as a *down* quark of a isospin symmetric doublet. Due to the possibility of transitions between the components, such an assignment is not possible for minimally doubled fermions. The component bilinears have different Dirac structure and thus different J^{PC} than the original interpolating operators. Moreover, contributions from the second set include oscillating terms with either $\xi_n = (-e^{+i2\varphi})^{n_{\underline{\alpha}}}$ or $\xi_n^* = (-e^{-i2\varphi})^{n_{\underline{\alpha}}}$. The fact that these oscillating factors have frequencies that are not integer multiples of $(2\pi)/(aN_{\underline{\alpha}})$ seems unusual given that the eigenfrequencies of the lattice are restricted to integer multiples of $(2\pi)/(aN_{\underline{\alpha}})$. However, the frequencies can be realised as maxima of distributions of discrete eigenfrequencies of the lattice. A harmonic oscillator and a one-dimensional fermion with imaginary mass serve as toy models that exhibit similar behaviour. These toy models are discussed in the appendix D to illustrate this phenomenon. It seems clear that these contributions are very sensitive to a mismatch $\delta c = (1 + d)\varphi$ of the relevant counterterm's coefficient. It is expected that this yields oscillating contributions in the parallel case ($\underline{\alpha} = 0$) and strong cancellations in perpendicular cases ($\underline{\alpha} \neq 0$). Oscillating contributions of this kind (though without dependence on a mismatched counterterm's coeffcient) are a well-known observation in simulations with staggered fermions [5]. The contributions from the second set interfere with contributions from the fourth set. The same considerations about Dirac structure and oscillating terms are valid for the lat-

ter. However, the fourth set includes contributions that suggest non-conservation of the components. If the components have any physical meaning, such processes must not survive in the continuum limit. Lastly, contributions of the fifth set violate symmetries of the action. They must either cancel mutually or vanish individually on every gauge configuration even at finite lattice spacing. Hence, these terms do not contribute to any observable quantities and can be neglected in the interpetation.

Since numerical simulations in section 4 are focused on only the connected contribution to two different mesonic channels ($\mathcal{M} = \mathcal{N} = \gamma^5$ and $\mathcal{M} = \mathcal{N} = \gamma^0$) with either $\underline{\alpha} = 0$ or $\underline{\alpha} = 3$, these mesonic correlations are constructed in detail. Using eqs. (3.42) and (3.51)-(3.57), $\mathcal{C}_{\gamma^5,\gamma^5}(t)$ for $\underline{\alpha} = 0$, $\vartheta = 0$ and an infinite lattice can be written as

$$\mathcal{C}_{\gamma^5,\gamma^5}(t) = \mathcal{C}^{\text{std}}_{\gamma^5,\gamma^5}(t) + \mathcal{C}^{\text{osc}}_{\gamma^0,\gamma^0}(t), \tag{3.59}$$

$$\mathcal{C}^{\text{std}}_{\gamma^5,\gamma^5}(t) = \Big\langle \sum_{n\in\Lambda^0_t} \text{tr}\Big(S^{\phi\bar\phi}_{w,k}(g^\phi_{0,k}[U])^\dagger\gamma^5(g^\phi_{0,l}[U])S^{\phi\bar\phi}_{l,v}(g^\phi_{n,v}[U])^\dagger\gamma^5(g^\phi_{n,w}[U])\Big)\Big\rangle_U$$

$$+ \Big\langle \sum_{n\in\Lambda^0_t} \text{tr}\Big(S^{\chi\bar\chi}_{w,k}(g^\chi_{0,k}[U])^\dagger\gamma^5(g^\chi_{0,l}[U])S^{\chi\bar\chi}_{l,v}(g^\chi_{n,v}[U])^\dagger\gamma^5(g^\chi_{n,w}[U])\Big)\Big\rangle_U$$

$$- \Big\langle \sum_{n\in\Lambda^0_t} \text{tr}\Big(S^{\phi\bar\chi}_{w,k}(g^\chi_{0,k}[U])^\dagger\gamma^5(g^\chi_{0,l}[U])S^{\chi\bar\phi}_{l,v}(g^\phi_{n,v}[U])^\dagger\gamma^5(g^\phi_{n,w}[U])\Big)\Big\rangle_U$$

$$- \Big\langle \sum_{n\in\Lambda^0_t} \text{tr}\Big(S^{\chi\bar\phi}_{w,k}(g^\phi_{0,k}[U])^\dagger\gamma^5(g^\phi_{0,l}[U])S^{\phi\bar\chi}_{l,v}(g^\chi_{n,v}[U])^\dagger\gamma^5(g^\chi_{n,w}[U])\Big)\Big\rangle_U, \tag{3.60}$$

$$\mathcal{C}^{\text{osc}}_{\gamma^0,\gamma^0}(t) = \Big\langle \sum_{n\in\Lambda^0_t} e^{-i(\pi+2\varphi)n_0}\, \text{tr}\Big(S^{\phi\bar\phi}_{w,k}(g^\phi_{0,k}[U])^\dagger\gamma^0(g^\chi_{0,l}[U])S^{\chi\bar\chi}_{n,v}(g^\chi_{n,v}[U])^\dagger\gamma^0(g^\phi_{n,w}[U])\Big)\Big\rangle_U$$

$$+ \Big\langle \sum_{n\in\Lambda^0_t} e^{+i(\pi+2\varphi)n_0}\, \text{tr}\Big(S^{\chi\bar\chi}_{w,k}(g^\chi_{0,k}[U])^\dagger\gamma^0(g^\phi_{0,l}[U])S^{\phi\bar\phi}_{n,v}(g^\phi_{n,v}[U])^\dagger\gamma^0(g^\chi_{n,w}[U])\Big)\Big\rangle_U$$

$$- \Big\langle \sum_{n\in\Lambda^0_t} e^{+i(\pi+2\varphi)n_0}\, \text{tr}\Big(S^{\chi\bar\phi}_{w,k}(g^\phi_{0,k}[U])^\dagger\gamma^0(g^\chi_{0,l}[U])S^{\chi\bar\phi}_{l,v}(g^\phi_{n,v}[U])^\dagger\gamma^0(g^\chi_{n,w}[U])\Big)\Big\rangle_U$$

$$- \Big\langle \sum_{n\in\Lambda^0_t} e^{-i(\pi+2\varphi)n_0}\, \text{tr}\Big(S^{\phi\bar\chi}_{w,k}(g^\chi_{0,k}[U])^\dagger\gamma^0(g^\phi_{0,l}[U])S^{\phi\bar\chi}_{l,v}(g^\chi_{n,v}[U])^\dagger\gamma^0(g^\phi_{n,w}[U])\Big)\Big\rangle_U. \tag{3.61}$$

The correlation function $\mathcal{C}_{\gamma^0,\gamma^0}(t)$ is obtained by the trivial replacement $\gamma^5 \leftrightarrow \gamma^0$ throughout the expressions. Correlation functions for $\underline{\alpha} = 3$ are obtained by the trivial replacement $0 \leftrightarrow 3$ in n_0 and γ^0 throughout the expressions. Unless the decomposition kernels are sufficiently localised, this correlation function cannot be interpreted in terms of any states formed from the fields ϕ and χ. However, if the decomposition kernels are sufficiently localised, each of the terms in $\mathcal{C}^{\text{std/osc}}_{\gamma^5,\gamma^5}(t)$ represents states with $J^{PC} = 0^{-+}$ propagating from time 0 to time t. Therefore, an oscillating contribution from 0^{-+} states should be be observed in the γ^0 channel. Each of the terms in $\mathcal{C}^{\text{std/osc}}_{\gamma^0,\gamma^0}(t)$ represents states with $J^{PC} = 0^{+-}$ that are not part of the QCD spectrum and contribute supposedly only noise. Hence, the formal decomposition suggest existence of 0^{-+} states in γ^5 and γ^0 channels. Numerical data indicating the presence of 0^{-+} states is presented in sections 4.3 and 4.4.

3.2 Remnant Θ symmetry and $\mathcal{O}(a)$ corrections

The Karsten-Wilczek term breaks n_α reflection and charge conjugation symmetries, $CP\Theta$ and both $C\Theta_{\underline{\alpha}}$ and $P_{\underline{\alpha}}$ are still good symmetries. Hence, generic observables that would have both symmetries if constructed using Wilson fermions may well have only $C\Theta_{\underline{\alpha}}$ symmetry if constructed using Karsten-Wilczek fermions. In particular, since correlation functions may well have only $C\Theta_{\underline{\alpha}}$ symmetry, they potentially lack symmetry under time reflection in the parallel case ($\underline{\alpha} = 0$). Nevertheless, both marginal anisotropic counterterms of eqs. (1.67) and (1.68) are symmetric under $n_{\underline{\alpha}}$ reflection and charge conjugation. Hence, the perturbative vacuum at one-loop has the symmetries of the gluonic counterterm. If the perturbative vacuum has higher symmetry than generic observables, the question arises whether this may apply to other (perturbative or non-perturbative) observables as well. In section 3.2.1, invariance of the pseudoscalar correlation function under $n_{\underline{\alpha}}$ reflection is derived analytically for free fields at first. Next, this invariance is deduced from $C\Theta_{\underline{\alpha}}$ symmetry. In section 3.2.2, general local correlation functions with charge conjugated gauge fields and an invariant vacuum are studied. It is shown that interpolating operators at source and sink with equal charge conjugation eigenvalue ensure symmetry under $n_{\underline{\alpha}}$ reflection and suppress $\mathcal{O}(a)$ corrections. This is a consequence of $C\Theta_{\underline{\alpha}}$ symmetry.

3.2.1 $C\Theta$ symmetry in the free theory

The pseudoscalar correlation function in the free theory

The pseudoscalar correlation function is a special case of eq. (3.48) and reads

$$\mathcal{C}_{5,5}(t) \equiv \mathcal{C}_{\gamma^5,\gamma^5}(t) = \big\langle \sum_{n\in\Lambda_t^0} -\mathrm{tr}\big(\bar{\psi}_0\gamma^5\psi_0\bar{\psi}_n\gamma^5\psi_n\big)\big\rangle_1. \tag{3.62}$$

The spinor fields are Wick contracted and yield propagators as

$$\mathcal{C}_{5,5}(t) = \big\langle \sum_{n\in\Lambda_t^0} \mathrm{tr}\big(S_{n,0}\gamma^5 S_{0,n}\gamma^5\big) - \mathrm{tr}\big(S_{0,0}\gamma^5\big)\mathrm{tr}\big(S_{n,n}\gamma^5\big)\big\rangle_1, \tag{3.63}$$

where the first piece is the connected and the second piece is the quark-disconnected contribution. For a γ^5 hermitian action, the connected contribution is written as

$$\mathcal{C}_{5,5}^{\mathrm{con.}}(t) = \big\langle \sum_{n\in\Lambda_t^0} \mathrm{tr}\big(S_{n,0}\gamma^5 S_{0,n}\gamma^5\big)\big\rangle_1 = \big\langle \sum_{n\in\Lambda_t^0} \mathrm{tr}\big(S_{n,0}S_{n,0}^\dagger\big)\big\rangle_1. \tag{3.64}$$

As gauge fields of the free theory are trivial ($U = 1$), the expectation value can be omitted here. Furthermore, explicit indication as connected contribution is omitted as well. The free correlation function in the chiral limit is cast into momentum space as

$$\mathcal{C}_{5,5}(t) = \sum_{n\in\Lambda_t^0} \int \frac{d^4p\,d^4k}{(2\pi)^8} e^{in\cdot p}\,\mathrm{tr}\Big(S(k+\tfrac{p}{2};\zeta,0,a)S^\dagger(k-\tfrac{p}{2};\zeta,0,a)\Big) \tag{3.65}$$

using the propagator of eq. (2.26). Summation of the sink slice introduces a delta function $\delta^{(3)}(\mathbf{p})$ for external three-momenta. The trace acts upon the numerator N as

$$N = \mathrm{tr}\left\{\left(-i(\gamma \cdot s_{k+\frac{p}{2}}) - i\tfrac{\zeta}{2}\gamma_{\underline{\alpha}}(\hat{s}_{k+\frac{p}{2}})_{\perp}^2\right)\left(+i(\gamma \cdot s_{k-\frac{p}{2}}) + i\tfrac{\zeta}{2}\gamma_{\underline{\alpha}}(\hat{s}_{k-\frac{p}{2}})_{\perp}^2\right)\right\}_{p=p_0\hat{e}_0}.$$

The abbreviations are defined in eqs. (2.21) and (2.22). The numerator is expanded as

$$N = \left\{4(s_{k+\frac{p}{2}} \cdot s_{k-\frac{p}{2}}) + \zeta^2(\hat{s}_{k+\frac{p}{2}})_{\perp}^2(\hat{s}_{k-\frac{p}{2}})_{\perp}^2 + 2\zeta\left(s_{k+\frac{p}{2}}^{\alpha}(\hat{s}_{k-\frac{p}{2}})_{\perp}^2 + s_{k-\frac{p}{2}}^{\alpha}(\hat{s}_{k+\frac{p}{2}})_{\perp}^2\right)\right\}_{p=p_0\hat{e}_0}$$

$$= \sum_{\mu}(s_k^{\mu}\hat{c}_p^{\mu})^2 - (c_k^0\hat{s}_p^0)^2 + \zeta\left\{\sum_{\mu\neq\underline{\alpha}}(s_k^{\alpha}\hat{c}_p^{\mu}(\hat{s}_k^{\mu}\hat{c}_{p/2}^{\mu})^2) + \varrho^{\alpha 0}s_k^{\alpha}\hat{c}_p^0(\hat{c}_k^0\hat{s}_{p/2}^0)^2\right\}$$

$$+ \zeta^2\left(\frac{1}{16}\left\{\sum_{\mu\neq\underline{\alpha}}(\hat{s}_k^{\mu}\hat{c}_{p/2}^{\mu})^2 + \varrho^{\alpha 0}(\hat{c}_k^0\hat{s}_{p/2}^0)^2\right\}^2 - \varrho^{\alpha 0}(s_k^0\hat{s}_p^0)^2\right), \tag{3.66}$$

until it finally simplifies to a manifestly even function of p_0. The denominator D reads

$$D = \left\{\left((s_{k+\frac{p}{2}})^2 + \frac{\zeta^2}{4}\left((\hat{s}_{k+\frac{p}{2}})_{\perp}^2\right)^2 + \zeta s_{k+\frac{p}{2}}^{\alpha}(\hat{s}_{k+\frac{p}{2}})_{\perp}^2\right)\right.$$

$$\left.\times \; \left((s_{k-\frac{p}{2}})^2 + \frac{\zeta^2}{4}\left((\hat{s}_{k-\frac{p}{2}})_{\perp}^2\right)^2 + \zeta s_{k-\frac{p}{2}}^{\alpha}(\hat{s}_{k-\frac{p}{2}})_{\perp}^2\right)\right\}_{p=p_0\hat{e}_0},$$

and is expanded as $D = X + Y + Z$ with

$$X = \left\{(s_{k+\frac{p}{2}})^2 + \tfrac{\zeta^2}{4}\left((\hat{s}_{k+\frac{p}{2}})_{\perp}^2\right)^2\right\}\left\{(s_{k-\frac{p}{2}})^2 + \tfrac{\zeta^2}{4}\left((\hat{s}_{k-\frac{p}{2}})_{\perp}^2\right)^2\right\} = \sum_{i=0}^{2}\left(\frac{\zeta^2}{4}\right)^i X_{2i}, \quad \text{(3.67)}$$

$$Y = \left\{\zeta s_{k+\frac{p}{2}}^{\alpha}(\hat{s}_{k+\frac{p}{2}})_{\perp}^2\right\}\left\{\zeta s_{k-\frac{p}{2}}^{\alpha}(\hat{s}_{k-\frac{p}{2}})_{\perp}^2\right\} \tag{3.68}$$

$$Z = z(+p) + z(-p) = \zeta Z_1 + \zeta^3 Z_3, \tag{3.69}$$

$$z(+p) = \left\{(s_{k+\frac{p}{2}})^2 + \tfrac{\zeta^2}{4}\left((\hat{s}_{k+\frac{p}{2}})_{\perp}^2\right)^2\right\}\left\{\zeta s_{k-\frac{p}{2}}^{\alpha}(\hat{s}_{k-\frac{p}{2}})_{\perp}^2\right\}, \tag{3.70}$$

where the restriction to $p = p_0\hat{e}_0$ is omitted. The individual terms read

$$X_0 = \frac{1}{16}\left(\sum_{\mu}\{(s_k^{\mu}\hat{c}_p^{\mu})^2 + (c_k^{\mu}\hat{s}_p^{\mu})^2\}\right)^2 - \left(\sum_{\mu}\{s_k^{\mu}c_k^{\mu}s_p^{\mu}\}\right)^2, \tag{3.71}$$

$$X_2 = \left(\frac{1}{4}\sum_{\mu}\{(s_k^{\mu}\hat{c}_p^{\mu})^2 + (c_k^{\mu}\hat{s}_p^{\mu})^2\}\right)\left\{\frac{1}{16}\left(\sum_{\nu\neq\underline{\alpha}}\{(\hat{s}_k^{\nu}\hat{c}_{p/2}^{\nu})^2 + (\hat{c}_k^{\nu}\hat{s}_{p/2}^{\nu})^2\}\right)^2 + \left(\sum_{\nu\neq\underline{\alpha}}\{s_k^{\nu}\hat{s}_p^{\nu}\}\right)^2\right\}$$

$$- \left(\sum_{\mu\neq\underline{\alpha}}\{(\hat{s}_k^{\mu}\hat{c}_{p/2}^{\mu})^2 + (\hat{c}_k^{\mu}\hat{s}_{p/2}^{\mu})^2\}\right)\left(\sum_{\nu}\{s_k^{\nu}c_k^{\nu}s_p^{\nu}\}\right)\left(\sum_{\lambda\neq\underline{\alpha}}\{s_k^{\lambda}\hat{s}_p^{\lambda}\}\right)\right), \tag{3.72}$$

$$X_4 = \left\{\left(\sum_{\mu\neq\underline{\alpha}}\{(\hat{s}_k^{\mu}\hat{c}_{p/2}^{\mu})^2 + (\hat{c}_k^{\mu}\hat{s}_{p/2}^{\mu})^2\}\right)^2 - \left(\sum_{\mu\neq\underline{\alpha}}\{s_k^{\mu}\hat{s}_p^{\mu}\}\right)^2\right\}^2, \tag{3.73}$$

$$Y = \tfrac{\zeta^2}{4}\{(\hat{s}_k^{\alpha}\hat{c}_{p/2}^{\alpha})^2 - (\hat{c}_k^{\alpha}\hat{s}_{p/2}^{\alpha})^2\}\left\{\tfrac{1}{16}\left(\sum_{\mu\neq\underline{\alpha}}\{(\hat{s}_k^{\mu}\hat{c}_{p/2}^{\mu})^2 + (\hat{c}_k^{\mu}\hat{s}_{p/2}^{\mu})^2\}\right)^2 - \left(\sum_{\mu\neq\underline{\alpha}}\{s_k^{\mu}\hat{s}_p^{\mu}\}\right)^2\right\}, \quad \text{(3.74)}$$

$$Z_1 = \frac{\left(\sum_\mu \{(s_k^\mu \hat{c}_p^\mu)^2 - (c_k^\mu \hat{s}_p^\mu)^2\}\right)}{4}\Big\{\frac{\left(s_k^{\underline{\alpha}}\hat{c}_{\overline{p}}^{\underline{\alpha}}\right)}{4}\Big(\sum_{\nu\neq\underline{\alpha}}\{(\hat{s}_k^\nu \hat{c}_{p/2}^\nu)^2 + (\hat{c}_k^\nu \hat{s}_{p/2}^\nu)^2\}\Big) + \big(c_k^{\underline{\alpha}}\hat{s}_{\overline{p}}^{\underline{\alpha}}\big)\Big(\sum_{\nu\neq\underline{\alpha}}\{s_k^\nu \hat{s}_p^\nu\}\Big)\Big\}$$

$$- \Big(\sum_\mu \{s_k^\mu c_k^\mu s_p^\mu\}\Big)\Big\{\frac{\left(c_k^{\underline{\alpha}}\hat{s}_{\overline{p}}^{\underline{\alpha}}\right)}{4}\Big(\sum_{\nu\neq\underline{\alpha}}\{(\hat{s}_k^\nu \hat{c}_{p/2}^\nu)^2 + (\hat{c}_k^\nu \hat{s}_{p/2}^\nu)^2\}\Big) + \big(s_k^{\underline{\alpha}}\hat{c}_{\overline{p}}^{\underline{\alpha}}\big)\Big(\sum_{\nu\neq\underline{\alpha}}\{s_k^\nu \hat{s}_p^\nu\}\Big)\Big\}, \quad (3.75)$$

$$Z_3 = 2\Big\{\frac{\left(s_k^{\underline{\alpha}}\hat{c}_{\overline{p}}^{\underline{\alpha}}\right)}{4}\Big(\sum_{\nu\neq\underline{\alpha}}\{(\hat{s}_k^\nu \hat{c}_{p/2}^\nu)^2 + (\hat{c}_k^\nu \hat{s}_{p/2}^\nu)^2\}\Big) - \big(c_k^{\underline{\alpha}}\hat{s}_{\overline{p}}^{\underline{\alpha}}\big)\Big(\sum_{\nu\neq\underline{\alpha}}\{s_k^\nu \hat{s}_p^\nu\}\Big)\Big\}$$

$$\times \Big\{\frac{1}{16}\Big(\sum_{\mu\neq\underline{\alpha}}\{(\hat{s}_k^\mu \hat{c}_{p/2}^\mu)^2 + (\hat{c}_k^\mu \hat{s}_{p/2}^\mu)^2\}\Big)^2 - \Big(\sum_{\mu\neq\underline{\alpha}}\{s_k^\mu \hat{s}_p^\mu\}\Big)^2\Big\}. \qquad (3.76)$$

Due to the delta function $\delta^{(3)}(\mathbf{p})$, these terms are simplified to

$$X_0 = \frac{1}{16}\Big\{\sum_\mu (s_k^\mu \hat{c}_p^\mu)^2 + (c_k^0 \hat{s}_p^0)^2\Big\}^2 - \{s_k^0 c_k^0 s_p^0\}^2, \qquad (3.77)$$

$$X_2 = \Bigg(\frac{1}{4}\Big\{\sum_\mu (s_k^\mu \hat{c}_p^\mu)^2 + (c_k^0 \hat{s}_p^0)^2\Big\}\Big(\frac{1}{16}\Big\{\sum_{\nu\neq\underline{\alpha}}(\hat{s}_k^\nu \hat{c}_{p/2}^\nu)^2 + \varrho^{\underline{\alpha}0}(\hat{c}_k^0 \hat{s}_{p/2}^0)^2\Big\}^2 + \varrho^{\underline{\alpha}0}\{s_k^0 \hat{s}_p^0\}^2\Big)$$

$$- \varrho^{\underline{\alpha}0}\Big\{\sum_{\mu\neq\underline{\alpha}}(\hat{s}_k^\mu \hat{c}_{p/2}^\mu)^2 + \varrho^{\underline{\alpha}0}(\hat{c}_k^0 \hat{s}_{p/2}^0)^2\Big\}\{s_k^0 c_k^0 s_p^0\}\{s_k^0 \hat{s}_p^0\}\Bigg), \qquad (3.78)$$

$$X_4 = \Bigg(\Big\{\sum_{\nu\neq\underline{\alpha}}(\hat{s}_k^\nu \hat{c}_{p/2}^\nu)^2 + \varrho^{\underline{\alpha}0}(\hat{c}_k^0 \hat{s}_{p/2}^0)^2\Big\}^2 - \varrho^{\underline{\alpha}0}\{s_k^0 \hat{s}_p^0\}^2\Bigg)^2, \qquad (3.79)$$

$$Y = \frac{\varsigma^2}{4}\Bigg\{\frac{\left(\hat{s}_k^{\underline{\alpha}}\hat{c}_{p/2}^{\underline{\alpha}}\right)^2}{16}\Big(\Big\{\sum_{\nu\neq\underline{\alpha}}(\hat{s}_k^\nu \hat{c}_{p/2}^\nu)^2 + \varrho^{\underline{\alpha}0}(\hat{c}_k^0 \hat{s}_{p/2}^0)^2\Big\}^2 + \varrho^{\underline{\alpha}0}\{s_k^0 \hat{s}_p^0\}^2\Big)$$

$$- \delta^{\underline{\alpha}0}(\hat{c}_k^0 \hat{s}_{p/2}^0)^2\Big\{\sum_{\nu\neq\underline{\alpha}}(\hat{s}_k^\nu \hat{c}_{p/2}^\nu)^2\Big\}^2\Bigg\}, \qquad (3.80)$$

$$Z_1 = \Big\{\sum_\mu (s_k^\mu \hat{c}_p^\mu)^2 - (c_k^0 \hat{s}_p^0)^2\Big\}\frac{\left(s_k^{\underline{\alpha}}\hat{c}_{\overline{p}}^{\underline{\alpha}}\right)}{16}\Big(\sum_{\nu\neq\underline{\alpha}}(\hat{s}_k^\nu \hat{c}_{p/2}^\nu)^2 + \varrho^{\underline{\alpha}0}(\hat{c}_k^0 \hat{s}_{p/2}^0)^2\Big)$$

$$- \{s_k^0 c_k^0 s_p^0\}\Big(\delta^{\underline{\alpha}0}\frac{\left(c_k^0 \hat{s}_p^0\right)}{4}\Big\{\sum_{\mu\neq\underline{\alpha}}(\hat{s}_k^\mu \hat{c}_{p/2}^\mu)^2\Big\} + \big(s_k^{\underline{\alpha}}\hat{c}_{\overline{p}}^{\underline{\alpha}}\big)\varrho^{\underline{\alpha}0}\{s_k^0 \hat{s}_p^0\}\Big), \qquad (3.81)$$

$$Z_3 = \frac{\left(s_k^{\underline{\alpha}}\hat{c}_{\overline{p}}^{\underline{\alpha}}\right)}{2}\Big(\sum_{\nu\neq\underline{\alpha}}(\hat{s}_k^\nu \hat{c}_{p/2}^\nu)^2 + \varrho^{\underline{\alpha}0}(\hat{c}_k^0 \hat{s}_{p/2}^0)^2\Big)\Big(\frac{1}{16}\Big\{\sum_{\nu\neq\underline{\alpha}}(\hat{s}_k^\nu \hat{c}_{p/2}^\nu)^2 + \varrho^{\underline{\alpha}0}(\hat{c}_k^0 \hat{s}_{p/2}^0)^2\Big\}^2 - \varrho^{\underline{\alpha}0}\{s_k^0 \hat{s}_p^0\}^2\Big).$$
$$(3.82)$$

Hence, all terms in the denominator are even functions of p_0. Because both numerator and denominator are even functions of p_0, the loop integral of the correlation function,

$$\widetilde{\mathcal{C}}(p_0) = \int \frac{d^4 k}{(2\pi)^4}\mathrm{tr}\Big(S(k + \hat{e}_0 \frac{p_0}{2}; \zeta, 0, a)S^\dagger(k - \hat{e}_0 \frac{p_0}{2}; \zeta, 0, a)\Big), \qquad (3.83)$$

79

is necessarily an even function of p_0. Thus, the exponential in eq. (3.65) can be replaced by a cosine and the connected part of the pseudoscalar correlation function is equal to

$$\mathcal{C}_{5,5}(t) = \int \frac{dp_0}{(2\pi)} \cos(tp_0) \frac{\widetilde{\mathcal{C}}(p_0) + \widetilde{\mathcal{C}}(-p_0)}{2}. \tag{3.84}$$

Hence, even though the propagators explicitly break $n_{\underline{\alpha}}$ reflection symmetry, the symmetry is restored in the pseudoscalar correlation function of the free theory. The free pseudoscalar correlation function is manifestly invariant under time reflection and parity for any version ($\underline{\alpha} = 0$ or $\underline{\alpha} \neq 0$) of the Karsten-Wilczek action. Though it is not a priori clear whether this remarkable result can be reproduced with interacting fields, it certainly warrants further analytical and numerical studies.

$C\Theta$, charge conjugation and reflection symmetry

In order to understand the presence of $n_{\underline{\alpha}}$ reflection symmetry, it is related to charge conjugation symmetry using $C\Theta_{\underline{\alpha}}$ symmetry of the theory. Using eq. (1.16), the pseudoscalar correlation function of eq. (3.62) is charge conjugated and reads

$$\mathcal{C}_{5,5}(t) = \langle \sum_{n \in \Lambda_t^0} -\mathrm{tr}\Big(\bar{\psi}_0 \gamma^5 \psi_0 \bar{\psi}_n \gamma^5 \psi_n\Big)\rangle_1 \xrightarrow{C}$$

$$\widehat{C}\mathcal{C}_{5,5}(t) \equiv \mathcal{C}_{5,5}^C(t) = \langle \sum_{n \in \Lambda_t^0} -\mathrm{tr}\Big(\bar{\psi}_0^C \gamma^5 \psi_0^C \bar{\psi}_n^C \gamma^5 \psi_n^C\Big)\rangle_{1C}$$

$$= \langle \sum_{n \in \Lambda_t^0} -\mathrm{tr}\Big((-\psi_0^T)C\gamma^5 C(\bar{\psi}_0^T)(-\psi_n^T)C\gamma^5 C(\bar{\psi}_n^T)\Big)\rangle_1, \tag{3.85}$$

where the charge conjugation matrix C is defined in eq. (A.33). The charge conjugated correlation function is simplified with basic Dirac and Grassmann algebra to

$$\mathcal{C}_{5,5}^C(t) = \langle \sum_{n \in \Lambda_t^0} -\mathrm{tr}\Big((\psi_0^T \gamma^{5T} \bar{\psi}_0^T)(\psi_n^T \gamma^{5T} \psi_n^T)\Big)\rangle_1 = \langle \sum_{n \in \Lambda_t^0} -\mathrm{tr}\Big((\bar{\psi}_0 \gamma^5 \psi_0)^T (\bar{\psi}_n \gamma^5 \psi_n)^T\Big)\rangle_1.$$

$$\tag{3.86}$$

When the transposition of both bilinears in the trace is removed, manifest invariance of the correlation function under charge conjugation becomes evident as

$$\mathcal{C}_{5,5}^C(t) = \langle \sum_{n \in \Lambda_t^0} -\mathrm{tr}\Big((\bar{\psi}_0 \gamma^5 \psi_0)(\bar{\psi}_n \gamma^5 \psi_n)\Big)\rangle_1 = \mathcal{C}_{5,5}(t). \tag{3.87}$$

The relation to reflection symmetries becomes apparent, once the spinor fields are Wick contracted to propagators. The charge conjugated connected piece of eq. (3.64) reads

$$\mathcal{C}_{5,5}^C(t) = \langle \sum_{n \in \Lambda_t^0} \mathrm{tr}\Big(S_{n,0}^C \gamma^5 S_{0,n}^C \gamma^5\Big)\rangle_1. \tag{3.88}$$

It is known from section 1.3.1 that the Karsten-Wilczek action has a $C\Theta_{\underline{\alpha}}$ symmetry, whose operator is the combination of charge conjugation and $n_{\underline{\alpha}}$ reflection operators. The consequence of $C\Theta_{\underline{\alpha}}$ symmetry is trivial for the perpendicular case ($\underline{\alpha} \neq 0$), since the spatial directions are summed in eq. (3.88). However, in the parallel case ($\underline{\alpha} = 0$), $C\Theta_{\underline{\alpha}}$ symmetry implies that

$$\mathcal{C}_{5,5}^C(t) = \langle \sum_{n \in \Lambda_t^0} \mathrm{tr}\Big(S_{n,0}^C \gamma^5 S_{0,n}^C \gamma^5\Big) \rangle_1 = \langle \sum_{n \in \Lambda_t^0} \mathrm{tr}\Big((\widehat{C}S_{n,0}\widehat{C}^\dagger)\gamma^5(\widehat{C}S_{0,n}\widehat{C}^\dagger)\gamma^5\Big) \rangle_1$$

$$= \langle \sum_{n \in \Lambda_{-t}^0} \mathrm{tr}\Big((\widehat{\Theta}S_{n,0}\widehat{\Theta}^\dagger)\gamma^5(\widehat{\Theta}S_{0,n}\widehat{\Theta}^\dagger)\gamma^5\Big) \rangle_1 = \langle \sum_{n \in \Lambda_{-t}^0} \mathrm{tr}\Big(S_{n,0}^\Theta \gamma^5 S_{0,n}^\Theta \gamma^5\Big) \rangle_1. \quad (3.89)$$

This expression is equal to the time-reflected correlation function defined as

$$\widehat{\Theta}\mathcal{C}_{5,5}(t) \equiv \mathcal{C}_{5,5}^\Theta(-t) = \langle \sum_{n \in \Lambda_{-t}^0} \mathrm{tr}\Big(S_{n,0}^\Theta \gamma^5 S_{0,n}^\Theta \gamma^5\Big) \rangle_1. \quad (3.90)$$

Because charge-conjugated and time-reflected correlation functions are equal and since the charge conjugated correlation function is equal to the original correlation function, it follows that the pseudoscalar correlation function is manifestly invariant under time reflection. Restriction to the pseudoscalar correlation function is not necessary, since the proof can be easily extended to a larger group of observables (such as generic mesonic correlation functions with equal Dirac matrices at source and sink). However, a crucial ingredient of the proof is invariance of the vacuum under charge conjugation. In the quenched approximation, sea quarks are neglected and gauge configurations are pure Yang-Mills fields. Therefore, gauge configurations in the quenched approximation correspond to a vacuum that is invariant under charge conjugation. Since all numerical simulations in this thesis are restricted to the quenched approximation, the unquenched case with sea quarks is not considered here. Whether or not the unquenched vacuum is charge conjugation invariant or not is an open and non-trivial problem.

3.2.2 $C\Theta$ symmetry in the interacting theory

Mesonic correlation functions consist of fermion loops with matrix insertions according to their interpolating operators. These operators may lead to non-trivial transformation behaviour under charge conjugation that is unrelated to the fermion action. After mesonic correlation functions with charge-conjugated gauge fields are discussed for invariant fermion actions (like naïve or Wilson fermions), the pattern is compared to Karsten-Wilczek fermions. In order to understand the different behaviour of Karsten-Wilczek fermions, charge conjugation of general next-neighbour lattice Dirac operators is considered. Charge conjugation of Minkowski space-time gauge fields A^μ is translated to gauge links U^μ on a Euclidean space-time lattice, which transform as

$$U_n^\mu \xrightarrow{C} U_n^{C\mu} = (U_n^\mu)^* = (U_n^{\mu\dagger})^T. \quad (3.91)$$

Thus, a general interacting Dirac operator

$$D_{n,m}[U] = \sum_\mu \mathcal{M}_+^\mu U_n^\mu \delta_{n+\hat{e}_\mu,m} - \mathcal{M}_-^\mu U_{n-\hat{e}_\mu,m}^{\mu\dagger} \delta_{n-\hat{e}_\mu} + \mathcal{M}_m \delta_{n,m} \tag{3.92}$$

with *hopping term matrices* $\mathcal{M}_\pm^\mu$ and a *mass matrix* $\mathcal{M}_m$ transforms as

$$D_{n,m}^C[U^C] = \sum_\mu C\mathcal{M}_+^\mu C U_n^{\mu*} \delta_{n+\hat{e}_\mu,m} - C\mathcal{M}_-^\mu C U_{n-\hat{e}_\mu}^{\mu\dagger*} \delta_{n-\hat{e}_\mu,m} + C\mathcal{M}_m C\delta_{n,m}. \tag{3.93}$$

Transposition in Dirac, colour and site space are labeled T_d, T_c and T_s. The definitions

$$(\widetilde{\mathcal{M}}_\pm^\mu)^{T_d} \equiv C\mathcal{M}_\pm^\mu C, \quad (\widetilde{\mathcal{M}}_m)^{T_d} \equiv C\mathcal{M}_m C. \tag{3.94}$$

allow for rewriting the charge conjugated Dirac operator with an overall transposition,

$$D_{n,m}^C[U^C] = \sum_\mu (\widetilde{\mathcal{M}}_+^\mu)^{T_d} (U_{m-\hat{e}_\mu}^{\mu\dagger})^{T_c} \delta_{m-\hat{e}_\mu,n}^{T_s} - (\widetilde{\mathcal{M}}_-^\mu)^{T_d} (U_m^\mu)^{T_c} \delta_{m+\hat{e}_\mu,n}^{T_s} + (\widetilde{\mathcal{M}}_m)^{T_d} \delta_{m,n}^{T_s}$$

$$= \sum_\mu \left(-\widetilde{\mathcal{M}}_-^\mu U_m^\mu \delta_{m+\hat{e}_\mu,n} + \widetilde{\mathcal{M}}_+^\mu C U_{m-\hat{e}_\mu}^{\mu\dagger} \delta_{m-\hat{e}_\mu,n} + \widetilde{\mathcal{M}}_m \delta_{m,n} \right)^T = (\widetilde{D}_{m,n}[U])^T, \tag{3.95}$$

where $\widetilde{D}$ is to be understood in the sense of eq. (3.94). Except for the overall transposition, the original Dirac structure is recovered if

$$\widetilde{\mathcal{M}}_\pm^\mu = -\mathcal{M}_\mp^\mu, \quad \widetilde{\mathcal{M}}_m = \mathcal{M}_m. \tag{3.96}$$

In the case of the Karsten-Wilczek operator, the matrices read

$$\mathcal{M}_\pm^\mu = +(1 + d\delta^{\alpha\mu})\gamma^\mu \mp i\zeta\varrho^{\alpha\mu}\gamma^\alpha, \quad \mathcal{M}_m = m_0\mathbf{1} + i\frac{3\zeta + c}{a}\gamma^\alpha, \tag{3.97}$$

$$\widetilde{\mathcal{M}}_\pm^\mu = -(1 + d\delta^{\alpha\mu})\gamma^\mu \pm i\zeta\varrho^{\alpha\mu}\gamma^\alpha, \quad \widetilde{\mathcal{M}}_m = m_0\mathbf{1} - i\frac{3\zeta + c}{a}\gamma^\alpha. \tag{3.98}$$

Thus, charge conjugation flips the sign of the Wilzcek parameter $(c(-\zeta) = -c(+\zeta))$

$$\widetilde{\mathcal{M}}_\pm^\mu(+\zeta) = -\mathcal{M}_\mp^\mu(-\zeta), \quad \widetilde{\mathcal{M}}_m(+\zeta) = \mathcal{M}_m(-\zeta), \quad \widetilde{D^f}[U](+\zeta) = D^f[U](-\zeta). \tag{3.99}$$

Charge conjugation invariant fermions

If eq. (3.96) is satisfied, the action is manifestly invariant under charge conjugation. Though naïve and Wilson fermions satisfy eq. (3.96), Karsten-Wilczek fermions satisfy eq. (3.99) instead. Because the Dirac operator of an invariant action transform as

$$D_{n,m}[U] \xrightarrow{C} CD_{n,m}[U^C]C = D_{n,m}^C[U^C] = (D_{m,n}[U])^T, \tag{3.100}$$

its inverse, the fermion propagator, must transform as

$$S_{n,m}^C[U^C] = (S_{m,n}[U])^T, \quad S_{n,m}[U^C] = C(S_{m,n}[U])^T C. \tag{3.101}$$

If a correlation function is computed from propagators that use charge conjugated gauge fields, it is related to correlation functions computed from propagators using the original gauge fields according to eq. (3.101) and reads

$$
\begin{aligned}
\mathcal{C}_{\mathcal{M},\mathcal{N}}(t)[U^C] &= \big\langle \sum_{n\in\Lambda_t^0} \mathrm{tr}\Big(S_{n,0}[U^C]\mathcal{M}S_{0,n}[U^C]\mathcal{N}\Big)\big\rangle_{U^C} \\
&= \big\langle \sum_{n\in\Lambda_t^0} \mathrm{tr}\Big((S_{0,n}[U])^T C\mathcal{M}C(S_{n,0}[U])^T C\mathcal{N}C\Big)\big\rangle_U \\
&= \big\langle \sum_{n\in\Lambda_t^0} \mathrm{tr}\Big(S_{n,0}[U]\widetilde{\mathcal{M}}S_{n,0}[U]\widetilde{\mathcal{N}}\Big)^T\big\rangle_U = \mathcal{C}_{\widetilde{\mathcal{M}},\widetilde{\mathcal{N}}}(t)[U].
\end{aligned}
\tag{3.102}
$$

The matrices $\widetilde{\mathcal{M}}$ and $\widetilde{\mathcal{N}}$ must be understood in the sense of eq. (3.94). If both matri-

$\mathcal{M},\mathcal{N}$	γ^ν	$\Sigma^{\mu\nu}$	$\mathbf{1}$	γ^5	$\gamma^5\gamma^\nu$
γ^θ	R	R	I	I	I
$\Sigma^{\chi\theta}$	R	R	I	I	I
$\mathbf{1}$	I	I	R	R	R
γ^5	I	I	R	R	R
$\gamma^5\gamma^\theta$	I	I	R	R	R

Table 3.2: Mesonic correlation functions for Wilson fermions are either purely real or purely imaginary. The format is 'R' for real and 'I' for imaginary correlation functions. Real correlators preserve their sign and imaginary correlators change their sign under charge conjugation. Correlators with naïve instead of Wilson fermions are always real and they are non-zero only if source and sink interpolators are symmetric ($\mathcal{M} = \mathcal{N}$).

ces transform with the same sign under left- and right-multiplication with the charge conjugation matrix C, the correlation function is independent of whether gauge fields are charge conjugated. Since all coefficients in Wilson and naïve Dirac operators are real, charge conjugation of gauge fields can only change the sign of the imaginary part of the correlation function. Hence, correlation functions must be purely real if both matrices transform with the same sign and purely imaginary if both matrices transform with different signs. This behaviour is observed within errors in numerical simulations with Wilson and naïve fermions and summarised in table 3.2, where rows and columns represent matrices $\mathcal{M}$ and $\mathcal{N}$ of source and sink interpolating operators.

Charge conjugation of Karsten-Wilczek fermions

For Karsten-Wilczek fermions, eq. (3.101) must be replaced due to eq. (3.99) by

$$
S_{n,m}^C[U^C] = (\widetilde{S}_{m,n}[U])^T, \quad S_{n,m}[U^C] = C(\widetilde{S}_{m,n}[U])^T C.
\tag{3.103}
$$

$\mathcal{M},\mathcal{N}$	$\gamma^{\underline{\alpha}}$	$\Sigma^{\underline{\alpha}\nu}$	γ^{ν}	$\Sigma^{\mu\nu}$	$\mathbf{1}$	$\gamma^5\gamma^{\underline{\alpha}}$	γ^5	$\gamma^5\gamma^{\mu}$
$\gamma^{\underline{\alpha}}$	+R	+R	-R	-R	+I	+I	-I	-I
$\Sigma^{\underline{\alpha}\theta}$	+R	+R	-R	-R	+I	+I	-I	-I
γ^{θ}	-R	-R	+R	+R	-I	-I	+I	+I
$\Sigma^{\chi\theta}$	-R	-R	+R	+R	-I	-I	+I	+I
$\mathbf{1}$	+I	+I	-I	-I	+R	+R	-R	-R
$\gamma^5\gamma^{\underline{\alpha}}$	+I	+I	-I	-I	+R	+R	-R	-R
γ^5	-I	-I	+I	+I	-R	-R	+R	+R
$\gamma^5\gamma^{\theta}$	-I	-I	+I	+I	-R	-R	+R	+R

Table 3.3: Local mesonic correlation functions with Karsten-Wilczek fermions are either real or imaginary. Some change sign for charge conjugated gauge fields. The format is '+' for positive sign and '-' for negative sign under charge conjugation and 'R' for real and 'I' for imaginary correlation functions. $\{\mu,\nu,\chi,\theta\} \neq \underline{\alpha}$.

Hence, instead of eq. (3.102), correlation functions are described by

$$
\begin{aligned}
\mathcal{C}_{\mathcal{M},\mathcal{N}}(t)[U^C] &= \langle \sum_{n\in\Lambda_t^0} \mathrm{tr}\Big(S_{n,0}[U^C]\mathcal{M}S_{0,n}[U^C]\mathcal{N}\Big)\rangle_{U^C} \\
&= \langle \sum_{n\in\Lambda_t^0} \mathrm{tr}\Big((\widetilde{S}_{0,n}[U])^T C\mathcal{M}C(\widetilde{S}_{n,0}[U])^T C\mathcal{N}C\Big)\rangle_{U} \\
&= \langle \sum_{n\in\Lambda_t^0} \mathrm{tr}\Big(\widetilde{S}_{n,0}[U]\widetilde{\mathcal{M}}\widetilde{S}_{n,0}[U]\widetilde{\mathcal{N}}\Big)\rangle_{U} \neq \mathcal{C}_{\widetilde{\mathcal{M}},\widetilde{\mathcal{N}}}(t)[U].
\end{aligned}
\tag{3.104}
$$

The Wilczek parameter ζ in the propagators $S[U^C]$ is replaced by $-\zeta$ in the propagators $\widetilde{S}[U]$. Hence, eq. (3.104) is rephrased with regard to the Wilczek parameter ζ as

$$
\mathcal{C}_{\mathcal{M},\mathcal{N}}(t;+\zeta)[U^C] = \mathcal{C}_{\widetilde{\mathcal{M}},\widetilde{\mathcal{N}}}(t;-\zeta)[U]
\tag{3.105}
$$

Given the Dirac matrices $\mathcal{M}$ and $\mathcal{N}$ of the interpolating operators, eq. (3.105) is an unambiguous statement about the ζ depence of the correlation function if and only if the vacuum is invariant under charge conjugation such as the pure Yang-Mills vacuum of the quenched approximation. It is not clear at present whether or not this invariance is realised for full QCD with dynamical Karsten-Wilczek fermions. However, this issue is of no concern for predictions about numerical simulations in the quenched approximation that are considered in this thesis. The change of the Wilczek parameter can be compensated by left- and right-multiplication of the propagators by matrices $\mathcal{R}_n = (-1)^{n_{\underline{\alpha}}}\mathcal{Q}$ and $\mathcal{R}_0 = \mathcal{Q}$ (cf. paragraph below eq. (2.33) or sections 2.5 and 3.1.2). As $1 = (\mathcal{R}_n)^2$ is plugged into the correlation functions on both sides of each propagator, $\mathcal{M}$ and $\mathcal{N}$ are also left-and right-multiplied by $\mathcal{Q}$. Denoting total powers of $\gamma^{\underline{\alpha}}$ and γ^5 in both interpolating operators as $N_{\underline{\alpha}}$ and N_5, they acquire factors $(-1)^{N_{\underline{\alpha}}+N_5}$ that must be combined with factors (±1) from left- and right-mutliplication with the charge conjugation matrix. Though mesonic correlation functions for Karsten-Wilczek fermions are purely real or

purely imaginary according to the same pattern as naïve and Wilson fermions. However, the pattern of signs in table 3.2 that real functions are positive and imaginary functions are negative under charge conjugation is broken up with extra factors $(-1)^{N_{\underline{\alpha}}+N_5}$. This behaviour is observed in numerical simulations and summarised in table 3.3, where rows and columns represent matrices $\mathcal{M}$ and $\mathcal{N}$ of source and sink interpolating operators. Because correlation functions for Karsten-Wilczek fermions satisfy eq. (3.105), those which are real and retain their sign under charge conjugation (indicated by +R in table 3.3) must be even functions of the Wilczek parameter ζ. Being even functions of ζ implies that they are invariant under $n_{\underline{\alpha}}$ reflection. This is a manifestation of the $C\Theta_{\underline{\alpha}}$ symmetry in correlation functions.

$C\Theta$ symmetry and $\mathcal{O}(a)$ corrections

Since invariance of correlation functions under $n_{\underline{\alpha}}$ reflection is linked to invariance under charge conjugation by $C\Theta_{\underline{\alpha}}$ symmetry, a condition for $n_{\underline{\alpha}}$ reflection symmetry of correlation functions can be formulated in an operator language for more general states. The Euclidean correlation function of the state $\mathcal{O}^\dagger|\Omega\rangle$ reads

$$\mathcal{C}_{\mathcal{O},\mathcal{O}^\dagger}(t) = \langle\Omega|\widehat{\mathcal{O}}e^{-\widehat{H}t}\widehat{\mathcal{O}}^\dagger|\Omega\rangle, \tag{3.106}$$

where $|\Omega\rangle$ is the vacuum. Since numerical simulations of this thesis use the quenched approximation, the vacuum of full QCD is not considered here. The pure Yang-Mills vacuum of the quenched approximation is strictly invariant under both $\widehat{C}$ and $\widehat{\Theta}_{\underline{\alpha}}$ of eqs. (1.16) and (1.46). The Hamiltonian $\widehat{H}$ has the same $C\Theta_{\underline{\alpha}}$ symmetry as the action,

$$\widehat{H} = (\widehat{\Theta_{\underline{\alpha}}C})\widehat{H}(\widehat{\Theta_{\underline{\alpha}}C})^\dagger, \tag{3.107}$$

where $\widehat{C}$ and $\widehat{\Theta}_{\underline{\alpha}}$ are the charge conjugation and $n_{\underline{\alpha}}$ reflection operators of eqs. (1.16) and (1.46). Then the correlation function is equal to

$$\mathcal{C}_{\mathcal{O},\mathcal{O}^\dagger}(t) = \langle\Omega|\widehat{\mathcal{O}}(\widehat{\Theta_{\underline{\alpha}}C})^\dagger e^{-\widehat{H}(\widehat{\Theta}_{\underline{\alpha}}t)}(\widehat{\Theta_{\underline{\alpha}}C})\widehat{\mathcal{O}}^\dagger|\Omega\rangle = \langle\Omega|\widehat{\mathcal{O}}\widehat{C}^\dagger\widehat{\Theta}_{\underline{\alpha}}^\dagger e^{-\widehat{H}(\widehat{\Theta}_{\underline{\alpha}}t)}\widehat{\Theta}_{\underline{\alpha}}\widehat{C}\widehat{\mathcal{O}}^\dagger|\Omega\rangle. \tag{3.108}$$

If the operator $\mathcal{O}^\dagger$ generates an eigenstate of charge conjugation, $\mathcal{O}^\dagger$ and $\mathcal{O}$ satisfy

$$\widehat{\mathcal{O}}^\dagger = \pm\widehat{C}\widehat{\mathcal{O}}^\dagger\widehat{C}^\dagger, \ \widehat{\mathcal{O}} = \pm\widehat{C}\widehat{\mathcal{O}}\widehat{C}^\dagger, \tag{3.109}$$

and the charge conjugation operators may be moved past the operators $\widehat{\mathcal{O}}$ and $\widehat{\mathcal{O}}^\dagger$.

$$\mathcal{C}_{\mathcal{O},\mathcal{O}^\dagger}(t) = \langle\Omega|\widehat{C}^\dagger\widehat{\mathcal{O}}\widehat{\Theta}_{\underline{\alpha}}^\dagger e^{-\widehat{H}(\widehat{\Theta}_{\underline{\alpha}}t)}\widehat{\Theta}_{\underline{\alpha}}\widehat{\mathcal{O}}^\dagger\widehat{C}|\Omega\rangle$$
$$= \langle\Omega|(\widehat{C}^\dagger\widehat{\Theta}_{\underline{\alpha}}^\dagger)(\widehat{\Theta}_{\underline{\alpha}}\widehat{\mathcal{O}}\widehat{\Theta}_{\underline{\alpha}}^\dagger)e^{-\widehat{H}(\widehat{\Theta}_{\underline{\alpha}}t)}(\widehat{\Theta}_{\underline{\alpha}}\widehat{\mathcal{O}}^\dagger\widehat{\Theta}_{\underline{\alpha}}^\dagger)(\widehat{\Theta}_{\underline{\alpha}}\widehat{C})|\Omega\rangle. \tag{3.110}$$

Since the vacuum satisfies $(\widehat{\Theta}_{\underline{\alpha}}\widehat{C})|\Omega\rangle = |\Omega\rangle$, the correlation function is expressed through $n_{\underline{\alpha}}$-reflected operators $(\widehat{\Theta}_{\underline{\alpha}}\mathcal{O}\widehat{\Theta}_{\underline{\alpha}}^\dagger)$ as an overall $n_{\underline{\alpha}}$-reflected correlation function,

$$\mathcal{C}_{\mathcal{O},\mathcal{O}^\dagger}(t) = \ = \mathcal{C}_{\widehat{\Theta}_{\underline{\alpha}}\mathcal{O}\widehat{\Theta}_{\underline{\alpha}}^\dagger,(\widehat{\Theta}_{\underline{\alpha}}\mathcal{O}\widehat{\Theta}_{\underline{\alpha}}^\dagger)^\dagger}(\widehat{\Theta}_{\underline{\alpha}}t) = \widehat{\Theta}_{\underline{\alpha}}\,\mathcal{C}_{\mathcal{O},\mathcal{O}^\dagger}(t). \tag{3.111}$$

In the parallel case of Karsten-Wilczek fermions ($\underline{\alpha} = 0$) , eq. (3.111) implies that the correlation function in any channel with definite charge conjugation quantum number is invariant under time reflection. The argument can be generalised to Boriçi-Creutz fermions at this stage. $n_{\underline{\alpha}}$ reflection is along the $\hat{f}_0$-direction (diagonal of the hypercube, cf. eq. (1.76)) for Boriçi-Creutz fermions. Therefore, $n_{\underline{\alpha}}$ reflection reflects all Euclidean directions at once. If the operators $\widehat{\mathcal{O}}^\dagger$ and $\widehat{\mathcal{O}}$ generate and destroy a state with definite parity and charge conjugation quantum numbers, the correlation function is invariant under any spatial reflection and under charge conjugation. Invariance under time reflection follows from the general $CP\Theta$ invariance and both invariance under charge conjugation ($\widehat{C}$) and under reflection of all spatial axes ($\widehat{P}$) of the correlation function. Hence, correlation functions of operators with definite charge conjugation and parity quantum numbers are invariant under time reflection for Boriçi-Creutz fermions.

Another consequence of $n_{\underline{\alpha}}$ reflection symmetry concerns $\mathcal{O}(a)$ corrections to the continuum limit. In both actions, any $\mathcal{O}(a)$-suppressed operators break charge conjugation and $n_{\underline{\alpha}}$ reflection symmetry to $C\Theta_{\underline{\alpha}}$ symmetry, whereas the leading order terms respect both symmetries. Hence, because $\mathcal{O}(a)$ corrections to any observable are generated by the $\mathcal{O}(a)$-suppressed operators (in diagrammatical terms only one $\mathcal{O}(a)$-suppressed insertion per diagram), they must also share their broken symmetry. If an observable has the unbroken symmetries, there cannot be any $\mathcal{O}(a)$ corrections. Therefore, leading corrections to correlation functions which respect both symmetries are of $\mathcal{O}(a^2)$. Of course, this statement is true only if the vacuum itself has the right symmetry and does not have $\mathcal{O}(a)$ corrections on its own. This is the case for the pure Yang-Mills vacuum of the quenched approximation. Whether or not this is the case for the full QCD vacuum is a non-trivial question that is not considered here. This is not the same as automatical $\mathcal{O}(a)$ improvement for Ginsparg-Wilson fermions, because the absence of $\mathcal{O}(a)$ corrections is exclusive to observables with additional symmetry.

3.3 Interim findings (II)

The preceding section contains analytical studies of Karsten-Wilczek fermions in terms of a decomposition of spinor fields ψ into a pair fields ϕ and χ with different four-momentum support and of higher symmetries of mesonic correlation functions.

Decomposition into a pair of fields ϕ and χ with different four-momentum support requires use of decomposition kernels which extend support over multiple lattice sites. Definition of fields with extended support is not feasible in a theory with an unmatched power divergent operator. Hence, a mismatch δc of the relevant operator's coefficient is absorbed into two phase factors that modify the boundary conditions of the fields ϕ and χ differently. This must not be mistaken for a removal of the counterterm or its coefficient. Since the decomposition relies on linearisation both in δc and in the lattice

spacing a for the lattice product rule of eq. (3.5), decomposition may well break down if either of δc or a is too large. Decomposition of interpolating operators yields bilinear forms of the fields ϕ and χ that form two strikingly different terms in mesonic correlation functions. Whereas the first term with the same fields (e.g. $\bar{\phi}$ and ϕ) has the same Dirac structure and J^{PC} as the correlation function for undoubled fermions, the second term with different fields (e.g. $\bar{\phi}$ and χ) has different Dirac structure and J^{PC} and also oscillates in the $\hat{e}_{\underline{\alpha}}$ direction. While such an oscillating term is well-known for staggered fermions [5], its frequency depends on the mismatch δc for Karsten-Wilczek fermions. It is certainly worthwhile to investigate whether this dependence on δc is a viable non-perturbative tuning criterion. Moreover, the second term with different fields and different J^{PC} may contribute additional low-lying states or even the ground state.

The decomposition is based on linearising in the mismatch δc and the lattice spacing a and may or may not be legitimate for numerical simulations. Moreover, as it makes use of unspecified decomposition kernels that are functionals of the local gauge fields, a rigorous perturbative calculation would require a perturbative expansion of the decomposition kernels as well. Therefore, identification of components in any pictorial representation lacks the field-theoretical rigour of Feynman diagrams. This problem is inherent in the treatment of any doubled lattice fermion in position-space. However, the decomposition suggests that general concepts concerning doubled fermions should be also applicable to Karsten-Wilczek fermions. The presence of oscillating contributions with different J^{PC} due to fermion modes in different parts of the Brillouin zone in correlation functions is known for staggered fermions [5, 80, 99]. It seems as if similar findings apply to Karsten-Wilczek fermions as well. Whether or not the frequency of the oscillations depends on the mismatch δc is put to a test in the numerical simulations that make up section 4.3.

Correlation functions can have a higher symmetry than the fermion action, if gauge configurations correspond to a vacuum $|\Omega\rangle$ that is invariant under $(\widehat{\Theta}_{\underline{\alpha}} \widehat{C})$. This is strictly satisfied for the pure Yang-Mills vacuum of the quenched approximation. Whether or not the full QCD vacuum has this symmetry is not within the scope of this thesis. For a symmetric vacuum, correlation functions with the same tree-level charge conjugation patterns at source and sink are also invariant under $n_{\underline{\alpha}}$ reflection as a consequence of $CP\Theta$ symmetry. This higher symmetry suggests that correlation functions with the same matrices in source and sink interpolating operators in the quenched approximation are symmetric under time reflection and have equal energies for forwards and backwards propagating states. Because $\mathcal{O}(a)$ terms in minimally doubled fermion actions break both symmetries explicitly, $\mathcal{O}(a)$ corrections should be absent in observables that retain the higher symmetry. Even if this behaviour were to hold true for the full QCD vacuum, this is not to be mistaken with $\mathcal{O}(a)$ improvement because it requires an extra symmetry of the observables. Nevertheless, symmetric correlation functions are tested for this higher symmetry in the numerical simulations that make up section 4.2.

Numerical studies

The central objective of lattice QCD is to study QCD in the non-perturbative regime, which can be achieved with numerical simulations. In these simulations, the QCD path integral (the Euclidean analogue of eq. (1.22) is evaluated on a limited number of field configurations, which are generated using an importance sampling method. A Markov process with a probabilistic acceptance condition is used to generate configurations. In order to satisfy detailed balance, the rejection probability is determined by the increase of the classical action. Field configurations are expressed in terms of gauge field variables that implicitly depend on sea quarks. Fermion fields are integrated out and yield the quark determinant, which is an additional contribution to an effective gauge field action. Once an ensemble of gauge configurations has been provided, observables are evaluated on each configuration as functions of fermionic and gluonic fields. Observables with valence fermions are calculated from a set of source fields on which the Dirac operator is inverted. These propagator components correspond to Wick contractions of fermion fields at different space-time points and are combined to form correlation functions of hadronic interpolating operators with appropriate spin and parity. Since interpolating operators have non-zero overlap with all physical states with the same quantum numbers, excited states as well as the ground state contribute in each channel. In order to cleanly extract the ground state, correlation functions are studied for long Euclidean time separation. The ground state is isolated, since spectral weights of all states exponentially decrease with their energies. A typical Euclidean correlation function for a lattice with infinite extent in the time direction reads

$$\mathcal{C}(t) = \sum_{k=0}^{\infty} A_k e^{-E_k t} = A_0 e^{-E_0 t} \sum_{k=0}^{\infty} \frac{A_k}{A_0} e^{-(E_k - E_0)t} \overset{t \to \infty}{\to} A_0 e^{-E_0 t} + \dots, \qquad (4.1)$$

where A_k are spectral weights (at $t = 0$) and E_k are the absolute energies of states. Whereas spectral weights depend on the peculiar details of the interpolating operators, the energies depend only on their quantum numbers. The set of spectral weights A_k can be manipulated in order to achieve dominance of the ground state for smaller t by applying smearing procedures, which alter geometrical shapes at source and sink. This

is of particular importance for the study of anisotropies in section 4.2. The energies of hadronic states satisfy dispersion relations $E_k(\mathbf{p}) = \sqrt{m_k^2 + \mathbf{p}^2}$, where $\mathbf{p}$ is the hadron's spatial momentum. Spatial momentum can be injected, if the local interpolating operator $O_\mathcal{N}(t)$ at the sink site $n = (t/a, \mathbf{n})$ is multiplied by a plane wave $e^{ia\mathbf{n}\cdot\mathbf{p}}$ before summation (cf. eq. (3.48)). The contribution of the ground state at smaller time separation is greatly enhanced with appropriate smearing techniques (cf. section 4.1). Due to the W_4 symmetry of the lattice, any direction may serve as time direction for calculating correlation functions. Furthermore, (anti-) periodicity of the finite space-time lattice is responsible for a superposition of hadronic states moving forward or backward in the time direction (cf. section 4.1). Therefore, a generic correlation function on a lattice with periodic boundary conditions in the time direction ($T = aN_t$, where N_t is the number of time slices) reads

$$\mathcal{C}_{PB}(t) = \sum_{k=0}^{\infty} A_k(e^{-E_k t} + e^{-E_k(T-t)}) \tag{4.2}$$

Correlation functions or ratios thereof on the full statistical ensemble are analysed with fit routines, which extract properties of hadronic states. The Jackknife method is applied for determination of statistical errors (cf. appendix C). In the *quenched approximation*, light quark masses close to the physical point lead to *exceptional configurations* for Wilson fermions. The inversion of the Wilson Dirac operator $D[U]$ breaks down for these exceptional configurations, which correspond to very small eigenvalues of the Wilson Dirac operator. Thus, Wilson fermions in the quenched approximation cannot reach pion masses below 300 MeV. Because minimally doubled fermions have chiral symmetry, they are supposed to be protected against exceptional configurations. It is expected that simulations with pion masses below 300 MeV are feasible with Karsten-Wilczek fermions. Nevertheless, most of the simulations within this thesis use heavier quark masses, because they are numerically cheaper. Hence, it is necessary to perform a chiral extrapolation of hadronic quantities towards either the chiral limit or the physical point using chiral perturbation theory. Lastly, since hadronic observables inherit discretisation errors from the action, a continuum extrapolation on lines of constant physics is necessary for extraction of the continuum limit. Technical apects of the numerical simulations in the quenched approximation are covered in section 4.1. Three different aspects of Karsten-Wilczek fermions are studied using data from numerical simulations. A study of the anisotropy of hadronic correlation functions [155] in section 4.2 and a study of oscillating correlation functions [154] in section 4.3 yield two independent tuning conditions for the relevant fermionic counterterm of eq. (1.66). Determination of a robust non-perturbative tuning condition for the marginal fermionic counterterm of eq. (1.67) is unsuccessful. Later on, in section 4.4, actual physical information on QCD concerning the chiral behaviour of pseudoscalar mesons is extracted with simulations that reach into the chiral regime that is inaccessible with Wilson fermions in the quenched approximation. Lastly, interim findings from numerical studies are summarised in section 4.5.

4.1 Setup of simulations

4.1.1 Karsten-Wilczek fermions in the quenched approximation

Numerical simulations of Karsten-Wilczek fermions as one example of minimally doubled fermion actions are performed for the first time. Gauge configurations are calculated in the quenched approximation, where the full QCD path integral

$$\langle \mathcal{O} \rangle = \frac{1}{Z} \int \mathcal{D}\bar{\psi}\mathcal{D}\psi\mathcal{D}U \ \mathcal{O}[\psi, \bar{\psi}, U] \ e^{-(S^f[\psi,\bar{\psi},U] + S^g[U])}$$
$$= \frac{1}{Z} \int \mathcal{D}U \ \det(D[U]) \ \mathcal{O}[\psi, \bar{\psi}, U] \ e^{-S^g[U]} \tag{4.3}$$

is approximated by setting the fermion determinant $\det(D[U])$ to 1 instead of including it into an effective gauge action $S^{\text{eff}}[U] = S^g[U] - \log\det(D[U])$ for full QCD. Herein, observables $\mathcal{O}[\psi, \bar{\psi}, U]$ are expressed in terms of fermion propagators and gauge fields. This amounts to neglecting vacuum fermion loops due to sea quarks and the quenched vacuum is the pure Yang-Mills vacuum. The absence of fermion loops in the quenched approximation implies that the gauge fields are not affected by the anisotropy of the fermion sector. Hence, simulations in the quenched approximation can forgo the gluonic counterterm of eq. (1.68), though both fermionic counterterms of eqs. (1.66) and (1.67) must be included. Due to the anisotropy of the fermion action, the QCD transfer matrix is anisotropic as well. Furthermore, the QCD transfer matrix lacks symmetry under $n_{\underline{\alpha}}$ reflection and charge conjugation, since both are broken explicitly by the Karsten-Wilczek term of eq. (1.61). It was seen in section 2.3.1 that requiring isotropy of the one-loop quark propagator is enough to fix the fermionic counterterms' coefficients perturbatively. It is worthwhile to investigate whether the requirement of isotropy for hadronic observables similarly provides a criterion for fixing the counterterms' coefficients. Even though 'Lorentz scalars' like hadron masses or pseudoscalar densities might be naïvely anticipated as isotropic like in perturbation theory (cf. section 2.3.2), this cannot be true in the non-perturbative context of a numerical simulation. Because they are calculated from directed correlation functions that require a choice of the Euclidean time direction (or *direction of correlation*), even the most simple hadronic quantity, which is the pseudoscalar ground state mass, is necessarily sensitive to the lack of isotropy in the fermion action. The anisotropy is studied by calculating correlation functions with different orientations of the direction of correlation with respect to the alignment of the Karsten-Wilczek term in sections 4.2 and 4.3. Section 3.2.2 suggests that correlation functions of states with definite charge conjugation quantum number on a pure Yang-Mills vacuum satisfy both $n_{\underline{\alpha}}$ reflection and charge conjugation symmetries. These considerations are put to a numerical test in section 4.2.2 and methods for dealing with a potential lack of time-reflection symmetry are developed.

4.1.2 Machine and code

Numerical simulations are performed on the Wilson cluster of the Institut für Kernphysik at Johannes Gutenberg-Universität Mainz. The simulation code is based on the Kpipi Code [73–75], which was originally designed for simulations of overlap fermions in the quenched approximation. The code is written in C, but makes frequent use of manual vectorisation using explicit inline assembly for SSE2 acceleration of particularly costly numerical operations. It was gradually adapted to numerical studies of minimally doubled fermion actions of Karsten-Wilczek and Boriçi-Creutz types. This section covers different stages of numerical simulations and summarises modifications to the code.

4.1.3 Lattice geometry

The preexisting Kpipi code sets the basic geometry constraints for numerical studies. The Euclidean direction N_0 is fixed as a free parameter T and the three other Euclidean directions N_1, N_2 and N_3 are fixed as another free parameter L at compile time. Both T and L must be integer multiples of 2 in the single processor version and of 8 in the parallelised version of the code. The parallelised version (cf. section 4.1.10) must have at least a 2×2 grid of local sublattices in $\hat{e}_0$ and $\hat{e}_1$ directions, where local sublattices must have lengths of at least 4 in both $\hat{e}_0$ and $\hat{e}_1$ directions. Moreover, the sublattice length in the $\hat{e}_1$ direction must be an integer multiple of 2, 3 or 5. Lattice sites are grouped together in the memory in an alignment of blocks, which improved performance when the code was initially written (ca. 2004). Some parts of the code rely on the specific form of the geometry arrays. Since the effort of a geometry change for this preexisting code exceeds its benefits, the geometry was left unchanged. Owing to the blocking structure, memory is not aligned in a pattern which allows for coherent even-odd ordering of sites, which is required for even-odd preconditioning of Dirac operators (cf. section 4.1.7). The problem was solved by introducing two additional geometry arrays, which provide a mapping between even-odd ordered and preexisting site-indices. Memory overhead due to two extra integer arrays is reasonably small and the loss of performance due to one additional intermediary hash table is acceptable.

4.1.4 Gauge configurations and scale setting

β	U_0^4	$a[\text{fm}]$	r_0	n_{JS}
5.8	0.567	0.136	3.668	30
6.0	0.594	0.093	5.368	40
6.2	0.614	0.068	7.360	140

Table 4.1: The scale a is set using eq. (4.5). Dimensionful quantities in lattice units are converted to physical quantities in units of $2\,\text{fm}^{-1}$ by multiplication with r_0. n_{JS} is the iteration count of the Jacobi smearing algorithm (cf. section 4.1.9).

The code providing gauge configurations was taken over without modification. Gauge

configurations are calculated with a Markov chain update procedure that satisfies a detailed balance condition. The update algorithm is a standard heatbath-overrelaxation algorithm. It consists of consecutive applications of the Cabibbo-Marinari heatbath algorithm [29,43] and microcanonical overrelaxation steps [2,158]. The individual update procedures – heatbath and overrelaxation – are described in detail in the fourth chapter of [65]. Gauge configurations throughout this thesis are always produced from a cold start with trivial gauge links $U_n^\mu = 1 \; \forall \; \mu, n$ (free theory). Each update cycle consists of sequences of one heatbath and five overrelaxation steps. The initial thermalisation uses 2000 iterations of the update cycle. Each configuration uses additional 100 iterations of the update cycle in order to reduce the correlation between configurations. The update algorithm provides gauge links in single precision. Double precision link variables are obtained as copies from the single precision gauge links, which are projected to SU(3) in double precision. Finally, double precision link variables are copied back to single precision links with an additional typecast. Otherwise, deviations between single and double precision fields occasionally cause exceptions in the code, which may halt execution of programs. The scale is set following [84] with the Sommer parameter r_0 as reference scale [143], which is defined by eq. (1.1) of [84] as

$$r_0 F(r_0) = 1.65, \tag{4.4}$$

where $F(r)$ is the force between static charges in the fundamental representation [143]. The constant on the right hand side of eq. (4.4) is chosen in order to fix the Sommer parameter at roughly 0.5 fm. In the range $5.7 \le \beta \le 6.57$, the inverse gauge coupling β is related to the lattice spacing a by eq. (2.18) of [84], which reads

$$\log\left(\frac{a}{r_0}\right) = -1.6805 - 1.7139(\beta - 6) + 0.8155(\beta - 6)^2 - 0.6667(\beta - 6)^3. \tag{4.5}$$

4.1.5 Dirac operators

Dirac operators for Karsten-Wilczek fermions and Boriçi-Creutz fermions of eqs. (1.69) and (1.90) are implemented using Dirac matrices in the chiral representation of eq. (A.27). However, instead of a direct implementation of the Dirac operator D, which is γ^5 hermitian, the hermitian Dirac operator $Q = \gamma^5 D$ is used. Dirac operators Q for implementation of Karsten-Wilczek and Boriçi-Creutz fermions are presented in appendix F.1. The propagator $S_{m,\underline{n}}[U]\eta_{\underline{n}}$ is obtained by solving the equation

$$\sum_{m,\alpha,a} Q_{\underline{n},m}^{\beta\alpha,ba} \phi_m^{\alpha,a} = \gamma^5 \eta_{\underline{n}}^{\beta,b} \tag{4.6}$$

with numerical methods (cf. sections 4.1.6 and 4.1.7). The source vector $\eta_{\underline{n}}$ and the solution vector ϕ_m are globally defined spinor fields. The solution ϕ_m, which is given by

$$\phi_m^{\alpha,a}(\eta_{\underline{n}}^{\beta,b}) = (Q^{-1})_{m,\underline{n}}^{\alpha\beta,ab} \gamma^5 \eta_{\underline{n}}^{\beta,b} = (D^{-1})_{m,\underline{n}}^{\alpha\beta,ab} \eta_{\underline{n}}^{\beta,b} \equiv S_{m,\underline{n}}^{\alpha\beta,ab}[U]\eta_{\underline{n}}^{\beta,b}, \tag{4.7}$$

is the inverse Dirac operator applied to the source $\eta_{\underline{n}}$ and describes the propagation of a fermion field from site $\underline{n}$ to all other sites m in the background of the gauge field U.

The source is a local point source with twelve complex components $\eta_{\underline{n}}^{\beta,\underline{b}}$ – three colour components $\underline{b}$ times four spin components β – at the site $\underline{n}$, which is always located at $\underline{n} = (0, 0, 0, 0)$ for simulations of this thesis. Propagator components $\phi_m^{\alpha,a}(\eta_{\underline{n}}^{\beta,\underline{b}})$ are obtained from twelve inversions, where different source components are set to 1. Smeared sources have the gauge-invariant smearing operator of eq. (4.18) applied n_{JS} times to local source components $\eta_{\underline{n}}^{\beta,\underline{b}}$ before the Dirac operator is inverted.

4.1.6 Mixed precision CG inverter

Starting conditions: $k = 0$

$$x_k = 0 \qquad\qquad (A)$$
$$r_k = b - Ax_k \qquad\qquad (B)$$
$$p_k = s_k = Ar_k \qquad\qquad (C)$$

Loop: iterate for $k = 0, 1, 2, \ldots$

$$q_k = Ap_k \qquad\qquad (a)$$
$$\lambda_k = |s_k|^2 / |q_k|^2 \qquad\qquad (b)$$
$$r_{k+1} = r_k - \lambda_k q_k \qquad\qquad (c)$$
$$x_{k+1} = x_k + \lambda_k p_k \qquad\qquad (d)$$
$$\nu_k = |s_k|^2 \qquad\qquad (e)$$
$$s_{k+1} = Ar_{k+1} \qquad\qquad (f)$$
$$\mu_k = |s_{k+1}|^2 / \nu_k \qquad\qquad (g)$$
$$p_{k+1} = s_{k+1} + \mu_k p_k \qquad\qquad (h)$$

until convergence is achieved and $|r_{k+1}|^2 < \epsilon^2$.

Figure 4.1: Pseudocode for the CG algorithm was taken from chapter thirteen of [12].

Since inversion of the Dirac operator is the bottleneck of any simulation in the quenched approximation, the inversion algorithm must be optimised and accelerated to the utmost. Minimally doubled Dirac operators are inverted using a conjugate gradient (CG) algorithm [71, 96] that was taken from chapter thirteen of [12] by solving eq. (4.6) as

$$Ax = b. \qquad\qquad (4.8)$$

Pseudocode of the CG algorithm is presented in figure 4.1. Convergence of a bi-conjugate gradient (Bi-CGstab) algorithm taken from chapter six of [65] is unstable for minimally doubled fermions.

The inverter uses mixed precision as a runtime option, which conducts calculations (a), (f) and (h) in single and (c) and (d) in double precision. Thus, whereas residue r_k and solution vector x_k are double precision fields, search vectors p_k, q_k and s_k use only single precision. This implementation of the CG algorithm restricts costly matrix-times-vector operations of (a) and (f) to single precision, if (f) is performed after a typecast of r_{k+1} to single precision, which can be stored in q_k. The mixed precision solver needs only one double precision spinor field r_k and three single precision spinor fields p_k, q_k and s_k as well as three doubles[1] λ_k, ν_k, μ_k as workspace, which seems to be the most cost-efficient implementation of a straight CG algorithm without preconditioning for minimally doubled fermions. In order to prevent the accumulation of numerical errors from single precision operations, convergence in double precision is ensured by recalculating the residue r_k from x_k using (B) in double precision after a fixed count $(\sim 10 - 30)$ of interations. In a final step after the precision goal $|r_{k+1}|^2 < \epsilon^2$ is reached, r_k is recalculated from x_k in double precision. In the rare case that the precision goal is missed, the solver runs through additional iterations at double precision[2], until the precision goal is met.

4.1.7 Even-odd preconditioning

In order to accelerate the inversion of Dirac operators for eqs. (1.69) and (1.90) with the CG algorithm, even-odd preconditioning [49] is used to reduce the condition number of the operator. Lattice sites are separated into two sets of even or odd lattice sites, which are defined by eq. (A.40). Thus, the Dirac equation of eq. (4.6) is recast into

$$
\begin{aligned}
Q^{ee}_{\underline{n},m}\phi^e_m + Q^{eo}_{\underline{n},m}\phi^o_m &= \gamma^5\eta^e_{\underline{n}}, \\
Q^{oe}_{\underline{n},m}\phi^e_m + Q^{oo}_{\underline{n},m}\phi^o_m &= \gamma^5\eta^o_{\underline{n}},
\end{aligned}
\tag{4.9}
$$

where colour and spinor indices are omitted and indices ^{o} and ^{e} label fields restricted to odd or even sites. Matrix multiplications with gauge fields occur only in the hopping terms $Q^{eo}_{n,m}$ and $Q^{oe}_{n,m}$. $Q^{ee}_{n,m}$ and $Q^{oo}_{n,m}$ are constant matrices of type $Q_0\delta_{n,m}$. Their colour structure is trivial and they are listed in table 4.2.

Action	Q_0	$\sqrt{\det Q_0}$
Wilson	$(\frac{4r}{a} + m_0)\mathbf{1}$	$\left(\frac{4r+am_0}{a}\right)^2$
Karsten-Wilczek	$i\frac{3\zeta+c}{a}\gamma^\alpha + m_0\mathbf{1}$	$\left(\frac{3\zeta+c}{a}\right)^2 + m_0^2$
Boriçi-Creutz	$i\frac{c-2\zeta}{a}\Gamma + m_0\mathbf{1}$	$\left(\frac{c-2\zeta}{a}\right)^2 + m_0^2$

Table 4.2: Constant matrices Q_0 have $\sqrt{\det Q_0} > 1/a^2$ and are easily inverted.

Following standard procedures, the upper row of eq. (4.9) is formally solved for ϕ^e_m,

$$
\phi^e_m = (Q^{ee\,-1})_{m,\underline{n}}\left(\gamma^5\eta^e_{\underline{n}} - Q^{eo}_{\underline{n},p}\phi^o_p\right).
\tag{4.10}
$$

---

[1] The double precision scalar ν_k can be omitted since λ_k can be reused to store $|s_k|^2$ as well.

[2] These final iterations require three additional double precision work space spinor fields, but ensure convergence in double precision. No more than two additional interations have been observed.

Using eq. (4.10), ϕ_m^e is eliminated from the lower row, which is reshuffled to

$$\left(Q_{\underline{n},m}^{oo} - Q_{\underline{n},m_0}^{oe}(Q^{ee\,-1})_{m_0,m_1}Q_{m_1,m}^{eo}\right)\phi_m^o = \gamma^5\eta_{\underline{n}}^o - Q_{\underline{n},m_2}^{oe}(Q^{ee\,-1})_{m_2,\underline{n}}\gamma^5\eta_{\underline{n}}^e. \qquad (4.11)$$

A new notation is introduced using a matrix $\widehat{Q}_{n,m}$ and a preconditioned source ξ_n^o,

$$\widehat{Q}_{n,m} = \left(\delta_{n,m} - (Q^{oo\,-1})_{n,m_1}Q_{m_1,m_2}^{oe}(Q^{ee\,-1})_{m_2,m_3}Q_{m_3,m}^{eo}\right), \qquad (4.12)$$

$$\xi_n^o = (Q^{oo\,-1})_{n,\underline{m}}\left(\gamma^5\eta_{\underline{m}}^o - Q_{\underline{m},m_1}^{oe}(Q^{ee\,-1})_{m_1,\underline{m}}\gamma^5\eta_{\underline{m}}^e\right). \qquad (4.13)$$

This notation allows for matching eq. (4.11) to the form of eq. (4.8) as

$$\widehat{Q}_{n,m}\phi_m^o = \xi_n^o. \qquad (4.14)$$

Hence, the CG inverter can be applied to the system of eq. (4.14). After the solution $\phi_m^o = (\widehat{Q}^{-1})_{m,n}\xi_n^o$ is obtained, the even components ϕ_m^e are calculated from eq. (4.10). The even-odd preconditioned operator $\widehat{Q}$ requires the same number of matrix-times-vector operations like the original operator Q, since the matrix multiplication is applied twice to only half the number of sites. However the condition number is reduced, since the gauge field dependent hopping term is suppressed against the constant on-site term by $(\det Q_0)^{1/2}$ instead of $(\det Q_0)^{1/4}$. Table 4.2 shows that suppression is best for Wilson fermions and worst for Boriçi-Creutz fermions. It should be noted here that even-odd preconditioning is computationally advantageous only if $Q_{n,m}^{ee}$ and $Q_{n,m}^{oo}$ can be inverted at marginal numerical cost.

4.1.8 Contractions and interpolating operators

Connected correlation functions are calculated according to eq. (3.48) from contractions of two fermion propagators at source and sink with a summation of the entire sink slice. Connected correlation functions depend on point-to-all propagators $S_{n,0}$ and all-to-point propagators $S_{0,n}$. The latter would require a prohibitive amount of inversions. However, the propagator inherits the γ^5 hermiticity from the Dirac operator and satisfies

$$S_{0,n} = \gamma^5(S^\dagger)_{n,0}\gamma^5. \qquad (4.15)$$

Therefore, connected correlation functions require only point-to-all propagators,

$$\mathcal{C}_{\mathcal{M},\mathcal{N}}(t) = \sum_{n\in\Lambda_t^0}\mathrm{tr}\left(S_{n,0}\mathcal{M}\gamma^5(S^\dagger)_{n,0}\gamma^5\mathcal{N}\right). \qquad (4.16)$$

Contraction of all twelve propagator components completes the trace at the source. Source Dirac matrices are implemented through contraction of different propagator components and multiplication with phase factors (± 1 or $\pm i$). The Dirac matrix at either source or sink must be transposed, since

$$\mathcal{C}_{\mathcal{M},\mathcal{N}}(t) = \sum_{n\in\Lambda_t^0}\mathrm{tr}_c\left(S_{n,0}^{\alpha\beta}(S^*)_{n,0}^{\delta\gamma}((\mathcal{M}\gamma^5)^T)^{\gamma\beta}(\gamma^5\mathcal{N})^{\delta\alpha}\right). \qquad (4.17)$$

Details of the procedure are listed in appendix F.2.

4.1.9 Smearing

A clean study of the anisotropy due to the Karsten-Wilczek action requires that other potential sources of anisotropy are avoided. Therefore, symmetric lattices are used. Compared to the usual choices for hadron spectroscopy, symmetric lattices have an unusually large spatial and unusually small temporal extent. These lattices have the disadvantage that the time interval in which the ground state is isolated becomes very short. It is therefore desirable to use smearing techniques to enhance the ground state's spectral weight. Local and smeared interpolating operators for creation and annihilation of mesons are implemented in order to improve the signal of the pseudoscalar ground state. There is a heuristic rule that the overlap of an interpolating operator with a meson's creation operator is considerably improved if the average smearing radius of the spatial distribution of the smeared source operator is of similar magnitude than the physical radius of that meson. Thus, spectral weights of excited states are reduced and the ground state is isolated already for shorter Euclidean time separations (cf. section 4.2). Gauge-invariant smearing is achieved with (iterative) *Jacobi smearing*[3] algorithms [4,87]. Jacobi smearing is an iterative procedure in which a gauge-invariant lattice Laplacian is added to the original spinor field with a fixed iteration count irrespective of convergence,

$$
O_{n,m}^{J}[U] = \frac{1}{1 + 6\kappa_{JS}} \left(\delta_{n,m} + \frac{\kappa_{JS}}{a} \sum_{\mu \neq 0} \left(U_n^\mu \delta_{n+\hat{e}_\mu, m} + U_{n-\hat{e}_\mu}^{\mu\dagger} \delta_{n-\hat{e}_\mu, m} \right) \right), \qquad (4.18)
$$

and includes a *normalisation factor* $1/(1 + 6\kappa_{JS})$, which prevents an unbounded growth of the smeared field. The smearing directions must be restricted to those perpendicular to the Euclidean time direction in order to avoid changes to the transfer matrix. In order to obtain a smooth spatial distribution, violent local fluctuations of spatial gauge fields have to be reduced. This is achieved with so-called *fat links*. Fat links V_n^μ are calculated from *thin links* U_n^μ (the usual link variables) of the update procedure with link smearing algorithms that average gauge fields locally. As elementary step, thin links are replaced by the SU(3) projected linear combinations of the thin links and their n_S pairs of *staples*,

$$
V_n^\mu = \text{Proj}_{SU(3)} \left[(1 - \xi) U_n^\mu + \frac{\xi}{2n_S} \sum_{\nu \neq \mu} U_n^\nu U_{n+\hat{e}_\nu}^\mu U_{n+\hat{e}_\mu}^{\mu\,\dagger} \right]. \qquad (4.19)
$$

In terms of the practical application, the smoothing properties of link smearing are similar to those of evolution with gradient flow [25, 112]. For the purpose of use in the numerical studies of this thesis, APE smearing [3] and HYP smearing [88] are implemented. The latter algorithm is applied with standard parameters ($\alpha = 0.75$, $\beta = 0.6$, $\gamma = 0.3$). This amounts to using a single pair of opposite staples with parameter $\xi = \gamma$ to get a first new set of links. Next, a second new set of links is constructed using the first set of new links for building two pairs of opposite staples with parameter $\xi = \beta$. Finally, the fat links are constructed using the second new set of links for building three pairs of

---

[3]Jacobi smearing is related to Wuppertal smearing (also called Gaussian smearing), where the smearing procedure is repeated until convergence is reached.

opposite staples with parameter $\xi = \alpha$. Three full iterations of HYP smearing are used to provide smooth links for smeared interpolating operators at the source of correlation functions.

The Jacobi smearing parameter is fixed as $\kappa_{JS} = 4.0$, which is a standard value used in many applications. The iteration number n_{JS} is adapted to the gauge coupling (cf. table 4.1) in order to achieve smearing radii of approximately $r \approx 0.5\,\mathrm{fm}$. This enhances the spectral weight of the pseudoscalar ground state. Lastly, it is noted that correlation functions which are smeared only at either the source or the sink may include states with negative spectral weights. In these cases, the correlation function is not necessarily a convex function and low-lying excited states may cancel partly with the ground state and reduce the quality of the signal.

4.1.10 Parallelisation

Memory considerations as well as the general need to minimise the computational effort strongly motivate parallelisation of numerical simulations. The full lattice Λ is subdivided into equally-sized local sublattices λ_j, which must communicate the fields in the neighbourhood of their boundaries $\partial \lambda_j$ to their neighbouring subprocesses after every modification. Communication between subprocesses is handled by MPI routines. Data is communicated via the Infiniband network of the Wilson cluster. In parallelised code, extra memory is required for the boundaries $\partial \lambda_j$, which store copies of fields from neighbouring sublattices. Thus, a finer division into local sublattices incurs a larger memory overhead for boundaries. Moreover, actual communication of boundary fields must wait for termination of the previous subprocess on all local sublattices and communication itself is a bottleneck for application of the Dirac operator.

For Karsten-Wilczek fermions with $\zeta = \pm 1$, kinetic terms of the Dirac operator in any direction other than the $\hat{e}_{\underline{\alpha}}$ direction have only one linearly independent pair of one lower and one upper Dirac component (cf. appendix F.1). After this pair has been relayed to neighbouring sublattices, missing components are automatically reconstructed in communication routines. The present simulation code comprises Karsten-Wilczek fermions for two different directions of the Karsten-Wilczek term, either $\underline{\alpha} = 0$ or $\underline{\alpha} = 3$, with arbitrary ζ or $\zeta = +1$. Boriçi-Creutz ($\zeta = +1$) and Wilson fermions are also available. The Dirac structure of hopping terms for some of these Dirac operators (e.g. $\frac{1 \pm \gamma^{\mu}}{2}$ for Wilson or $\frac{\gamma^{\mu} \mp i\zeta\gamma^{\underline{\alpha}}}{2}$ for $\mu \neq \underline{\alpha}$ for Karsten-Wilczek fermions) allows for reconstruction of some Dirac components from the others, which allows a reduction of the computational cost. This is due to a reduced number of SU(3) multiplications and also due to a reduced number of components that have to be communicated across the boundaries. Each Dirac operator has its own optimised set of boundary field communication buffers and routines, which are initialised automatically in simulations.

4.2 Anisotropy of hadronic quantities

β	$a\,[fm]$	r_0	L	n_{cfg}	am_0	c	d
6.0	0.093	5.368	32	100	$0.02, 0.03, 0.04, 0.05$	$[-1.2, +0.3]$	0.0
6.0	0.093	5.368	32	100	$0.01, 0.02, 0.03, 0.04, 0.05$	$[-0.65, -0.20]$	$[-0.08, +0.02]$
6.0	0.093	5.368	48	40	0.02	$[-0.65, +0.0]$	0.0
6.2	0.068	7.360	32	100	$0.01, 0.02, 0.03, 0.04, 0.05$	$[-0.65, -0.20]$	$[-0.08, +0.04]$
6.2	0.068	7.360	48	40	0.02	$[-0.65, +0.0]$	0.0
5.8	0.136	3.668	32	100	$0.02, 0.04, 0.05$	$[-0.65, +0.0]$	$[0.0, +0.02]$

Table 4.3: Symmetric lattices ($T = L$) are used in studies of the anisotropy. The parameter c is varied in small steps close to the perturbative estimates (cf. table 2.2).

Numerical studies [155] of the anisotropy are performed with Karsten-Wilczek fermions of eqs. (1.69) and (1.70) in order to tune the coefficients c and d non-perturbatively. Boosted perturbation theory (BPT) provides an initial guess for the coefficients (cf. table 2.2), where the plaquette is used to estimate non-perturbative parameters from one-loop results (cf. section 2.4). Symmetric lattices with $T = L$ and periodic boundary conditions in all directions avoid anisotropic finite volume or boundary effects that might obscure the anisotropy due to the fermion action. Since simulations utilise the quenched approximation, the coefficient d_p of the gluonic counterterm is set to zero. Correlation functions are calculated using Karsten-Wilczek fermion propagators with $\zeta = +1$ and alignment $\underline{\alpha} = 0$ (cf. section 4.1.5), where the direction of correlation is either the $\hat{e}_0$ or $\hat{e}_3$ direction. With respect to the alignment of the Karsten-Wilczek operator, $\hat{e}_0$ yields *parallel* and $\hat{e}_3$ yields *perpendicular correlation functions*. The statistical basis are 100 configurations (cf. section 4.1.4) of 32^4 lattices and 40 configurations of 48^4 lattices. Lattice parameters are listed in table 4.3. Correlation functions use source-smeared interpolating operators (cf. section 4.1.9) with a smearing radius of $r \approx 0.5\,\mathrm{fm}$, since the direction of correlation is quite short ($T = 32$) and isolation of the ground state is not guaranteed otherwise. Scale setting using the Sommer parameter [143] is accomplished via eq. (4.5).

4.2.1 Tuning with the mass anisotropy

The gauge coupling is chosen as $\beta = 6.0$ for initial scans of parameter space. The bare fermion mass am_0 is set to a relatively high value, which allows for inversions of the Dirac operator with moderate computational cost. The marginal counterterm's coefficient is fixed as $d = 0$ initially, because BPT suggests that its effects are mild (cf. table 2.2) compared to the relevant parameter c. c is varied in small steps near the BPT estimate ($c \approx c_{BPT}$) and in wide steps in more outlying regions of parameter space ($c \not\approx c_{BPT}$). The pseudoscalar (PS) correlation function with vanishing hadron

momentum (cf. eq. (4.16))

$$\mathcal{C}_{PS}^{\parallel,\perp}(t) \equiv \mathcal{C}_{\gamma^5,\gamma^5}(n_{\parallel,\perp}) \equiv \mathcal{C}_{5,5}(n_{\parallel,\perp}) = \sum_{n \in \Lambda_t^{\parallel,\perp}} \sum_{a,b} \sum_{\alpha,\beta} |S_{n,0}^{\alpha\beta,ab}|^2 \qquad (4.20)$$

is computed in numerical simulations using Karsten-Wilczek fermion propagators with $\underline{\alpha} = 0$. The direction of correlation is either $\hat{e}_t = \hat{e}_0$ for the *parallel* (wrt the Karsten-Wilczek term) or $\hat{e}_t = \hat{e}_3$ for the *perpendicular correlation function*. It is analysed by performing fits, which extract the mass $M_{PS}^{\parallel,\perp}$ of the pseudoscalar ground state. Statistical errors are determined with the Jackknife method (cf. appendix C). Since the study of the anisotropy is restricted to the pseudoscalar channel, the index 'PS' is omitted in the remainder of section 4.2. The mass $M_\parallel$, which is calculated from the parallel correlation function $\mathcal{C}^\parallel(t)$ is called the *parallel mass*, and the mass $M_\perp$, which is calculated from the perpendicular correlation function $\mathcal{C}^\perp(t)$, is called the *perpendicular mass*. The *mass anisotropy* is the difference of squared pseudoscalar masses,

$$\Delta(M_{PS}^2) \equiv \left(M_\parallel^2\right) - \left(M_\perp^2\right). \qquad (4.21)$$

which is employed as a tuning criterion for c, while the other parameters β, m_0 and d are kept at fixed values. The mass anisotropy is interpolated as a function of c. The extremum of the mass anisotropy defines the non-perturbatively tuned coefficient c_M[4]. In the next step, the bare fermion mass am_0 is lowered towards the chiral limit. An extrapolation of c_M to the chiral limit is performed in order to compare with estimates from BPT. In the following step, sensitivity to variation of d is studied. Lastly, the coupling β is varied and the procedure is repeated for different lattice spacings.

4.2.2 Determination of the pseudoscalar mass

Because the fermion action of eq. (1.69) lacks a simple transformation behaviour under $n_{\underline{\alpha}}$ reflection, backward (b) and forward (f) propagating states will in general be different in parallel correlation functions. Masses and spectral weights of backwards and forwards states are treated as independent. If both masses differ, $M_\parallel$ cannot be unambiguously defined. In line with section 3.1.4, no oscillations are expected in the γ^5 channel. Hence, this correlation function can be described for vanishing hadronic momenta as

$$\mathcal{C}(t) = \sum_{k=0}^{\infty} \left(\frac{A_k^f}{2M_k^f} e^{-M_k^f \cdot t} + \frac{A_k^b}{2M_k^b} e^{-M_k^b \cdot (T-t)} \right) \qquad (4.22)$$

and reaches asymptotic behaviour for large T and $t \approx T/2$ as

$$\mathcal{C}(t) = \frac{A_0^f}{2M_0^f} e^{-M_0^f \cdot t} + \frac{A_0^b}{2M_0^b} e^{-M_0^b \cdot (T-t)} + \dots. \qquad (4.23)$$

---

[4]c_M labels the value of c that is eventually obtained by tuning with the mass anisotropy. The label is used to allow a distinction to c from other methods of tuning (cf. sections 4.3.3,4.5).

Using eq. (4.23) as a four-parametric fit function with adequate fit ranges in clearly separated intervals of the Euclidean time direction simultaneously extracts masses of backwards and forwards states as independent parameters. A local effective mass of either backwards or forwards states is another tool for isolating their respective masses.

Local effective mass
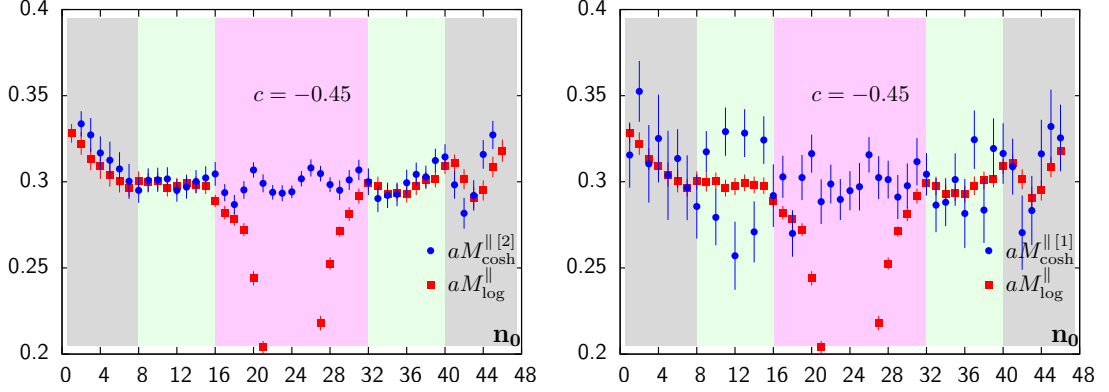
Figure 4.2: Left: $M_{\text{cosh}}^{[2]}(t)$ and $M_{\text{log}}(t)$ agree in the plateau region within errors. Right: Fluctuations around $M_{\text{log}}(t)$ beset $M_{\text{cosh}}^{[1]}(t)$ even in the plateau region. Symbols and data sets are explained in the text.

Such a local effective mass, which is called the *log mass*, is calculated as

$$M_{\text{log}}^{[s]}(t) = \frac{1}{s} \log \frac{|\mathcal{C}(t)|}{|\mathcal{C}(t+s)|} \tag{4.24}$$

and reaches a plateau for large times if the oncoming state is negligible. The parameter s is the step size and is usually set to one. In an interval around the midpoint of a periodic lattice, the log mass is a poor quantity for deciding whether the ground state has been reached because of the oncoming state's contribution. Another definition of a local effective mass is the *cosh mass*, which is calculated as

$$M_{\text{cosh}}^{[s]}(t) = \frac{1}{s} \log \left(R + \sqrt{R^2 - 1} \right), \ \ R = \frac{|\mathcal{C}(t+s)| + |\mathcal{C}(t-s)|}{2|\mathcal{C}(t)|}. \tag{4.25}$$

Effective mass plots in figure 4.2 have a lilac shaded band centered around midpoint ($t = T/2$), where the log mass (red filled squares) drops towards zero. Neither backwards nor forwards contributions are negligible in the central region. The grey-shaded bands near the temporal boundary of the lattice yield higher $M_{\text{log}}(t)$, since excited states cannot be neglected and the ground state is not isolated. In the green shaded plateau regions, $M_{\text{log}}(t)$ is constant within errors, since excited as well as oncoming states are negligible. Therefore, local effective masses in the green bands isolate the backward or forward propagating ground states repectively. The parallel pseudoscalar correlation function is

Eff. mass	Fit range [...]	Cor. fit $M^{[1]}$	χ^2/dof	Uncor. fit $M^{[1]}$	χ^2/dof	Cor. fit $M^{[2]}$	χ^2/dof	Uncor. fit $M^{[2]}$	χ^2/dof
cosh	$[8-16]$	0.305(3)	0.950	0.305(3)	2.800	0.299(3)	0.692	0.300(3)	0.237
cosh	$[32-40]$	0.304(3)	1.399	0.301(3)	0.915	0.305(2)	1.352	0.301(3)	1.406
cosh	$[8-16, 32-40]$	0.306(2)	1.447	0.303(3)	1.769	0.303(2)	2.225	0.300(2)	0.786
cosh	$[8-40]$	0.299(1)	5.801	0.301(1)	1.349	0.297(1)	7.148	0.299(1)	1.126
log	$[8-16]$	0.294(2)	1.633	0.297(3)	0.833	0.293(2)	1.910	0.296(3)	0.886
log	$[32-40]$	0.301(2)	1.461	0.299(2)	1.197	0.299(1)	2.303	0.299(2)	1.700
log	$[8-16, 32-40]$	0.299(1)	2.100	0.298(2)	1.006	0.302(1)	3.916	0.298(2)	1.965

Table 4.4: Fits to the effective mass mostly agree within $1-2\sigma$. $M^{[2]}_{\mathrm{cosh}}$ is more stable than $M^{[1]}_{\mathrm{cosh}}$. The data set is the same as in figure 4.2.

obtained with $\beta = 6.0$ and $c = -0.45$ on a 48^4 lattice from table 4.3. The pseudoscalar mass is $M^{\parallel}_{PS} \approx 630\,\mathrm{MeV}$. The cosh mass with $s = 2$ (blue bullets in the left plot of figure 4.2) agrees very well with $M_{\log}(t)$ in the plateau region. Moreover, $M^{[2]}_{\mathrm{cosh}}(t)$ maintains the plateau value within errors within the central region around midpoint. Since the cosh mass with $s = 1$ (blue bullets in the right plot of figure 4.2) strongly fluctuates around the plateau value of $M_{\log}(t)$, $M^{[1]}_{\mathrm{cosh}}(t)$ should not be used. The local effective mass is fitted as a constant within the plateau regions. Fit results in table 4.4 provide no numerical evidence of different backwards and forwards masses. However, χ^2/dof is very large and its considerable variation between different fits is not understood at present.

Parallel correlation functions

Independent parameters	Fit range [...]	Correlated fit M^f	M^b	χ^2/dof	Uncorrelated fit M^f	M^b	χ^2/dof
M^f_0, A^f_0	$[8-16]$	0.301(3)		1.261	0.298(3)		0.038
M^b_0, A^b_0	$[32-40]$		0.300(2)	0.690		0.297(3)	0.059
$M^f_0 = M^b_0, A^f_0 = A^b_0$	$[8-16]$	0.302(3)		1.154	0.299(3)		0.035
$M^f_0 = M^b_0, A^f_0 = A^b_0$	$[32-40]$		0.301(2)	0.740		0.298(3)	0.036
$M^f_0, M^b_0, A^f_0, A^b_0$	$[8-40]$	0.300(1)	0.299(1)	3.923	0.298(2)	0.299(2)	0.038
$M^f_0, M^b_0, A^f_0, A^b_0$	$[10-38]$	0.300(1)	0.296(1)	2.827	0.298(2)	0.299(2)	0.039
$M^f_0, M^b_0, A^f_0, A^b_0$	$[8-16, 32-40]$	0.304(3)	0.303(2)	1.402	0.299(3)	0.298(3)	0.036
$M^f_0, M^b_0, A^f_0, A^b_0$	$[10-16, 32-38]$	0.301(3)	0.301(3)	1.424	0.299(4)	0.296(3)	0.033
$M^f_0, M^b_0, A^f_0, A^b_0$	$[8-14, 34-40]$	0.303(3)	0.302(3)	1.858	0.299(4)	0.298(3)	0.042

Table 4.5: Backwards and forwards fit masses agree within errors. Fits with different functions or fit ranges are consistent but strongly deviate in their correlated χ^2/dof. The data set is the same as in figure 4.2.

An alternative approach uses fits to the correlation function with an ansatz like eq. (4.23). If the fit range is restricted to one of the plateau regions, backwards or forwards states are isolated for all fits of table 4.5. Fits with independent parameters for forwards and backwards states simultaneously extract properties of backwards or forwards ground

Fit range	Correlated fit			Uncorrelated fit		
[...]	M	$A \; [\times 10^{-3}]$	χ^2/dof	M	$A \; [\times 10^{-3}]$	χ^2/dof
$[10-38]$	0.2983(5)	6.02(10)	3.215	0.298(1)	6.2(2)	0.566
$[9-39]$	0.2988(5)	6.12(8)	3.120	0.298(1)	6.2(1)	0.585
$[8-40]$	0.2996(4)	6.24(8)	3.839	0.298(1)	6.2(1)	0.612
$[8-14, 34-40]$	0.304(2)	6.6(3)	1.795	0.299(3)	6.3(3)	0.985
$[8-16, 32-40]$	0.304(2)	6.6(2)	1.432	0.299(3)	6.3(3)	0.969
$[10-16, 32-38]$	0.301(2)	6.4(2)	1.272	0.298(3)	6.2(3)	0.989

Table 4.6: $M_\parallel$ is determined with a symmetrised fit. Though correlated χ^2/dof strongly depends on the fit range, results are stable and agree with uncorrelated fits within errors. The data set is the same as in figure 4.2.

states. Examples of fit results are listed in table 4.5. There is no numerical evidence for different backwards and forwards masses and consistency between both fit strategies is evident. Hereafter, $n_{\underline{\alpha}}$ reflection symmetry is assumed and $M_\parallel$ is defined as the fit mass obtained with a symmetrised fit ansatz. Local effective masses are calculated as cosh masses with step size $s = 2$ due to better numerical stability. Fit results are stable (cf. table 4.6), though correlated fits have large χ^2/dof if the interval around midpoint ($t \approx T/2$) is included.

Perpendicular correlation functions
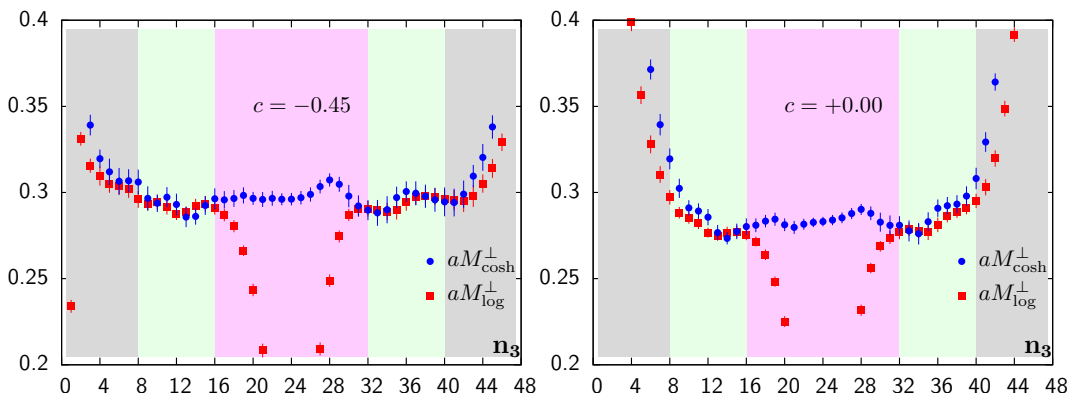
Figure 4.3: Left: $M_{\text{cosh}}(t)$ and $M_{\text{log}}(t)$ agree in the plateau region within errors at $c = -0.45 \approx c_{BPT}$. Right: $M_{\text{cosh}}(t)$ and $M_{\text{log}}(t)$ agree only for $t/a \in [13, 16] \cup [32, 35]$ at $c = +0.00$. Symbols and data sets are explained in the text.

Time reflection symmetry of perpendicular correlation functions is strictly satisfied and the asymptotic form of a correlation function is given by

$$\mathcal{C}(t) = \frac{A_0}{2M_0} \left(e^{-M_0 \cdot t} + e^{-M_0 \cdot (T-t)} \right) + \dots, \tag{4.26}$$

which can be used as a two-parametric fit function. The local effective masses shown in figure 4.3 are obtained from perpendicular pseudoscalar correlation functions with $\beta = 6.0$

Fit range	c = −0.45				c = +0.00			
	Cor. fit		Unc. fit		Cor. fit		Unc. fit	
[...]	$M^{[2]}$	χ^2/dof	$M^{[1]}$	χ^2/dof	$M^{[2]}$	χ^2/dof	$M^{[1]}$	χ^2/dof
[16−32]	0.297(1)	0.862	0.299(2)	0.061	0.283(1)	1.583	0.284(1)	0.069
[14−34]	0.296(1)	0.709	0.298(1)	0.078	0.2829(9)	1.363	0.284(1)	0.101
[12−36]	0.2953(8)	1.640	0.297(1)	0.121	0.2821(8)	1.913	0.283(1)	0.153
[10−38]	0.2960(7)	1.863	0.296(1)	0.192	0.2840(6)	2.114	0.283(1)	0.211
[8−40]	0.2953(4)	1.729	0.296(1)	0.266	0.2835(3)	6.716	0.283(1)	0.290
[8−14, 34−40]	0.293(1)	1.306	0.293(2)	0.354	0.283(1)	2.631	0.284(2)	0.597
[8−16, 32−40]	0.295(1)	1.243	0.293(2)	0.304	0.2834(9)	2.076	0.283(2)	0.510
[10−16, 32−38]	0.295(1)	0.912	0.292(2)	0.208	0.282(1)	1.633	0.281(2)	0.374

Table 4.7: Fits to perpendicular functions hint at increasing mass for fit ranges closer to midpoint, but agree within errors. The data set is the same as in figure4.3.

Fit range	Correlated fit			Uncorrelated fit		
[...]	M	$A\ [\times 10^{-3}]$	χ^2/dof	M	$A\ [\times 10^{-3}]$	χ^2/dof
[10−38]	0.2960(7)	3.05(5)	1.863	0.296(1)	3.10(8)	0.192
[9−39]	0.2953(4)	3.02(4)	1.820	0.296(1)	3.08(8)	0.223
[8−40]	0.2953(4)	3.01(3)	1.729	0.296(1)	3.06(8)	0.266
[8−14, 34−40]	0.293(1)	2.92(6)	1.306	0.293(2)	2.93(9)	0.354
[8−16, 32−40]	0.295(1)	2.96(5)	1.243	0.293(2)	2.93(9)	0.304
[10−16, 32−38]	0.295(1)	3.05(8)	0.912	0.292(2)	2.9(1)	0.208

Table 4.8: $M_\perp$ is determined with a symmetrised fit ansatz. The data set is the same as in figure4.3 for $c = -0.45$.

on a 48^4 lattice from table 4.3. The fit mass has a peculiar dependence on the fit range. Table 4.7 shows that the mass increases and χ^2/dof decreases, if the fit range is contracted towards the central region around midpoint ($t \approx T/2$). Excited states contributing with negative spectral weights are a possible explanation for this counterintuitive behaviour. Such behaviour is possible as the correlation functions is smeared only at the source (cf. section 4.1.9). Fit results are listed in table 4.8 for comparison with parallel correlation functions (cf. table 4.6).

4.2.3 Minimisation of the mass anisotropy

Interpolation of fit parameters

A fit to the pseudoscalar correlation function extracts the parameter M for the ground state's mass. Residual mass anisotropy can persist at finite lattice spacing even after tuning the counterterms' coefficients. Calculating the mass anisotropy from squared pseudoscalar masses is beneficial for a chiral extrapolation that assumes Goldstone boson-like properties. An ansatz for the squared masses $M^2_{\parallel,\perp}$ as quadratic functions in c,

$$M^2_{\parallel,\perp}(c) = a_0^{\parallel,\perp} + a_1^{\parallel,\perp} c + a_2^{\parallel,\perp} c^2,\tag{4.27}$$
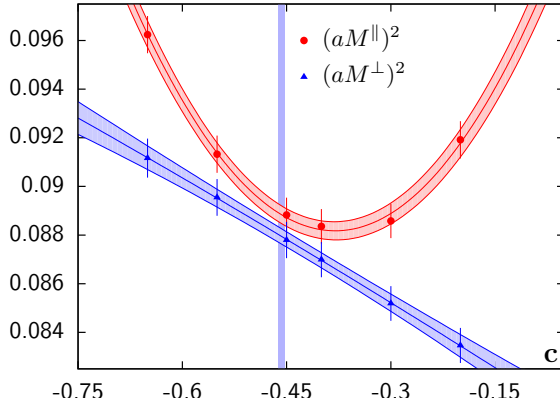
Figure 4.4: Interpolation of $M_\parallel^2$ and $M_\perp^2$ in c: Both squared masses are interpolated within $c \in [-0.65, -0.2]$. Correlators have $\beta = 6.0$ on a 48^4 lattice from table 4.3. The pseudoscalar mass is $M_{PS} \approx 630\,\text{MeV}$ for $c = c_M$.

is motivated by the expectation to achieve an minimum of the anisotropy after tuning. An example for the interpolation within $c \in [-0.65, -0.2]$ is shown in figure 4.4. All data within the range are matched within standard errors, but $M_\parallel^2$ at $c = 0.0$ requires additional higher order terms. Fit masses $M_{\parallel,\perp}^2$ do not match but retain a small difference, which is of the same order as statistical uncertainties. Therefore, the absolute mass anisotropy of eq. (4.21) is not necessarily a good observable. The extremum of the mass anisotropy is calculated from the difference of interpolations as

$$c_M = -\frac{a_1^\parallel - a_1^\perp}{2(a_2^\parallel - a_2^\perp)} \qquad (4.28)$$

and indicated as the blue vertical band in figure 4.4.

| Fit range | c_M for $c \in [-0.65, -0.20]$ | | c_M for $c \in [-0.65, +0.00]$ | |
[...]	Cor. fit	Unc. fit	Cor. fit	Unc. fit
$[10-38]$	$-0.460(5)$	$-0.457(6)$	$-0.457(4)$	$-0.456(4)$
$[9-39]$	$-0.519(9)$	$-0.457(5)$	$-0.494(6)$	$-0.455(4)$
$[8-40]$	$-0.508(9)$	$-0.457(5)$	$-0.486(5)$	$-0.455(4)$

Table 4.9: Extrema of $\Delta(M_{PS}^2)$ are stable within errors only for uncorrelated fits to the correlation function. The data set has $\beta = 6.0$ on a 48^4 lattice from table 4.3.

Though the fit range dependence of c_M for interpolations of fit masses from correlated fits to the correlation function exceeds the statistical uncertainty, it is consistent with uncorrelated results for shorter fit intervals. This is shown in table 4.9.

Smaller lattices

Smaller lattices (32^4) of table 4.3 are used for scans of the parameter space in m_0 and d due to their smaller numerical cost. However, the time direction for symmetric lattices
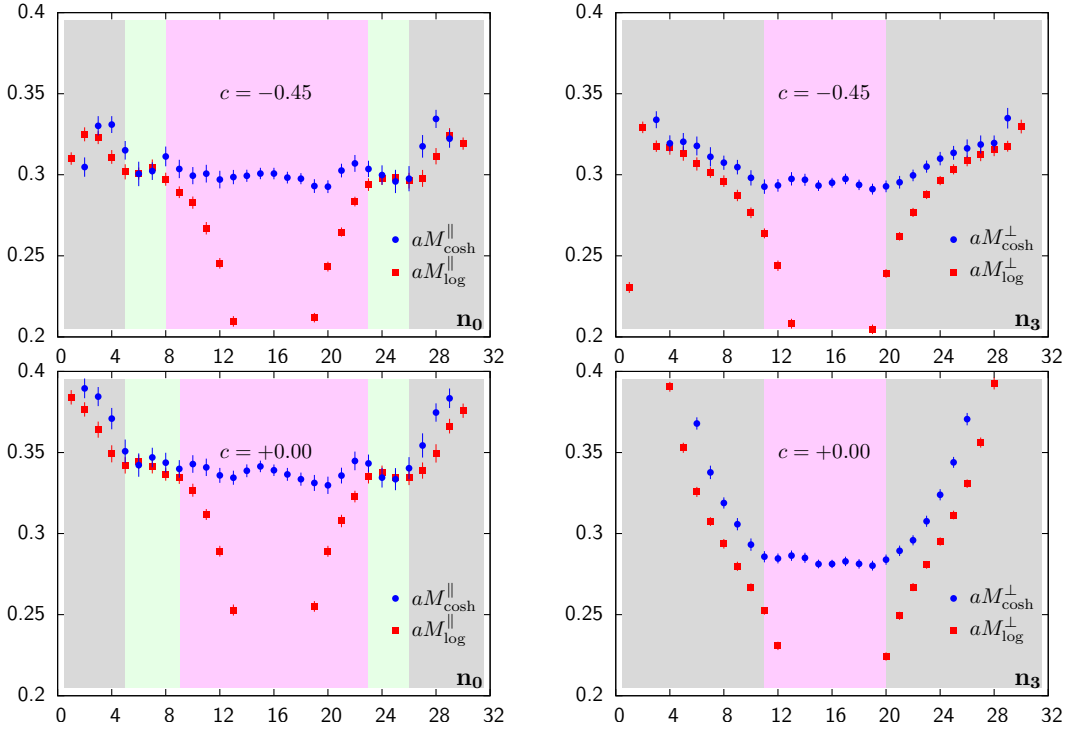
Figure 4.5: Left: Plateaus of $M_{\mathrm{cosh}}^{\parallel}(t)$ and $M_{\mathrm{log}}^{\parallel}(t)$ are very short. Right: $M_{\mathrm{log}}^{\perp}(t)$ lacks the plateau of $M_{\mathrm{cosh}}^{\perp}(t)$. Symbols and data sets are explained in the text.

with $T = L$ might be too short for a clean extraction of the ground state, which introduces systematical uncertainties. Scans of parameter space are required for clarification of the dependence of the mass anisotropy on d and for an extrapolation of c_M to the chiral limit. Local effective mass plateaus, which are invariably shorter due to the shorter time direction, are presented in figure 4.5. The cosh mass with $s = 2$ is represented by blue bullets and the log mass with $s = 1$ by red squares. The cosh mass plateau of the perpendicular correlation function is very short. The pseudoscalar correlation functions have $c = -0.45$ in the upper plots and $c = 0.0$ in the lower plots. Data are obtained with $\beta = 6.0$, $m_0 = 0.02$ and $d = 0.0$ on a 32^4 lattice from table 4.3. The pseudoscalar mass for $c = -0.45$ is $M_{PS} \approx 630\,\mathrm{MeV}$ and consistent with 48^4 within combined errors.

| Fit range | c_M for $c \in [-0.65, -0.20]$ | | c_M for $c \in [-0.70, +0.00]$ | |
$[\dots]$	Cor. fit	Unc. fit	Cor. fit	Unc. fit
$[12-20]$	$-0.448(8)$	$-0.449(8)$	$-0.450(6)$	$-0.453(7)$
$[10-22]$	$-0.444(6)$	$-0.442(6)$	$-0.446(5)$	$-0.447(5)$
$[9-23]$	$-0.446(6)$	$-0.442(5)$	$-0.447(5)$	$-0.446(5)$
$[8-24]$	$-0.440(6)$	$-0.442(5)$	$-0.442(5)$	$-0.445(4)$

Table 4.10: c_M is slightly less negative on smaller volumes (cf. table 4.9). The data set has $\beta = 6.0$, $m_0 = 0.02$ and $d = 0.0$ on a 32^4 lattice from table 4.3.
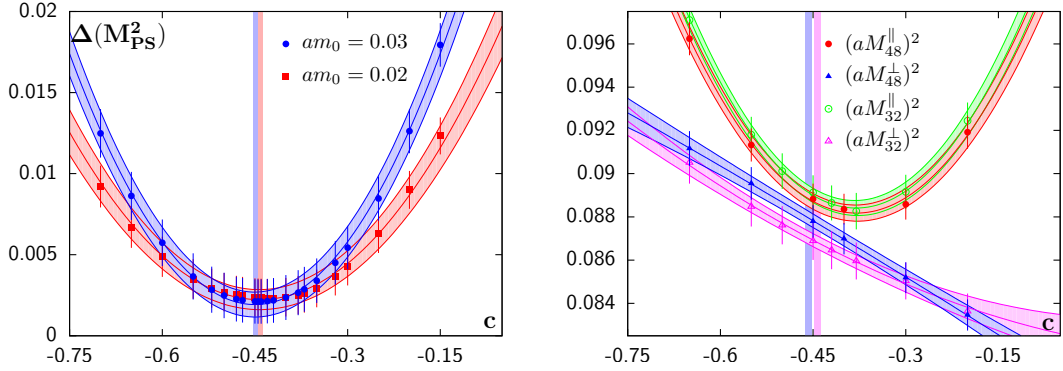
Figure 4.6: Left: The extremum is shallower for lighter masses. Right: The mass anisotropy is consistent within errors. Symbols and data sets are explained in the text.

Direct subtraction of the interpolations yields $\Delta(M_{PS}^2)$ of eq. (4.21). The left plot of figure 4.6 displays the dependence of $\Delta(M_{PS}^2)$ on the fermion mass parameter in the neighbourhood of c_M, where the two overlapping vertical bands indicate c_M for the different masses. The lower mass $am_0 = 0.02$ (red squares) yields a shallower interpolation than the higher mass $am_0 = 0.03$ (blue bullets). Interpolations of fit masses for different lattice sizes are plotted together in the right plot of figure 4.6. Masses on the smaller lattice are denoted by open symbols. Though the mass splitting is slightly wider on the smaller lattice as $M_{32}^{\parallel} > M_{48}^{\parallel}$ and $M_{32}^{\perp} < M_{48}^{\perp}$, the masses agree within errors. Minimisation results for $\beta = 6.0$, $m_0 = 0.02$ and $d = 0.0$ using different fit and interpolation ranges are stable within errors (cf. table 4.10). Values for the larger ($c_M^{(48)}$, cf. table 4.9) and smaller ($c_M^{(32)}$, cf. table 4.10) lattices are indicated as vertical blue and lilac bands in the figure. Their difference $\Delta_{c_M}^{\text{fs}} \equiv c_M^{(48)} - c_M^{(32)} \approx -0.01$ provides an estimate of finite size effects, which are considered as systematical errors.

Chiral extrapolation of the minimum of the mass anisotropy

Fit range	c_M, linear in m_0		c_M, quadratic in m_0	
$[\ldots]$	Cor. fit	Unc. fit	Cor. fit	Unc. fit
$[12-20]$	$-0.448(11)$	$-0.451(12)$	$-0.429(22)$	$-0.436(21)$
$[10-22]$	$-0.439(8)$	$-0.439(9)$	$-0.425(14)$	$-0.422(14)$
$[9-23]$	$-0.440(8)$	$-0.437(13)$	$-0.429(13)$	$-0.421(12)$
$[8-24]$	$-0.429(8)$	$-0.435(7)$	$-0.411(12)$	$-0.419(11)$

Table 4.11: Quadratic instead of linear chiral extrapolation yields more negative c_M with larger errors. Correlators have $\beta = 6.0$ on a 32^4 lattice from table 4.3.

Extrema of $\Delta(M_{PS}^2)$ on the 32^4 lattice with $\beta = 6.0$ and $d = 0.0$ are extrapolated towards the chiral limit. Linear and quadratic extrapolations of c_M are displayed in the
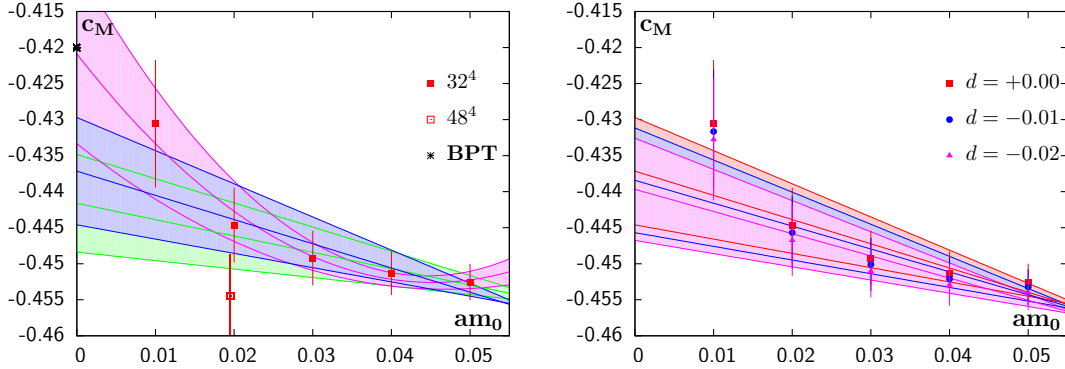
Figure 4.7: Left: A chiral extrapolation of c_M can be compared to c_{BPT}. Finite size effects seem to point to c_M being more negative by $\Delta^{\text{fs}}_{c_M} \approx -0.01$. Right: Dependence on d is not resolved by c_M. Symbols and data sets are explained in the text.
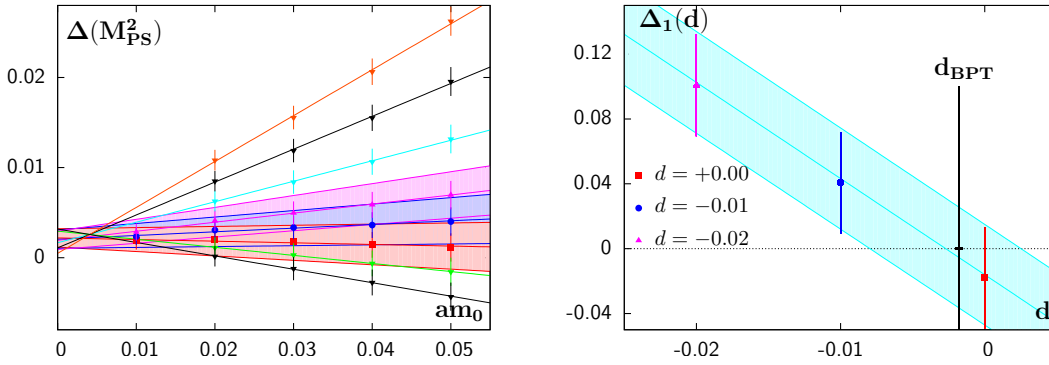

Figure 4.8: Left: $\Delta(M^2_{PS})$ for $c = c_M$ is linear in m_0. Right: The slope $\Delta_1(d)$ is linear in d and vanishes close to d_{BPT}. Symbols and data are explained in the text.

left plot of figure 4.7 and listed in table 4.11. The data set contains all masses and $c \in [-0.65, -0.2]$ from table 4.3 for fit ranges of $t/a \in [9 - 23]$ for 32^4. The lightest mass ($am_0 = 0.01$) is not matched well in a linear extrapolation (blue line). However, curvatures of quadratic extrapolations (lilac line) seem too high as the extrapolation bends upwards at the highest mass ($am_0 = 0.05$). It is probably pure coincidence that its endpoint is very close to the perturbative estimate c_{BPT} (black burst). A linear extrapolation with the lightest mass left out yields slightly more negative c_M, but still agrees with the extrapolation of the full sample within errors. The 48^4 lattice (open symbol at $am_0 = 0.02$, slightly shifted to the left for distinction of error bars) indicates more negative c_M (by $\Delta^{\text{fs}}_{c_M} \approx -0.01$) than the 32^4 lattice (filled symbols). Thus, c_M for the lightest mass ($am_0 = 0.01$) agrees with the central value of the fit within combined statistical and estimated finite size errors. Variation of d on the 32^4 lattice is shown in the right plot of figure 4.7. Since results for $d = 0.0$ (red squares), $d = -0.01$ (blue bullets) and $d = -0.02$ (lilac triangles) are consistent within fractions of the errors, the

tuning condition $c = c_M$ can be considered as independent of d.

Once c is tuned to c_M, the interpolating function for $\Delta(M_{PS}^2)$ yields the residual mass anisotropy, which is shown for a 32^4 lattice at $\beta = 6.0$ in the left plot of figure 4.8. The data set covers $d \in [-0.08, +0.02]$ and is extrapolated linearly in the mass,

$$\Delta(M_{PS}^2) = \Delta_0 + \Delta_1(d)\, m_0. \tag{4.29}$$

The crossing of lines at $am_0 > 0$ indicates that tuning does not remove the anisotropy completely. The slope parameter $\Delta_1(d)$ is linear in d (cf. right plot of figure 4.8) and is dominated by the d dependence of $M_{\parallel}^2$. The turquoise line is a regression line between $d = 0.0$ and $d = -0.02$. The vertical line marks the BPT estimate ($d_{BPT} = -0.00179$).

4.2.4 Dependence of the mass anisotropy on the gauge coupling
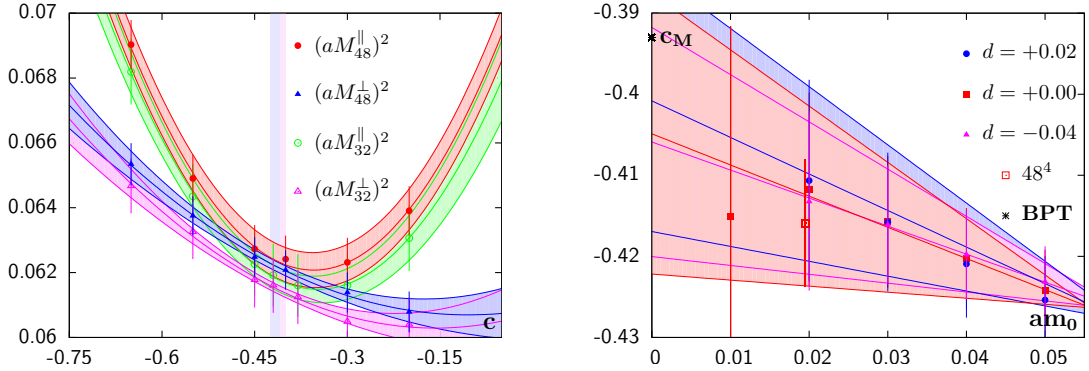
Finer lattices: $\beta = 6.2$

Figure 4.9: Left: The mass anisotropy is consistent within errors. The pseudoscalar mass is $M_{PS} \approx 725 \,\text{MeV}$ for $c = c_M$. Right: c_M is insensitive to d within errors. Symbols and data are explained in the text.

The gauge coupling is changed to $\beta = 6.2$, which is closer to the continuum limit. The previous procedure for determination of the mass and interpolation using eq. (4.27) is repeated (cf. interpolations for $am_0 = 0.02$ in the left plot of figure 4.9). The smaller physical lattice size primarily affects perpendicular correlation functions and reasonable fit ranges are very short. Due to large variations of c_M for changes of the fit range, systematical uncertainties due to the fit range are estimated as $\Delta_{c_M}^{\text{fr}} \approx 0.02$. A linear chiral extrapolation of c_M is conducted on the 32^4 lattice with $\beta = 6.2$ as in section 4.2.3. Large statistical errors are observed and c_M is quite insensitive to d (right plot of figure 4.9). The estimate c_{BPT} (black burst) lies within the error bands of c_M. The 48^4 lattice (open symbol at $am_0 = 0.02$, slightly shifted to the left) suggests more negative values of c_M than the 32^4 lattice (filled symbols), which is also indicated by the two overlapping vertical bands (blue for 48^4, lilac for 32^4) in the left plot. Chiral behaviour of the residual
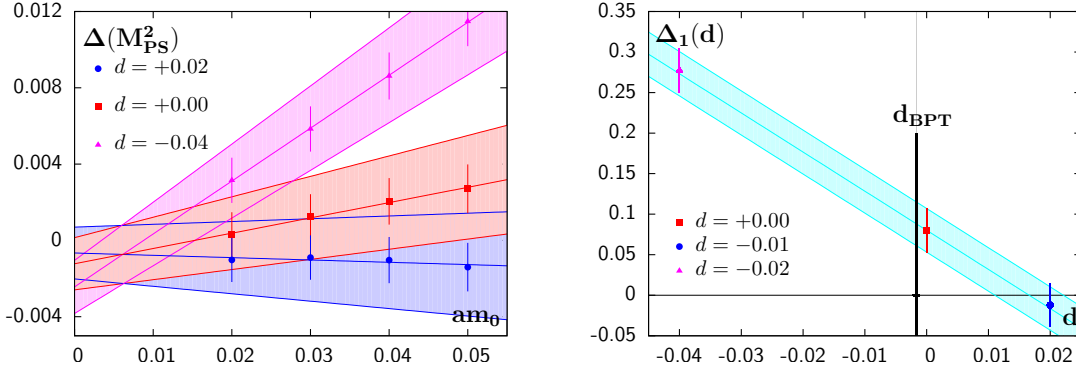
Figure 4.10: Left: $\Delta(M_{PS}^2)$ for $c = c_M$ is linear in m_0. Right: The slope $\Delta_1(d)$ is linear in d and vanishes close to $d \approx +0.015$. Symbols and data are explained in the text.

mass anisotropy $\Delta(M_{PS}^2)$ for $c = c_M$ is described by eq. (4.29) within errors. In the left plot of figure 4.10, it is shown that Δ_0 is consistent with zero but changes its sign with respect to $\beta = 6.0$. The right plot displays the linear regression of $\Delta_1(d)$. The vertical line marks the BPT estimate.
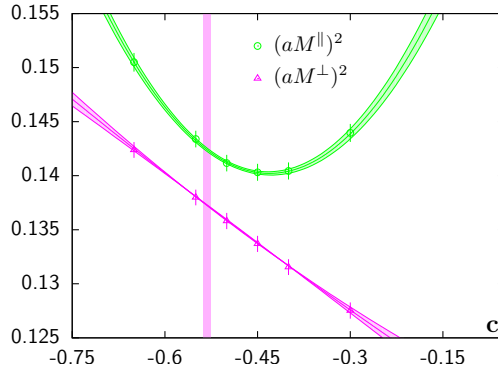
Coarser lattices: $\beta = 5.8$

Figure 4.11: The coarser lattice with $\beta = 5.8$ is more anisotropic. Pseudoscalar masses for $am_0 = 0.02$ are $M_{PS}^{\parallel} \approx 545\,\mathrm{MeV}$ and $M_{PS}^{\perp} \approx 535\,\mathrm{MeV}$ for $c = c_M$. Symbols and data sets are explained in the text below.

Figure 4.11 shows that the mass anisotropy between parallel (green circles) and perpendicular (lilac triangles) masses is larger than for $\beta = 6.0$. c_M is indicated by the lilac vertical band. Because data for larger lattices with $\beta = 5.8$ is not available, uncertainties due to finite size of the lattice are estimated to be as large as for $\beta = 6.0$ ($\Delta_{c_M}^{\mathrm{fs}} \equiv c_M^{(48)} - c_M^{(32)} \approx -0.01$ as defined in section 4.2.3). Significant dependence on the fit range (for fits to the correlation function) is not observed. The left plot of figure
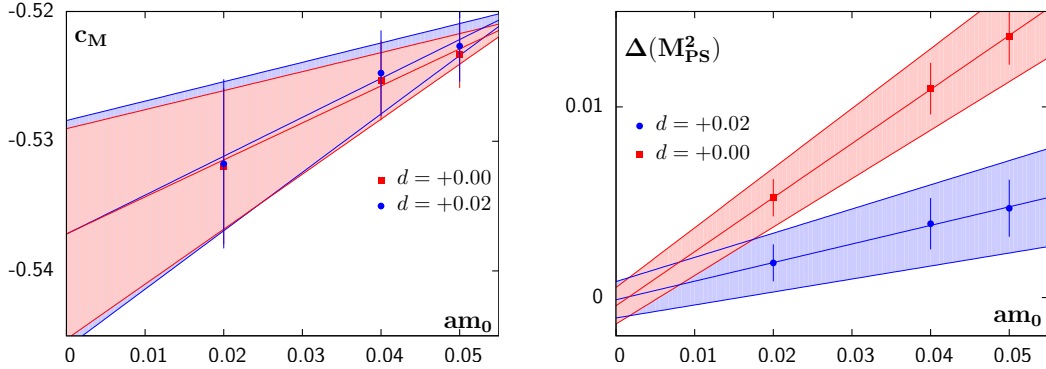
109

Figure 4.12: Left: The chiral extrapolation of c_M has a positive slope. Right: $d_0 \approx +0.03$ would flat approach the chiral limit flatly. Symbols and data sets are explained below.

4.12 shows that c_M for $d = +0.00$ (red squares) and $d = +0.02$ (blue bullets) is independent of d within errors. The positive slope of the chiral extrapolation starkly differs from results for finer lattices. The estimate $c_{BPT} = -0.454$ is more than 15% less negative than c_M. The residual mass anisotropy $\Delta(M_{PS}^2)$ suggests that the slope $\Delta_1(d)$ of the approach to the chiral limit vanishes for $d \approx +0.03$. At present, no particular reason is known why trends in the chiral extrapolation for $\beta = 5.8$ and $\beta = 6.0$ or $\beta = 6.2$ are opposite. However, data are compatible with c_M being independent of am_0.

Qualitative aspects of gauge coupling dependence

The non-perturbative value c_M is slightly more neagtive than the estimate c_{BPT}. Unsurprisingly, this difference $(c_{BPT} - c_M)$ increases for coarser lattices. c_M for all three gauge couplings is summarised in table 4.12. Dominant sources for systematical uncertainties are finite size effects, dependence on the fit range and the chiral extrapolation. Because the lightest mass is $M_{PS} \approx 450\,\text{MeV}$, the study of the anisotropy has not necessarily reached the chiral regime. Perpendicular correlation functions receive contributions from long-lived excited states. An increase of effective mass plateaus towards the midpoint of the lattice for source-smeared correlation functions suggests that these excited states may have negative spectral weights (cf. section 4.2.2). Their contribution seems to become more important with detuning of c. The associated systematical uncertainty is estimated to be similar in size to the other sources of systematical uncertainty.

β	$a\,[fm]$	c_M	M_{PS} for $c = c_M$
5.8	0.136	$-0.537(8)(10)$	540 MeV
6.0	0.093	$-0.437(7)(10)$	450 MeV
6.2	0.068	$-0.405(17)(20)$	515 MeV

Table 4.12: The format $c_M(\delta)(\sigma)$ includes statistical and systematical errors. The last column indicates the lightest pseudoscalar mass in the chiral extrapolation of $\Delta\left(M_{PS}^2\right)$.

4.3 Oscillating correlation functions

β	a [fm]	r_0	T	n_{cfg}	am_0	c	d
6.0	0.093	5.368	48	20	0.02	-0.45	-0.001
6.2	0.068	7.360	128	10	0.00730	$[-0.50, -0.30]$	-0.001
6.0	0.093	5.368	128	10	0.01000	$[-0.55, -0.35]$	-0.001
5.8	0.136	3.668	128	10	0.01464	$[-0.60, -0.40]$	-0.002

Table 4.13: Oscillating correlation functions are studied with $L = 24$.

Pseudoscalar correlation functions in the γ^5 channel do not exhibit visible oscillations. Nevertheless, oscillations are observed in many other channels of *parallel correlation functions* for $q\bar{q}$ states, while they are not observed in the same channels of *perpendicular correlation functions* for $q\bar{q}$ states. The direction of correlation is parallel to the Karsten-Wilczek term for parallel correlation functions and perpendicular to the Karsten-Wilczek term for perpendicular correlation functions. Moreover, the frequency of the oscillations depends on the relevant counterterm's coefficient c. Hence, the aim of this section is to clarify the origin and physical relevance of these oscillations without making explicit use of the decomposition that is defined in section 3.1 by answering the following questions:

1. Are the states of the QCD spectrum observed in channels that contain oscillations?

2. Are the differences between parallel and perpendicular correlation functions a result of residual anisotropies that can be removed with better tuning?

3. Is it possibile to use the c dependence of the frequency for non-perturbative tuning?

The first question is answered by comparing the ground state masses of the $J = 0$ sector for Karsten-Wilczek fermions with tuned parameters to the ground state masses for Wilson fermions, which are known to correctly reproduce the spectrum of QCD. The second question is answered by a comparison to correlation functions for naïve fermions, which exhibit a similar pattern of oscillations without being anisotropic. Though naïve fermions are unphysical, they show a pattern of oscillating correlation functions that is similar to both tuned parallel Karsten-Wilczek fermions and staggered fermions [5]. This pattern is due to the presence of an additional pole of the quark propagators in the direction of correlation. Naïve fermions are realised with the routines for Karsten-Wilczek fermions by setting the Wilczek parameter ζ and all counterterms to zero and require no additional coding effort. In section 4.3.1, the naïve fermion action of eq. (1.39) is contrasted with the Wilson fermion action, which includes eq. (1.50). Next, approximately tuned *parallel and perpendicular Karsten-Wilzcek fermions*[5] are juxtaposed in section 4.3.2. The Wilczek parameter is set to $\zeta = +1$ and the counterterm coefficients

---

[5]Parallel and perpendicular Karsten-Wilzcek fermions amount to calculation of parallel or perpendicular correlation functions (direction of correlation wrt alignment of the Karsten-Wilczek term).

are tuned to $c = -0.45$ and $d = -0.001$. Contrary to the approach in section 4.2, perpendicular Karsten-Wilczek fermions are implemented by changing the direction of the Karsten-Wilczek term ($\underline{\alpha} = 3$) while keeping the direction of correlation in the $\hat{e}_t = \hat{e}_0$ direction. All of these correlation functions are computed on 20 configurations of a 48×24^3 lattice at $\beta = 6.0$. This approach has the benefit of a longer time direction despite the reduction of the numerical cost due to smaller spatial volumes. This longer time direction is advantageous for isolating the ground state, in particular for perpendicular correlation functions. Moreover, local fluctuations of gauge links along the time direction are the same for both parallel and perpendicular correlation functions. The mass splitting between γ^5 channels for both parallel and perpendicular Karsten-Wilzcek fermions is consistent with zero and indicates that anisotropies discussed in section 4.2 have been removed even for lattices with $T \neq L$. The third question in the list is anwered in section 4.3.3, where a non-perturbative tuning condition is derived from a Fourier analysis of ratios of correlation functions.

4.3.1 Naïve and Wilson fermions

Correlation functions for Wilson fermions use $am_0 = -0.788$. The bare mass parameter takes the critical mass $am_{cr} = -0.808$ of Wilson fermions into account, which is determined as $am_0 = 1/(2\kappa) - 4$ from the critical hopping parameter $\kappa_{cr} = 0.157131(9)$ for unimproved Wilson fermions at $\beta = 6.0$ that was taken from [85]. Correlation functions for naïve fermions use $am_0 = 0.02$. Free naïve fermions have 16 real fermion modes localised in the Brillouin zone at the naïve doublers of eq. (1.48) and satisfy a residual chiral symmetry. However, naïve fermions do not reproduce the spectrum of QCD due to their unphysically large number of degenerate fermions. Though the bare parameters of both actions correspond to a bare quark mass of $am_q \approx 0.02$, it must be kept in mind that use of the same bare mass parameter does not imply matching hadron masses for different fermion actions. The displayed absolute values of correlation functions are calculated with source-smeared interpolating operators. $\mathcal{C}(n_0) \geq 0$ is indicated as red squares and $\mathcal{C}(n_0) < 0$ as blue bullets in the following figures. The time direction in the following figures is always the $\hat{e}_0$ direction. Ground state masses of these correlation functions are summarised in table 4.14 at the end.

Correlation functions for Wilson fermions in the γ^5 and $\gamma^5\gamma^0$ channels are displayed in the upper row of figure 4.13. Both quark bilinears $\bar{\psi}\gamma^5\psi$ and $\bar{\psi}\gamma^5\gamma^0\psi$ have $J^{PC} = 0^{-+}$ and have the same ground state mass within statistical errors. Correlation functions for Wilson fermions in the γ^0 and $\mathbf{1}$ channels are shown in the lower row of figure 4.13. Whereas the quark bilinear $\bar{\psi}\mathbf{1}\psi$ has $J^{PC} = 0^{++}$, the other quark bilinear $\bar{\psi}\gamma^0\psi$ has $J^{PC} = 0^{+-}$. As there are no physical mesons with $J^{PC} = 0^{+-}$, no statistically significant signal is seen in the γ^0 channel and the correlation function rapidly plummets into statistical noise that is consistent with zero. The correlation function in the $\mathbf{1}$ channel shows a clear signal of a state that is heavier than the ground state of the γ^5 channel. The change of sign for $n_0 \in [25, 31]$ is just a fluctuation that consistent with zero within errors. These observations reflect the meson spectrum of QCD.
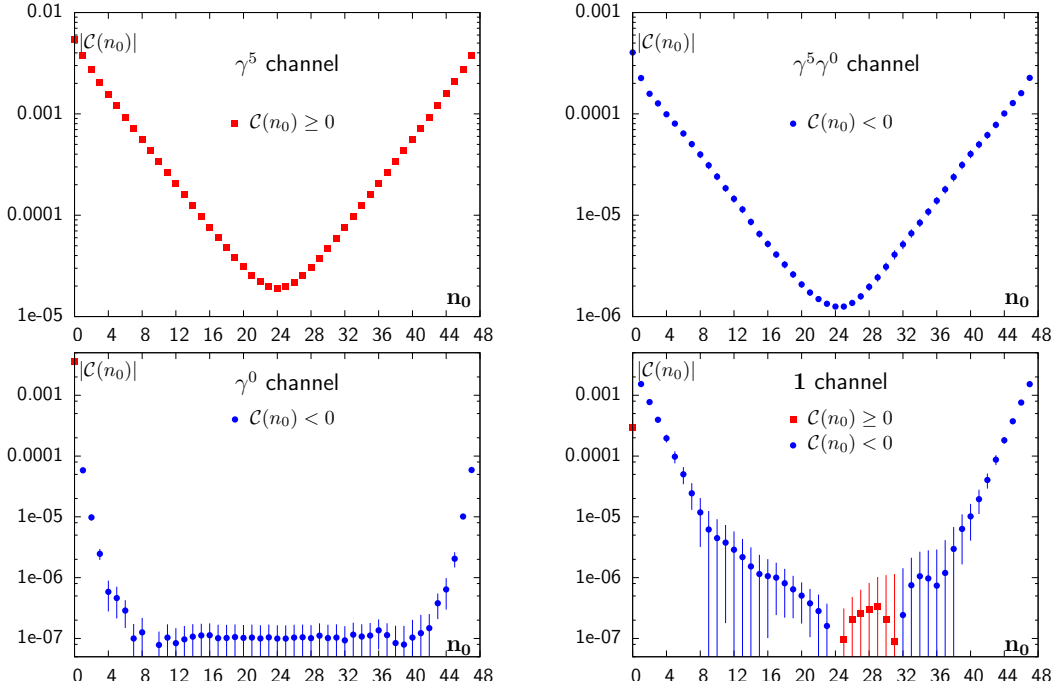
Figure 4.13: Upper row: γ^5 (left) and $\gamma^5\gamma^0$ channels (right) are mass degenerate for Wilson fermions. Lower row: For Wilson fermions, the γ^0-channel (left) contains only noise, whereas the **1**-channel (right) contains low-lying scalar states.

Correlation functions for naïve fermions in the γ^5 or γ^0 channels are displayed in the upper row of figure 4.14. As there are no physical mesons with $J^{PC} = 0^{+-}$, no statistically significant signal is expected for the γ^0 channel. However, the empirical observation is that the absolute value of both correlation functions agrees at machine precision and their ratio satisfies on all time slices (up to machine precision)

$$R_{05}(n_0) \equiv R_{\gamma^0, \gamma^5}(n_0) = \frac{\mathcal{C}_{\gamma^0, \gamma^0}(n_0)}{\mathcal{C}_{\gamma^5, \gamma^5}(n_0)} = (-1)^{n_0}. \tag{4.30}$$

Hence, there is an additional oscillating contribution in the γ^0 channel, which correponds to states that are mass-degenerate with states in the γ^5 channel (and have the same spectral weights). For naïve fermions, the spectra of the interpolating operators $\bar{\psi}\gamma^5\psi$ and $\bar{\psi}\gamma^0\psi$ are degenerate, but the non-oscillating contribution in the γ^5 channel is alternating in the other.

Most other correlation functions are more complicated. An example is presented in the lower row of figure 4.14. Without any regard to a physical interpretation, the correlation functions have a form which appears to be a superposition of two different contributions on odd and even time slices or a superposition of a non-oscillating and an alternating contribution. The latter assessment is supported by the observation that the ratio of
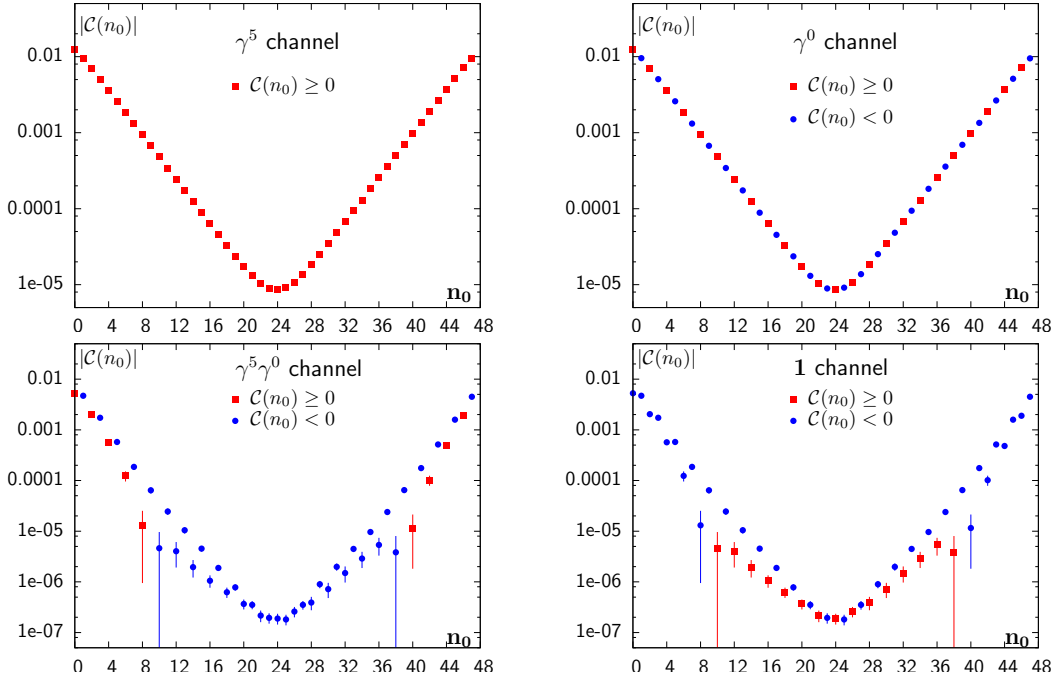
Figure 4.14: Upper row: γ^5 (left) and γ^0 channels (right) have identical magnitude for naïve fermions. Lower row: $\gamma^5\gamma^0$ (left) or $\mathbf{1}$ channels contain superpositions of oscillating and non-oscillating terms for naïve fermions.

correlators in $\gamma^5\gamma^0$ and $\mathbf{1}$ channels satisfies (up to machine precision) the same empirical relation up to a global factor (-1),

$$R_{\mathbf{1},\gamma^5\gamma^0}(n_0) = \frac{\mathcal{C}_{\mathbf{1},\mathbf{1}}(n_0)}{\mathcal{C}_{\gamma^5\gamma^0,\gamma^5\gamma^0}(n_0)} = -(-1)^{n_0}. \tag{4.31}$$

Thus, for naïve fermions, the interpolating operators $\bar{\psi}\gamma^5\gamma^0\psi$ and $\bar{\psi}\mathbf{1}\psi$ have degenerate spectra and the non-oscillating contributions in either of the channels are the alternating contributions in the other.

It is known from Wilson fermions that both $\bar{\psi}\gamma^5\psi$ and $\bar{\psi}\gamma^5\gamma^0\psi$ generate 0^{-+} states. Therefore, if there were an exclusive relation between interpolating operators for naïve fermions and J^{PC}, both interpolating operators would have to generate the same 0^{-+} states. Spectral weights would be different and even masses may differ due to lattice artefacts. However, it is evident from the correlation functions that the spectra of both interpolating operators generate different states in the oscillating contribution. Hence, an exclusive relation between interpolating operators for naïve fermions and J^{PC} cannot apply and their spectra may include different J^{PC}. Thus, it is concluded that both $\bar{\psi}\gamma^5\gamma^0\psi$ and $\bar{\psi}\mathbf{1}\psi$ generate 0^{-+} and 0^{++} states. Since both J^{PC} are relevant for physical mesons, both the non-oscillating and the alternating contribution are observed in the correlation function. This conclusion is consistent with the observation for the γ^5 and γ^0 channels (the 0^{+-} contribution is only noise) and can be generalised even further. For

114

every channel of $q\bar{q}$ states, an empirical correpondence to another channel is observed (up to machine precision):

$$R_{\mathcal{M}_\pm, \gamma^5\gamma^0\mathcal{M}_\pm}(n_0) = \pm (-1)^{n_0}, \qquad \begin{cases} \mathcal{M}_+ \in & \{\gamma^5, \gamma^0, \gamma^5\gamma^i, \gamma^0\gamma^i\} \\ \mathcal{M}_- \in & \{\mathbf{1}, \gamma^5\gamma^0, \gamma^i, \gamma^j\gamma^k\} \end{cases} . \qquad (4.32)$$
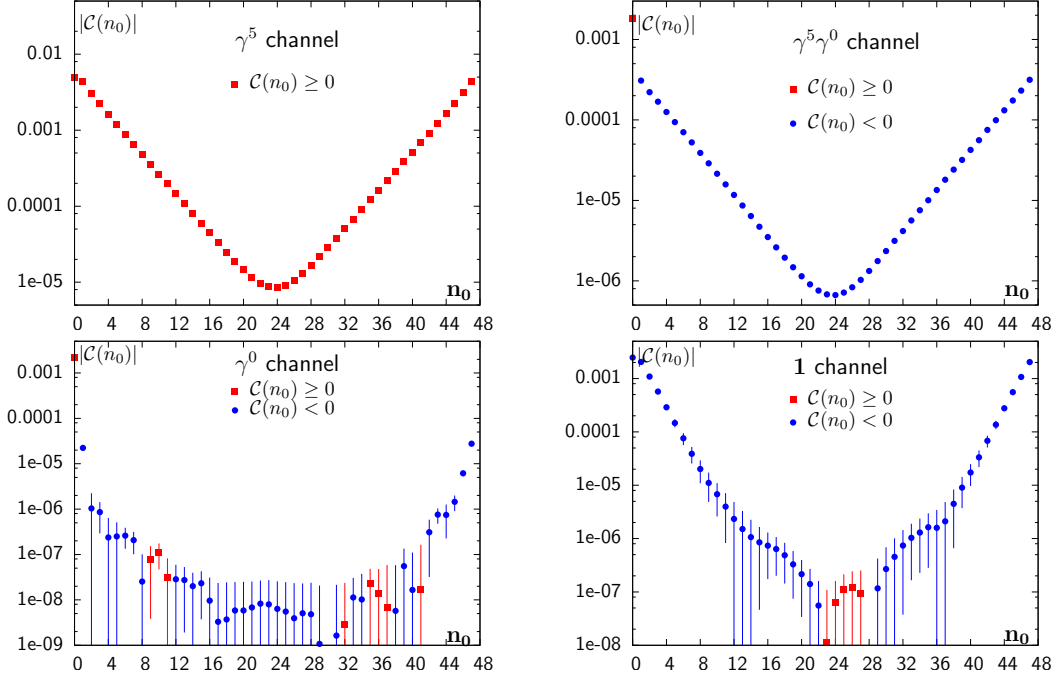
4.3.2 Oscillations of Karsten-Wilczek fermions

Figure 4.15: Upper row: γ^5 (left) and $\gamma^5\gamma^0$ channels (right) are mass degenerate for perpendicular Karsten-Wilczek fermions. Lower row: The γ^0 channel (left) contains only noise and the $\mathbf{1}$ channel (right) contains scalar states for perpendicular Karsten-Wilczek fermions.

Perpendicular Karsten-Wilczek fermions yield mass degenerate ground states in γ^5 and $\gamma^5\gamma^0$ channels (cf. upper row of figure 4.15). The γ^0 channel contains only statistical noise, while the $\mathbf{1}$ channel exhibits a low-lying scalar state (cf. lower row of figure 4.15). Thus, perpendicular Karsten-Wilczek fermions seem to closely resemble Wilson fermions. It appears appropriate to assign the same J^{PC}.

Parallel Karsten-Wilczek correlation functions in γ^5 and γ^0 channels are displayed in the upper row of figure 4.16 and exhibit striking similarity to naïve correlation functions in figure 4.14. There are no visible oscillations in the γ^5 channel and only oscillating terms in the γ^0 channel. Nonetheless, γ^5 and γ^0 channels for Karsten-Wilczek fermions do not have a common ground state mass. These observations would be expected if interpolating
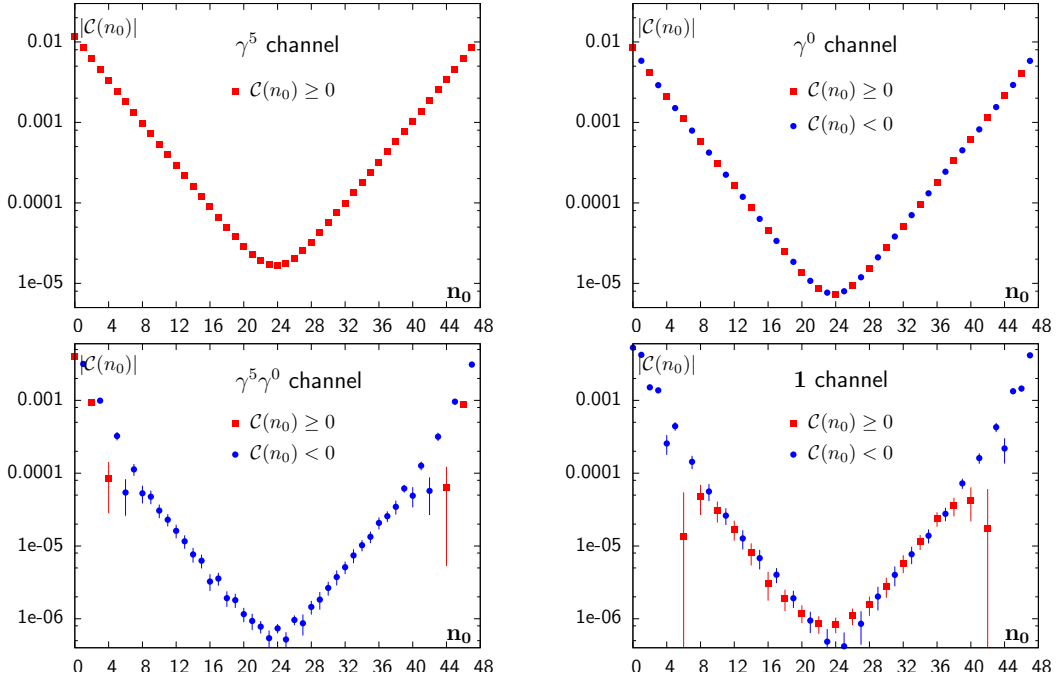
115

Figure 4.16: Upper row: γ^5 (left) and γ^0 channels (right) have similar but different magnitude for parallel Karsten-Wilczek fermions. The masses are different. Lower row: $\gamma^5\gamma^0$ (left) or $\mathbf{1}$ channels show both parity partners for parallel Karsten-Wilczek fermions.

operators for Karsten-Wilczek fermions would overlap with states with the same J^{PC} as interpolating operators for naïve fermions. The ground state of the γ^0 channel would be considered to have $J^{PC} = 0^{-+}$ and the mass splitting would suggest that gauge fields discriminate between states with the same J^{PC} in different channels. Furthermore, the observed similarity of $\gamma^5\gamma^0$ and $\mathbf{1}$ channels for naïve fermions is preserved for parallel Karsten-Wilczek fermions. These channels are shown in the lower row of figure 4.16. The oscillating terms in the $\gamma^5\gamma^0$ channel are observed only close to the boundaries ($n_0 \leq 8$ or $n_0 \geq 40$) and quickly fall to amplitudes close to noise level. On the contrary, the oscillations are long-lived in the $\mathbf{1}$ channel. These observations lead to the conclusion that the ground state of the $\mathbf{1}$ channel must belong to the oscillating contribution, while the ground state of the $\gamma^5\gamma^0$ channel must belong to the non-oscillating contribution. These observations would be expected if interpolating operators for Karsten-Wilczek fermions would overlap with states with the same J^{PC} as interpolating operators for naïve fermons. The ground state of both channels would have $J^{PC} = 0^{-+}$ and would belong to the non-oscillating contribution in the $\gamma^5\gamma^0$ channel and to the oscillating contribution in the $\mathbf{1}$ channel. Because the other contributions in both channels would have $J^{PC} = 0^{++}$, their signal would be much weaker.

Figure 4.17 displays local effective masses for γ^0 (blue bullets) and γ^5 channels (red squares). The former (aM_{00}) exceeds the latter (aM_{55}) consistently by approximately one or two standard errors over the full range of the effective mass plateau and precisely
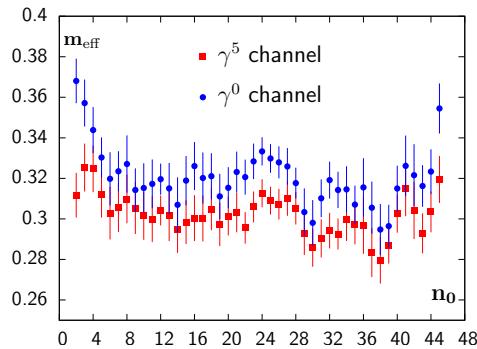
116

Figure 4.17: There is a mass splitting between cosh masses of γ^0 and γ^5 channels. Symbols and data sets are explained in the text.

follows suit in any fluctuations of the plateau value. The mass splitting is

$$aM_{00} - aM_{55} \approx 0.02 \qquad (4.33)$$

and amounts to ten standard errors on the level of the fit mass. This smallness of the mass splitting raises the question whether the splitting decreases or increases for finer lattices. A decreasing splitting would be interpreted as a lattice artefact and the γ^0 channel's ground state would have to be considered as a physical state that is mass-degenerate with the γ^5 channel's ground state in the continuum limit. An increasing splitting would have to be considered as an indication that the γ^0 channel's ground state were an unphysical state. This question is answered in a detailed study of the chiral behaviour and continuum extrapolation of both ground state masses in section 4.4.

Action	aM_{55}	aM_{00}	$aM_{50\,50}$	$aM_{\mathbf{11}}$
Naïve	0.339(1)	0.339(1)	0.381(21)	0.383(22)
KW $\parallel$	0.299(2)	0.319(2)	0.333(12)	0.332(23)
KW $\perp$	0.299(2)		0.301(2)	
Wilson	0.254(2)		0.261(5)	

Table 4.14: Pseudoscalar fit masses aM_{55} are obtained using γ^5, $aM_{50\,50}$ using $\gamma^5\gamma^0$, aM_{00} using γ^0 and $aM_{\mathbf{11}}$ using $\mathbf{1}$ in the interpolating operators. The data set of table 4.13 is used and parameters are explained in the text. aM_{55} corresponds to $M_{PS} \approx 630\,\text{MeV}$ for Karsten-Wilczek fermions and $M_{PS} \approx 540\,\text{MeV}$ for Wilson fermions.

Fits to the correlation function for naïve and parallel Karsten-Wilczek fermions are performed with the ansatz

$$\mathcal{C}(t) = \frac{A_0}{2M_0} \left(e^{-M_0 \cdot t} + e^{-M_0 \cdot (T-t)} \right) + \frac{\widetilde{A}_0}{2\widetilde{M}_0} (-1)^{t/a} \left(e^{-\widetilde{M}_0 \cdot t} + e^{-\widetilde{M}_0 \cdot (T-t)} \right), \qquad (4.34)$$

where $A_0, M_0, \widetilde{A}_0, \widetilde{M}_0$ are four independent parameters. For the γ^5 or γ^0 channels, where only either the non-oscillating or the oscillating contribution is observed, one term in the

117

ansatz of eq. (4.34) is omitted in the fit function. Because they are considered as different J^{PC}, both contributions each have their own ground state. Fit masses of pseudoscalar states for naïve, parallel as well as perpendicular Karsten-Wilczek and Wilson fermions are summarised in table 4.14. It is noted again that the common bare quark mass parameter does not imply similar hadron masses because different fermion actions are used. The following empirical symmetry patterns are observed:

- For Wilson and perpendicular Karsten-Wilczek fermions, the following are common observations: The γ^5 and $\gamma^5\gamma^0$ channels are mass degenerate (within errors) and both identified as 0^{-+}. The $\mathbf{1}$ channel is heavier than 0^{-+} and identified as 0^{++}. The γ^0 channel contains only noise, because 0^{+-} is not realised in physical mesons.

- For naïve and parallel Karsten-Wilczek fermions, the following are common observations: Oscillating and non-oscillating contributions are observed in most channels. The non-oscillating contributions are interpreted as the same J^{PC} that is identified for Wilson fermions in the same channel. J^{PC} for the oscillating contributions is deduced by multiplying the Dirac matrix of the interpolating operators by $\gamma^5\gamma^0$. Thus, the γ^5 channel contains no visible oscillations and is interpreted as 0^{-+}. The γ^0 channel contains only oscillating contributions that are also interpreted as 0^{-+}. Contributions due to 0^{+-} in both channels may exist, but are indistinduishable from noise. The $\gamma^5\gamma^0$ and $\mathbf{1}$ channels are interpreted as containing both 0^{-+} and 0^{++}. For the $\gamma^5\gamma^0$ channel, non-oscillating contributions are interpreted as 0^{-+}. For the $\mathbf{1}$ channel, non-oscillating contributions are interpreted as 0^{++}. The oscillating contribution is interpreted as the other J^{PC}.

- For parallel and perpendicular Karsten-Wilczek fermions the following is observed: The γ^5 channels for both and the $\gamma^5\gamma^0$ channel for perpendicular Karsten-Wilczek fermions are mass degenerate (within errors). This indicates that the action is tuned correctly even for $T \neq L$. The masses of γ^0, $\gamma^5\gamma^0$ and $\mathbf{1}$ channels for parallel Karsten-Wilczek fermions are a few percent larger than the γ^5 channel's mass. The mass in the γ^0 channel is slightly lower than in $\gamma^5\gamma^0$ and $\mathbf{1}$ channels, but all three masses are consistent within errors. The larger errors in the $\gamma^5\gamma^0$ and $\mathbf{1}$ channels are a consequence of the oscillating contribution that generally enlarges the uncertainty of the fits.

- For naïve fermions: Correlation functions satisfy the empirical relation of eq. (4.32) at machine precision. Therefore, both the pair of γ^5 and γ^0 channels and the pair of $\gamma^5\gamma^0$ and $\mathbf{1}$ channels are mass-degenerate pairs. The mass splitting between the γ^5 and $\gamma^5\gamma^0$ channels is larger than for parallel Karsten-Wilczek fermions.

The observation of oscillations for naïve and parallel Karsten-Wilczek fermions in the same channels make it clear that oscillations are not due to anisotropy. As the anisotropy of the pseudoscalar mass is succesfully removed, incomplete tuning is not responsible for the oscillating terms. These oscillating terms are generated by the presence of the Dirac operator's extra pole in the direction of correlation and mass splittings between states with the same J^{PC} in different channels persist in the tuned theory.
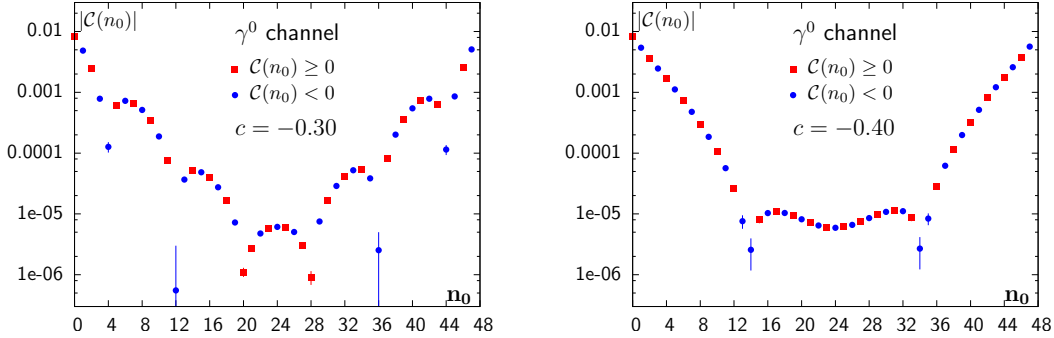
4.3.3 Tuning with the frequency spectrum

Figure 4.18: The γ^0 channel exhibits oscillations whose frequency depends on the parameter c. Data sets are explained in the text below.

Correlation functions for approximately tuned parallel Karsten-Wilczek fermions (section 4.3.2) exhibit alternating terms in the same channels as correlation functions for naïve fermions (section 4.3.1). However, these patterns vary as the coefficients of the counterterms are changed, which is shown in figure 4.18. The depicted correlation functions in the γ^0 channel for $c = -0.30$ (left) and $c = -0.40$ (right) use $\beta = 6.0$, $am_0 = 0.02$ and $d = 0.0$ on a 48^4 lattice of table 4.3 and clearly show that the pattern of oscillations depends on the choice of the relevant counterterm's coefficient c. These patterns have to be contrasted with approximately tuned Karsten-Wilczek fermions ($c = -0.45$ for $\beta = 6.0$) that are shown in the upper right plot in figure 4.16. The rapid oscillation of the parallel correlation function for approximately tuned Karsten-Wilczek fermions, which is described well by a factor $(-1)^{n_0}$, is modified for detuned Karsten-Wilczek fermions. Thus, the question whether the change in oscillation patterns can serve as a criterion for tuning the relevant counterterm's coefficient. Figure 4.18 indicates that the modification of the oscillation's pattern becomes more pronounced as c is detuned further. Hence, the oscillation's frequency Ω can be parameterised as

$$\Omega = \pi + \omega_c, \quad \partial\omega_c/\partial c \text{ finite}, \tag{4.35}$$

where the *frequency shift* ω_c is a smooth function of c that vanishes in the tuned theory. Its variation may serve as an observable indicating a mismatch δc. c_0 is defined as the value of c that restores the frequency spectrum to its tree level form (the *tuned frequency spectrum*) so that the coefficient c can be written as $c = c_0 + \delta_c$. If ω_c vanishes, the mismatch δc is zero and the coefficient is tuned correctly to $c_0 = c(g_0)$. Though there is no apparent link between a full restoration of hypercubic symmetry and the frequency spectrum, it is clear that neither restoration of hypercubic symmetry nor restoration of the frequency spectrum is possible unless c is tuned correctly. Instead of attempting a fit to an oscillating correlation function, where the frequency is an unknown parameter, methods of Fourier analysis are applied to a ratio of correlation functions. The frequency distribution of lattice eigenfrequencies is peaked at the oscillation frequencies Ω, even

though Ω does not have to be an eigenfrequency of the lattice. Two simple toy models in appendix D elucidate this concept. Of course, the resolution of a discrete Fourier transform is limited by the width of the frequency bins,

$$\omega_b = \frac{2\pi}{N_0}, \tag{4.36}$$

which depends only on N_0, the temporal extent of the lattice. If $|\omega_c| < \omega_b/2$, the time direction is too short to provide sufficient resolution of the spectrum. Thus, N_0 should be as large as possible and lattices of table 4.13 with very long time direction ($N_0 = 128$) are applied for this purpose.
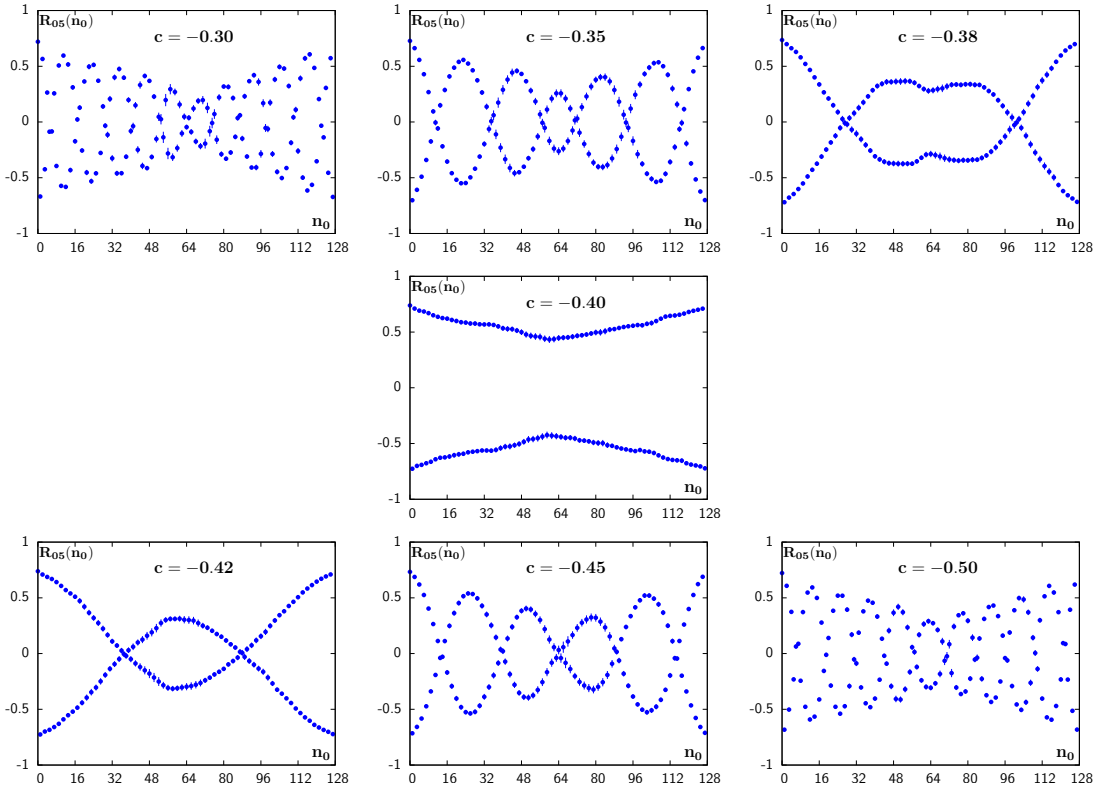

Figure 4.19: Correlator ratios $R_{05}(n_0)$ on a 128×24^3 lattice at $\beta = 6.2$ from table 4.13 provide unmistakable evidence of the c dependence of the frequency shift ω_c.

It is observed in eq. (4.33) that the mass splitting between γ^0 and γ^5 channels is very small. Therefore, the leading order quark mass dependence cancels in the ratio $R_{05}(n_0)$ of these correlators, which is defined in eq. (4.30) for naïve fermions. Though eq. (4.30) is satified only approximately for tuned parallel Karsten-Wilczek fermions due to the small mass splitting, the residual decay of the correlator ratios (due to the mass splitting) is smaller for finer lattices. Because peaks in the frequency spectrum are narrower for a smaller residual decay, the following discussion is focused on $\beta = 6.2$. However, it must be kept in

mind that both correlation functions (γ^0 and γ^5 channels) have different excited states. Hence, even if the mass splitting between the ground states were zero, there would still be a residual decay due to the presence of different excited states. Seven ratios for $\beta = 6.2$ and $c \in [-0.30, -0.50]$ are shown in figure 4.19. $c_M = -0.405(17)(20)$, the non-perturbative value that is obtained from the mass anisotropy in section 4.2, agrees within errors with the parameter $c = -0.40$ of the central plot. Correlator ratios $R_{05}(n_0)$ for $\beta = 6.0$ and $\beta = 5.8$ are shown in figures E.1 and E.3 in appendix E. These ratios contain stronger exponential decays due to larger ground state mass differences.
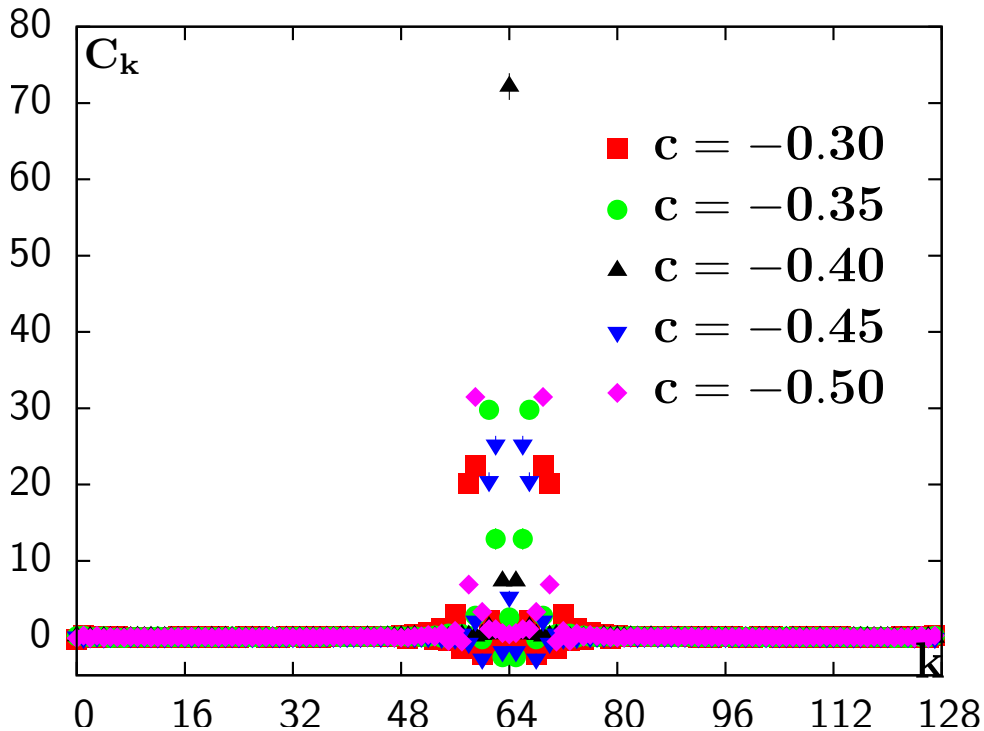

Figure 4.20: The two peaks of the Fourier spectrum of the correlator ratio $\mathcal{R}_{05}(n_0)$ approach a single peak at $k = N_0/2$ if the coefficient c is tuned properly.

In order to obtain a frequency spectrum with two peaks near zero, an alternating factor $(-1)^{n_0}$ (due to $\Omega = \pi$ in the tuned frequency spectrum) is multiplied with the ratio before it is submitted to a discrete Fourier transform using the GSL FFT library [62]. The Fourier coefficients C_k are computed as

$$C_k = \sum_{n_0=0}^{N_0-1} \mathcal{R}_{05}(n_0)(-1)^{n_0} e^{-2\pi i \frac{k n_0}{N_0}}. \tag{4.37}$$

Because the FFT of the ratios is conducted independently on each sample of the full ensemble, no statistical information is lost in this process and statistical uncertainties of the spectra can be calculated with the Jackknife method. Fourier spectra that are

121

defined without the alternating factor $(-1)^{n_0}$ are shown in figure 4.20. Two peaks are observed in the spectra that approach a single peak at $k = N_0/2$ for $c = c_0$. The spectra are symmetric (up to machine precision) about $k = N_0/2$. Distinction between $c > c_0$ and $c < c_0$ on the basis of the spectra in figure 4.20 is impossible. Outside of the peak region, the spectrum is almost consistent with zero. The power spectral density (PSD) takes advantage of the frequency spectrum's symmetry. Its definition is taken from [132],

$$
\begin{aligned}
\mathcal{P}(f_0) &= \tfrac{1}{N^2}|C_0|^2 \\
\mathcal{P}(f_k) &= \tfrac{1}{N^2}\left(|C_k|^2 + |C_{N-k}|^2\right) \qquad k = 1, 2, \ldots, \left(\tfrac{N}{2} - 1\right) , \\
\mathcal{P}(f_{N/2}) &= \tfrac{1}{N^2}|C_{N/2}|^2
\end{aligned}
\tag{4.38}
$$

where the C_k are the Fourier coefficients defined in eq. (4.37). The two peaks of the frequency spectrum are mapped onto a single peak of the power spectral density. The power spectral densities within the frequency range $\omega \in [0, 0.3\pi]$ are shown in figure 4.21. They are sharply peaked distributions with noise which is typically suppressed by $3-6$ orders of magnitude. Due to the aforementioned residual exponential decays of the ground state mass difference and excited state contributions, which are not known in detail, the exact form of the frequency spectrum is unknown.
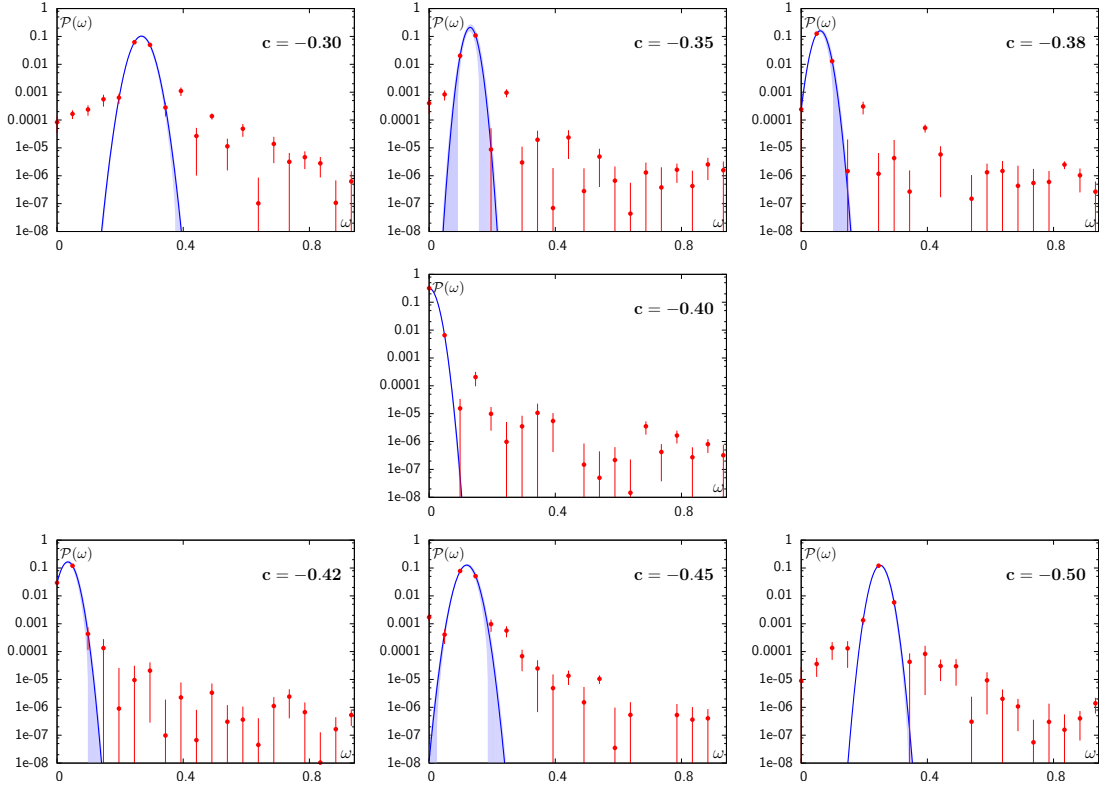

Figure 4.21: Power spectral densities are displayed on a logarithmic scale. The curve is a gaussian function, which is used for estimating the maximum of the distribution.

An estimate of the peak frequency and its systematical uncertainty are obtained as the maximum ω_c and the width σ of a gaussian distribution,

$$g(\omega) = \frac{P_0}{\sqrt{2\pi\sigma^2}} e^{-\frac{(\omega-\omega_c)^2}{2\sigma^2}}, \tag{4.39}$$

which is matched with a least squares fit to the power spectral density on each sample. If the peak frequency ω_c is smaller than $\omega_b/2$, all samples evaluate to $\omega_c = 0$ and the statistical uncertainty vanishes. If $\omega_c = 0$ with $\delta_{\omega_c} = 0$ were used in an interpolation in c, it would completely dominate the interpolation[6]. Hence, a balanced and sensitive approach to interpolation must combine statistical and systematical uncertainties. Systematic uncertainties are estimated as the root of the variance of the gaussian distribution. In the following, they are treated as independent errors and combined quadratically,

$$\delta_{\omega_c} = \sqrt{(\delta_{\omega_c})^2 + \sigma^2}. \tag{4.40}$$

$\beta = 5.8$							
c	-0.40	-0.45	-0.48	-0.50	-0.53	-0.55	-0.60
ω_c	155(2)(37)	74(1)(38)	26(2)(38)	11(2)(26)	14(4)(35)	40(2)(33)	116(2)(35)

$\beta = 6.0$							
c	-0.35	-0.40	-0.42	-0.45	-0.47	-0.50	-0.55
ω_c	124(1)(12)	54(1)(13)	25(1)(13)	0(0)(15)	32(1)(13)	74(1)(13)	141(1)(13)

$\beta = 6.2$							
c	-0.30	-0.45	-0.38	-0.40	-0.42	-0.45	-0.50
ω_c	134(1)(11)	65(1)(7)	30(1)(8)	0(0)(9)	17(1)(9)	60(1)(11)	125(1)(9)

Table 4.15: The peak frequency ω_c of the power spectral densities seems to be linear in $|\delta_c|$. ω_c in the table must be multiplied by 10^{-3}. Statistical (δ_{ω_c}) and systematical (σ) uncertainties are in brackets. Ratios are calculated on 128×24^3-lattices from table 4.13.

Peak frequencies with statistical and systematical uncertainties in the format $\omega_c(\delta_{\omega_c})(\sigma)$ for $\beta = 6.2$, 6.0 and 5.8 are summarised in table 4.15. Power spectral densities of ratios for $\beta = 6.0$ and $\beta = 5.8$ are presented in figures E.2 and E.4 in appendix E. The width of the peak is larger on the coarse lattice ($\beta = 5.8$), which is immediately clear from a comparison of the figures. This is the reason why the systematical errors for $\beta = 5.8$ considerably exceed their counterparts on finer lattices ($\beta = 6.0$, $\beta = 6.2$). The ratios contain stronger exponential decays due to larger ground state mass differences. It is seen in figure 4.20 and in table 4.15 that the frequency shift ω_c does not allow for a distinction between $\delta_c > 0$ and $\delta_c < 0$. Two different approaches are applied. First, the peak frequencies ω_c are interpolated with the function

$$\omega_c = A \cdot |c - c_0|, \tag{4.41}$$

---

[6]If multiple coefficients c have $\omega_c = 0$ and $\delta_{\omega_c} = 0$, linear interpolation of ω_c necessarily fails.

which precludes from using a simple linear fit. Second, peak frequencies ω_c for $c < c_{\min}$ with $\omega_{c_{\min}} \leq \omega_c \ \forall \ c$ are multiplied by (-1) and a linear interpolation is conducted with

$$\omega_c = A(c - c_0). \tag{4.42}$$

Both approaches are consistent. Interpolations of peak frequencies are displayed in figure 4.22 and their zeros c_0 are listed in table 4.16. The frequency shift ω_c is described extraordinarily well over the full range of data (at $\beta = 6.2$ and $\beta = 6.0$) by the ansatz of eq. (4.41). Hence, even a shorter $\hat{e}_0$ direction (e.g. $N_0 = 48$) yields sufficient resolution for linear interpolation. c_0 is consistent with c_M within combined errors. Since oscillations are exclusive to parallel correlation functions, c_0 is obtained without use of perpendicular correlation functions (correlation functions, where the direction of correlation is perpendicular to alignment of the Karsten-Wilczek term). Therefore, restoration of the frequency spectrum to its tree-level form is a tuning condition that disregards the anisotropy. If an observable with sensitivity to the anisotropy, good statistical accuracy and strong sensitivity to d were discovered, the residual anisotropy after setting $c = c_0$ could be employed for tuning d non-perturbatively.
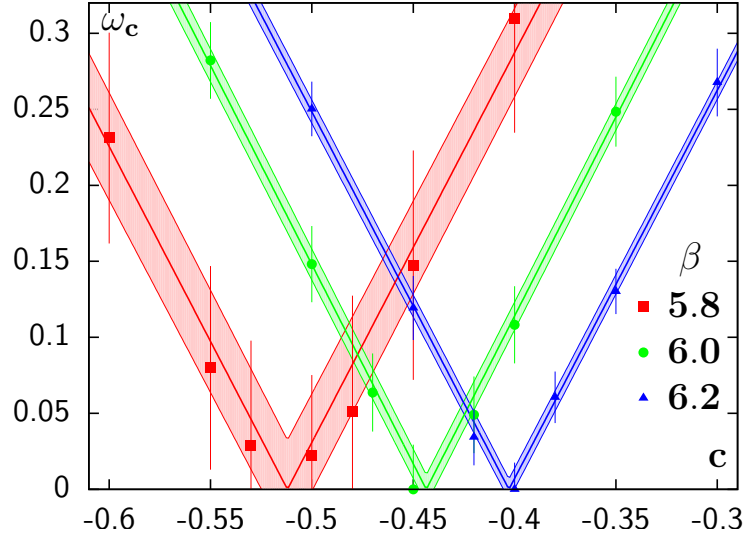
Figure 4.22: Peak frequencies ω_c for $\beta = 5.8$, $\beta = 6.0$ and $\beta = 6.2$ are interpolated in c using eq. (4.41). Error bands are dominated by systematical errors.

β	$a\,[fm]$	c_0
5.8	0.136	$-0.5120(7)(100)$
6.0	0.093	$-0.4435(8)(37)$
6.2	0.068	$-0.4028(5)(27)$

Table 4.16: The zero crossing c_0 of eq. (4.42) is obtained for ratios with $N_0 = 128$. The format $c_0(\delta)(\sigma)$ includes statistical and systematical errors.

4.4 Chiral behaviour of the pseudoscalar ground state

β	am_0	(r_0m_0)	(r_0M_{55})	M_{55} [MeV]	(r_0M_{00})	M_{00} [MeV]	$\mathcal{B}_{55}$
5.8	0.02928	0.107	1.655(2)	653(1)	1.858(3)	733(1)	25.5(1)
5.8	0.02000	0.073	1.379(1)	544(1)	1.612(3)	636(1)	25.9(1)
5.8	0.01464	0.054	1.188(1)	469(1)	1.450(4)	572(2)	26.2(1)
5.8	0.01000	0.037	0.989(1)	390(1)	1.294(5)	511(2)	26.6(1)
5.8	0.00732	0.027	0.851(1)	336(1)	1.194(6)	471(2)	26.9(1)
5.8	0.00534	0.020	0.731(1)	288(1)	1.115(8)	440(3)	27.2(1)
6.0	0.02000	0.107	1.597(4)	630(1)	1.695(5)	669(2)	23.8(1)
6.0	0.01371	0.074	1.333(4)	526(1)	1.444(5)	570(2)	24.2(1)
6.0	0.01000	0.054	1.149(4)	453(2)	1.274(5)	503(2)	24.6(2)
6.0	0.00685	0.037	0.963(4)	380(2)	1.109(6)	438(2)	25.3(2)
6.0	0.00500	0.027	0.832(4)	328(2)	0.997(7)	393(3)	25.9(3)
6.0	0.00365	0.020	0.719(5)	284(2)	0.905(8)	357(3)	26.5(3)
6.2	0.01460	0.107	1.567(7)	618(3)	1.602(7)	632(3)	23.0(2)
6.2	0.01000	0.074	1.305(8)	515(3)	1.346(7)	531(3)	23.4(3)
6.2	0.00730	0.054	1.124(8)	444(3)	1.173(8)	463(3)	23.8(4)
6.2	0.00500	0.037	0.943(9)	372(4)	1.004(9)	396(3)	24.5(5)
6.2	0.00365	0.027	0.815(10)	322(4)	0.889(10)	351(4)	25.1(6)
6.2	0.00266	0.020	0.704(12)	278(5)	0.793(11)	313(4)	25.8(9)
6.2	0.00194	0.014	0.607(14)	240(5)	0.712(12)	281(5)	26.4(12)

Table 4.17: The tuned action is studied on lattices with $T = 48$. $L = 24$ for $\beta = 5.8$, 6.0 and $L = 32$ for $\beta = 6.2$ are used.

β	c	d	T	L	n_{cfg}
5.8	-0.51	-0.002	48	24	200
6.0	-0.45	-0.001	48	24	200
6.2	-0.40	-0.001	48	32	100

Table 4.18: c is tuned non-perturbatively and $\Delta(M_{PS}^2)$ as well as ω_c are consistent with zero within errors. d is fixed perturbatively. The Wilczek parameter is set to $\zeta = +1$.

The preceding two sections concern non-perturbative tuning of Karsten-Wilczek fermions. The counterterm's coefficient c of the Karsten-Wilczek action is tuned non-perturbatively by either making use of minimisation of the pseudoscalar mass anisotropy (section 4.2) or restoration of the tree-level frequency spectrum (section 4.3). The counterterm coefficient d is tuned using boosted perturbation theory. Simulation parameters are listed in table 4.18. Properties of QCD are studied using the Karsten-Wilczek fermion action. The scale is set with the Sommer parameter r_0 [143] from table 4.1. The only remaining simulation parameter is the bare fermion mass am_0, which is listed in table 4.17 together with fit masses of the pseudoscalar ground states of the γ^5 channel (M_{55}) and of the γ^0 channel (M_{00}). Chiral behaviour is studied by varying am_0 within a factor of $6-7$.

The 3rd column of table 4.17 is the bare mass $r_0 m_0$ in physical units $(2 \, \text{fm}^{-1})$. Because mass renormalisation is required but not performed, different $r_0 M_{55}$ (in the 4th column) is obtained for the same $r_0 m_0$ at different β. Since M_{55} and M_{00} are quite similar and a pseudoscalar ground state is expected in both channels, both are tentatively treated as approximate Goldstone bosons with different discretisation effects. Local effective mass plots indicating the fit ranges are displayed in figure E.6 in the appendix.

4.4.1   Chiral behaviour of the γ^5 channel

In full QCD, chiral perturbation theory (ChPT) at next-to-leading order [63,64] predicts that the pion mass scales with the average light quark mass m_{ud} and the strange quark mass m_s as

$$M_{\pi,2}^2 = 2B_0 m_{ud}, \quad M_{\eta,2}^2 = \frac{2}{3} B_0 (m_{ud} + 2m_s), \tag{4.43}$$

$$M_{\pi,4}^2 = M_{\pi,2}^2 \left\{ 1 + X + \frac{M_{\pi,2}^2}{32\pi^2 F_0^2} \log\left(\mu^{-2} M_{\pi,2}^2\right) - \frac{M_{\eta,2}^2}{96\pi^2 F_0^2} \log\left(\mu^{-2} M_{\eta,2}^2\right) \right\}, \tag{4.44}$$

$$X = \frac{16}{F_0^2} \left\{ (2m_{ud} + m_s) B_0 (2L_6^r - L_4^r) + (m_{ud} + m_s) B_0 (2L_8^r - L_5^r) \right\}.$$

The notation follows [139], where $M_{\pi,2n}^2$ and $M_{\eta,2n}^2$ indicate the pion and eta meson masses for degenerate up and down quarks at chiral order $2n$. $2B_0$ and F_0 are the chiral condensate and the pion decay constant in the chiral limit. X is the sum of two contributions that depend on the quark masses, B_0, F_0 and four renormalised low-energy constants L_i^r from the chiral Lagrangian at chiral order four. All of these (quark masses, B_0, F_0 and L_i^r) are undetermined parameters that must be obtained by matching ChPT calculations to calculations in QCD or to experimental data. The ratio $\mathcal{B}_{55}$ in the 8th column of table 4.17 is defined as

$$\mathcal{B}_{55} \equiv \frac{(r_0 M_{55})^2}{(r_0 m_0)}. \tag{4.45}$$

Comparison of eq. (4.45) with eqs. (4.43) and (4.44) suggests that $\mathcal{B}_{55}$ is related to $2B_0$ in partially quenched QCD (the strange quark is considered as heavy) as

$$\mathcal{B}_{55} \propto 2B_0 \{ 1 + X_0 m_{ud} + X_1 m_{ud} \log\left(a m_{ud}\right) \}. \tag{4.46}$$

As factors X_0 and X_1 are numerically positive, the prediction of partially quenched QCD is a monotonical increase of $\mathcal{B}_{55}$ with the quark mass. Instead, a decrease is observed at fixed β. There are two possible causes why this increase is not reflected in the data.

The first cause is that the quenched approximation neglects virtual quark loops, which cancel hairpin diagrams [21,142] that contribute to mesonic correlation functions. Lack of this cancellation leads to additional logarithmic contributions to the pion mass [21] in the form of quenched chiral logarithms,

$$M_\pi^2 = M_{\pi,2}^2 \left\{ (1 - \delta) - \delta \log\left(\mu^{-2} M_{\pi,2}^2\right) \right\} + \mathcal{O}(M_{\pi,2}^4), \tag{4.47}$$

126

where the new parameter δ is related to the pseudoscalar flavour singlet mass M_0^2 by

$$\delta = \frac{M_0^2}{N_f(4\pi F_0)^2}. \tag{4.48}$$

The parameter M_0^2 is related to the topological susceptibility χ_t through the Witten-Veneziano formula [150, 161]. A phenomenological estimate of M_0^2 is obtained in terms of physical meson masses,

$$M_0^2 = M_{\eta'}^2 + M_\eta^2 - 2M_K^2, \tag{4.49}$$

which yields $\delta \approx 0.18$. Since δ is positive, quenched chiral logarithms cause a logarithmic divergence of $\mathcal{B}_{55}$ in the chiral limit.

The second cause for a rise of $\mathcal{B}_{55}$ in the chiral limit are uncertainties in the choice of the coefficients. The anisotropy study in section 4.2 demonstrates that the mass anisotropy $\Delta(M_{PS}^2)$ in the chiral limit is not removed perfectly at finite lattice spacing, which implies a mass shift in at least one of the correlation functions. As c is tuned only with a few percent accuracy and d only using perturbation theory, incomplete tuning must be considered another potential source of non-vanishing contributions to the ground state mass in the chiral limit. Nevertheless, a chiral extrapolation as

$$r_0^2 M^2 = r_0^2 M_{\text{res}}^2 + 2B_0(r_0 m_0)\left\{(1-\delta) - \delta\log\left(m_0/r_0\right)\right\} \tag{4.50}$$

is suited for both γ^5 and γ^0 channels. The small mass splitting of eq. (4.33) between γ^5 and γ^0 channels indicates that the latter channel's ground state is a pseudoscalar which is affected by mild discretisation effects. Spontaneous chiral symmetry breaking would still affect all non-singlet pseudoscalars, if such discretisation effects could be treated like the quark mass as perturbations in a ChPT for Karsten-Wilczek fermions[7].

M_{55} is extracted by fitting a cosh to the correlation function for each fermion mass parameter am_0. Fit masses are squared and subjected to a chiral extrapolation with

$$M^2(am_0) = C + (am_0) \cdot \{A + B\log\left(am_0\right)\} \tag{4.51}$$

and $\delta = B/(B-A)$. The same chiral extrapolation is conducted in one case with three independent fit parameters (upper row of figure 4.23) and in another case with the constraint $C = 0$ (lower row of figure 4.23). Results of both chiral extrapolations are shown in table 4.19. Extrapolation results with an offset C agree well with each other and with the phenomenological estimate ($\delta \approx 0.18$). If the offset is fixed to $C = 0$, $\chi^2/$dof increases and δ varies within a factor of two for $\beta = 6.0$ and $\beta = 6.2$. Since δ is only a phenomenological estimate and the spread of other lattice results for δ [162] is consistent with this result, strong conclusions must be avoided at this point. The variation might indicate incomplete tuning in the sense that the counterterms are tuned better for $\beta = 5.8$ than for $\beta = 6.0$ and $\beta = 6.2$. A partial reexamination of the study with improved counterterm coefficients[8] may partly solve this problem. Because M_{55}^2 in

---

[7]ChPT for staggered fermions in [109] includes non-singlet discretisation effects in the chiral expansion. This sets the example that should be followed for Karsten-Wilczek fermions.

[8]The simulation parameter d for $\beta = 6.0$ and $\beta = 6.2$ is closer to d_{1L} than to d_{BPT}.
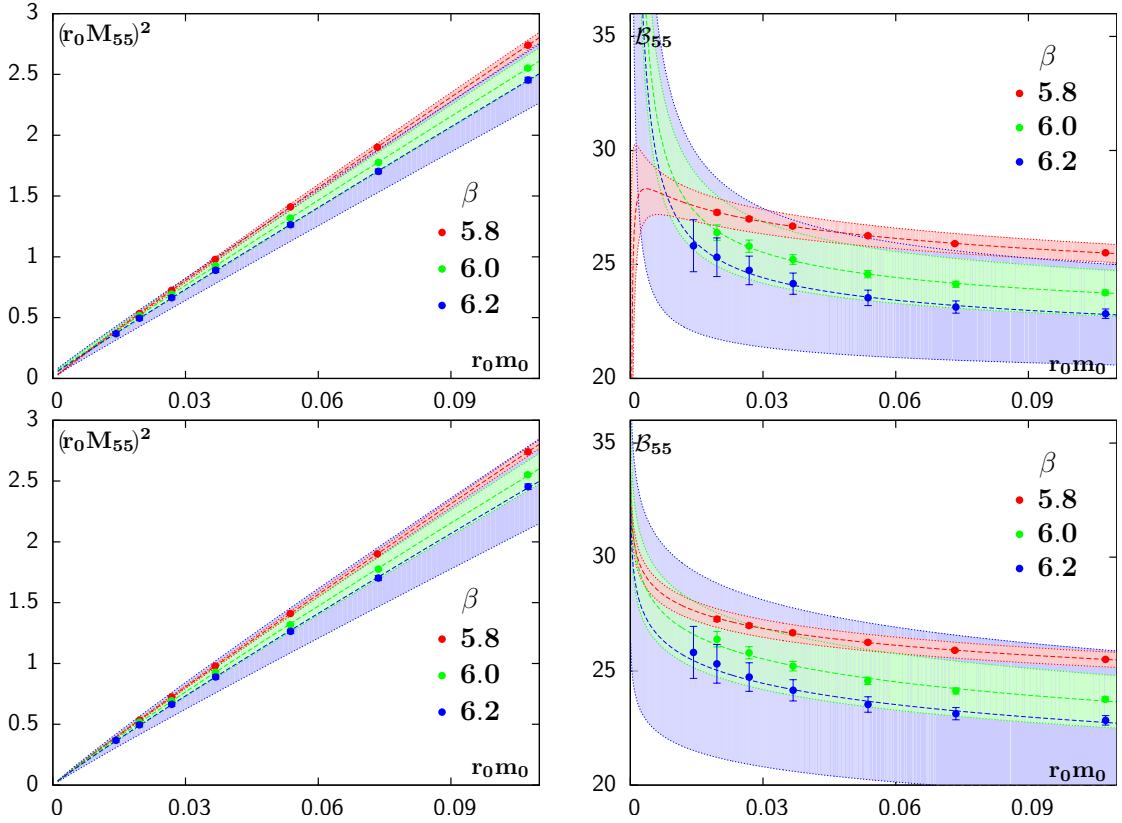
Figure 4.23: Upper row: C is included as parameter in the chiral extrapolation of M_{55}^2. At $\beta = 5.8$, it partly compensates for the rise of $\mathcal{B}_{55}$ due to quenched chiral logarithms. Lower row: The offset parameter C in the chiral extrapolation of M_{55}^2 is fixed to 0.

the chiral limit at $\beta = 5.8$ is consistent with zero within less than 2σ, data support the claim that the ground state of the γ^5 channel behaves as a (Pseudo-) Goldstone boson.

β	$r_0 A$	$r_0 B$	δ	$r_0^2 C$	χ^2/dof	$r_0 A$	$r_0 B$	δ	χ^2/dof
5.8	21.5(2)	$-4.2(2)$	0.16(1)	$-0.004(3)$	0.05	21.8(2)	$-3.9(2)$	0.15(1)	0.04
6.0	20.6(4)	$-3.9(7)$	0.15(1)	0.036(8)	0.10	18.0(6)	$-7.8(8)$	0.30(2)	0.59
6.2	19.7(9)	$-5.0(19)$	0.20(6)	0.031(21)	0.05	17.1(16)	$-9.9(28)$	0.37(7)	0.16

Table 4.19: The chiral extrapolation of M_{55}^2 with an offset in the chiral limit reproduces the phenomenological value of $\delta \approx 0.18$ very well.

4.4.2 Interpretation of the γ^0 channel

For Wilson fermions, interpolating operators of the γ^0 channel are related to $J^{PC} = 0^{+-}$ and do not generate physical $q\bar{q}$ states from the vacuum. Hence, the physical significance of the γ^0 channel's ground state for Karsten-Wilczek fermions is not immediately evident.

However, the mass splitting between the ground states of γ^0 and γ^5 channels is about 3-15% and decreases for finer lattices. The ground state would have to be considered as an unphysical state, if the mass splitting increased for finer lattices. Because the trend in data is opposite, the state must correspond to a physical meson in the continuum limit. Within this mass range, there are no states in the QCD spectrum other than isospin non-singlet pseudoscalars. Therefore, the continuum limit of the ground state must be a (Pseudo-) Goldstone boson in the chiral limit. Assuming that the discretisation effects that eventually break the symmetries can be treated as perturbations within some parameter range (which is a priori unknown), its mass M_{00} is tentatively squared and extrapolated using eq. (4.51). The same chiral extrapolation is conducted in one case with three independent fit parameters and in another case with $B = 0$ (upper and lower rows of figure E.5 in appendix E.3). Results of both chiral extrapolations are in perfect agreement (cf. table 4.20) and provide no numerical evidence for quenched chiral logarithms in the γ^0 channel.

β	$r_0 A$	$r_0 B$	$r_0^2 C$	χ^2/dof	$r_0 A$	$r_0^2 C$	χ^2/dof
5.8	25.2(2)	0.0003(120)	0.75(2)	0.002	25.1(2)	0.75(2)	0.002
6.0	23.3(1)	$-0.03(2)$	0.37(2)	0.11	23.4(2)	0.37(2)	0.08
6.2	22.0(2)	0.008(30)	0.20(2)	0.04	22.0(2)	0.20(2)	0.03

Table 4.20: The chiral extrapolation of M_{00}^2 produces a large offset in the chiral limit.

In order to shed light on the physical interpretation of the γ^0 channel, the quadratic mass difference $(M_{00}^2 - M_{55}^2)$ is expressed in units of r_0^2,

$$\Delta_{05} \equiv r_0^2 \left(M_{00}^2 - M_{55}^2 \right). \tag{4.52}$$

Because there are strong cancellations between statistical fluctuations in the difference of the squared masses, its statistical error decreases (compared to the individual masses) and turns out to be too small for covering the difference's variations over the full quark mass range. The difference in the chiral limit is obtained as the difference of the offset parameters C (rescaled with r_0^2) of the chiral extrapolations of the ground state masses of both channels and included as 'ch.l.' in the table 4.21. Δ_{05} is remarkably stable over the full range of quark masses and decreases towards the continuum limit. The scaling behaviour of its approach to the continuum limit is determined by the scaling behaviour of both correlation functions. Since the results of section 3.2 indicate that mesonic correlation functions with definite charge conjugation quantum numbers on quenched cofigurations do not have $\mathcal{O}(a)$ corrections, leading discretisation effects of Δ_{05} are $\mathcal{O}(a^2)$. Therefore, Δ_{05} can be extrapolated to the continuum limit as

$$\Delta_{05} = \Delta_0 + a^2 \Delta_2 + \mathcal{O}(a^3). \tag{4.53}$$

Continuum extrapolation is conducted with different functions $f_{02}(a)$ and $f_2(a)$,

$$f_{02}(a^2) = \Delta_0 + a^2 \Delta_2, \tag{4.54}$$

$$f_2(a^2) = a^2 \Delta_2. \tag{4.55}$$

β	$(r_0 m_0)$	$(r_0 M_{55})^2$	$(r_0 M_{00})^2$	Δ_{05}
5.8	0.107	2.740(5)	3.454(11)	0.714(8)
5.8	0.073	1.901(4)	2.597(11)	0.696(9)
5.8	0.054	1.410(3)	2.103(12)	0.692(10)
5.8	0.037	0.979(3)	1.674(13)	0.696(12)
5.8	0.027	0.725(2)	1.427(15)	0.702(14)
5.8	0.020	0.534(2)	1.243(17)	0.709(17)
5.8	ch.l.	$-0.004(3)$	0.751(17)	0.755(17)
6.0	0.107	2.552(12)	2.873(15)	0.321(5)
6.0	0.074	1.776(10)	2.085(14)	0.309(6)
6.0	0.054	1.319(9)	1.623(13)	0.304(6)
6.0	0.037	0.927(8)	1.229(13)	0.302(7)
6.0	0.027	0.693(7)	0.994(13)	0.302(8)
6.0	0.020	0.517(7)	0.818(14)	0.301(10)
6.0	ch.l.	0.036(8)	0.366(15)	0.330(13)
6.2	0.107	2.454(22)	2.566(22)	0.112(5)
6.2	0.073	1.703(20)	1.812(19)	0.110(5)
6.2	0.054	1.264(18)	1.377(18)	0.112(5)
6.2	0.037	0.889(17)	1.008(17)	0.119(5)
6.2	0.027	0.665(17)	0.791(17)	0.127(5)
6.2	0.020	0.496(17)	0.629(17)	0.134(6)
6.2	0.014	0.369(16)	0.507(17)	0.139(7)
6.2	ch.l.	0.031(21)	0.196(18)	0.165(13)

Table 4.21: The difference Δ_{05} of the squared ground state masses of γ^0 and γ^5 channels has only a mild fermion mass dependence. The statistical errors of Δ_{05} are greatly reduced due to cancellations of fluctuations between both channels.

Both extrapolations are displayed in figure 4.24 and their coefficients are listed in table 4.22. The extrapolation with $f_{02}(a^2)$, which is non-zero in the continuum limit, agrees well with data and χ^2/dof is reasonably small, whereas $f_2(a^2)$ seems to be disfavoured. This may have different reasons, among which incomplete tuning, fluctuations in the data points or unresolved higher order effects are the most obvious. Resolution of higher order discretisation effects is not deemed feasible with only three data points. Incomplete tuning is particularly suggestive because C is non-vanishing in the chiral extrapolation of the γ^5 channel for both finer lattices ($\beta = 6.0$ and $\beta = 6.2$). It is pointed out with regard to eq. (4.52) that the value of the expansion coefficient Δ_0 is numerically consistent with $-C$ for $\beta = 6.0$ and $\beta = 6.2$ in table 4.19, which suggests that $r_0^2 M_{00}^2$ is consistent with zero in the combined chiral and continuum limit. Therefore, chiral behaviour of the ground state of the γ^0 channel is consistent with a (Pseudo-) Goldstone boson in the continuum limit. As the fermion mass dependence of Δ_{05} is rather mild, this conclusion seems to be extendable to finite fermion mass. The difference at finite lattice spacing
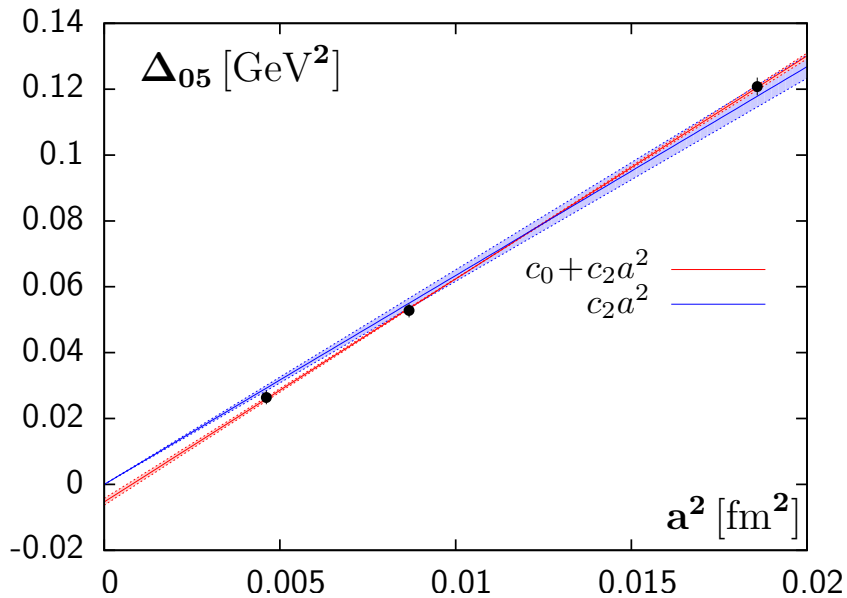
Figure 4.24: The continuum extrapolation of Δ_{05} is conducted with two functions $f_{02}(a^2)$ (red) and $f_2(a^2)$ (blue). Data clearly supports $f_{02}(a^2)$.

extrapolation	Δ_0	Δ_2	χ^2/dof
$f_{02}(a)$	$-0.033(6)$	$42.3(6)$	0.15
$f_2(a)$	0 by def.	$39.6(11)$	2.11

Table 4.22: The continuum extrapolation of Δ_{05} disfavours restriction to $\mathcal{O}(a^2)$ corrections. This could be either due to incomplete tuning or due to higher orders.

is evidence of discretisation effects that distinguish between both pseudoscalar states. This result is the analogue to taste-breaking effects for staggered fermions [24, 104]. It appears that (quenched) chiral perturbation theory is applicable and captures the quark mass dependence correctly even for (Pseudo-) Goldstone bosons that are beset by these lattice artifacts. This remarkable result certainly warrants further dedicated studies.

4.5 Interim findings (III)

In an initial discussion, foreseeable difficulties in numerical studies with minimally doubled fermions are pointed out and technical details of the implementation are covered. Only some of these difficulties can be understood purely in terms of the broken discrete symmetries of the theory. The appearance of oscillating terms in certain channels can be interpreted in term of the decomposition of the spinor fields of section 3.1. Two different approaches to non-perturbative tuning of Karsten-Wilczek fermions are developed. They make use of the anisotropy of the pseudoscalar mass or shifted frequency spectra of oscillating ratios of correlation functions. Lastly, a spectroscopic study of mesonic correlation functions in two different channels determines the chiral behaviour of their ground states and identifies them as pseudoscalars, which are degenerate in the continuum limit.

The first approach to non-perturbative renormalisation compares hadronic correlation functions, which use different directions of correlation – parallel or perpendicular to the $\hat{e}_{\underline{\alpha}}$ direction of the Karsten-Wilczek term. Without appropriately tuned counterterms, observables which are related to these correlators are anisotropic. The condition that the mass anisotropy $\Delta(M_{PS}^2)$ of the pseudoscalar ground state has a mininum is used to tune the relevant counterterm's coefficient to a value c_M. This approach has three main weaknesses. First, because the mass anisotropy $\Delta(M_{PS}^2)$ is a very shallow function of the relevant counterterm's coefficient, c_M has relatively large uncertainties. Second, since $\Delta(M_{PS}^2)$ is not independent of the marginal counterterm's coefficient, disentangling the dependence on both coefficients is a non-trivial issue. Third, correlation functions with the direction of correlation perpendicular to the alignment of the Karsten-Wilczek term have short plateaus. It appears as if they include low-lying excited state contributions, which seem to have negative spectral weights in source-smeared correlation functions. These issues seem less prominent if $c \approx c_M$.

Two non-trivial aspects in the numerical evaluation in correlation functions with the direction of correlation parallel to the alignment of the Karsten-Wilczek term were studied in detail. First, signatures of the broken time-reflection symmetry are not observed in numerical data for the pseudoscalar channel. Due to the considerations about the $C\Theta_{\underline{\alpha}}$ symmetry in section 3.2, this is not surprising. Second, in all mesonic channels other than the γ^5 channel, an oscillating contribution can be observed directly. A possible explanation of the oscillatory pattern is offered by the formal decomposition in section 3.1. In particular, a very small mass splitting between the ground states of γ^0 and γ^5 channels is observed and their ratio $R_{05}(n_0)$ for the finest lattice with $\beta = 6.2$ is almost purely oscillating with only a very small exponential decay. If the relevant counterterm is not fully tuned, the ratio's frequency spectrum has two peaks that are aligned symmetrically around π/a, while the peak is at π/a in the frequency spectra for naïve or free Karsten-Wilczek fermions. The frequency shift's parameter dependence is

empirically found to be $\omega_c \propto |\delta c|$. The formal decomposition in section 3.1 also suggests oscillations with frequencies that are close to π/a but shifted linearly in δ_c. The condition that the frequency spectrum of $R_{05}(n_0)$ is restored to its tree-level form is used to tune the relevant counterterm's coefficient to c_0 in this second approach.
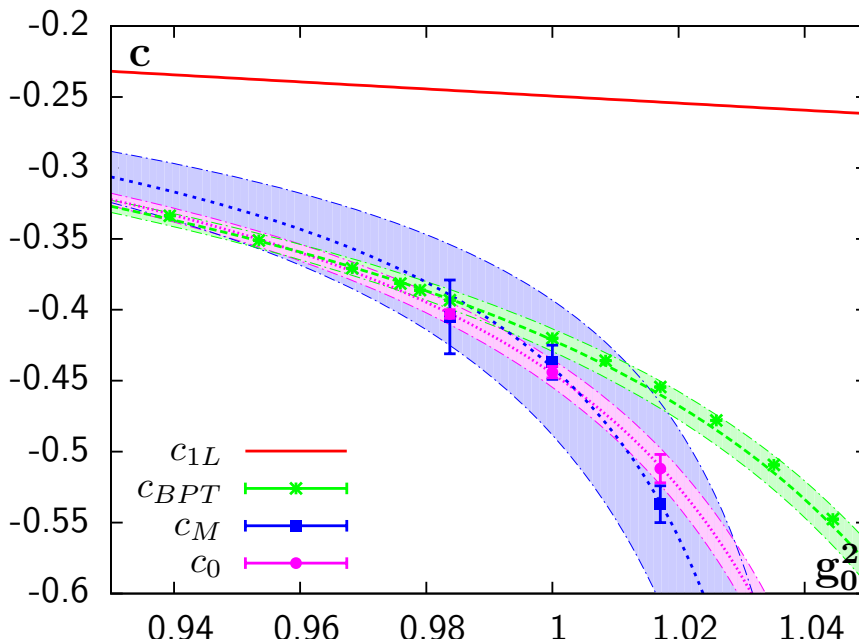
Figure 4.25: Non-perturbative renormalisation schemes for $c(g_0^2)$ agree within errors. One-loop results are clearly too small, but BPT undershoots only by a few percent.

β	$a\,[fm]$	c_{BPT}	$\frac{c_0 - c_{BPT}}{c_0}$	c_M	c_0
5.8	0.136	-0.454	11%	$-0.537(8)(10)$	$-0.5120(7)(100)$
6.0	0.093	-0.420	5%	$-0.437(7)(10)$	$-0.4435(8)(37)$
6.2	0.068	-0.393	2%	$-0.405(17)(20)$	$-0.4028(5)(27)$

Table 4.23: Two different non-perturbative tuning schemes yield c_M and c_0 for the relevant counterterm. The first error is statistical, the second error is an estimate of systematical uncertainty. Results agree very well though c_0 yields smaller uncertainties.

Non-perturbative results for the relevant counterterm's coefficient $c(g_0^2)$ are summarised in table 4.23 and figure 4.25. c_M and c_0 at each gauge coupling are in good agreement and are slightly (cf. fourth column in table 4.23) more negative than the estimate c_{BPT} from boosted perturbation theory. The systematical uncertainty of c_M is due to finite size effects, the fit range dependence of correlation functions with direction of correlation perpendicular to the alignment of the Karsten-Wilczek term and uncertainties of the chiral extrapolation. The systematical uncertainty of c_0 is due to the width of the peak

Scheme	c_M	c_0
n_2	$+0.2255(27)$	$+0.2163(8)$
d_1	$-0.9459(53)$	$-0.9256(18)$
χ^2/dof	0.458	0.081

Table 4.24: The Padé approximation of c_0 using eq. (4.56) has the smallest uncertainties and agrees with c_{BPT} for fine lattices within 1σ.

in the power spectral density, which is dominated by the ground state mass difference. Variation of c_0 due to different m_0 or d or for different lattice sizes is within statistical uncertainties. The coefficient in each scheme is interpolated with a Padé approximant using $n_1 \equiv c_{1L} = -0.249351$, which ensures that the interpolation reproduces the one-loop result for small couplings. The interpolation

$$c(g_0^2) = \frac{n_1 g_0^2 + n_2 g_0^4}{1 + d_1 g_0^2} \tag{4.56}$$

yields parameters that are listed in table 4.24. Finding a numerically robust approach to non-perturbative tuning of the marginal counterterm's coefficient d is still an open problem. Because estimates from BPT (d_{BPT} from table 2.2) are very small, they may well be sufficient for non-perturbative tuning within uncertainties.

The spectroscopic study of the ground state of γ^5 and γ^0 channels with an approximately tuned action verifies that M_{55}^2 receives contributions from quenched chiral logarithms, which agree within uncertainties with phenomenological estimates for all studied couplings. Thus, data are consistent with an interpretation as a (Pseudo-) Goldstone boson at finite lattice spacing. Consistency of the logarithms amongst different β and with phenomenological estimates improves if a finite offset is included in the chiral extrapolation of M_{55}^2. This might indicate incomplete tuning of the counterterms. Data provide no numerical evidence for quenched chiral logarithms in the ground state mass M_{00}^2 of the γ^0 channel. Instead, it has a residual mass in the chiral limit that vanishes as $\mathcal{O}(a^2)$ in the continuum limit. Deviation of the squared ground states mass difference Δ_{05} from zero in the continuum limit is very small and consistent with the negative offset of M_{55}^2 for the finer lattices. Results are inconclusive whether these deviations are due to systematical uncertainties (e.g. incomplete tuning), due to neglecting higher order terms or simply due to statistical fluctuations. The ground states of γ^5 and γ^0 channels for tuned parallel Karsten-Wilczek fermions are degenerate in the continuum limit within these uncertainties. Thus, the γ^0 channel's ground state is interpreted as a (Pseudo-) Goldstone boson in the continuum limit. The non-vanishing residual mass term can be understood as a consequence of the explicitly broken non-singlet chiral symmetry at finite lattice spacing cf. section 2.5). Lastly, a spectroscopic study in the quenched approximation with pseudoscalar masses below $300\,\text{MeV}$ would not have been feasible with Wilson fermions due to exceptional configurations. Clearly, Karsten-Wilczek fermions are protected from exceptional configurations by their residual chiral symmetry.

Conclusions

For the first time, perturbative studies of minimally doubled fermions have been published in [36, 37]. The first non-perturbative studies in the quenched approximation have been published in [154, 155]. This thesis wraps up the results of these studies and presents new unpublished research about minimally doubled fermions in lattice QCD. The perturbative studies include two varieties of minimally doubled fermions – Boriçi-Creutz and Karsten-Wilczek fermions – whereas the numerical studies are restricted to Karsten-Wilczek fermions. Minimally doubled fermions are among the few types of lattice fermions with an exact local chiral symmetry at finite lattice spacing and an ultralocal Dirac operator that can be inverted with moderate numerical cost. Because minimally doubled fermions reproduce two mass-degenerate quarks, numerical results can be interpreted in terms of QCD in the isospin-symmetric limit.

Minimally doubled fermions realise an exact chiral symmetry at finite lattice spacing whilst explicitly breaking the hypercubic symmetry and symmetry under both charge conjugation and reflections of one particular direction. This particular direction, along which the two poles of their Dirac operators are aligned, is different for Boriçi-Creutz and Karsten-Wilczek fermions and reflects the orientation of the dimension five operators in their actions. Nevertheless, the actions are invariant under the combination of charge conjugation and the broken reflection symmetry such that $CP\Theta$ symmetry is always maintained. Due to the broken symmetries, renormalisation requires three counterterms, whose forms are determined by the broken symmetries and whose coefficients have been computed perturbatively in [36, 37]. There are two fermionic counterterms – a relevant counterterm with dimension three and a marginal counterterm with dimension four – and a marginal gluonic counterterm with dimension four. The broken symmetries are manifest in the form of anisotropies unless the counterterms are tuned properly. Conservation of ultralocal vector and axial symmetry currents is verified on the one-loop level such that the PCAC relation is satisfied exactly. Estimates for the non-perturbative coefficients are obtained using boosted perturbation theory.

Different aspects of Karsten-Wilczek fermions are explored in numerical studies using the quenched approximation. In particular, the influence of the relevant counterterm's coefficient is studied extensively. Signatures of the broken reflection symmetry, which would be seen as a mass splitting between forward and backward propagating states in correlation functions parallel to the Karsten-Wilczek term's alignment, are consistent with zero. Interpretation as a consequence of $CP\Theta$ symmetry of the action using pure Yang-Mills gauge configurations is suggestive. Anisotropies due to inaccurately tuned counterterms are observed in the mass determination for the pseudoscalar channel in directions which are either parallel or perpendicular to the alignment of the Karsten-Wilczek term. Minimisation of the anisotropy is used as a scheme for non-perturbative tuning of the relevant counterterm. Though the anisotropy depends on the marginal counterterm as well, the sensitivity is insufficient for the given statistical accuracy. Hence, use of its estimate from boosted perturbation theory seems to be numerically sufficient as it is very small.

Numerical studies reveal that the connection between interpolating operators for Karsten-Wilczek fermions and J^{PC} of hadrons is more complicated than for Wilson-type fermions, but correlation functions of Dirac bilinears can still be interpreted straightforwardly in terms of mesonic channels. These complications are indicated by the empirical observation of oscillations for most mesonic correlation functions in a direction that is parallel to the alignment of the Karsten-Wilczek term. These oscillations are most significant in the γ^0 and $\mathbf{1}$ channels, where the ground state belongs to the oscillating contribution. Nevertheless, no oscillations are observed in correlation functions in a direction that is perpendicular to the Karsten-Wilczek term's alignment. The oscillating contributions are interpreted in the spirit of a formal decomposition of spinor fields and of their bilinear operators that are used in correlation functions. Conclusions from this decomposition about J^{PC} of the states in the oscillating contributions are consistent with their masses in numerical studies. Empirical observations indicate that the oscillation pattern changes upon variation of the relevant counterterm's coefficient. Frequency spectra for ratios of correlation functions in the direction that is parallel to the Karsten-Wilczek term's alignment are obtained with methods of discrete Fourier analysis. The numerical result that the frequency spectrum is restored to its tree-level form upon tuning of the relevant counterterm's coefficient serves as a second scheme for non-perturbative tuning. Conclusions from the formal decomposition about the frequency's dependence on the coefficient are consistent with observations. The results from the two different non-perturbative tuning schemes differ at the level of a few percent but are consistent within the overall uncertainties (cf. table 4.23).

Correlation functions in the pseudoscalar sector are studied in the chiral regime for pseudoscalar masses well below $300\,\mathrm{MeV}$. This mass range is inaccessible with Wilson fermions in the quenched approximation due to exceptional configurations. The study shows that Karsten-Wilczek fermions are not affected by exceptional configurations. A chiral extrapolation of the pseudoscalar mass is performed in the spirit of chiral pertur-

bation theory. Strictly speaking, the chiral limit does not exist due to pathologies of the quenched approximation, which manifest themselves in the form of quenched chiral logarithms. Their size as estimated from numerical data agrees with other determinations. The pseudoscalar mass is consistent with zero in the limit of vanishing quark mass. An approximate degeneracy between the ground state of the oscillating contribution in the γ^0 channel and the ground state of the pseudoscalar channel is observed empirically. This mass splitting is nearly independent of the quark mass and consistent with zero in the continuum limit. Since this state is interpreted as $J^{PC} = 0^{-+}$ in the spirit of the formal decomposition, both ground states are interpreted as pion states.

As a natural next step it is necessary to move on from the quenched approximation to simulations with *dynamical minimally doubled fermions*. The best chances for success rests with an implementation of Karsten-Wilczek fermions within very general, preexisting frameworks such as USQCD [93] or the MILC [113] code. In a simulation with dynamical fermions, the gluonic counterterm will be tuned by the prescription that the average plaquette value of *parallel* and *perpendicular plaquettes* (including or excluding the direction of the Karsten-Wilczek term's alignment) must be equal. Whether or not this prescription is sufficiently independent of the other counterterms' coefficients remains to be seen, but the idea seems very straightforward compared to the fermionic counterterms. The method of stochastic sources can be applied to deal with the second systematical deficit of present simulations, as it may be applied in a calculation of *quark-disconnected contributions*. These quark-disconnected contributions which discriminate between charged and neutral pions are indispensable for an unambiguous identification of the physical pion states that are seen in the different channels containing pseudoscalars. The analytical and numerical studies within this thesis are the first proof that non-perturbative studies of QCD with minimally doubled fermions are feasible and yield a mass spectrum which exhibits the correct features as expected from QCD. Even though studies in the quenched approximation are in a way dissatisfying compared to the success of Lattice QCD with dynamical fermions using other discretisations, the present study will be the cornerstone upon which any future application with minimally doubled fermions will rest.

Acknowledgements

Conventions

A.1 Physical constants

This section declares the unit conventions throughout this thesis. Natural units are applied throughout this thesis, i.e.

$$c = 1 = \hbar. \tag{A.1}$$

Therefore, physical quantities have the following length dimensions:

$$[\text{length}] = [\text{time}] = [\text{energy}]^{-1} = [\text{mass}]^{-1}. \tag{A.2}$$

For the purpose of conversion to other systems of units, the product of the quantum of action and the speed of light in vacuum as well as the speed of light in vacuum are given in SI units by

$$\hbar c = 197.326968(17)\,\text{MeV fm}, \quad c = 299792458\,\text{m s}^{-1}. \tag{A.3}$$

A.2 Indices

This section declares the index conventions throughout this thesis.

Space-time indices

Space-time indices are labelled by Greek letters mostly from the middle of the Greek alphabet. If they are applied in Minkowski space-time $\mathbb{M}^4$, their range is $\mu \in \{0, 1, 2, 3\}$. If they are applied in Euclidean space-time $\mathbb{R}^4$, their range is $\mu \in \{0, 1, 2, 3\}$ as well.

Space-time indices, which occur multiply are always considered to be summed over. Exceptions are explicitly highlighted. Fixed indices, which are never summed are marked by an underscore, e.g. $\underline{\mu}$.

Spinor indices

Spinor indices are labelled by Greek letters mostly from the beginning of the Greek alphabet. Their range is $\alpha \in \{1, 2, 3, 4\}$. Spinor indices which occur twice are always considered to be summed over according to Einstein's summation convention.

Colour indices

Colour indices are labelled by Latin letters mostly from the start of the alphabet. The range of colour indices is $a \in \{1, 2, 3\}$ for the fundamental representation and $a \in \{1, 2, 3, 4, 5, 6, 7, 8\}$ for the adjoint representation. Colour indices which occur twice in either the fundamental or adjoint representation are always considered to be summed over according to Einstein's summation convention. Exceptions are explicitly highlighted. Fixed indices, which are never summed are marked by an underscore, e.g. $\underline{a}$.

Flavour indices

Flavour indices in the fundamental representation are labelled by bracketed numbers. Their general range is $f \in \{1, 2, 3, 4, 5, 6\}$ and they are sorted in the order of ascending quark mass. The spinor's symbol ψ can be replaced by the one-letter label of the flavours, e.g. $\psi^{(1)} \equiv u$, $\psi^{(2)} \equiv d$, ... and the quark mass parameters can be labeled as $m^{(1)} = m_u$, $m^{(2)} = m_d$, ... Summation of flavour indices is always declared explicitly.

Space-time coordinates

Space-time coordinates x of field variables ψ defined on a space-time continuum are represented as arguments of the fields, e.g. $\psi(x)$. Space-time coordinates are labelled with latin letters from the end of the alphabet. In the contrary, site labels n on discretised space-time lattice are dimensionless numbers defined as $n_\mu = x_\mu/a$. Site labels are represented as site indices ψ_n. Sites labels are usually labelled by letters from the middle of the alphabet. Integration over space-time coordinates or summation over site labels are always declared explicitly. The summation range of site labels is usually omitted.

Momentum space coordinates

The vector space of four-momenta is referred to as momentum space throughout this thesis. Its coordinates k_μ are always represented as arguments of the fields, $\psi(k)$. Integration over momentum space coordinates is always declared explicitly.

A.3 SU(N) Matrices

This section declares the conventions concerning SU(N) matrices.

SU(2) – Pauli matrices

The Pauli matrices σ^μ are defined by

$$\sigma^1 = \begin{pmatrix} 0 & 1 \\ 1 & 0 \end{pmatrix}, \quad \sigma^2 = \begin{pmatrix} 0 & -i \\ i & 0 \end{pmatrix}, \quad \sigma^3 = \begin{pmatrix} 1 & 0 \\ 0 & -1 \end{pmatrix}. \tag{A.4}$$

The 2×2-unit matrix is included as

$$\sigma^0 = \begin{pmatrix} 1 & 0 \\ 0 & 1 \end{pmatrix}. \tag{A.5}$$

As generators of the symmetry group SU(2), they are defined with an extra factor $1/2$,

$$\tau_j = \frac{1}{2}\sigma^j \tag{A.6}$$

and satisfy

$$\tau^i\tau^j = \frac{1}{2}\left(\delta^{ij} + i\epsilon^{ijk}\tau^k\right). \tag{A.7}$$

SU(3) – Gell-Mann matrices

The Gell-Mann matrices λ^j are defined by

$$\lambda^1 = \begin{pmatrix} 0 & 1 & 0 \\ 1 & 0 & 0 \\ 0 & 0 & 0 \end{pmatrix}, \qquad \lambda^2 = \begin{pmatrix} 0 & -i & 0 \\ i & 0 & 0 \\ 0 & 0 & 0 \end{pmatrix}, \qquad \lambda^3 = \begin{pmatrix} 1 & 0 & 0 \\ 0 & -1 & 0 \\ 0 & 0 & 0 \end{pmatrix},$$

$$\lambda^4 = \begin{pmatrix} 0 & 0 & 1 \\ 0 & 0 & 0 \\ 1 & 0 & 0 \end{pmatrix}, \qquad \lambda^5 = \begin{pmatrix} 0 & 0 & -i \\ 0 & 0 & 0 \\ i & 0 & 0 \end{pmatrix}, \qquad \lambda^6 = \begin{pmatrix} 0 & 0 & 0 \\ 0 & 0 & 1 \\ 0 & 1 & 0 \end{pmatrix},$$

$$\lambda^7 = \begin{pmatrix} 0 & 0 & 0 \\ 0 & 0 & -i \\ 0 & i & 0 \end{pmatrix}, \qquad \lambda^8 = \frac{1}{\sqrt{3}}\begin{pmatrix} 1 & 0 & 0 \\ 0 & 1 & 0 \\ 0 & 0 & -2 \end{pmatrix}. \tag{A.8}$$

As generators of the symmetry group SU(3), they are defined with an extra factor $1/2$,

$$T_j = \frac{1}{2}\lambda^j \tag{A.9}$$

and satisfy

$$T^iT^j = \frac{1}{2}\left(\frac{1}{3}\delta^{ij}\mathbf{1} + (d^{ijk} + if^{ijk})T_k\right). \tag{A.10}$$

Casimir operators

The Casimir operators of the group SU(N) are given by

$$C(R) = \frac{1}{2} = \text{Tr}(T_{\underline{a}}T_{\underline{a}}) \tag{A.11}$$

$$C_2(R)1_{N \times N} = \sum_a T_a T_a = \frac{N^2 - 1}{2N}1_{N \times N}, \quad C_2(R) \equiv C_F \tag{A.12}$$

$$C_2 \equiv C_2(G) = C(G) = f^{\underline{acd}}f^{\underline{acd}} = N, \tag{A.13}$$

where R is the fundamental and G is the adjoint representation.

A.4   Minkowski and Euclidean space-time

This section declares the conventions concerning Minkowski and Euclidean space-time throughout this thesis. Quantities defined on a Minkowski or Euclidean space-time are always labelled with upper indices M or E if there is any possibility of an ambiguity. If ambiguities can be excluded, these labels are omitted.

A.4.1   Coordinates and four-vectors

This thesis mostly uses Euclidean space-time. Four-vectors defined on Euclidean space-time are connected with four-vectors on Minkowski space-time by a Wick rotation. The Wick rotation of the x_0 coordinate is defined as

$$x_0^E \equiv ix_0^M. \tag{A.14}$$

The Minkowski space-time coordinate x_0^M is identical to the usual physical time t. Four-momenta p_μ, derivatives ∂_μ as well as four-vector fields $A_\mu(x)$ have their temporal components transformed by the Wick-rotation with the conjugate factor $(-i)$,

$$p_0^E = -ip_0^M, \tag{A.15}$$

$$\partial_0^E = \frac{\partial}{\partial x^{0\,E}} = \frac{1}{i}\frac{\partial}{\partial x^{0\,M}} = -i\partial_0^M, \tag{A.16}$$

$$A_0^E(x^E) = -iA_0^M(x^M). \tag{A.17}$$

Four-vectors are defined in Minkowski and Euclidean space-time by

$$x^{M\,\mu} = (x_0^M, \mathbf{x}^M), \tag{A.18}$$

$$x_\mu^M = g_{\mu\nu}x^{M\,\mu} = (x_0^M, -\mathbf{x}^M), \tag{A.19}$$

$$x_\mu^E = x^{E\,\mu} = (x_0^E, \mathbf{x}^E) \tag{A.20}$$

and scalar products are

$$x^M \cdot y^M = x_\mu^M y^{M\,\mu} = (x_0^M y_0^M) - (\mathbf{x}^M \cdot \mathbf{y}^M), \tag{A.21}$$

$$x^E \cdot y^E = x_\mu^E y_\mu^E = (x_0^E y_0^E) + (\mathbf{x}^E \cdot \mathbf{y}^E). \tag{A.22}$$

Three-dimensional vectors are in bold print (e.g. $\mathbf{x}$). The scalar product of four-vectors and three-vectors are both abbreviated as dot products. The metric of Minkowski space-time is defined as

$$g_{\mu\nu} = \text{diag}\,(+1, -1, -1, -1). \tag{A.23}$$

Due to the aforementioned transformation properties of derivatives in eq. (A.16) and vector fields in eq. (A.17), the field strength tensor $F_{\mu\nu}(x)$ transforms as

$$F^{E\,\mu\nu}(x^E) = F_{\mu\nu}^E(x^E) = (-i)^{(\delta^{\mu 0} + \delta^{\nu 0})}\, F_{\mu\nu}^M(x^M) = i^{(\delta^{\mu 0} + \delta^{\nu 0})}\, F^{M\,\mu\nu}(x^M). \tag{A.24}$$

Thus, the product $F_{\mu\nu}^E(x^E)F_{\mu\nu}^E(x^E) = F_{\mu\nu}^M(x^M)F^{M\,\mu\nu}(x^M)$ is not multiplied by any extra factors in the Wick rotation.

Spinor fields and adjoint spinor fields are treated as independent degrees of freedom in the Osterwalder-Schrader approach [124, 126] to a Euclidean field theory, but are otherwise left unchanged:

$$\psi^E(x^E) = \psi^M(x^M), \quad \bar{\psi}^E(x^E) = \bar{\psi}^M(x^M). \tag{A.25}$$

While this is not of particular importance in the path integral approach, which already treats ψ and $\bar{\psi}$ as independent field in Minkowski space-time, the OS approach causes a loss of hermiticity for the Dirac action, which can be avoided by Waldron's elaborate scheme for the Wick rotation including spinor rotations [148, 149, 153]. Throughout this thesis, the OS approach to Euclidean field theories is applied.

A.4.2 Dirac matrices

Dirac matrices are defined as

$$\gamma^{M\,0} = \begin{pmatrix} 0 & \sigma^0 \\ \sigma^0 & 0 \end{pmatrix}, \qquad \gamma^{M\,j} = \begin{pmatrix} 0 & \sigma^j \\ -\sigma^j & 0 \end{pmatrix}, \tag{A.26}$$

$$\gamma^{E\,0} = \begin{pmatrix} 0 & \sigma^0 \\ \sigma^0 & 0 \end{pmatrix} = \gamma^{M\,0}, \qquad \gamma^{E\,j} = \begin{pmatrix} 0 & -i\sigma^j \\ i\sigma^j & 0 \end{pmatrix} = -i\gamma^{M\,j}, \tag{A.27}$$

which corresponds to the chiral representation in both Minkowski and Euclidean space-time. The Dirac matrix γ^0 is real, wheres the spatial Dirac matrices are anti-hermitian in Minkowski space-time and hermitian in Euclidean space-time. They satisfy the Clifford algebra,

$$\left\{ \gamma^{M\,\mu}, \gamma^{M\,\nu} \right\} = 2g^{\mu\nu}, \quad \left\{ \gamma^{E\,\mu}, \gamma^{E\,\nu} \right\} = 2\delta^{\mu\nu}. \tag{A.28}$$

143

Contrary to standard conventions, Euclidean space-time Dirac matrices are usually written with upper indices throughout the thesis. The chirality matrix γ^5, which anticommutes with all Dirac matrices γ^μ, is defined by

$$\gamma^{M\,5} = i\gamma^{M\,0}\gamma^{M\,1}\gamma^{M\,2}\gamma^{M\,3}, \quad \gamma^{E\,5} = \gamma^{E\,0}\gamma^{E\,1}\gamma^{E\,2}\gamma^{E\,3} \tag{A.29}$$

and is equal in Minkowski and Euclidean space-time:

$$\gamma^5 = \gamma^{M\,5} = \gamma^{E\,5} = \begin{pmatrix} \sigma^0 & 0 \\ 0 & -\sigma^0 \end{pmatrix}. \tag{A.30}$$

The chirality matrix is usually written with an upper index as γ^5 in this thesis. The chirality projectors are defined as

$$P_R = \frac{1}{2}(1 + \gamma^5), \quad P_L = \frac{1}{2}(1 - \gamma^5) \tag{A.31}$$

and parity projectors (for fermions) are defined as

$$P_+ = \frac{1}{2}(1 + \gamma^0), \quad P_- = \frac{1}{2}(1 - \gamma^0). \tag{A.32}$$

The charge conjugation matrix C is defined as

$$C = i\gamma_0\gamma_2 = C^\dagger = C^{-1} = -C^T \tag{A.33}$$

both on Minkowski and Euclidean space-times and satisifies

$$\gamma^\mu C = C^T \gamma^{\mu\,T}. \tag{A.34}$$

A.4.3   Continuous space-time and discrete space-time lattices

Events in a four-dimensional continuous space-time V of infinite extent,

$$V = \{x = (x_0, x_1, x_2, x_3) \mid -\infty < x_\mu < \infty\}, \tag{A.35}$$

are labelled by four-component coordinate vectors x, which have the dimension of a [length]. This definition can be restricted to any subspace of finite extent,

$$V = \{x = (x_0, x_1, x_2, x_3) \mid 0 < x_\mu < L_\mu\}, \tag{A.36}$$

where the size of the subspace introduces a length scale. Any finite subspace must be supplied with appropriate boundary conditions. Throughout this thesis, boundary conditions will be generally chosen as periodic or anti-periodic, e.g. any function satisfies

$$f(x_\mu + L_\mu) = \pm f(x_\mu). \tag{A.37}$$

In a discretisation, continuous space-time is replaced by a finite space-time lattice Λ,

$$\Lambda = \{n = (n_0, n_1, n_2, n_3) \mid 0 \le n_\mu < N_\mu\}. \tag{A.38}$$

144

Events on this lattice are labelled by a four-component site vector n, which is dimensionless. It is connected to a coordinate vector of dimension [length] as

$$x_\mu = a n_\mu \tag{A.39}$$

by a lattice spacing a, which defines the intrinsic length scale of the system (the intrinsic length scale of the continuous system is defined in terms of the lattice spacing and the number of sites: $L_\mu = a N_\mu$). Sites n of a discretised space-time lattice can be sorted into even and odd sites, which are distinguished by whether the sum of components

$$n_\Sigma = \sum_{\mu=0}^{3} n_\mu \tag{A.40}$$

is an even or an odd number. The volume is defined as $V = a^4 |\Lambda|$, where $|\Lambda| = \prod_\mu N_\mu$ takes the role of a dimensionless volume. Slices of the lattice are defined for any direction by

$$\Lambda_m^{\underline{\mu}} = \{ n \in \Lambda \, | n_{\underline{\mu}} = m = \text{const} \}. \tag{A.41}$$

A.5   Fourier transformations

Fourier transformations connect space-time V to its Fourier space $\widetilde{V}$, which is usually called momentum space throughout this thesis.

Infinite space-time

The Fourier space $\widetilde{V}$ of an infinite space-time V is also infinite. The Fourier transform $\widetilde{f}(p)$ of a real function $f(x)$ is defined by

$$\widetilde{f}(p) = \int_V f(x) e^{-ix\cdot p} d^4 x, \tag{A.42}$$

$$f(x) = \int_{\widetilde{V}} \widetilde{f}(p) e^{ix\cdot p} \frac{d^4 p}{(2\pi)^4}. \tag{A.43}$$

145

Hence, complex functions $\phi(x)$ are transformed to $\widetilde{\phi}(p)$ according to

$$\widetilde{\phi}(p) = \int_V \phi(x)e^{-ix\cdot p}d^4x, \tag{A.44}$$

$$\phi(x) = \int_{\widetilde{V}} \widetilde{\phi}(p)e^{ix\cdot p}\frac{d^4p}{(2\pi)^4}, \tag{A.45}$$

$$\widetilde{\phi^\dagger}(p) = \int_V \phi^\dagger(x)e^{ix\cdot p}d^4x, \tag{A.46}$$

$$\phi^\dagger(x) = \int_{\widetilde{V}} \widetilde{\phi^\dagger}(p)e^{-ix\cdot p}\frac{d^4p}{(2\pi)^4}. \tag{A.47}$$

Because it is always clear from the arguments, the Fourier transforms of the fields ψ, $\bar\psi$ and A are not marked with a tilde ($\widetilde{}$) explicitly. Delta functions, which naturally arise in Fourier transformations of local products of fields, are generated as

$$\delta(p-q) \equiv \delta(p_0-q_0)\delta(p_1-q_1)\delta(p_2-q_2)\delta(p_3-q_3) = \int_V e^{-ix\cdot(p-q)}d^4x, \tag{A.48}$$

$$\delta(x-y) \equiv \delta(x_0-y_0)\delta(x_1-y_1)\delta(x_2-y_2)\delta(x_3-y_3) = \int_{\widetilde{V}} e^{i(x-y)\cdot p}\frac{d^4p}{(2\pi)^4}. \tag{A.49}$$

Finite space-time lattice

The discretised Fourier space is the Brillouin zone, $\widetilde{V} = (2\pi/a)^4 = |\Lambda| \prod_\mu(2\pi/(aN_\mu))$. The Fourier transform $f(k)$ of a real function f_n on a finite space-time lattice is defined by (complex functions are analogous to eqs. (A.44)-(A.47))

$$\widetilde{f}(k) = \frac{1}{\sqrt{|\Lambda|}} \sum_{n\in\Lambda} f_n e^{-ian\cdot k}, \tag{A.50}$$

$$f_n = \frac{1}{\sqrt{|\Lambda|}} \sum_{k\in\widetilde{\Lambda}} \widetilde{f}(k) e^{ian\cdot k}. \tag{A.51}$$

The analogues of the delta functions of eqs. (A.48) and (A.49) are given by

$$\delta(k,l) \equiv \delta_{k_0 l_0}\delta_{k_1 l_1}\delta_{k_2 l_2}\delta_{k_3 l_3} = \frac{1}{|\Lambda|} \sum_{n\in\Lambda} e^{-ian\cdot(k-l)}, \tag{A.52}$$

$$\delta_{n,m} \equiv \delta_{n_0 m_0}\delta_{n_1 m_1}\delta_{n_2 m_2}\delta_{n_3 m_3} = \frac{1}{|\Lambda|} \sum_{k\in\widetilde{\Lambda}} e^{ia(n-m)\cdot k}. \tag{A.53}$$

Generalisation of the (inverse) discrete Fourier transform of real functions to complex functions is analogous to the treatment in the continuous case (cf. A.5).

Addendum to perturbative studies

This appendix covers some particularly lengthy expression, which appear in perturbative calculations, in more detail.

B.1 Recursion relations for bosonic integrals

This appendix summarises the recursion relations for basic bosonic integrals in LPT and clarifies the nomenclature. All recursion relations have been taken from [31], chapter 18. Their practical application is done with a FORM [106, 151] program, which has been provided by Stefano Capitani. The basic integrals of eq. (2.14) satisfy recursion relations. Absent momentum components in the numerator are left out in the nomenclature, e.g.

$$\mathcal{B}(p; n_0, n_3) \equiv \mathcal{B}(p; n_0, 0, 0, n_3), \quad \mathcal{B}(p) \equiv \mathcal{B}(p; 0, 0, 0, 0). \tag{B.1}$$

The first set of recursion relations removes a first power of a momentum component $\hat{k}_\mu^2$ in the numerator,

$$4\mathcal{B}(p; 1) = \mathcal{B}(p-1) - M^2 \mathcal{B}(p) \tag{B.2}$$

$$3\mathcal{B}(p; x, 1) = \mathcal{B}(p-1; x) - \mathcal{B}(p; x+1) - M^2 \mathcal{B}(p; x) \tag{B.3}$$

$$2\mathcal{B}(p; x, y, 1) = \mathcal{B}(p-1; x, y) - \mathcal{B}(p; x+1, y) - \mathcal{B}(p; x, y+1) - M^2 \mathcal{B}(p; x, y) \tag{B.4}$$

$$\mathcal{B}(p; x, y, z, 1) = \mathcal{B}(p-1; x, y, z) - \mathcal{B}(p; x+1, y, z) - \mathcal{B}(p; x, y+1, z)$$
$$- \mathcal{B}(p; x, y, z+1) - M^2 \mathcal{B}(p; x, y, z). \tag{B.5}$$

The second recursion relation lowers the power of a momentum component $\hat{k}_\mu^{2r}$ in the numerator,

$$\mathcal{B}(p; \ldots, r) = \frac{r-1}{p-1}\mathcal{B}(p-1; \ldots, r-1) - \frac{4r-6}{p-1}\mathcal{B}(p-1; \ldots, r-2) + 4\mathcal{B}(p; \ldots, r-1). \tag{B.6}$$

B.2 Addendum to the self-energy calculation

B.2.1 Sunset diagram for Karsten-Wilczek fermions

Various particular unwieldy expressions of the one-loop calculation of the fermionic self-energy are presented only in this addendum to the perturbative studies. The algebraically simplified numerators of $J_3^\chi(\zeta, a)$ read

$$N_0 = s_k^\chi \big(\{ 2(\hat{c}_k^\chi)^2 - (\hat{c}_k)^2 \} + \delta^{\chi\underline{\alpha}}\zeta^2(\hat{s}_k)_\perp^2 \big)$$
$$+ \zeta \big\{ 4s_k^{\underline{\alpha}}s_k^\chi \varepsilon^{\underline{\alpha}\chi} + \delta^{\chi\underline{\alpha}} \big(4(s_k)_\perp^2 + \tfrac{1}{2}(\hat{s}_k)_\perp^2 \{ 2(\hat{c}_k^{\underline{\alpha}})^2 - (\hat{c}_k)^2 + \zeta^2(\hat{s}_k)_\perp^2 \} \big) \big\} \tag{B.7}$$

$$N_1 = s_k^\chi \Big(\{ 4(s_k)^2 + \zeta^2(1 + 2\delta^{\chi\underline{\alpha}}) \{ (\hat{s}_k)_\perp^2 \}^2 \} + \zeta(\hat{s}_k)_\perp^2 \{ 4s_k^{\underline{\alpha}}s_k^\chi + \delta^{\chi\underline{\alpha}} \big(2(s_k)^2 + \tfrac{\zeta^2}{2} \{ (\hat{s}_k)_\perp^2 \}^2 \big) \} \Big). \tag{B.8}$$

The denominators of the sunset diagram that contribute to wavefunction renormalisation and the marginal counterterm's coefficient for Karsten-Wilczek fermions read

$$D_4 = D^{KW}(k; \zeta, M, a) D^g(-k; M, a), \tag{B.9}$$

$$D_5 = D^{KW}(k; \zeta, M, a) \left(D^g(-k; M, a) \right)^2, \tag{B.10}$$

$$D_6 = D^{KW}(k; \zeta, M, a) \left(D^g(-k; M, a) \right)^3. \tag{B.11}$$

Five numerators N_4 - N_8 contribute to wavefunction renormalisation and to the marginal counterterm's coefficient. The full numerators N_4 and N_5 of the part in Feynman gauge $(J_4^{\chi\theta}|_{\xi=1})$ read

$$N_4 = \sum_{\mu,\nu,\lambda} \frac{\delta^{\mu\nu}}{8} \mathrm{tr} \Big\{ \big(\gamma^\chi \delta^{\mu\theta} \left(-\gamma^\mu \hat{s}_k^\mu + \zeta\gamma^{\underline{\alpha}}\varepsilon^{\underline{\alpha}\mu}\hat{c}_k^\mu \right) \left(\gamma^\lambda s_k^\lambda + \zeta\gamma^{\underline{\alpha}}\varepsilon^{\underline{\alpha}\lambda} \{ 1 - c_k^\lambda \} \right) \left(\gamma^\nu \hat{c}_k^\nu + \zeta\gamma^{\underline{\alpha}}\varepsilon^{\underline{\alpha}\nu}\hat{s}_k^\nu \right) \big)$$
$$+ \big(\gamma^\chi \delta^{\nu\theta} \left(\gamma^\mu \hat{c}_k^\mu + \zeta\gamma^{\underline{\alpha}}\varepsilon^{\underline{\alpha}\mu}\hat{s}_k^\mu \right) \left(\gamma^\lambda s_k^\lambda + \zeta\gamma^{\underline{\alpha}}\varepsilon^{\underline{\alpha}\lambda} \{ 1 - c_k^\lambda \} \right) \left(-\gamma^\nu \hat{s}_k^\nu + \zeta\gamma^{\underline{\alpha}}\varepsilon^{\underline{\alpha}\nu}\hat{c}_k^\nu \right) \big) \Big\}, \tag{B.12}$$

$$N_5 = \sum_{\mu,\nu,\lambda} \frac{\delta^{\mu\nu}}{4} \mathrm{tr} \Big\{ \gamma^\chi \left(\gamma^\mu \hat{c}_k^\mu + \zeta\gamma^{\underline{\alpha}}\varepsilon^{\underline{\alpha}\mu}\hat{s}_k^\mu \right) \left(\gamma^\lambda s_k^\lambda + \zeta\gamma^{\underline{\alpha}}\varepsilon^{\underline{\alpha}\lambda} \{ 1 - c_k^\lambda \} \right) \left(\gamma^\nu \hat{c}_k^\nu + \zeta\gamma^{\underline{\alpha}}\varepsilon^{\underline{\alpha}\nu}\hat{s}_k^\nu \right) \Big\} \left(\hat{c}_k^\theta \hat{s}_k^\theta \right), \tag{B.13}$$

and the numerators N_6, N_7 and N_8 of the gauge fixing part $\left(-(1-\xi) \left(\partial J_4^{\chi\theta}/\partial\xi \right) \right)$ read

$$N_6 = \sum_{\mu,\nu,\lambda} \frac{1}{8} \mathrm{tr} \Big\{ \big(\gamma^\chi \delta^{\mu\theta} \left(-\gamma^\mu \hat{s}_k^\mu + \zeta\gamma^{\underline{\alpha}}\varepsilon^{\underline{\alpha}\mu}\hat{c}_k^\mu \right) \left(\gamma^\lambda s_k^\lambda + \zeta\gamma^{\underline{\alpha}}\varepsilon^{\underline{\alpha}\lambda} \{ 1 - c_k^\lambda \} \right) \left(\gamma^\nu \hat{c}_k^\nu + \zeta\gamma^{\underline{\alpha}}\varepsilon^{\underline{\alpha}\nu}\hat{s}_k^\nu \right) \big)$$
$$+ \big(\gamma^\chi \delta^{\nu\theta} \left(\gamma^\mu \hat{c}_k^\mu + \zeta\gamma^{\underline{\alpha}}\varepsilon^{\underline{\alpha}\mu}\hat{s}_k^\mu \right) \left(\gamma^\lambda s_k^\lambda + \zeta\gamma^{\underline{\alpha}}\varepsilon^{\underline{\alpha}\lambda} \{ 1 - c_k^\lambda \} \right) \left(-\gamma^\nu \hat{s}_k^\nu + \zeta\gamma^{\underline{\alpha}}\varepsilon^{\underline{\alpha}\nu}\hat{c}_k^\nu \right) \big) \Big\} (\hat{s}_k^\mu \hat{s}_k^\nu), \tag{B.14}$$

$$N_7 = \sum_{\mu,\nu,\lambda} -\frac{\delta^{\mu\theta}\hat{c}_k^\mu \hat{s}_k^\nu + \delta^{\nu\theta}\hat{s}_k^\mu \hat{c}_k^\nu}{8} \mathrm{tr} \Big\{ \gamma^\chi \left(\gamma^\mu \hat{c}_k^\mu + \zeta\gamma^{\underline{\alpha}}\varepsilon^{\underline{\alpha}\mu}\hat{s}_k^\mu \right) \left(\gamma^\lambda s_k^\lambda + \zeta\gamma^{\underline{\alpha}}\varepsilon^{\underline{\alpha}\lambda} \{ 1 - c_k^\lambda \} \right) \left(\gamma^\nu \hat{c}_k^\nu + \zeta\gamma^{\underline{\alpha}}\varepsilon^{\underline{\alpha}\nu}\hat{s}_k^\nu \right) \Big\}, \tag{B.15}$$

$$N_8 = \sum_{\mu,\nu,\lambda} -\frac{(\hat{c}_k^\theta \hat{s}_k^\theta)(\hat{s}_k^\mu \hat{s}_k^\nu)}{2} \mathrm{tr} \Big\{ \gamma^\chi \left(\gamma^\mu \hat{c}_k^\mu + \zeta\gamma^{\underline{\alpha}}\varepsilon^{\underline{\alpha}\mu}\hat{s}_k^\mu \right) \left(\gamma^\lambda s_k^\lambda + \zeta\gamma^{\underline{\alpha}}\varepsilon^{\underline{\alpha}\lambda} \{ 1 - c_k^\lambda \} \right) \left(\gamma^\nu \hat{c}_k^\nu + \zeta\gamma^{\underline{\alpha}}\varepsilon^{\underline{\alpha}\nu}\hat{s}_k^\nu \right) \Big\}. \tag{B.16}$$

Summation of Euclidean indices and evaluation of the trace simplifies the numerators to

$$N_4 = s_k^\theta s_k^\chi \left\{ 2(1 - 2\delta^{\theta\chi}) + \zeta^2 \left(-1 + 2\delta^{\theta\underline{\alpha}} + 4\delta^{\chi\underline{\alpha}} - \delta^{\theta\chi} \{ 4\delta^{\chi\underline{\alpha}} + (\hat{s_k})_\perp^2 \varepsilon^{\chi\underline{\alpha}} \} \right) \right\}$$
$$+ \zeta \left\{ s_k^{\underline{\alpha}} \delta^{\theta\chi} \left((\hat{c}_k^\theta)^2 - \delta^{\theta\underline{\alpha}} \{ (\hat{c}_k^\theta)^2 + (\hat{s}_k)_\perp^2 \} \right) + s_k^\theta \delta^{\chi\underline{\alpha}} \varepsilon^{\theta\underline{\alpha}} \left(2(\hat{c}_k^\theta)^2 + (1 + \zeta^2)(\hat{s}_k)_\perp^2 \right) \right\}, \quad \text{(B.17)}$$

$$N_5 = -2 s_k^\theta s_k^\chi \left\{ (\hat{c}_k)^2 - 2(\hat{c}_k^\theta)^2 - \zeta^2 \delta^{\chi\underline{\alpha}} (\hat{s}_k)_\perp^2 \right\}$$
$$- 2\zeta s_k^\theta \left\{ 4 s_k^{\underline{\alpha}} s_k^\chi + \delta^{\chi\underline{\alpha}} \left(4 \{ (s_k)_\perp^2 - (s_k^\chi)^2 \} + \frac{1}{2} (\hat{s}_k)_\perp^2 \left\{ 2(\hat{c}_k^\chi)^2 - (\hat{c}_k)^2 + \zeta^2 (\hat{s})_\perp^2 \right\} \right) \right\}, \quad \text{(B.18)}$$

$$N_6 = -2(\hat{s}_k^\theta)^2 \delta^{\theta\chi} (s_k)^2 + \zeta^2 \left\{ 2 s_k^\theta s_k^\chi \varepsilon^{\chi\underline{\alpha}} - \delta^{\theta\chi} (\hat{s}_k^\theta)^2 ((\hat{s}_k)_\perp^2)^2 \right\}$$
$$+ \zeta (\hat{s}_k)_\perp^2 \left\{ (\hat{s}_k^\theta)^2 \left(s_k^\chi \delta^{\theta\underline{\alpha}} - s_k^\theta \delta^{\chi\underline{\alpha}} - 3 s_k^{\underline{\alpha}} \delta^{\theta\chi} \right) + \zeta^2 s_k^\theta \delta^{\chi\underline{\alpha}} (\hat{s}_k)_\perp^2 \right\}, \quad \text{(B.19)}$$

$$N_7 = -2 \delta^{\theta\chi} (\hat{c}_k^\theta)^2 \left\{ (s_k)^2 + \zeta^2 ((\hat{s}_k)_\perp^2)^2 \right\} - 2\zeta^2 s_k^\theta s_k^\chi (\hat{s}_k)_\perp^2 \left\{ -2 + \delta^{\theta\underline{\alpha}} + 2\delta^{\chi\underline{\alpha}} \varepsilon^{\theta\chi} \right\}$$
$$+ \zeta \left(-2 s^{\underline{\alpha}} \delta^{\theta\chi} (\hat{c}_k^\theta)^2 (\hat{s}_k)_\perp^2 - s_k^\theta \varepsilon^{\theta\underline{\alpha}} \left\{ 4\delta^{\chi\underline{\alpha}} (s_k)^2 + \zeta^2 ((\hat{s}_k)_\perp^2)^2 \right\} \right), \quad \text{(B.20)}$$

$$N_8 = -16 s_k^\theta s_k^\chi \left\{ (s_k)^2 + \frac{\zeta^2}{4} (2\delta^{\chi\underline{\alpha}} + 1) \{ (\hat{s}_k)_\perp^2 \}^2 \right\} - 8\zeta s_k^\theta (\hat{s}_k)_\perp^2 \left\{ 2 s_k^\chi s_k^{\underline{\alpha}} + \delta^{\chi\underline{\alpha}} \left(1 + \frac{\zeta^2}{8} \{ (\hat{s}_k)_\perp^2 \}^2 \right) \right\}. \quad \text{(B.21)}$$

These numerators simplify further since the denominator includes odd powers of only $k^{\underline{\alpha}}$. The next step of the calculation is shown in eqs. (2.81) - (2.85) in the main part.

B.2.2 Sunset diagram for Boriçi-Creutz fermions

Boriçi-Creutz fermions involve one-loop calculations that are even more cumbersome than those for Karsten-Wilczek fermions. Since every Euclidean component k_μ contributes as an odd power that multiplies ζ in the denominator, simplification of the numerator using symmetry arguments is only possible in terms which are individually even in ζ and loop momenta. However, any odd function of loop momenta in the numerators contributes to the integrals, since it combines to an even power with terms like $\zeta(s_k)$ in the denominator. The integral of eq. (2.89) is split into a Feynman gauge part ($\mathcal{J}_0 = J_3^\chi|_{\xi=1}$) and a gauge fixing part ($\mathcal{J}_1 = (\xi - 1)(\partial J_3^\chi/\partial\xi)$), which is the rest of eq. (2.89). Numerators N_0 of $\mathcal{J}_0$ and N_1 of $\mathcal{J}_1$ are simplified algebraically to

$$N_0 = s_k^\chi \{ 2(\hat{c}_k^\chi)^2 - (\hat{c}_k)^2 \} + \zeta^2 \left\{ \{ 6(\hat{s}_k^\chi)^2 + (\hat{s}_k)^2 \} s_k^\chi - \{ 2(\hat{s}_k^\chi)^2 + \frac{1}{2} (\hat{s}_k)^2 \} (s_k) - (s_k \hat{s}_k \hat{s}_k) \right\}$$
$$+ \zeta \left\{ 2(s_k)^2 + 4(s_k) s_k^\chi - 8(s_k^\chi)^2 + \frac{1}{4} \{ 2(\hat{c}_k^\chi)^2 - (\hat{c}_k)^2 \} \{ 2(\hat{s}_k^\chi)^2 - (\hat{s}_k)^2 \} \right.$$
$$+ \zeta^2 \left(\frac{1}{4} \{ (\hat{s}_k)^2 - 2(\hat{s}_k^\chi)^2 \} (\hat{s}_k)^2 + \frac{1}{2} \{ 2(\hat{s}_k^\chi)^4 - (\hat{s}_k)^4 \} \right) \right\}, \quad \text{(B.22)}$$

$$N_1 = s_k^\chi \left(4(s_k)^2 + \zeta^2 \{ -(\hat{s}_k)^4 + 2((\hat{s}_k)^2)^2 + 2(s_k \hat{s}_k)^2 \} \right)$$
$$+ \zeta^2 \left(\{ (\hat{s}_k^\chi)^2 (\hat{s}_k)^2 + \frac{1}{2} ((\hat{s}_k)^2)^2 \} (s_k) + 2 \{ (\hat{s}_k^\chi)^2 - (\hat{s}_k)^2 \} (s_k \hat{s}_k \hat{s}_k) \right)$$
$$+ \zeta \left(\{ (\hat{s}_k)^2 - 4(\hat{s}_k^\chi)^2 \} (s_k)^2 + 2 \{ 2(s_k \hat{s}_k \hat{s}_k) - (s_k)(\hat{s}_k)^2 \} s_k^\chi + \frac{\zeta^2}{2} \{ (\hat{s}_k^\chi)^2 - \frac{1}{2} (\hat{s}_k)^2 \} (\hat{s}_k)^4 \right). \quad \text{(B.23)}$$

The terms in eqs. (B.22) and (B.23), are either even in ζ and odd in k or odd in ζ and even in k. Since the denominator $D^{BC}(k; \zeta, M, a)$ consists of terms that are either even or odd in both ζ and k, the full integral $J_3^\chi(\zeta, a)$ is necessarily an odd function of ζ, since integrands which are odd in any loop momentum component k_μ vanish upon integration.

Further simplification of N_0 or N_1 due to symmetry arguments yields

$$
\begin{aligned}
N_0 &= s_k^\chi \{2(\hat{c}_k^\chi)^2 - (\hat{c}_k)^2\} + \zeta^2 \{\{6(\hat{s}_k^\chi)^2 + (\hat{s}_k)^2\} s_k^\chi - \{2(\hat{s}_k^\chi)^2 + \tfrac{1}{2}(\hat{s}_k)^2\}(s_k) - (s_k \hat{s}_k \hat{s}_k)\} \\
&\quad + \zeta \Big\{ 2(s_k)^2 - 4(s_k^\chi)^2 + \tfrac{1}{4}\{2(\hat{c}_k^\chi)^2 - (\hat{c}_k)^2\}\{2(\hat{s}_k^\chi)^2 - (\hat{s}_k)^2\} \\
&\quad + \zeta^2 \big(\tfrac{1}{4}\{(\hat{s}_k)^2 - 2(\hat{s}_k^\chi)^2\}(\hat{s}_k)^2 + \tfrac{1}{2}\{2(\hat{s}_k^\chi)^4 - (\hat{s}_k)^4\} \big) \Big\},
\end{aligned}
\tag{B.24}
$$

$$
\begin{aligned}
N_1 &= s_k^\chi \big(4(s_k)^2 + \zeta^2 \{ -(\hat{s}_k)^4 + 2((\hat{s}_k)^2)^2 + 2(s_k \hat{s}_k)^2 \} \big) \\
&\quad + \zeta^2 \big(\{(\hat{s}_k^\chi)^2(\hat{s}_k)^2 + \tfrac{1}{2}((\hat{s}_k)^2)^2\}(s_k) + 2\{(\hat{s}_k^\chi)^2 - (\hat{s}_k)^2\}(s_k \hat{s}_k \hat{s}_k) \big) \\
&\quad + \zeta \big(\{(\hat{s}_k)^2 - 4(\hat{s}_k^\chi)^2\}(s_k)^2 + \{2(s_k^\chi)^2 + \tfrac{\zeta^2}{4}(\hat{s}_k)^4\}\{2(\hat{s}_k^\chi)^2 - (\hat{s}_k)^2\} \big).
\end{aligned}
\tag{B.25}
$$

The integral $J_m(\zeta, M, a)$ of eq. (2.91) contributes to mass renormalisation. It is split into a Feynman gauge part ($\mathcal{J}_2 = J_m|_{\xi=1}$) and a gauge fixing part ($\mathcal{J}_3 = (\xi - 1)(\partial J_m / \partial \xi)$). Numerators N_2 of $\mathcal{J}_2$ and N_3 of $\mathcal{J}_3$ are simplified algebraically to

$$
N_2 = (\hat{c}_k)^2 + \zeta^2 (\hat{s}_k)^2 + 2\zeta(s_k),
\tag{B.26}
$$

$$
N_3 = 4(s_k)^2 + \zeta^2 (\hat{s}_k)^4 + 2\zeta(s_k \hat{s}_k \hat{s}_k).
\tag{B.27}
$$

The presence of an odd term in both ζ and k is a remarkable difference to the case of Karsten-Wilczek fermions, where such terms had explicitly cancelled. Since it vanishes unless it is combined with the odd term in ζ and k of the denominator, the overall integral $J_m(\zeta, M, a)$ is an even function of ζ. The presence of these odd terms considerably increases the numerical effort of the numerical integration for Boriçi-Creutz fermions compared to Karsten-Wilczek fermions.

The most laboriuous part of the self-energy calculation is $J_4(p; \zeta, M, a)$, which contributes to the wavefunction renormalisation and the marginal counterterm. The denominators of the sunset diagram that contribute to wavefunction renormalisation and the marginal counterterm's coefficient for Boriçi-Creutz fermions read

$$
D_4 = D^{BC}(k; \zeta, M, a) D^g(-k; M, a),
\tag{B.28}
$$

$$
D_5 = D^{BC}(k; \zeta, M, a) \left(D^g(-k; M, a) \right)^2,
\tag{B.29}
$$

$$
D_6 = D^{BC}(k; \zeta, M, a) \left(D^g(-k; M, a) \right)^3.
\tag{B.30}
$$

Five numerators N_4 - N_8 contribute to wavefunction renormalisation and to the marginal counterterm's coefficient. The full numerators N_4 and N_5 of the part in Feynman gauge ($J_4^{\chi\theta}|_{\xi=1}$) read

$$
\begin{aligned}
N_4 &= \sum_{\mu,\nu,\lambda} \frac{\delta^{\mu\nu}}{8} \mathrm{tr}\Big\{ \Big(\gamma^\chi \delta^{\mu\theta} \left(-\gamma^\mu \hat{s}_k^\mu - \zeta\gamma^{\mu'} \hat{c}_k^\mu \right) \left(\gamma^\lambda s_k^\lambda - \zeta\gamma^{\lambda'}\{1 - c_k^\lambda\} \right) \left(\gamma^\nu \hat{c}_k^\nu - \zeta\gamma^{\nu'}\hat{s}_k^\nu \right) \Big) \\
&\quad + \Big(\gamma^\chi \delta^{\nu\theta} \left(\gamma^\mu \hat{c}_k^\mu - \zeta\gamma^{\mu'}\hat{s}_k^\mu \right) \left(\gamma^\lambda s_k^\lambda - \zeta\gamma^{\lambda'}\{1 - c_k^\lambda\} \right) \left(-\gamma^\nu \hat{s}_k^\nu - \zeta\gamma^{\nu'}\hat{c}_k^\nu \right) \Big) \Big\},
\end{aligned}
\tag{B.31}
$$

$$
N_5 = \sum_{\mu,\nu,\lambda} \frac{\delta^{\mu\nu}}{4} \mathrm{tr}\Big\{ \gamma^\chi \left(\gamma^\mu \hat{c}_k^\mu - \zeta\gamma^{\mu'}\hat{s}_k^\mu \right) \left(\gamma^\lambda s_k^\lambda - \zeta\gamma^{\lambda'}\{1 - c_k^\lambda\} \right) \left(\gamma^\nu \hat{c}_k^\nu - \zeta\gamma^{\nu'}\hat{s}_k^\nu \right) \Big\} \left(\hat{c}_k^\theta \hat{s}_k^\theta \right),
\tag{B.32}
$$

and the numerators N_6, N_7 and N_8 of the gauge fixing part $\left(-(1-\xi)\left(\partial J_4^{\chi\theta}/\partial\xi\right)\right)$ read

$$N_6 = \sum_{\mu,\nu,\lambda} \frac{1}{8}\mathrm{tr}\Big\{ \Big(\gamma^\chi\delta^{\mu\theta}\left(-\gamma^\mu\hat{s}_k^\mu - \zeta\gamma^{\mu\prime}\hat{c}_k^\mu\right)\left(\gamma^\lambda s_k^\lambda - \zeta\gamma^{\lambda\prime}\{1-c_k^\lambda\}\right)\left(\gamma^\nu\hat{c}_k^\nu - \zeta\gamma^{\nu\prime}\hat{s}_k^\nu\right)\Big)$$
$$+ \Big(\gamma^\chi\delta^{\nu\theta}\left(\gamma^\mu\hat{c}_k^\mu - \zeta\gamma^{\mu\prime}\hat{s}_k^\mu\right)\left(\gamma^\lambda s_k^\lambda - \zeta\gamma^{\lambda\prime}\{1-c_k^\lambda\}\right)\left(-\gamma^\nu\hat{s}_k^\nu - \zeta\gamma^{\nu\prime}\hat{c}_k^\nu\right)\Big)\Big\}\left(\hat{s}_k^\mu\hat{s}_k^\nu\right), \tag{B.33}$$

$$N_7 = \sum_{\mu,\nu,\lambda} -\frac{\delta^{\mu\theta}\hat{c}_k^\mu\hat{s}_k^\nu + \delta^{\nu\theta}\hat{s}_k^\mu\hat{c}_k^\nu}{8}\mathrm{tr}\Big\{\gamma^\chi\left(\gamma^\mu\hat{c}_k^\mu - \zeta\gamma^{\mu\prime}\hat{s}_k^\mu\right)\left(\gamma^\lambda s_k^\lambda - \zeta\gamma^{\lambda\prime}\{1-c_k^\lambda\}\right)\left(\gamma^\nu\hat{c}_k^\nu - \zeta\gamma^{\nu\prime}\hat{s}_k^\nu\right)\Big\}, \tag{B.34}$$

$$N_8 = \sum_{\mu,\nu,\lambda} -\frac{(\hat{c}_k^\theta\hat{s}_k^\theta)(\hat{s}_k^\mu\hat{s}_k^\nu)}{2}\mathrm{tr}\Big\{\gamma^\chi\left(\gamma^\mu\hat{c}_k^\mu - \zeta\gamma^{\mu\prime}\hat{s}_k^\mu\right)\left(\gamma^\lambda s_k^\lambda - \zeta\gamma^{\lambda\prime}\{1-c_k^\lambda\}\right)\left(\gamma^\nu\hat{c}_k^\nu - \zeta\gamma^{\nu\prime}\hat{s}_k^\nu\right)\Big\}. \tag{B.35}$$

Summation of Euclidean indices and evaluation of the trace simplifies numerators to

$$N_4 = s_k^\theta\{1-2\delta^{\theta\chi}\}\Big\{2(1-\zeta^2)s_k^\chi + \zeta^2(s_k)\Big\} + \zeta^2\Big(\{\delta^{\theta\chi} - \frac{1}{4}\}\{4(s_k^\theta)^2 - (\hat{s}_k^\theta)^4\} - c_k^\theta\{(\hat{s}_k^\chi)^2 + \varepsilon^{\theta\chi}(\hat{s}_k)^2\}\Big)$$
$$+ \zeta\Big\{s_k^\theta(1-2\delta^{\theta\chi})\Big(\{1+\zeta^2\}\{(\hat{s}_k^\chi)^2 - \frac{1}{2}(\hat{s}_k)^2\} - \zeta^2(\hat{s}_k^\theta)^2\Big) + 2c_k^\theta\big(s_k^\theta + s_k^\chi + \delta^{\theta\chi}\{(s_k) - 4s_k^\theta\}\big)\Big\}, \tag{B.36}$$

$$N_5 = +2s_k^\theta\Big(s_k^\chi\{2(\hat{c}_k^\chi)^2 - (\hat{c}_k)^2\} + \zeta^2\big\{\{6(\hat{s}_k^\chi)^2 + (\hat{s}_k)^2\}s_k^\chi - \{2(\hat{s}_k^\chi)^2 + \frac{1}{2}(\hat{s}_k)^2\}(s_k) - (s_k\hat{s}_k\hat{s}_k)\big\}$$
$$+ \zeta\Big\{2(s_k)^2 + 4(s_k)s_k^\chi - 8(s_k^\chi)^2 + \frac{1}{4}\{2(\hat{c}_k^\chi)^2 - (\hat{c}_k)^2\}\{2(\hat{s}_k^\chi)^2 - (\hat{s}_k)^2\}$$
$$+ \zeta^2\big(\frac{1}{4}\{(\hat{s}_k)^2 - 2(\hat{s}_k^\chi)^2\}(\hat{s}_k)^2 + \frac{1}{2}\{2(\hat{s}_k^\chi)^4 - (\hat{s}_k)^4\}\big)\Big\}\Big), \tag{B.37}$$

$$N_6 = -2(\hat{s}_k^\theta)^2\delta^{\theta\chi}(s_k)^2 + \zeta^2\Big\{s_k^\theta\big(\{4\delta^{\theta\chi} - 1\}(s_k\hat{s}_k\hat{s}_k) + 2s_k^\theta(\hat{s}_k^\chi)^2 + 2s_k^\chi(\hat{s}_k)^2 + (s_k)\{(\hat{s}_k)^2 - 2(\hat{s}_k^\chi)^2\}\big)$$
$$- (\hat{s}_k^\theta)^2\big(c_k^\theta\{2(\hat{s}_k^\chi)^2 + (\hat{s}_k)^2\} + \frac{1}{4}(\hat{s}_k)^2 + \frac{1}{2}\{\delta^{\theta\chi}(\{(\hat{s}_k)^2\}^2 + (\hat{s}_k)^4) + (\hat{s}_k^\chi)^2(\hat{s}_k^\theta)^2\}\big)\Big\}$$
$$+ \zeta\Big\{s_k^\chi(\hat{s}_k^\theta)^2\{(\hat{s}_k)^2 + (\hat{s}_k^\theta)^2 + c_k^\theta\} + s_k^\theta\big(\{2(s_k)^2 - \frac{\zeta^2}{2}(\hat{s}_k)^4\}\{1-2\delta^{\theta\chi}\} - 4s_k^\chi s_k^\theta - (\hat{s}_k^\theta)^2(\hat{s}_k)^2\big)\Big\}, \tag{B.38}$$

$$N_7 = -\delta^{\theta\chi}(\hat{c}_k^\theta)^2\big(2(s_k)^2 + \frac{\zeta^2}{2}\{((\hat{s}_k)^2)^2 - (\hat{s}_k)^4 + (\hat{s}_k)^2(\hat{s}_k^\chi)^2\}\big)$$
$$+ \zeta^2 s_k^\theta\big(\{3s_k^\theta - 2s_k^\chi - (s_k)\}(\hat{s}_k)^2 + (1 - 4\delta^{\theta\chi})(s_k\hat{s}_k\hat{s}_k)\big)$$
$$+ \zeta\big((\hat{c}_k^\theta)^2\{(\hat{s}_k)^2\{s_k^\chi - s_k^\theta\} + 2s_k^\theta(\hat{s}_k^\chi)^2\} + s_k^\theta\{4s_k^\theta s_k^\chi - \{2(s_k)^2 - \frac{\zeta^2}{2}(\hat{s}_k)^4\}(1-2\delta^{\theta\chi})\}\big), \tag{B.39}$$

$$N_8 = -4s_k^\theta\Big\{s_k^\chi\big(4(s_k)^2 + \zeta^2\{-(\hat{s}_k)^4 + 2((\hat{s}_k)^2)^2 + 2(s_k\hat{s}_k)^2\}\big)$$
$$+ \zeta^2\big(\{(\hat{s}_k^\chi)^2(\hat{s}_k)^2 + \frac{1}{2}((\hat{s}_k)^2)^2\}(s_k) + 2\{(\hat{s}_k^\chi)^2 - (\hat{s}_k)^2\}(s_k\hat{s}_k\hat{s}_k)\big)$$
$$+ \zeta\big(\{(\hat{s}_k)^2 - 4(\hat{s}_k^\chi)^2\}(s_k)^2 + 2\{2(s_k\hat{s}_k\hat{s}_k) - (s_k)(\hat{s}_k)^2\}s_k^\chi + \frac{\zeta^2}{2}\{(\hat{s}_k^\chi)^2 - \frac{1}{2}(\hat{s}_k)^2\}(\hat{s}_k)^4\big)\Big\}. \tag{B.40}$$

It is observed that each numerator consists of terms which are either even or odd in both ζ and k. Since these odd powers of k vanish unless combined with the denominator's term that is odd in ζ and k, both contributions to Σ_1 and d_{1L} are necessarily even functions of ζ. Further simplification is achieved by noting that odd powers of loop momentum components k_μ in terms of the numerators which are even in powers k (with

151

arbitrary Euclidean indices) are integrated to zero.

$$
\begin{aligned}
N_4 = & -(s_k^\theta)^2\{2\delta^{\theta\chi} - \zeta^2\} + \zeta^2\Big(\{\delta^{\theta\chi} - \tfrac{1}{4}\}\{4(\hat{s}_k^\theta)^2 - (\hat{s}_k^\theta)^4\} - c_k^\theta\{(\hat{s}_k^\chi)^2 + \varepsilon^{\theta\chi}(\hat{s}_k)^2\}\Big) \\
& + \zeta\{s_k^\theta(1 - 2\delta^{\theta\chi})(\{1 + \zeta^2\}\{(\hat{s}_k^\chi)^2 - \tfrac{1}{2}(\hat{s}_k)^2\} - \zeta^2(\hat{s}_k^\theta)^2) + 2c_k^\theta(s_k^\theta + s_k^\chi + \delta^{\theta\chi}\{(s_k) - 4s_k^\theta\})\},
\end{aligned}
$$
(B.41)

$$
\begin{aligned}
N_5 = & -2s_k^\theta\Big(s_k^\theta\big(\delta^{\theta\chi}\{(\hat{c}_k)^2 - 2(\hat{c}_k^\theta)^2\} - \zeta^2\{(2\delta^{\theta\chi} - 1)\{2(\hat{s}_k^\chi)^2 + (\hat{s}_k^\theta)^2 + \tfrac{1}{2}(\hat{s}_k)^2\}\}\big) \\
& - \zeta\Big\{2(s_k)^2 + 4(s_k)s_k^\chi - 8(s_k^\chi)^2 + \tfrac{1}{4}\{2(\hat{c}_k^\chi)^2 - (\hat{c}_k)^2\}\{2(\hat{s}_k^\chi)^2 - (\hat{s}_k)^2\} \\
& + \zeta^2\big(\tfrac{1}{4}\{(\hat{s}_k)^2 - 2(\hat{s}_k^\chi)^2\}(\hat{s}_k)^2 + \tfrac{1}{2}\{2(\hat{s}_k^\chi)^4 - (\hat{s}_k)^4\}\big)\Big\}\Big),
\end{aligned}
$$
(B.42)

$$
\begin{aligned}
N_6 = & -2(\hat{s}_k^\theta)^2\delta^{\theta\chi}(s_k)^2 + \zeta^2\Big\{(s_k^\theta)^2\big(2\delta^{\theta\chi}\{2(\hat{s}_k^\theta)^2 + (\hat{s}_k)^2\} + (\hat{s}_k)^2 - (\hat{s}_k^\theta)^2\big) \\
& - (\hat{s}_k^\theta)^2\big(c_k^\theta\{2(\hat{s}_k^\chi)^2 + (\hat{s}_k)^2\} + \tfrac{1}{4}(\hat{s}_k)^2 + \tfrac{1}{2}\{\delta^{\theta\chi}(\{(\hat{s}_k)^2\}^2 + (\hat{s}_k)^4) + (\hat{s}_k^\chi)^2(\hat{s}_k^\theta)^2\}\big)\Big\} \\
& + \zeta\Big\{s_k^\chi(\hat{s}_k^\theta)^2\{(\hat{s}_k)^2 + (\hat{s}_k^\theta)^2 + c_k^\theta\} + s_k^\theta\big(\{2(s_k)^2 - \tfrac{\zeta^2}{2}(\hat{s}_k)^4\}\{1 - 2\delta^{\theta\chi}\} - 4s_k^\chi s_k^\theta - (\hat{s}_k^\theta)^2(\hat{s}_k)^2\big)\Big\},
\end{aligned}
$$
(B.43)

$$
\begin{aligned}
N_7 = & -\delta^{\theta\chi}(\hat{c}_k^\theta)^2\big(2(s_k)^2 + \tfrac{\zeta^2}{2}\{((\hat{s}_k)^2)^2 - (\hat{s}_k)^4 + (\hat{s}_k)^2(\hat{s}_k^\chi)^2\}\big) + \zeta^2(s_k^\theta)^2\big(2\varepsilon^{\theta\chi}(\hat{s}_k)^2 + (1 - 4\delta^{\theta\chi})(\hat{s}_k^\theta)^2\big) \\
& + \zeta\big((\hat{c}_k^\theta)^2\{(\hat{s}_k)^2\{s_k^\chi - s_k^\theta\} + 2s_k^\theta(\hat{s}_k^\chi)^2\} + s_k^\theta\{4s_k^\theta s_k^\chi - \{2(s_k)^2 - \tfrac{\zeta^2}{2}(\hat{s}_k)^4\}(1 - 2\delta^{\theta\chi})\}\big),
\end{aligned}
$$
(B.44)

$$
\begin{aligned}
N_8 = & -4s_k^\theta\Big\{s_k^\theta\{\delta^{\theta\chi}\big(4(s_k)^2 + \zeta^2\{-(\hat{s}_k)^4 + 2((\hat{s}_k)^2)^2 + 2(s_k\hat{s}_k)^2\}\big) \\
& + \zeta^2\big(\{(\hat{s}_k^\chi)^2(\hat{s}_k)^2 + \tfrac{1}{2}((\hat{s}_k)^2)^2\} + 2\{(\hat{s}_k^\chi)^2 - (\hat{s}_k)^2\}(\hat{s}_k^\theta)^2\big)\} \\
& + \zeta\big(\{(\hat{s}_k)^2 - 4(\hat{s}_k^\chi)^2\}(s_k)^2 + 2\{2(s_k\hat{s}_k\hat{s}_k) - (s_k)(\hat{s}_k)^2\}s_k^\chi + \tfrac{\zeta^2}{2}\{(\hat{s}_k^\chi)^2 - \tfrac{1}{2}(\hat{s}_k)^2\}(\hat{s}_k)^4\big)\Big\}.
\end{aligned}
$$
(B.45)

In particular, odd powers in ζ in the numerators multiply various different combinations of odd powers of loop momentum components, which cannot be reduced because the denominator includes a sum of all loop momentum components in its odd term. This is the main reason why numerical integration is considerably more expensive for Boriçi-Creutz fermions than for Karsten-Wilczek fermions.

Statistical analysis

In the following, a brief overview of the statistical analysis within this thesis is given. This overview closely follows [65]. The terminology of primary and secondary observables as well as correlated and uncorrelated fits are clarified. The subject of autocorrelations is touched and methods for estimating whether observables are sufficiently uncorrelated or not are discussed. Finally, the Jackknife method which is used in the statistical analysis of this thesis is discussed.

A primary observable X is calculated on N different configurations, where X_i denotes the value of X on the ith sample. The expectation value of $\langle X \rangle$ and the variance σ_X^2 are defined as

$$\langle X \rangle = \langle X_i \rangle, \tag{C.1}$$

$$\sigma_X^2 = \langle (X_i - \langle X_i \rangle)^2 \rangle. \tag{C.2}$$

Stochastic estimators $\langle \widehat{X} \rangle$ and $\widehat{\sigma}_X^2$ are defined accordingly for $\langle X \rangle$ and σ_X^2,

$$\widehat{X} = \frac{1}{N} \sum_{i=1}^{N} X_i, \tag{C.3}$$

$$\widehat{\sigma}_X^2 = \frac{1}{N-1} \sum_{i=1}^{N} (X_i - X)^2. \tag{C.4}$$

The expectation value of the estimator $\langle \widehat{X} \rangle$ agrees with the mean as $\langle \widehat{X} \rangle = \langle X \rangle$. If the X_i are uncorrelated, their expectation values factorise for $i \neq j$ as

$$\langle X_i X_j \rangle = \langle X_i \rangle \langle X_j \rangle = \langle X \rangle^2 \tag{C.5}$$

153

and the variance $\sigma_{\widehat{X}}^2$ of the estimator is given by

$$
\sigma_{\widehat{X}}^2 = \langle \left(\langle \widehat{X} \rangle - \langle X \rangle \right)^2 \rangle = \langle \left(\frac{1}{N} \sum_{i=1}^{N} (X_i - \langle X \rangle) \right)^2 \rangle
$$

$$
= \frac{1}{N} \langle X^2 \rangle - \langle X \rangle^2 + \frac{1}{N^2} \sum_{i \neq j=1}^{N} \langle X_i X_j \rangle. \tag{C.6}
$$

The last term yields $\sum_{i \neq j=1}^{N} \langle X_i X_j \rangle = N(N-1) \langle X \rangle^2$ for uncorrelated observables due to eq. (C.5) and the variance of the estimator is related to the variance of the observable by $\sigma_{\widehat{X}}^2 = \sigma_X^2 / N$. Using the estimator of the variance $\widehat{\sigma}_X^2$ instead of σ_X^2, the statistical error of the estimator $\widehat{X}$ is given by

$$
\sigma = \frac{\widehat{\sigma}_X}{\sqrt{N}}. \tag{C.7}
$$

Since observables, which are computed from the same Markov chain are necessarily correlated to some extent, these correlations have to be accounted for. In principle, it would be necessary to calculate the autocorrelation function,

$$
C_X(t) \equiv C_X(X_i, X_{i+t}) = (X_i - \langle X_i \rangle)(X_{i+t} - \langle X_{i+t} \rangle), \tag{C.8}
$$

and the integrated autocorrelation time,

$$
\tau_{X,\text{int}} = \frac{1}{2} + \sum_{t=1}^{N} \Gamma_X(t), \quad \Gamma_X(t) = \frac{C_X(t)}{C_X(0)}, \tag{C.9}
$$

where t is the computer time of the Markov chain update algorithm. The variance of the estimator which would yield the statistical error including autocorrelations reads

$$
\sigma_{\widehat{X}}^2 = \frac{1}{N^2} \sum_{i,j} C_X(|i-j|) = \frac{C_X(0)}{N} \sum_{t=-N}^{N} \Gamma_X(|t|) \left(1 - \frac{|t|}{N} \right) \approx \frac{\sigma_X^2}{N} 2\tau_{X,\text{int}}, \tag{C.10}
$$

where $C_X(0) = \sigma_X^2$ is used. However, calculation of the integrated autocorrelation time requires a cutoff of the summation for values of t where $\Gamma_X(t)$ becomes unreliable. Since usually extremely large ensembles with at least $1000\,\tau_{X,\text{int}}$ samples are required for a reliable estimate of $\tau_{X,\text{int}}$, this method is impractical for the small statistical ensembles of the numerical studies of chapter 4.

A typical representative of a secondary observable Y is a parameter obtained from a fit to a correlation function. The statistical error of Y is obtained as the square root of the diagonal elements of the covariance matrix

$$
COV(Y, Z) = \lim_{N \to \infty} \frac{1}{N} \sum_{i,j=1}^{N} \frac{\partial Y}{\partial X_i} \frac{\partial Z}{\partial X_j} \langle X_i X_j \rangle_N \tag{C.11}
$$

Since the secondary observables Y are usually non-linear functions of the primary observables X, the covariance matrix is not exactly known. The fit is performed as a minimisation of χ^2 that is defined as

$$\chi^2 = \sum_{s,s'=n_{\min}}^{n_{\max}} \left(X(s) - f(Y,s)\right) w(s,s') \left(X(s') - f(Y,s')\right) \tag{C.12}$$

by varying the set of fit parameters Y. The indices s, s' denote the sampling range of the minimisation and typically represent indices of time slices. Ideally the inverse of the exact covariance matrix would be used as statistical weights $w(s,s') = COV(s,s')$. However, since only a stochastic estimator $COV_N(s,s')$ of the covariance matrix on N samples is known,

$$COV_N(s,s') = \frac{1}{N-1} \langle \left(X(s) - \langle X(s) \rangle_N \right) \left(X(s') - \langle X(s') \rangle_N \right) \rangle_N \tag{C.13}$$

is inverted numerically and used as a weight $w(s,s')) = COV_N(s,s')^{-1}$ in the definition of χ^2. In the case of truly uncorrelated data, the covariance matrix is diagonal and the weights take the form $w(s,s') = \delta_{s,s'}/\sigma_X^2(s)$. If the estimator of the covariance is badly determined due to statistical fluctuations, it may acquire accidental small eigenvalues that are detrimental to the stability of the fit. As a result, despite reasonably small values of χ^2, the fit fails to agree with the primary observables. In such a case, the covariance matrix must either be smoothly approximated or the off-diagonal elements of the covariance matrix must be neglected. The latter case is the familiar form of an uncorrelated fit.

The numerical correlation of data is estimated in the statistical analysis with three different approaches. The first approach is data blocking. The ensemble is divided in N/K subsets, which are indicated by $k \in [1, \ldots, N/K]$. The mean value $\langle \widehat{X}_k \rangle$ and variance $\sigma_{\widehat{X}_k}^2$ are calulated on each subset k with K samples each. If the variance scales like $1/K$ upon variation of K, the original observables can be considered sufficiently uncorrelated. The second approach omits samples of the total ensemble in a simplified version of the statistical bootstrap. This is done by either using only a subset of K samples which would be counted as the kth subset in the data blocking approach or by using only every kth sample and varying the offset i of the first sample within $i \in [0, K-1]$. If the mean $\langle X_k \rangle$ fluctuates between the subsets only within the statistical errors of any of the subsets, data can be considered sufficiently uncorrelated.

The third approach uses the Jackknife method. The Jackknife method computes sample averages of the original data, where the ith sample is removed. Hence, the Jackknife bins read

$$X_i^J = \frac{1}{N-1} \left(N\widehat{X} - X_i\right) \tag{C.14}$$

and the variance is given by

$$\sigma_{\widehat{X}}^2 = \frac{N-1}{N} \sum_{i=1}^{N} \left(X_i^J - \langle \widehat{X} \rangle\right)^2 \tag{C.15}$$

155

The Jackknife method can be freely combined with the aforementioned blocking procedures. Its advantage is that secondary observables Y^J that are computed from primary observables X^J that have been processed with the Jackknife procedure are automatically stochastic estimators for $\langle Y \rangle$. Their covariance matrix reads

$$COV(Y, Z) = \lim_{N \to \infty} \frac{N-1}{N} \sum_{i=1}^{N} \left(Y_i^J - \langle Y \rangle \right) \left(Z_i^J - \langle Z \rangle \right). \qquad \text{(C.16)}$$

Once the secondary observables Y^J are obtained with the Jackknife method, they can be used instead of primary observables in eq. (C.12), any secondary observables Y can be used to define a sampling range and the covariance matrix of the primary observables can be replaced by eq. (C.16).

Fits to secondary observables are performed for all extrapolations of fit parameters. The sampling range is defined in terms of simulation parameters of the primary simulations. The covariance matrix of fit parameters appears unstable using correlated fits for extrapolations due to having only small data sets. Thus, secondary observables from correlated fits are fitted with uncorrelated fits within this thesis.

Lastly, some values of the simulation parameter c in the analysis of power spectral densities in section 4.3.3 yield frequencies $\omega_c \le \omega_B/2$, which are too close to zero for obtaining any statistical variation. In these cases, the analysis which determines the statistical error from Jackknife bins of secondary observables fails and yields zero as the statistical error. Thus, the statistical error is combined quadratically with an estimate of the systematical error and an uncorrelated fit using routines from the GSL library is conducted on any sample Y^J. The combined statistical and systematical errors are used in the definition of the weights of the secondary observables. The statistical error is then calculated from the variance of ternary observabless and the systematical error is estimated from the variance-covariance matrix of ternary observables.

Oscillating lattice toy models

Application of the decomposition of spinor fields in section 3.1.4 indicates that mesonic correlation functions receive oscillating contributions with a frequency that is a continuous function of the counterterms' coefficients. Thus, this frequency is not necessarily an eigenfrequency of a periodic lattice for arbitrary choices of the parameters. This appendix contains two toy models that show how oscillations with arbitrary frequencies are realised on a lattice with periodic boundary conditions.

D.1   Harmonic oscillator as a toy model

The first toy model is a simple harmonic oscillator. Its equation of motion reads

$$\left(\frac{d^2}{dt^2} + \omega_0^2\right) q(t) = 0 \tag{D.1}$$

and its solutions are

$$q(t) = A\cos(\omega_0 t) + B\sin(\omega_0 t). \tag{D.2}$$

For a periodic system with $q(t + T) = q(t)$, it is obvious that the only permissible homogenous solutions are those with $\omega_0 \overset{!}{=} \frac{2\pi n}{T}$. However, the situation is different for inhomogenous solutions. The Green's function of the harmonic oscillator is defined by

$$\left(\frac{d^2}{dt^2} + \omega_0^2\right) G(t, t_0) = \delta(t - t_0), \tag{D.3}$$

and reads

$$G(t, t_0) = \frac{1}{2\pi} \int_{-\infty}^{+\infty} dk \frac{e^{ik(t-t_0)}}{\omega_0^2 - k^2 + i\epsilon}. \tag{D.4}$$

If the harmonic oscillator is set up with periodic boundary conditions $q(t + T) = q(t)$, the Green's function becomes (T is the physical length of the periodic direction)

$$G(t, t_0) = \frac{1}{T} \sum_{n_k=0}^{\infty} \frac{e^{i \frac{2\pi n_k}{T}(t-t_0)}}{\omega_0^2 - \left(\frac{2\pi n_k}{T}\right)^2} \tag{D.5}$$

due to its restricted frequency range ($k = \frac{2\pi n_k}{T}$). The real part of the Green's function of eq. (D.5)– which is the same as the sum of Green's function and reflected Green's function – is plotted as the points in figure D.5) for $T = 64$ for three oscillator frequencies $\frac{T\omega_0}{128\pi} = \left\{\frac{1}{11}, \frac{2}{11}, \frac{3}{11}\right\}$. The continuous curves are obtained by truncating the sum in eq. (D.5) at $n_k = T - 1$. Effects of the truncation are visible near the inhomogenity. It is clearly visible that the Green's function oscillates with oscillator frequency ω_0 even though it is not a permissible frequency k for homogenous solutions.
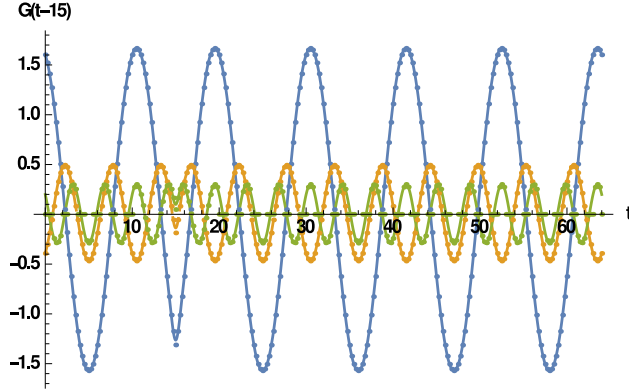
Figure D.1: Green's functions for harmonic oscillators of frequencies $\frac{T\omega_0}{128\pi} = \left\{\frac{1}{11}, \frac{2}{11}, \frac{3}{11}\right\}$ (blue, yellow, green) oscillate with ω_0.

The power spectral density, which is defined in eq. (4.38), is computed from a discrete Fourier transform of the Green's function and plotted in figure D.2. The curves are given by $1/[N^3(\omega_0^2 - k^2)^2]$ and diverge at the peaks of the power spectral densities. The peak positions are not at frequencies k that are permissible in terms of the periodic boundary conditions, but at the eigenfrequencies ω_0 of the harmonic oscillators.

Next, the harmonic oscillator is formulated on a lattice. This introduces an upper bound for the frequencies. One example of a discretised action for a harmonic oscillator on a lattice is given by

$$S[q] = \frac{m}{2a} \sum_{n=0}^{N-1} q_n \left(((a\omega)^2 - 2)q_n + q_{n-1} + q_{n+1} \right). \tag{D.6}$$
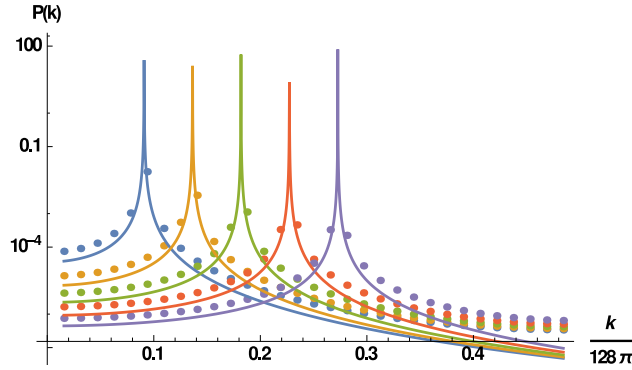
Figure D.2: The peaks of the power spectral densities mark the oscillators' frequencies $\frac{T\omega_0}{64} = \frac{2\pi}{22} \times \{2, 3, 4, 5, 6\}$, which lie in between the lattice frequencies k.

With a Fourier transform of the variable q_n, the action is expressed in frequency space,

$$
\begin{aligned}
S[q] &= \frac{m}{2aN} \frac{1}{\sqrt{N}^2} \sum_{n_k, n_\ell = 0}^{N-1} q(2\pi \frac{n_k}{aN}) q(2\pi \frac{n_\ell}{aN}) \sum_{n=0}^{N-1} e^{i(n_k+n_\ell)n \frac{2\pi}{N}} \left((a\omega_0)^2 - 2 + e^{+ia\ell} + e^{-ia\ell} \right) \\
&= \frac{m}{aN} \sum_{n_k=0}^{N-1} q\left(2\pi \frac{n_k}{aN}\right) q\left(2\pi \frac{N - n_k}{aN}\right) \left(\cos\left(2\pi \frac{n_k}{N}\right) - 1 + \frac{(a\omega)^2}{2} \right),
\end{aligned}
\tag{D.7}
$$

where the different modes decouple. Hence, the equation of motion is

$$
\left(\cos\left(2\pi \frac{n_k}{N}\right) - 1 + \frac{(a\omega_0)^2}{2} \right) q\left(\frac{2\pi n_k}{aN}\right) = 0
\tag{D.8}
$$

and turns into a standard harmonic oscillator $(-k^2 + \omega_0^2)q(k) = 0$ in its continuum limit $(a \to 0$ and $k = \frac{2\pi}{a} \frac{n_k}{N})$. The homogenous solution of the lattice equation requires

$$
\frac{2\pi}{a} \frac{n_k}{N} = \omega_0^{\text{lat}} \equiv \frac{1}{a} \arccos\left(1 - \frac{(a\omega_0)^2}{2} \right),
\tag{D.9}
$$

where n_k is an integer that labels one of the lattice eigenfrequencies. Due to the discretised second derivative, the lattice Green's function reads

$$
G(n, n_0) = \frac{a}{N} \sum_{n_k=0}^{N-1} \frac{e^{i2\pi \frac{n_k}{N}(n-n_0)}}{1 - \frac{(a\omega_0)^2}{2} - \cos\left(2\pi \frac{n_k}{N}\right)}.
\tag{D.10}
$$

The power spectral density is computed from a discrete Fourier transform of the lattice Green's function and plotted in figure D.3 together with curves that are given by

$$
C(n_k, \omega_0) = \frac{1}{N^3} \frac{1}{1 - \frac{(a\omega_0)^2}{2} - \cos\left(2\pi \frac{n_k}{N}\right)}.
\tag{D.11}
$$

The curves $C(n_k, \omega_0)$ diverge at the peaks of the power spectral densities, which match the discretised oscillator's frequencies ω_0^{lat} instead of the lattice eigenfrequencies $\frac{2\pi}{a} \frac{n_k}{N}$.

159
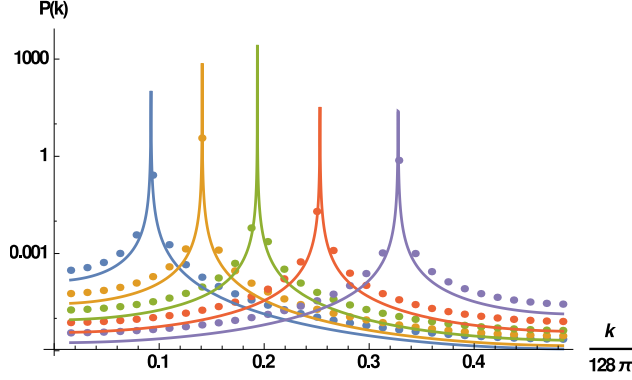
Figure D.3: The peaks of the power spectral densities mark the discretised oscillators' frequencies $\omega_0^{\text{lat}}(\omega_0)$, $a\omega_0 = \frac{2\pi}{22} \times \{2, 3, 4, 5, 6\}$.

D.2 One-dimensional, spinless lattice fermion

The second toy model, a one-dimensional colourless and spinless fermion field with imaginary mass $i\omega_0$ is closer to the thesis' main topic. The field's action is given by

$$S[\psi, \psi^\dagger] = \sum_{n=0}^{N-1} \psi_n^\dagger \{\frac{\psi_{n+1} - \psi_{n-1}}{2a} + i\omega_0\psi_n\}. \tag{D.12}$$

The equation of motion reads

$$\frac{\psi_{n+1} - \psi_{n-1}}{2a} + i\omega_0\psi_n = 0 \tag{D.13}$$

and decouples in frequency space as

$$\frac{i}{a}\left\{\sin\left(2\pi\frac{n_k}{N}\right) + a\omega_0\right\}\psi\left(2\pi\frac{n_k}{N}\right) = 0. \tag{D.14}$$

Similar to the discretised harmonic oscillator, homogenous solutions require

$$\frac{2\pi}{a}\frac{n_k}{N} = \left\{\begin{array}{c} \Omega_1 \\ \Omega_2 \end{array}\right. \equiv \left\{\begin{array}{c} -\omega_0^{\text{lat}} \\ \frac{\pi}{a} + \omega_0^{\text{lat}} \end{array}\right., \quad \omega_0^{\text{lat}} \equiv \frac{1}{a}\arcsin\left(a\omega_0\right), \tag{D.15}$$

where n_k is an integer that labels one of the lattice eigenfrequencies. Due to the discretised derivative, the lattice Green's function – the one-dimensional fermion propagator – reads

$$G(n, n_0) = \frac{-i}{N}\sum_{n_k=0}^{N-1} \frac{e^{i2\pi\frac{n_k}{N}(n-n_0)}}{(a\omega_0) + \sin\left(2\pi\frac{n_k}{N}\right)}. \tag{D.16}$$

The Green's function for $N = 128$ is plotted in figure D.4 and exhibits interference patterns that are analysed in terms of its power spectral density, which is plotted in figure D.5. The continuous curves in the plot of the power spectral density are given by

$$C(k, \omega_0) = \frac{1}{N^4}\frac{1}{(a\omega_0) + \sin\left(2\pi\frac{n_k}{N}\right)}. \tag{D.17}$$
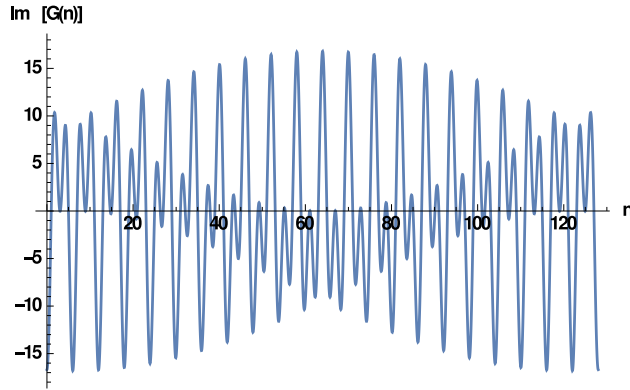
160

Figure D.4: The Green's function $G(n, 0)$ for $\frac{a\omega_0}{2\pi} = -\frac{3}{22}$ exhibits interference patterns.

The power spectral density is peaked at the frequencies Ω_1 and Ω_2 that are defined in eq. (D.15). Each lattice frequency $\frac{2\pi}{a}\frac{n_k}{N}$ contributes with different weigths to each of the peaks for Ω_1 and Ω_2, whose interference pattern is visible in the Green's function.
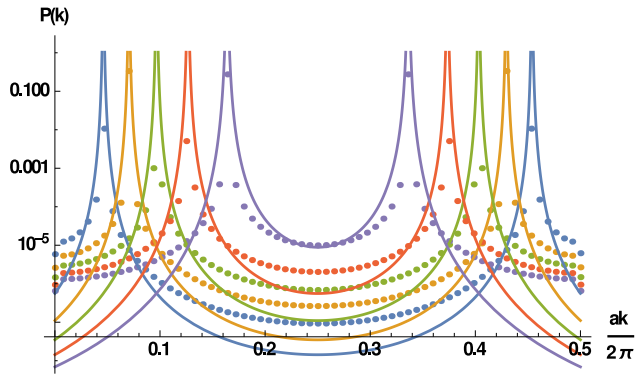

Figure D.5: The peaks of the power spectral densities mark both frequencies Ω_1 and Ω_2, which are defined as functions of ω_0^{lat}, where $a\omega_0 = -\frac{2\pi}{22} \times \{2, 3, 4, 5, 6\}$.

In the next step of the toy model, a mesonic correlation function is created from the contraction of two Green's functions as in eqs. (3.48) or (4.17),

$$G_M(n, n_0) = |G(n, n_0)|^2. \tag{D.18}$$

This correlation function is manifestly positive and contains a constant and an oscillating term with equal weights as is depicted in figure D.6. Hence, the correlation function can be written in terms of the oscillation frequency Ω as

$$G_M(n) \propto 1 + \frac{\cos\left(a\Omega\frac{N}{2}\right)}{1 + \cos\left(a\Omega N\right)} \cos\left(a\Omega(n - \frac{N}{2})\right). \tag{D.19}$$

Thus, the toy model's correlation function formally resembles the decomposed correlation function in eqs. (3.59)-(3.61) that is derived from a spinor decomposition in section 3.1.
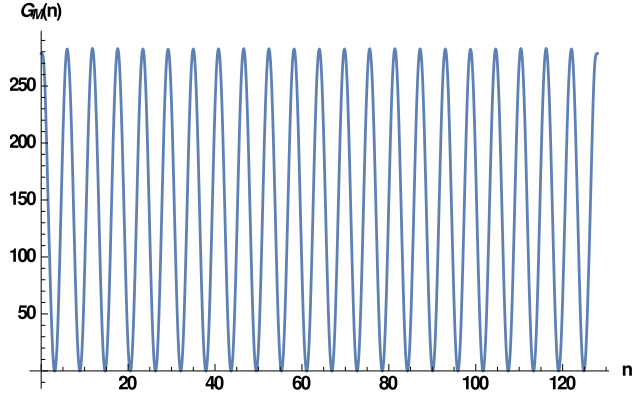
161

Figure D.6: The mesonic correlation function for $\frac{a\omega_0}{2\pi} = -\frac{3}{22}$ has oscillating and non-oscillating contributions.

Its frequency Ω is analysed in terms of the mesonic correlation function's power spectral density, which is plotted in figure D.7. The first peak is exactly at the lattice's eigenfrequency $\frac{2\pi}{a}\frac{n_k}{N} = 0$. The second peak has its maximum at

$$\Omega \equiv \Omega_2 - \Omega_1 = \frac{\pi}{a} + 2\omega_0^{\text{lat}}, \tag{D.20}$$

which implies that the oscillation is due to the product of different fermionic modes (counted as Ω_1 and Ω_2) in both Green's functions. Frequencies other than the lattices's eigenfrequencies can be realised in terms of the peak position of the spectral distribution of the lattice's eigenfrequencies. Since this toy model is essentially a one-dimensional, non-interacting Karsten-Wilczek fermion, it is not suprising that similar features are reproduced in the numerical results of section 4.3.
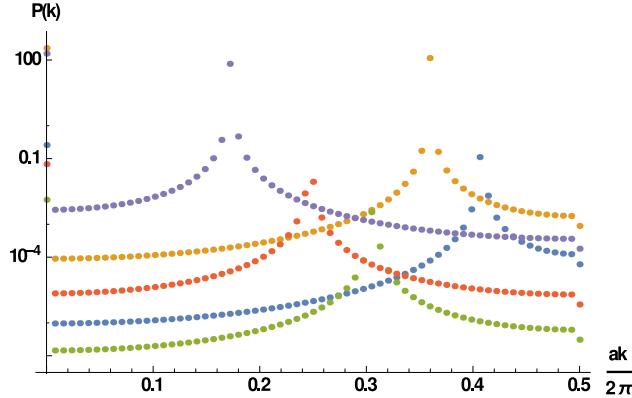

Figure D.7: The peak of the mesonic correlation function's power spectral densities marks the frequency difference $\Omega = \Omega_2 - \Omega_1$. Both Ω_1 and Ω_2 are defined as functions of ω_0^{lat}, where $a\omega_0 = -\frac{2\pi}{22} \times \{2, 3, 4, 5, 6\}$.

Simulation parameters and data sets

E.1 Summary of data sets

This appendix summarises all parameters sets of simulations for this thesis in tabular form. Karsten-Wilczek fermions are always simulated with $\zeta = +1$.

β	T	n_{cfg}	c	d	am_0
5.8	32	100	$0.0, -0.3, -0.4, -0.45, -0.5, -0.55, -0.65$	$0, 0.02$	$0.02, 0.04, 0.05$
6.0	32	100	$-0.2, -0.3, -0.38, -0.42, -0.45, -0.5, -0.55, -0.65$	$-0.02, -0.01, 0$	$0.01, 0.02, 0.03, 0.04, 0.05$
6.0	32	100	$-0.3, -0.38, -0.42, -0.45, -0.5, -0.55$	$-0.08, -0.06, -0.04, +0.01, +0.02$	$0.02, 0.03, 0.04, 0.05$
6.0	32	100	$+0.3, +0.2, +0.1, 0.0, -0.1, -0.15, -0.2, -0.25, -0.3, -0.32, -0.35, -0.37, -0.38, -0.40, -0.42, -0.43, -0.44, -0.4445, -0.45, -0.47, -0.48, -0.5, -0.52, -0.55, -0.6, -0.65, -0.7, -0.8, -0.9, -1.0, -1.1, -1.2$	0	$0.02, 0.03, 0.04, 0.05$
6.0	48	40	$0.0, -0.2, -0.3, -0.4, -0.45, -0.55, -0.65$	0	0.02
6.2	32	100	$-0.2, -0.3, -0.38, -0.42, -0.45, -0.55, -0.65$	0	0.01
6.2	32	100	$-0.2, -0.3, -0.38, -0.42, -0.45, -0.55, -0.65$	$-0.08, -0.04, +0.02$	$0.02, 0.03, 0.04, 0.05$
6.2	32	100	$-0.15, -0.2, -0.25, -0.27, -0.3, -0.32, -0.33, -0.35, -0.37, -0.38, -0.42, -0.43, -0.45, -0.47, -0.50, -0.55, -0.6, -0.65$	0	$0.02, 0.03, 0.04, 0.05$
6.2	48	40	$0.0, -0.2, -0.3, -0.4, -0.45, -0.55, -0.65$	0	0.02

Table E.1: The anisotropy study covers a wide range of parameter values. Parallel and perpendicular source-smeared correlators are available in γ^5, $\mathbf{1}$ and all γ^μ channels.

163

β	n_{cfg}	c		d	am_0	$r_0 m_0$
5.8	10	$-0.4, -0.45, -0.48, -0.5, -0.53, -0.55, -0.6$		-0.002	0.01464	0.054
6.0	10	$-0.35, -0.40, -0.42, -0.45, -0.47, -0.50, -0.55$		-0.001	0.01	0.054
6.2	10	$-0.3, -0.35, -0.38, -0.40, -0.42, -0.45, -0.50$		-0.001	0.0073	0.054

Table E.2: All datasets of the frequency study use the same bare mass ($r_0 m_0$) in physical units. Mesonic correlators are source smeared and available in all $\mathcal{M}, \mathcal{N}$ channels.

Action	β	n_{cfg}	c	d	m_{cr}	m_0	$(r_0 M_{55})$ [MeV]
Karsten-Wilczek, $\parallel$	6.0	20	-0.45	-0.001	n.a	0.02	642(4)
Karsten-Wilczek, $\perp$	6.0	20	-0.45	-0.001	n.a	0.02	642(4)
Naïve	6.0	20	n.a.	n.a	n.a	0.02	728(2)
Wilson	6.0	20	n.a.	n.a	-0.808	-0.788	545(4)

Table E.3: Different values of $r_0 M_{55}$ for equal bare masses m_0 (or $m_0 - m_{cr}$ for Wilson fermions) are due to use of different fermion actions.

β	L	n_{cfg}	c	d	am_0	$(r_0 m_0)$	$(r_0 M_{55})$	M_{55} [MeV]	$\mathcal{B}_{55}$
5.8	24	200	-0.51	-0.002	0.02928	0.107	1.655(2)	653(1)	25.5(1)
5.8	24	200	-0.51	-0.002	0.02000	0.073	1.379(1)	544(1)	25.9(1)
5.8	24	200	-0.51	-0.002	0.01464	0.054	1.188(1)	469(1)	26.3(1)
5.8	24	200	-0.51	-0.002	0.01000	0.037	0.990(1)	391(1)	26.7(1)
5.8	24	200	-0.51	-0.002	0.07320	0.027	0.852(1)	336(1)	27.0(1)
5.8	24	200	-0.51	-0.002	0.05340	0.020	0.731(1)	288(1)	27.3(1)
6.0	24	200	-0.45	-0.001	0.02000	0.107	1.598(3)	631(1)	23.8(1)
6.0	24	200	-0.45	-0.001	0.01371	0.074	1.333(3)	526(1)	24.2(1)
6.0	24	200	-0.45	-0.001	0.01000	0.054	1.149(3)	453(1)	24.6(1)
6.0	24	200	-0.45	-0.001	0.06850	0.037	0.964(4)	380(1)	25.3(2)
6.0	24	200	-0.45	-0.001	0.00500	0.027	0.833(4)	329(2)	25.9(3)
6.0	24	200	-0.45	-0.001	0.03650	0.020	0.719(4)	284(2)	26.4(3)
6.2	32	100	-0.40	-0.001	0.01460	0.107	1.575(5)	621(2)	23.1(2)
6.2	32	100	-0.40	-0.001	0.01000	0.074	1.312(6)	518(2)	23.4(2)
6.2	32	100	-0.40	-0.001	0.07300	0.054	1.131(6)	446(2)	23.8(3)
6.2	32	100	-0.40	-0.001	0.00500	0.037	0.947(7)	374(3)	24.4(3)
6.2	32	100	-0.40	-0.001	0.03650	0.027	0.819(7)	323(3)	25.0(4)
6.2	32	100	-0.40	-0.001	0.02660	0.020	0.709(8)	280(3)	25.7(6)
6.2	32	100	-0.40	-0.001	0.01940	0.014	0.615(8)	243(3)	26.5(7)

Table E.4: Chiral behaviour is studied on lattices with $T = 48$. Different $r_0 M_{55}$ for equal $r_0 m_0$ at different β indicates lack of mass renormalisation.

E.2 Addendum to tuning with the frequency spectrum

Ratios $R_{05}(n_0)$ of correlation functions for the coarser lattices ($\beta = 6.0$, $\beta = 5.8$) are displayed in the following. Since the ratio at the source $R_{05}(0)$ varies only within one or two standard errors over the range of c for all lattices, the ratio of renormalisation factors of the γ^5 and γ^0 bilinears seems to have only a weak dependence on c.
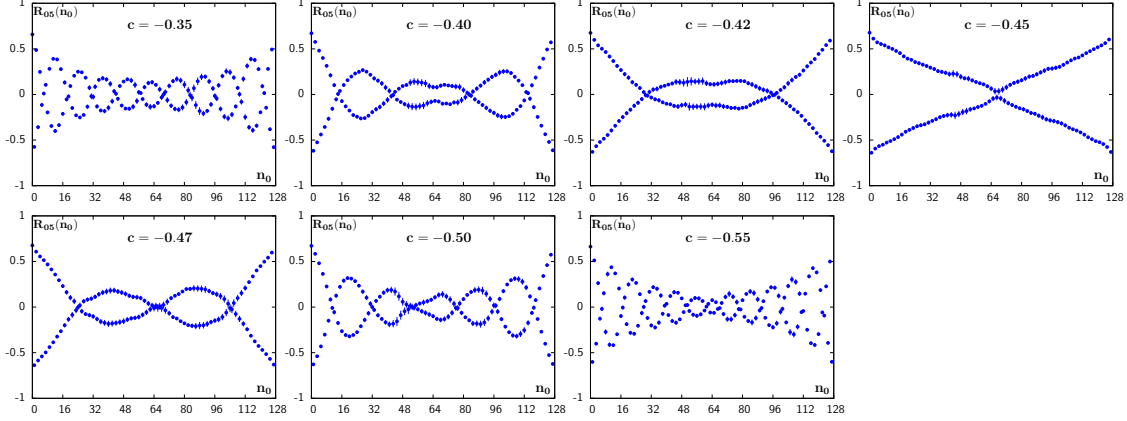
Figure E.1: Ratios $R_{05}(n_0)$ on a 128×24^3 lattice at $\beta = 6.0$ from table 4.13 are unmistakable evidence of the c dependence of the frequency shift.

Figure E.2: Power spectral densities ($\beta = 6.0$) are displayed on a logarithmic scale. The curve is a gaussian function, which is used to estimate the maximum of the distribution.

The residual exponential decay at $\beta = 6.0$ can be approximated linearly (cf. $c = -0.45$ in figure E.1). Hence, peak broadening in the power spectral density is still relatively mild and the peaks consist of $3-4$ data points. The width of the peak does not increase significantly above the mininum that is defined by half of the bin size,

$$\sigma_{\min} = \omega_b/2. \tag{E.1}$$

165

The residual exponential decay for $\beta = 5.8$ cannot be approximated as a linear funciton (cf. $c = -0.50$ in figure E.3) and oscillations can hardly be resolved visually. Presumably, the oscillation can be isolated cleanly if the ratio is divided by a hyperbolic cosine of the ground state mass difference for $c \approx c_0$.
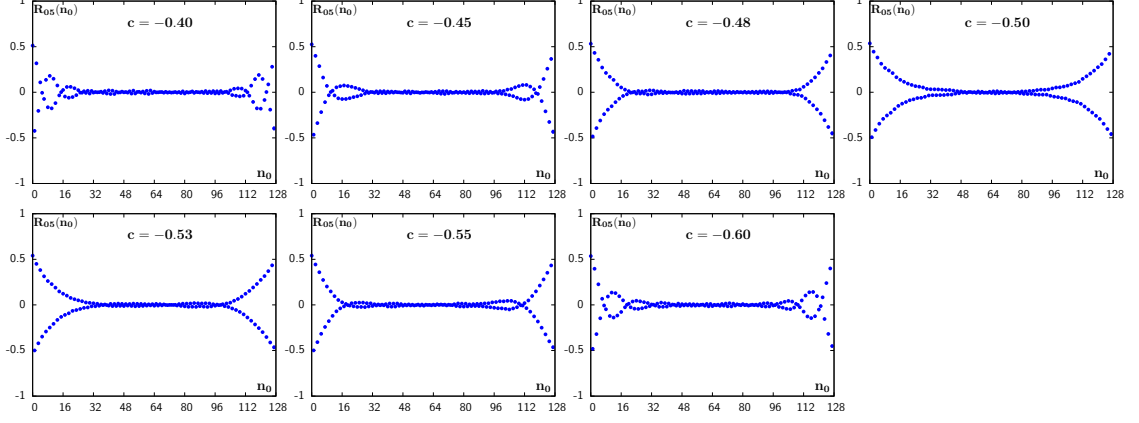
Figure E.3: Ratios $R_{05}(n_0)$ on a 128×24^3 lattice for $\beta = 5.8$ from table 4.13 still feature large exponential decays.

Peak broadening in the power spectral density is quite severe and each peak consists of $7-10$ data points (cf. figure E.4). Its width is therefore approximately three times as large as the minimal width of eq. (E.1). Thus, the systematical error can be presumably reduced by a factor $2-4$, if the residual decay is removed.
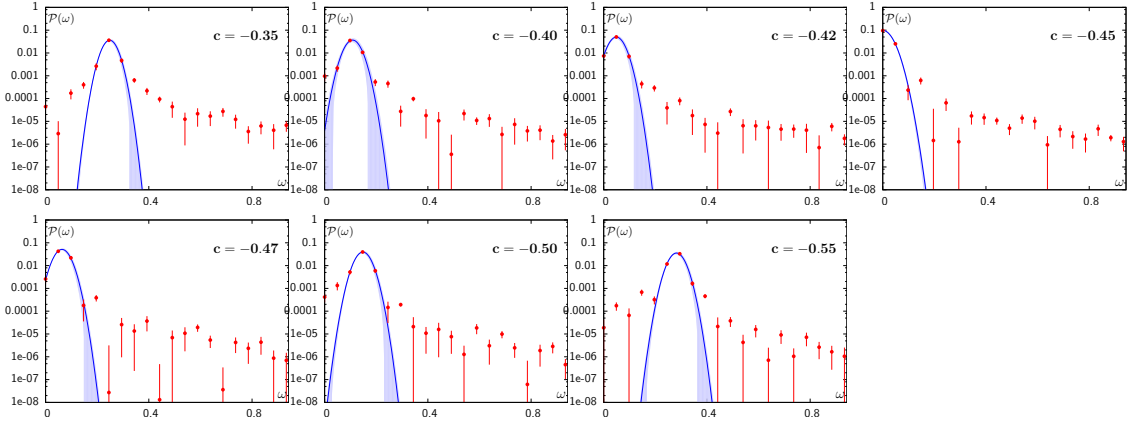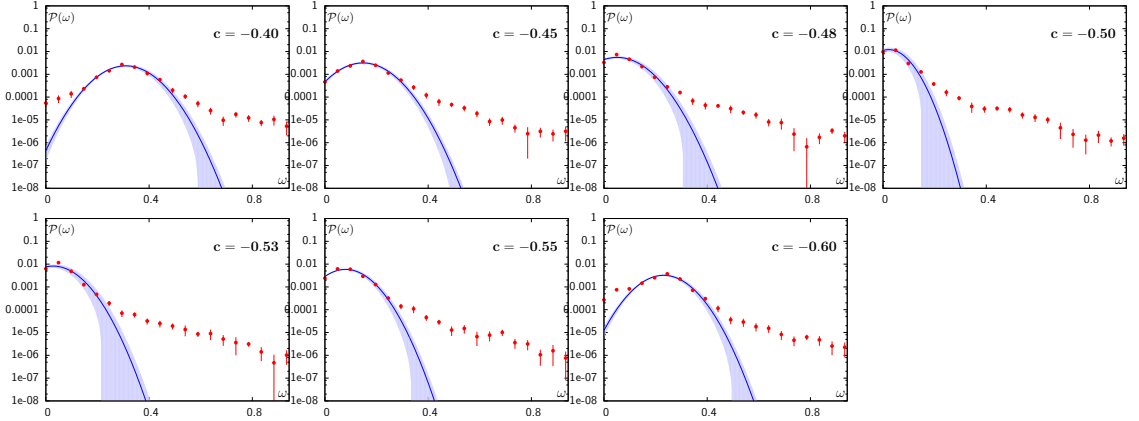

Figure E.4: Power spectral densities ($\beta = 5.8$) are displayed on a logarithmic scale. The curve is a gaussian function, which is used to estimate the maximum of the distribution.

166

E.3 Addendum to chiral behaviour of the pseudoscalar ground state

The ground state mass M_{00} is extracted with a fit using eq. (4.51). The left column of figure E.5 shows $\mathcal{B}_{00} = (r_0 M_{00})^2/(r_0 m_0)$, the analogue of $\mathcal{B}_{55}$ defined in eq. (4.45).
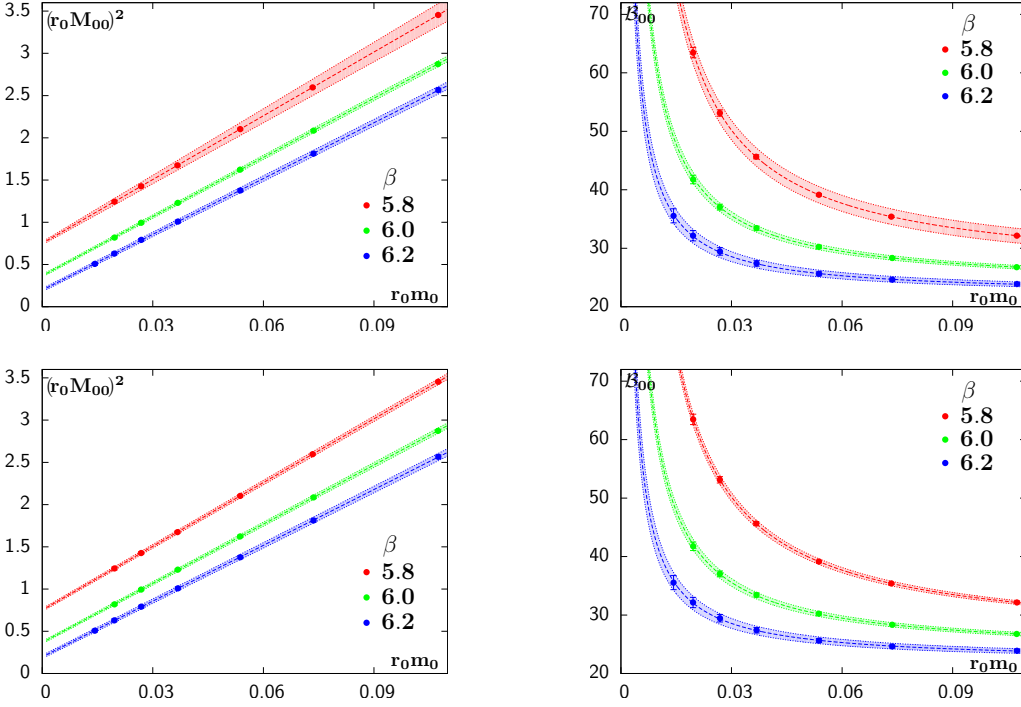
Figure E.5: Upper row: The chiral extrapolation of M_{00}^2 including quenched chiral logarithms obtains the residual mass M_{res}^2 with small errors. Lower row: Without logarithms, the extrapolation of M_{00}^2 has narrower error bands.

The study of the chiral behaviour of the pseudoscalar ground states of γ^5 and γ^0 channels involves fits to correlation functions. Local effective (cosh) masses are displayed in the following together with the fit masses with $1\sigma$ bands within the fit ranges. The grey-shaded bands are considered as potentially affected by excited states. Fit parameters are stable within 1σ upon variation of the fit range within the central region. The error bands of the γ^0 channel are wider by a factor $1.5 \sim 2$. Fluctuations as well as errors increase with a decrease of the lattice spacing as well as with a decrease of the quark mass. Since fluctuations of both channels are very similar, there are large cancellations in the ratio of correlation functions, which explain the decrease of the error of the mass difference in the chiral limit.
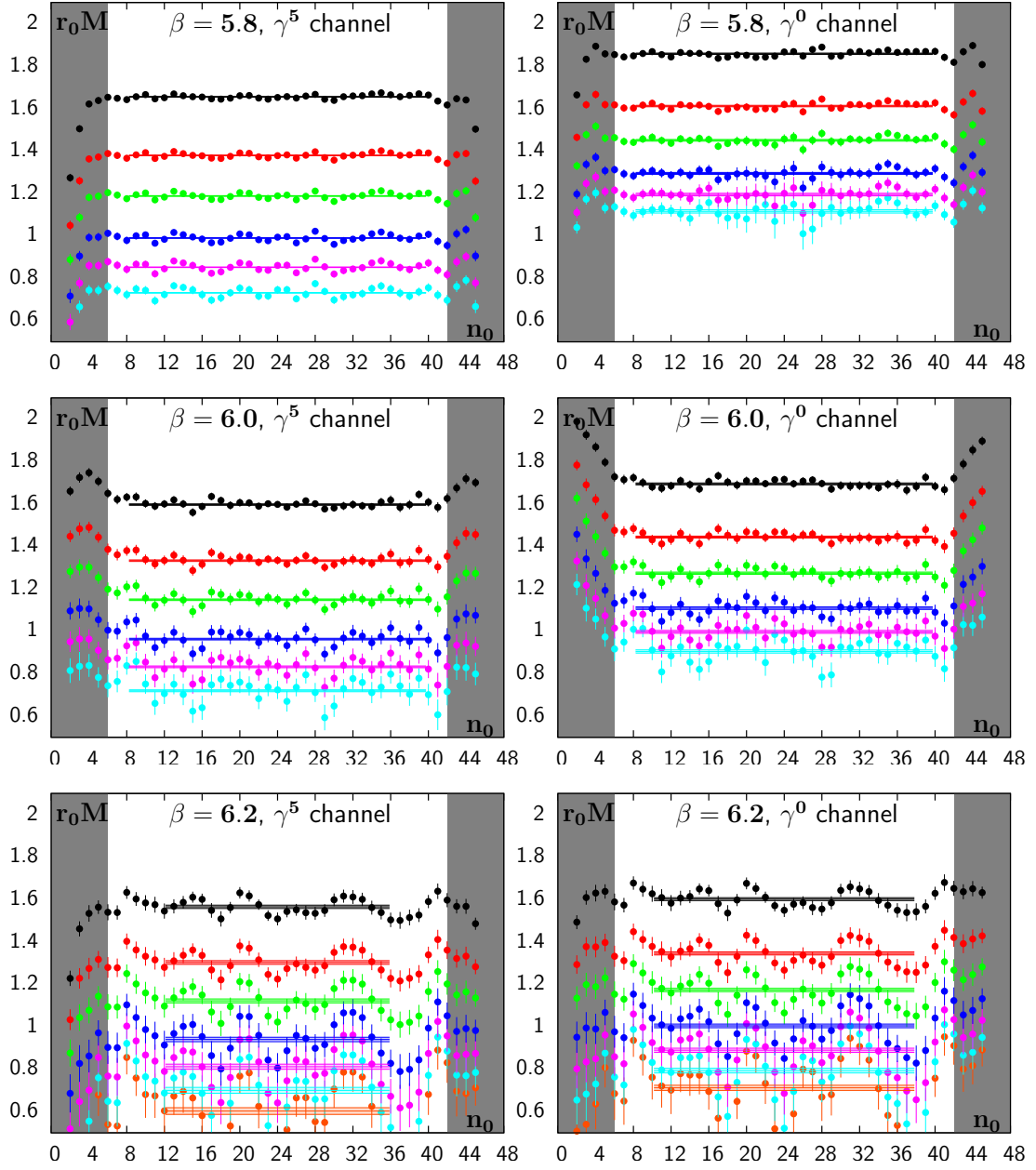
Figure E.6: Local effective mass plots of the γ^5 and γ^0 channels exhibit almost the same fluctuations for all masses from table 4.17.

168

Numerical implementation

F.1 Lattice Dirac operators

This appendix covers the implementation of the Karsten-Wilczek and the Boriçi-Creutz
Dirac operators in numerical studies of minimally doubled fermions. The hermitian
Dirac operators $Q = \gamma^5 D$ are applied in numerical simulations. The application of Q is
implemented with an input field ϕ and an output field ψ as

$$\psi = Q\phi = \delta_m \psi + \frac{1}{2} \sum_\mu \left(\delta_+^\mu \psi + \delta_-^\mu \psi \right). \tag{F.1}$$

The on-site term $\delta_m \psi$ and the hopping terms $\delta_\pm^\mu \psi$ are defined for Karsten-Wilczek and
Boriçi-Creutz operators in the following.

F.1.1 Karsten-Wilczek Dirac operator

The Karsten-Wilczek Dirac operator with $\underline{\alpha} = 0$ is taken from eq. (1.69). The hopping
terms $\delta_\pm^\mu \psi$ of eq. (F.1) add 1/2 times the following contributions:

$$\left\{ \begin{array}{rcl}
\delta_-^0 \psi_n^1 &=& U_n^{0\dagger}(- [1+d] \, \phi_{n-\hat{e}_0}^3) \\
\delta_-^0 \psi_n^2 &=& U_n^{0\dagger}(- [1+d] \, \phi_{n-\hat{e}_0}^4) \\
\delta_-^0 \psi_n^3 &=& U_n^{0\dagger}(+ [1+d] \, \phi_{n-\hat{e}_0}^1) \\
\delta_-^0 \psi_n^4 &=& U_n^{0\dagger}(+ [1+d] \, \phi_{n-\hat{e}_0}^2)
\end{array} \right\}
\left\{ \begin{array}{rcl}
\delta_+^0 \psi_n^1 &=& U_n^0 \, (+ [1+d] \, \phi_{n+\hat{e}_0}^3) \\
\delta_+^0 \psi_n^2 &=& U_n^0 \, (+ [1+d] \, \phi_{n+\hat{e}_0}^4) \\
\delta_+^0 \psi_n^3 &=& U_n^0 \, (- [1+d] \, \phi_{n+\hat{e}_0}^1) \\
\delta_+^0 \psi_n^4 &=& U_n^0 \, (- [1+d] \, \phi_{n+\hat{e}_0}^2)
\end{array} \right\} \tag{F.2}$$

$$\left\{ \begin{array}{rcl}
\delta_-^3 \psi_n^1 &=& U_n^{3\dagger}(-i \, [1+\zeta] \, \phi_{n-\hat{e}_3}^3) \\
\delta_-^3 \psi_n^2 &=& U_n^{3\dagger}(+i \, [1-\zeta] \, \phi_{n-\hat{e}_3}^4) \\
\delta_-^3 \psi_n^3 &=& U_n^{3\dagger}(-i \, [1-\zeta] \, \phi_{n-\hat{e}_3}^1) \\
\delta_-^3 \psi_n^4 &=& U_n^{3\dagger}(+i \, [1+\zeta] \, \phi_{n-\hat{e}_3}^2)
\end{array} \right\}
\left\{ \begin{array}{rcl}
\delta_+^3 \psi_n^1 &=& U_n^3 \, (+i \, [1-\zeta] \, \phi_{n+\hat{e}_3}^3) \\
\delta_+^3 \psi_n^2 &=& U_n^3 \, (-i \, [1+\zeta] \, \phi_{n+\hat{e}_3}^4) \\
\delta_+^3 \psi_n^3 &=& U_n^3 \, (+i \, [1+\zeta] \, \phi_{n+\hat{e}_3}^1) \\
\delta_+^3 \psi_n^4 &=& U_n^3 \, (-i \, [1-\zeta] \, \phi_{n+\hat{e}_3}^2)
\end{array} \right\} \tag{F.3}$$

$$\begin{cases} \delta^1_- \psi^1_n = U^{1\dagger}_n(+i\left[\phi^4_{n-\hat{e}_1} - \zeta\phi^3_{n-\hat{e}_1}\right]) \\ \delta^1_- \psi^2_n = U^{1\dagger}_n(+i\left[\phi^3_{n-\hat{e}_1} - \zeta\phi^4_{n-\hat{e}_1}\right]) \\ \delta^1_- \psi^3_n = U^{1\dagger}_n(+i\left[\phi^2_{n-\hat{e}_1} + \zeta\phi^1_{n-\hat{e}_1}\right]) \\ \delta^1_- \psi^4_n = U^{1\dagger}_n(+i\left[\phi^1_{n-\hat{e}_1} + \zeta\phi^2_{n-\hat{e}_1}\right]) \end{cases} \begin{cases} \delta^1_+ \psi^1_n = U^1_n(-i\left[\phi^4_{n-\hat{e}_1} + \zeta\phi^3_{n-\hat{e}_1}\right]) \\ \delta^1_+ \psi^2_n = U^1_n(-i\left[\phi^3_{n-\hat{e}_1} + \zeta\phi^4_{n-\hat{e}_1}\right]) \\ \delta^1_+ \psi^3_n = U^1_n(-i\left[\phi^2_{n-\hat{e}_1} - \zeta\phi^1_{n-\hat{e}_1}\right]) \\ \delta^1_+ \psi^4_n = U^1_n(-i\left[\phi^1_{n-\hat{e}_1} - \zeta\phi^2_{n-\hat{e}_1}\right]) \end{cases}$$
$$(\text{F.4})$$

$$\begin{cases} \delta^2_- \psi^1_n = U^{2\dagger}_n(+\left[\phi^4_{n-\hat{e}_2} - i\zeta\phi^3_{n-\hat{e}_2}\right]) \\ \delta^2_- \psi^2_n = U^{2\dagger}_n(-\left[\phi^3_{n-\hat{e}_2} + i\zeta\phi^4_{n-\hat{e}_2}\right]) \\ \delta^2_- \psi^3_n = U^{2\dagger}_n(+\left[\phi^2_{n-\hat{e}_2} + i\zeta\phi^1_{n-\hat{e}_2}\right]) \\ \delta^2_- \psi^4_n = U^{2\dagger}_n(-\left[\phi^1_{n-\hat{e}_2} - i\zeta\phi^2_{n-\hat{e}_2}\right]) \end{cases} \begin{cases} \delta^2_+ \psi^1_n = U^2_n(-\left[\phi^4_{n-\hat{e}_2} + i\zeta\phi^3_{n-\hat{e}_2}\right]) \\ \delta^2_+ \psi^2_n = U^2_n(+\left[\phi^3_{n-\hat{e}_2} - i\zeta\phi^4_{n-\hat{e}_2}\right]) \\ \delta^2_+ \psi^3_n = U^2_n(-\left[\phi^2_{n-\hat{e}_2} - i\zeta\phi^1_{n-\hat{e}_2}\right]) \\ \delta^2_+ \psi^4_n = U^2_n(+\left[\phi^1_{n-\hat{e}_2} + i\zeta\phi^2_{n-\hat{e}_2}\right]) \end{cases},$$
$$(\text{F.5})$$

and the on-site term $\delta_m\psi$ of eq. (F.1) contributes

$$\begin{cases} \delta_m\psi^1_n = (+m_0\phi^1_n + i\frac{3\zeta+c}{a}\phi^3_n) \\ \delta_m\psi^2_n = (+m_0\phi^2_n + i\frac{3\zeta+c}{a}\phi^4_n) \\ \delta_m\psi^3_n = (-m_0\phi^3_n - i\frac{3\zeta+c}{a}\phi^1_n) \\ \delta_m\psi^4_n = (-m_0\phi^4_n - i\frac{3\zeta+c}{a}\phi^2_n) \end{cases}.$$
$$(\text{F.6})$$

Some spatial hopping terms $\delta^j_\pm\psi$ for $\underline{\alpha} = 0$ and $\zeta = \pm 1$ are related (cf. table F.1). Components which are linearly related are reconstructed with reduced numerical effort.

$\delta^1_- \psi^1_n = \mp\zeta\delta^1_- \psi^2_n,$	$\delta^1_- \psi^3_n = \pm\zeta\delta^1_- \psi^4_n,$	$\delta^1_+ \psi^1_n = \pm\zeta\delta^1_+ \psi^2_n,$	$\delta^1_+ \psi^3_n = \mp\zeta\delta^1_+ \psi^4_n,$
$\delta^2_- \psi^1_n = \pm i\zeta\delta^2_- \psi^2_n,$	$\delta^2_- \psi^3_n = \mp i\zeta\delta^2_- \psi^4_n,$	$\delta^2_+ \psi^1_n = \mp i\zeta\delta^2_+ \psi^2_n,$	$\delta^2_+ \psi^3_n = \pm i\zeta\delta^2_+ \psi^4_n,$
	$\zeta = +1:$	$\delta^3_- \psi^2_n = \delta^3_- \psi^3_n = 0,$	$\delta^3_+ \psi^1_n = \delta^3_+ \psi^4_n = 0,$
	$\zeta = -1:$	$\delta^3_- \psi^1_n = \delta^3_- \psi^4_n = 0,$	$\delta^3_+ \psi^2_n = \delta^3_+ \psi^3_n = 0.$

Table F.1: For $\underline{\alpha} = 0$ and $\zeta = \pm 1$, the Dirac components of $\delta^1_\pm\psi$ and $\delta^1_\pm\psi$ are linearly dependent and half of the $\delta^3_\pm\psi$ trivially vanish. Moreover, the communications for spatial boundaries are halved in each spatial direction.

The Karsten-Wilczek Dirac operator with $\underline{\alpha} = 3$ is used for studies of the anisotropy. The hopping terms $\delta^\mu_\pm\psi$ of eq. (F.1) add $1/2$ times the following contributions:

$$\begin{cases} \delta^0_- \psi^1_n = U^{0\dagger}_n(-\left[1 - \zeta\right]\phi^3_{n-\hat{e}_0}) \\ \delta^0_- \psi^2_n = U^{0\dagger}_n(-\left[1 + \zeta\right]\phi^4_{n-\hat{e}_0}) \\ \delta^0_- \psi^3_n = U^{0\dagger}_n(+\left[1 - \zeta\right]\phi^1_{n-\hat{e}_0}) \\ \delta^0_- \psi^4_n = U^{0\dagger}_n(+\left[1 + \zeta\right]\phi^2_{n-\hat{e}_0}) \end{cases} \begin{cases} \delta^0_+ \psi^1_n = U^0_n(+\left[1 + \zeta\right]\phi^3_{n+\hat{e}_0}) \\ \delta^0_+ \psi^2_n = U^0_n(+\left[1 - \zeta\right]\phi^4_{n+\hat{e}_0}) \\ \delta^0_+ \psi^3_n = U^0_n(-\left[1 + \zeta\right]\phi^1_{n+\hat{e}_0}) \\ \delta^0_+ \psi^4_n = U^0_n(-\left[1 - \zeta\right]\phi^2_{n+\hat{e}_0}) \end{cases}$$
$$(\text{F.7})$$

$$\begin{cases} \delta^3_- \psi^1_n = U^{3\dagger}_n(-i\left[1 + d\right]\phi^3_{n-\hat{e}_3}) \\ \delta^3_- \psi^2_n = U^{3\dagger}_n(+i\left[1 + d\right]\phi^4_{n-\hat{e}_3}) \\ \delta^3_- \psi^3_n = U^{3\dagger}_n(-i\left[1 + d\right]\phi^1_{n-\hat{e}_3}) \\ \delta^3_- \psi^4_n = U^{3\dagger}_n(+i\left[1 + d\right]\phi^2_{n-\hat{e}_3}) \end{cases} \begin{cases} \delta^3_+ \psi^1_n = U^3_n(+i\left[1 + d\right]\phi^3_{n+\hat{e}_3}) \\ \delta^3_+ \psi^2_n = U^3_n(-i\left[1 + d\right]\phi^4_{n+\hat{e}_3}) \\ \delta^3_+ \psi^3_n = U^3_n(+i\left[1 + d\right]\phi^1_{n+\hat{e}_3}) \\ \delta^3_+ \psi^4_n = U^3_n(-i\left[1 + d\right]\phi^2_{n+\hat{e}_3}) \end{cases}$$
$$(\text{F.8})$$

$$
\left\{
\begin{array}{rcl}
\delta^1_- \psi^1_n &=& U^{1\dagger}_n (+i\left[\phi^4_{n-\hat{e}_1} - i\zeta\phi^3_{n-\hat{e}_1}\right]) \\
\delta^1_- \psi^2_n &=& U^{1\dagger}_n (+i\left[\phi^3_{n-\hat{e}_1} + i\zeta\phi^4_{n-\hat{e}_1}\right]) \\
\delta^1_- \psi^3_n &=& U^{1\dagger}_n (+i\left[\phi^2_{n-\hat{e}_1} + i\zeta\phi^1_{n-\hat{e}_1}\right]) \\
\delta^1_- \psi^4_n &=& U^{1\dagger}_n (+i\left[\phi^1_{n-\hat{e}_1} - i\zeta\phi^2_{n-\hat{e}_1}\right])
\end{array}
\right\}
\left\{
\begin{array}{rcl}
\delta^1_+ \psi^1_n &=& U^1_n (-i\left[\phi^4_{n-\hat{e}_1} + i\zeta\phi^3_{n-\hat{e}_1}\right]) \\
\delta^1_+ \psi^2_n &=& U^1_n (-i\left[\phi^3_{n-\hat{e}_1} - i\zeta\phi^4_{n-\hat{e}_1}\right]) \\
\delta^1_+ \psi^3_n &=& U^1_n (-i\left[\phi^2_{n-\hat{e}_1} - i\zeta\phi^1_{n-\hat{e}_1}\right]) \\
\delta^1_+ \psi^4_n &=& U^1_n (-i\left[\phi^1_{n-\hat{e}_1} + i\zeta\phi^2_{n-\hat{e}_1}\right])
\end{array}
\right\}
$$
$$\text{(F.9)}$$

$$
\left\{
\begin{array}{rcl}
\delta^2_- \psi^1_n &=& U^{2\dagger}_n (+\left[\phi^4_{n-\hat{e}_2} + \zeta\phi^3_{n-\hat{e}_2}\right]) \\
\delta^2_- \psi^2_n &=& U^{2\dagger}_n (-\left[\phi^3_{n-\hat{e}_2} + \zeta\phi^4_{n-\hat{e}_2}\right]) \\
\delta^2_- \psi^3_n &=& U^{2\dagger}_n (+\left[\phi^2_{n-\hat{e}_2} - \zeta\phi^1_{n-\hat{e}_2}\right]) \\
\delta^2_- \psi^4_n &=& U^{2\dagger}_n (-\left[\phi^1_{n-\hat{e}_2} - \zeta\phi^2_{n-\hat{e}_2}\right])
\end{array}
\right\}
\left\{
\begin{array}{rcl}
\delta^2_+ \psi^1_n &=& U^2_n (-\left[\phi^4_{n-\hat{e}_2} - \zeta\phi^3_{n-\hat{e}_2}\right]) \\
\delta^2_+ \psi^2_n &=& U^2_n (+\left[\phi^3_{n-\hat{e}_2} - \zeta\phi^4_{n-\hat{e}_2}\right]) \\
\delta^2_+ \psi^3_n &=& U^2_n (-\left[\phi^2_{n-\hat{e}_2} + \zeta\phi^1_{n-\hat{e}_2}\right]) \\
\delta^2_+ \psi^4_n &=& U^2_n (+\left[\phi^1_{n-\hat{e}_2} + \zeta\phi^2_{n-\hat{e}_2}\right])
\end{array}
\right\},
$$
$$\text{(F.10)}$$

and the on-site term $\delta_m \psi$ of eq. (F.1) contributes

$$
\left\{
\begin{array}{rcl}
\delta_m \psi^1_n &=& (+m_0 \phi^1_n + \frac{3\zeta+c}{a}\phi^3_n) \\
\delta_m \psi^2_n &=& (+m_0 \phi^2_n - \frac{3\zeta+c}{a}\phi^4_n) \\
\delta_m \psi^3_n &=& (-m_0 \phi^3_n - \frac{3\zeta+c}{a}\phi^1_n) \\
\delta_m \psi^4_n &=& (-m_0 \phi^4_n + \frac{3\zeta+c}{a}\phi^2_n)
\end{array}
\right\}.
$$
$$\text{(F.11)}$$

Perpendicular hopping terms $(\delta^0_\pm \psi, \ \delta^1_\pm \psi, \ \delta^2_\pm \psi)$ for $\underline{\alpha} = 3$ and $\zeta = \pm 1$, are related (cf. table F.2). Components which are linearly related are reconstructed with reduced numerical effort.

$\delta^1_- \psi^1_n = \mp i\zeta\delta^1_- \psi^2_n,$	$\delta^1_- \psi^3_n = \pm i\zeta\delta^1_- \psi^4_n,$	$\delta^1_+ \psi^1_n = \pm i\zeta\delta^1_+ \psi^2_n,$	$\delta^1_+ \psi^3_n = \mp i\zeta\delta^1_+ \psi^4_n,$
$\delta^2_- \psi^1_n = \mp\zeta\delta^2_- \psi^2_n,$	$\delta^2_- \psi^3_n = \pm\zeta\delta^2_- \psi^4_n,$	$\delta^2_+ \psi^1_n = \pm\zeta\delta^2_+ \psi^2_n,$	$\delta^2_+ \psi^3_n = \mp\zeta\delta^2_+ \psi^4_n,$
	$\zeta = +1:$	$\delta^0_- \psi^1_n = \delta^0_- \psi^3_n = 0,$	$\delta^0_+ \psi^2_n = \delta^0_+ \psi^4_n = 0,$
	$\zeta = -1:$	$\delta^0_- \psi^2_n = \delta^0_- \psi^4_n = 0,$	$\delta^0_+ \psi^1_n = \delta^0_+ \psi^3_n = 0.$

Table F.2: For $\underline{\alpha} = 3$ and $\zeta = \pm 1$, the Dirac components of $\delta^1_\pm \psi$ and $\delta^1_\pm \psi$ are linearly dependent and half of the $\delta^0_\pm \psi$ trivially vanish. Moreover, the communications for spatial boundaries are halved in each perpendicular direction.

Independent of the particular choice of $\underline{\alpha}$, the tally of floating point operations, which is dominated by the SU(3) matrix-times-vector operations in the $\delta^\mu_\pm \psi$, is reduced to approximately 5/8 for $\zeta = \pm 1$, if the symmetries of $\delta^\mu_\pm \psi$ are incorporated into the code. It is reasonable to provide extra versions of the Karsten-Wilczek Dirac operator for $\zeta = \pm 1$ due to their superior numerical efficiency.

F.1.2 Boriçi-Creutz Dirac operator

The Boriçi-Creutz Dirac operator is taken from eq. (1.90). The hopping terms $\delta^\mu_\pm \psi$ of eq. (F.1) add $1/2$ times the following contributions:

$$
\left\{
\begin{aligned}
\delta^0_- \psi^1_n &= U^{0\dagger}_n ((-1-i\zeta)\phi^3_{n-\hat{e}_0} + (i\zeta + d/2)\left[(-1+i)\phi^3_{n-\hat{e}_0} + (+1+i)\phi^4_{n-\hat{e}_0}\right]) \\
\delta^0_- \psi^2_n &= U^{0\dagger}_n ((-1-i\zeta)\phi^4_{n-\hat{e}_0} + (i\zeta + d/2)\left[(-1+i)\phi^3_{n-\hat{e}_0} + (-1-i)\phi^4_{n-\hat{e}_0}\right]) \\
\delta^0_- \psi^3_n &= U^{0\dagger}_n ((+1+i\zeta)\phi^1_{n-\hat{e}_0} + (i\zeta + d/2)\left[(+1+i)\phi^1_{n-\hat{e}_0} + (+1+i)\phi^2_{n-\hat{e}_0}\right]) \\
\delta^0_- \psi^4_n &= U^{0\dagger}_n ((+1+i\zeta)\phi^2_{n-\hat{e}_0} + (i\zeta + d/2)\left[(-1+i)\phi^1_{n-\hat{e}_0} + (+1-i)\phi^2_{n-\hat{e}_0}\right])
\end{aligned}
\right.
\tag{F.12}
$$

$$
\left\{
\begin{aligned}
\delta^0_+ \psi^1_n &= U^{0}_n ((+1-i\zeta)\phi^3_{n+\hat{e}_0} + (i\zeta - d/2)\left[(+1-i)\phi^3_{n-\hat{e}_0} + (-1-i)\phi^4_{n-\hat{e}_0}\right]) \\
\delta^0_+ \psi^2_n &= U^{0}_n ((+1-i\zeta)\phi^4_{n+\hat{e}_0} + (i\zeta - d/2)\left[(+1-i)\phi^3_{n-\hat{e}_0} + (+1+i)\phi^4_{n-\hat{e}_0}\right]) \\
\delta^0_+ \psi^3_n &= U^{0}_n ((-1+i\zeta)\phi^1_{n+\hat{e}_0} + (i\zeta - d/2)\left[(-1-i)\phi^1_{n-\hat{e}_0} + (-1-i)\phi^2_{n-\hat{e}_0}\right]) \\
\delta^0_+ \psi^4_n &= U^{0}_n ((-1+i\zeta)\phi^2_{n+\hat{e}_0} + (i\zeta - d/2)\left[(+1-i)\phi^1_{n-\hat{e}_0} + (-1+i)\phi^2_{n-\hat{e}_0}\right])
\end{aligned}
\right.
\tag{F.13}
$$

$$
\left\{
\begin{aligned}
\delta^1_- \psi^1_n &= U^{1\dagger}_n ((+i-\zeta)\phi^3_{n-\hat{e}_1} + (i\zeta + d/2)\left[(-1+i)\phi^3_{n-\hat{e}_1} + (+1+i)\phi^4_{n-\hat{e}_1}\right]) \\
\delta^1_- \psi^2_n &= U^{1\dagger}_n ((+i-\zeta)\phi^4_{n-\hat{e}_1} + (i\zeta + d/2)\left[(-1+i)\phi^3_{n-\hat{e}_1} + (-1-i)\phi^4_{n-\hat{e}_1}\right]) \\
\delta^1_- \psi^3_n &= U^{1\dagger}_n ((+i-\zeta)\phi^1_{n-\hat{e}_1} + (i\zeta + d/2)\left[(+1+i)\phi^1_{n-\hat{e}_1} + (+1+i)\phi^2_{n-\hat{e}_1}\right]) \\
\delta^1_- \psi^4_n &= U^{1\dagger}_n ((+i-\zeta)\phi^2_{n-\hat{e}_1} + (i\zeta + d/2)\left[(-1+i)\phi^1_{n-\hat{e}_1} + (+1-i)\phi^2_{n-\hat{e}_1}\right])
\end{aligned}
\right.
\tag{F.14}
$$

$$
\left\{
\begin{aligned}
\delta^1_+ \psi^1_n &= U^{1}_n ((-i-\zeta)\phi^3_{n+\hat{e}_1} + (i\zeta - d/2)\left[(+1-i)\phi^3_{n-\hat{e}_1} + (-1-i)\phi^4_{n-\hat{e}_1}\right]) \\
\delta^1_+ \psi^2_n &= U^{1}_n ((-i-\zeta)\phi^4_{n+\hat{e}_1} + (i\zeta - d/2)\left[(+1-i)\phi^3_{n-\hat{e}_1} + (+1+i)\phi^4_{n-\hat{e}_1}\right]) \\
\delta^1_+ \psi^3_n &= U^{1}_n ((-i-\zeta)\phi^1_{n+\hat{e}_1} + (i\zeta - d/2)\left[(-1-i)\phi^1_{n-\hat{e}_1} + (-1-i)\phi^2_{n-\hat{e}_1}\right]) \\
\delta^1_+ \psi^4_n &= U^{1}_n ((-i-\zeta)\phi^2_{n+\hat{e}_1} + (i\zeta - d/2)\left[(+1-i)\phi^1_{n-\hat{e}_1} + (-1+i)\phi^2_{n-\hat{e}_1}\right])
\end{aligned}
\right.
\tag{F.15}
$$

$$
\left\{
\begin{aligned}
\delta^2_- \psi^1_n &= U^{2\dagger}_n ((+1+i\zeta)\phi^3_{n-\hat{e}_2} + (i\zeta + d/2)\left[(-1+i)\phi^3_{n-\hat{e}_2} + (+1+i)\phi^4_{n-\hat{e}_2}\right]) \\
\delta^2_- \psi^2_n &= U^{2\dagger}_n ((-1-i\zeta)\phi^4_{n-\hat{e}_2} + (i\zeta + d/2)\left[(-1+i)\phi^3_{n-\hat{e}_2} + (-1-i)\phi^4_{n-\hat{e}_2}\right]) \\
\delta^2_- \psi^3_n &= U^{2\dagger}_n ((+1+i\zeta)\phi^1_{n-\hat{e}_2} + (i\zeta + d/2)\left[(+1+i)\phi^1_{n-\hat{e}_2} + (+1+i)\phi^2_{n-\hat{e}_2}\right]) \\
\delta^2_- \psi^4_n &= U^{2\dagger}_n ((-1-i\zeta)\phi^2_{n-\hat{e}_2} + (i\zeta + d/2)\left[(-1+i)\phi^1_{n-\hat{e}_2} + (+1-i)\phi^2_{n-\hat{e}_2}\right])
\end{aligned}
\right.
\tag{F.16}
$$

$$
\left\{
\begin{aligned}
\delta^2_+ \psi^1_n &= U^{2}_n ((-1+i\zeta)\phi^3_{n+\hat{e}_2} + (i\zeta - d/2)\left[(+1-i)\phi^3_{n-\hat{e}_2} + (-1-i)\phi^4_{n-\hat{e}_2}\right]) \\
\delta^2_+ \psi^2_n &= U^{2}_n ((+1-i\zeta)\phi^4_{n+\hat{e}_2} + (i\zeta - d/2)\left[(+1-i)\phi^3_{n-\hat{e}_2} + (+1+i)\phi^4_{n-\hat{e}_2}\right]) \\
\delta^2_+ \psi^3_n &= U^{2}_n ((-1+i\zeta)\phi^1_{n+\hat{e}_2} + (i\zeta - d/2)\left[(-1-i)\phi^1_{n-\hat{e}_2} + (-1-i)\phi^2_{n-\hat{e}_2}\right]) \\
\delta^2_+ \psi^4_n &= U^{2}_n ((+1-i\zeta)\phi^2_{n+\hat{e}_2} + (i\zeta - d/2)\left[(+1-i)\phi^1_{n-\hat{e}_2} + (-1+i)\phi^2_{n-\hat{e}_2}\right])
\end{aligned}
\right.
\tag{F.17}
$$

$$\begin{cases}
\delta_-^3 \psi_n^1 &= U_n^{3\dagger}((-i+\zeta)\phi_{n-\hat{e}_3}^3 + (i\zeta+d/2)\left[(-1+i)\phi_{n-\hat{e}_3}^3 + (+1+i)\phi_{n-\hat{e}_3}^4\right]) \\
\delta_-^3 \psi_n^2 &= U_n^{3\dagger}((+i-\zeta)\phi_{n-\hat{e}_3}^4 + (i\zeta+d/2)\left[(-1+i)\phi_{n-\hat{e}_3}^3 + (-1-i)\phi_{n-\hat{e}_3}^4\right]) \\
\delta_-^3 \psi_n^3 &= U_n^{3\dagger}((-i+\zeta)\phi_{n-\hat{e}_3}^1 + (i\zeta+d/2)\left[(+1+i)\phi_{n-\hat{e}_3}^1 + (+1+i)\phi_{n-\hat{e}_3}^2\right]) \\
\delta_-^3 \psi_n^4 &= U_n^{3\dagger}((+i-\zeta)\phi_{n-\hat{e}_3}^2 + (i\zeta+d/2)\left[(-1+i)\phi_{n-\hat{e}_3}^1 + (+1-i)\phi_{n-\hat{e}_3}^2\right])
\end{cases}$$
(F.18)

$$\begin{cases}
\delta_+^3 \psi_n^1 &= U_n^3 ((+i+\zeta)\phi_{n+\hat{e}_3}^3 + (i\zeta-d/2)\left[(+1-i)\phi_{n-\hat{e}_3}^3 + (-1-i)\phi_{n-\hat{e}_3}^4\right]) \\
\delta_+^3 \psi_n^2 &= U_n^3 ((-i-\zeta)\phi_{n+\hat{e}_3}^4 + (i\zeta-d/2)\left[(+1-i)\phi_{n-\hat{e}_3}^3 + (+1+i)\phi_{n-\hat{e}_3}^4\right]) \\
\delta_+^3 \psi_n^3 &= U_n^3 ((+i+\zeta)\phi_{n+\hat{e}_3}^1 + (i\zeta-d/2)\left[(-1-i)\phi_{n-\hat{e}_3}^1 + (-1-i)\phi_{n-\hat{e}_3}^2\right]) \\
\delta_+^3 \psi_n^4 &= U_n^3 ((-i-\zeta)\phi_{n+\hat{e}_3}^2 + (i\zeta-d/2)\left[(+1-i)\phi_{n-\hat{e}_3}^1 + (-1+i)\phi_{n-\hat{e}_3}^2\right])
\end{cases},$$
(F.19)

and the on-site term $\delta_m\psi$ of eq. (F.1) is

$$\begin{cases}
\delta_m\psi_n^1 &= (+m_0\phi_n^1 + \frac{2\zeta+c}{2}\left[(+1+i)\phi_n^3 + (+1-i)\phi_n^4\right]) \\
\delta_m\psi_n^2 &= (+m_0\phi_n^2 + \frac{2\zeta+c}{2}\left[(+1+i)\phi_n^3 + (-1+i)\phi_n^4\right]) \\
\delta_m\psi_n^3 &= (-m_0\phi_n^3 + \frac{2\zeta+c}{2}\left[(+1-i)\phi_n^1 + (+1-i)\phi_n^2\right]) \\
\delta_m\psi_n^4 &= (-m_0\phi_n^4 + \frac{2\zeta+c}{2}\left[(+1+i)\phi_n^1 + (-1-i)\phi_n^2\right])
\end{cases}.$$
(F.20)

For $\zeta = +1$, all coefficients of Boriçi-Creutz hopping terms $\delta_\pm^\mu\psi$ in the linear combinations on the right hand sides of eqs. (F.12), ..., (F.19) are covered by three real constants,

$$\begin{aligned}
h_{1+} &= 1 + d/2 \\
h_{1-} &= 1 - d/2 \quad, \\
h_{3+} &= 3 + d/2
\end{aligned}$$
(F.21)

which can be used to minimise the tally of complex-times-vector operations. This is the most efficient implementation of the Boriçi-Creutz Dirac operator at present knowledge.

F.2 Contractions

Contractions of two fermionic propagators into mesonic correlation functions rely on eq. (4.17), which reads

$$\mathcal{C}_{\mathcal{M},\mathcal{N}}(t) = \sum_{n\in\Lambda_t^0} \operatorname{tr}_c\Big(S_{n,0}^{\alpha\beta}(S^*)_{n,0}^{\delta\gamma}((\mathcal{M}\gamma^5)^T)^{\gamma\beta}(\gamma^5\mathcal{N})^{\delta\alpha}\Big).$$
(F.22)

Propagator components (hereafter: propagators) are stored in the memory as spinor fields 'ψ' which are defined on the full lattice in a memory alignment of 24 doubles following

$$\operatorname{Re}\psi_1^1 \operatorname{Im}\psi_1^1 \operatorname{Re}\psi_1^2 \ldots \operatorname{Im}\psi_1^3 \quad \operatorname{Re}\psi_2^1 \ldots \operatorname{Im}\psi_2^3 \quad \operatorname{Re}\psi_3^1 \ldots \operatorname{Im}\psi_3^3 \quad \operatorname{Re}\psi_4^1 \ldots \operatorname{Im}\psi_4^3.$$
(F.23)

In the following, the indication of Dirac matrices within the simulation program for interpolating operators at source and sink is outlined in table F.3. The simulation uses Dirac matrices in the chiral representation that are defined in eq. (A.27). Instead of using the original matrices $\mathcal{M}$ and $\mathcal{N}$ in interpolating operators, contractions directly use the transposed matrix product $(\mathcal{M}\gamma^5)^T$ for the source and the matrix product $(\gamma^5\mathcal{N})$ for the sink:

$$\mathcal{M} \to (\mathcal{M}\gamma^5)^T, \qquad \mathcal{N} \to (\gamma^5\mathcal{N}). \tag{F.24}$$

Dirac matrix $\mathcal{M},\mathcal{N}$	γ^μ	$\mathbf{1}$	γ^5	$\gamma^5\gamma^\mu$	$\gamma^0\gamma^i$	$\gamma^i\gamma^j, i<j$
Index μ	μ	4	5	$6+\mu$	$9+i$	$10+i+j$

Table F.3: 16 Dirac matrices that are used in interpolating operators are labeled by only one index μ. Care has to be taken since only γ^μ, $\mathbf{1}$ and γ^5 are hermitian.

Propagators are calculated one by one in sequence, where the colour component ranges between $i_c \in [1,2,3]$ in an outer loop and the spin component (or Dirac component) ranges between $i_d \in [1,2,3,4]$ in an inner loop. Each Dirac component is directly used in the calculation of 2-point functions with either $\mathbf{1}$ or γ^5 at the source and added up to the total correlation function. Once the second ($i_d = 2$) Dirac component (or fourth ($i_d = 4$) Dirac component) is available, 2 contributions to correlation functions with source interpolators with tensor structure ($\gamma^\mu\gamma^\nu$) are calculated. The propagator is contracted with the first ($j_d = 1$) Dirac component (or third ($j_d = 3$) Dirac component) for $\mu = \{10,11,14,15\}$ and it is contracted with itself for $\mu = \{12,13\}$. Next, contractions of j_d with i_d are performed for $\mu = \{10,11,14,15\}$ and of j_d with j_d for $\mu = \{12,13\}$ added to the total correlation functions. Once the third ($i_c = 3$) Dirac component is available, 2 contributions to correlation functions with source interpolators with vector (γ^μ) or axial vector ($\gamma^5\gamma^\mu$) structure are calculated. The propagator is contracted with the first ($j_d^0 = 1$) Dirac component for $\mu = \{0,3,6,9\}$ and it is contracted with the second ($j_d^1 = 2$) for $\mu = \{1,2,7,8\}$. Next, contractions of $j_d^{0,1}$ with i_d are performed and added to the total correlation functions. Once the fourth ($i_d = 3$) Dirac component is available, 2 contributions to correlation functions with source interpolators with vector (γ^μ) or axial vector ($\gamma^5\gamma^\mu$) structure are calculated. The propagator is contracted with the first ($j_d^1 = 1$) Dirac component for $\mu = \{1,2,7,8\}$ and it is contracted with the second ($j_d^0 = 2$) for $\mu = \{0,3,6,9\}$ and added to the total correlation function. Next, contractions of $j_d^{0,1}$ with i_d are performed and added to the total correlation functions. Finally, the last 2 contributions to correlation functions with source interpolators with tensor structure ($\gamma^\mu\gamma^\nu$) are calculated as described above.

The procedure is repeated for all colour components. Propagators are temporarily dumped to the hard disk for later use as j_d component in contractions. For the contractions, these dumped propagators are restored and kept in work space that is reserved for the CG solver in the rest of the program. After processing the fourth $i_d = 4$ components, the dumped propagators are deleted.

The subroutine

void *add_to_MM_2pt* (**int** *p1*, **int** *p2*, **int** *l*, **int** *mu*, **int** *nu*, **int** *dir*,
$\qquad\qquad$ **int** **vect_ps*, **complex_dble** **corr*),

which performs the contractions, receives the locations *p1*, *p2* in memory for 2 possibly different propagators that are computed by the inverter for different Dirac operators or for different smearing options at source or sink. The index $l = 3(i_d - 1) + (i_c - 1)$ denotes which propagator is treated and is factored into a macro that determines whether the contribution is added or subtracted from the correlator. The indices *mu* and *nu* label the Dirac matrices of interpolating operators at sink (*mu*) and source (*nu*). The index *nu* determines the Dirac components that are accessed in the contractions of j_d^0, j_d^1 or j_d with i_d. Either index j_d^0, j_d^1 or j_d is calculated only once for every i_d and replaces l within the subroutine. The index *dir* incidates the Euclidean time direction and may be either set to 0 or 3. The contractions are performed for all lattice sites individually and all sites in a slice that is perpendicular to this time direction are summed up in the aftermath. The pointer **vect_ps* indicates a four-component array, which holds integers that determine an external momentum insertion at the sink. The momentum is given by $p_\mu = 2\pi/a \cdot (vect\_ps[\mu]/N\mu)$. Only three components have a physical role as spatial hadron momenta. However, due to the flexibility in terms of defining the time direction, external momenta are handled most naturally as a four-component field. Finally, the pointer *corr* indicates an array, which stores the value of the correlation function.

mu	*amu*	*tmu*	*imu*
$0 \leq mu < 5$	0	0	*mu*
$mu = 5$	1	0	4
$6 \leq mu < 10$	1	0	$mu - 6$
$10 \leq mu < 15$	0	1	$mu - 10$

Table F.4: Flags for contractions are used for determination of signs with simple integer operations. Flags *anu*, *tnu* and *inu* are defined accordingly.

In each call of the subroutine, eight integers (*amu*, *tmu*, *imu*, *xmu*, *anu*, *tnu*, *inu*, *xnu*) are defined according to table F.4. *amu* is set to one, if the sink Dirac structure contains γ^5 and to zero otherwise. *tmu* is set to one if the sink Dirac structure has two Euclidean indices and to zero otherwise. *xmu* is defined as one if the sink Dirac structure is imaginary and zero otherwise,

$$xmu = (((imu\&1)\&\&(!tmu))||(((imu)\hat{}1)\&\&((imu)\hat{}4)\&\&(tmu))). \qquad (F.25)$$

anu, *tnu*, *xnu* are defined accordingly. *imu* is an index running within 0 and 5, which is used within the macros **k(imu, tmu, j)**, **f(imu, amu, tmu, j)**, **g(inu, anu, tnu, l)**. The 24 real components of the propagators are looped with an index *j* using steps of two. The spinor component of the second propagator is determined by the macro **k(imu, tmu, j)**,

175

which is not affected by the replacement rule of eq. (F.24). Variation of the sign due to different components of the Dirac matrices at source and sink are determined by the macros $\mathbf{g(inu, anu, tnu, l)}$ and $\mathbf{f(imu, amu, tmu, j)}$, which take the matrix products of eq. (F.24) into account. Then the full contraction for one sink site is given by

$$
A = \sum_{j'=0}^{j'<12} \delta_{j,2j'}\ \mathbf{f} \cdot \mathbf{g} \cdot ((\mathbf{double}*)(\psi_0^0[p1] + j) * (\mathbf{double}*)(\psi_0^0[p2] + \mathbf{k})
$$
$$
+ (\mathbf{double}*)(\psi_0^0[p1] + j + 1) * (\mathbf{double}*)(\psi_0^0[p2] + \mathbf{k} + 1))
$$
(F.26)

$$
B = \sum_{j'=0}^{j'<12} \delta_{j,2j'}\ \mathbf{f} \cdot \mathbf{g} \cdot ((\mathbf{double}*)(\psi_0^0[p1] + j) * (\mathbf{double}*)(\psi_0^0[p2] + \mathbf{k} + 1)
$$
$$
- (\mathbf{double}*)(\psi_0^0[p1] + j + 1) * (\mathbf{double}*)(\psi_0^0[p2] + \mathbf{k})), \quad \text{(F.27)}
$$

where k, f and g are determined with the macros for each j. After the summation, $\mathbf{Re(xmu, xnu, A, B)}$ is added to the real part and $\mathbf{Im(xmu, xnu, A, B)}$ is added to the imaginary part of the correlator for this sink site. The calculation is repeated for all sink sites. The role of the index j_d for the contraction at the source is mirrored by the index k for the contraction at the sink.

Macro k=**k(imu, tmu, j)**:

k=(tmu ? (imu&2) ? (j)
               : (1-((((j)/6)&1)« 1))*6+(j)
     : (imu&4) ? (j)
               : (imu%3) ? ((j)%6+6*(3-((j)/6)))
                       : (((j)+12)%24))

Macro f=**f(imu, amu, tmu, j)**:

f= (tmu ? (imu&2)   ? (((j)/6)%imu) ? (imu&1)   ? (-1) : $(+1)$
                                 : (imu&1)   ? $(+1)$: (-1)
                   : (imu&4)   ? (imu&1)   ? (((j)/6)»1) ? (-1) : $(+1)$
                                            : (((j)/6)%3)? $(+1)$: (-1)
                           : (imu&1)   ? (((j)/6)%2)? (-1) : $(+1)$
                                            : (-1)
       : ((imu&(~1)) ? (imu&(~3))   ? (amu)   ? $(+1)$
                                          : (((j)/6)»1) ? (-1) : $(+1)$
                           : (((j)/6)%(2ˆamu)) ? (-1) : $(+1)$
                   : ((imu&1)ˆamu) ? (amu)   ? (-1) : $(+1)$
                         : ((((j)/6)»1)ˆ(amu)) ? $(+1)$: (-1))))))

Macro g=**g(inu, anu, tnu, l)**:

g= (tnu ? (inu&2)   ? (((l)/3)%inu) ? (inu&1)   ? (-1) : $(+1)$
                                 : (inu&1)   ? $(+1)$: (-1)
                   : (inu&4)   ? (inu&1)   ? (((l)/3)»1)   ? (-1) : $(+1)$
                                            : (((l)/3)%3)   ? (-1) : $(+1)$
                           : (inu&1)   ? (((l)/3)%2)   ? $(+1)$: (-1)
                                            : (-1)
       : ((inu&(~1)) ? (inu&(~3))   ? (anu)   ? $(+1)$
                                          : (((l)/3)»1)   ? (-1) : $(+1)$
                         : (((l)/3)%(2ˆanu)) ? ((inu&1)ˆanu) ? $(+1)$: (-1)
                   : ((inu&1)ˆanu)   : ((inu&1)ˆanu) ? (-1) : $(+1)$
                   : ((inu&1)ˆanu) ? (anu)   ? $(+1)$: (-1)
                         : ((((l)/3)»1)ˆ(anu)) ? $(+1)$: (-1))))))

Macros Re=**Re(xmu, xnu, A, B)**, Im=**Im(xmu, xnu, A, B)**:

Re= (((xmu)ˆ(xnu)) ? (-B)
               : ((xmu)&&(xnu)) ? (-A) : (+A))
Im= (((xmu)ˆ(xnu)) ? (A)
               : ((xmu)&&(xnu)) ? (-B) : (+B))

Figure F.1: Macros for contractions spread out factors ± 1, factors i and selection of components due to Dirac structure of interpolators to different parts of the program.

Bibliography

[1] Georges Aad et al. Observation of a new particle in the search for the Standard Model Higgs boson with the ATLAS detector at the LHC. *Phys.Lett.*, B716:1–29, 2012.

[2] Stephen L. Adler. An Overrelaxation Method for the Monte Carlo Evaluation of the Partition Function for Multiquadratic Actions. *Phys.Rev.*, D23:2901, 1981.

[3] M. Albanese et al. Glueball Masses and String Tension in Lattice QCD. *Phys.Lett.*, B192:163–169, 1987.

[4] C.R. Allton et al. Gauge invariant smearing and matrix correlators using Wilson fermions at Beta = 6.2. *Phys.Rev.*, D47:5128–5137, 1993.

[5] R. Altmeyer et al. The Hadron spectrum in QCD with dynamical staggered fermions. *Nucl.Phys.*, B389:445–512, 1993.

[6] C. D. Anderson. The Positive Electron. *Physical Review*, 43:491–494, March 1933.

[7] Carl D. Anderson and Seth H. Neddermeyer. Cloud chamber observations of cosmic rays at 4300 meters elevation and near sea-level. *Phys. Rev.*, 50:263–271, Aug 1936.

[8] H. L. Anderson, E. Fermi, R. Martin, and D. E. Nagle. Angular distribution of pions scattered by hydrogen. *Phys. Rev.*, 91:155–168, Jul 1953.

[9] H. L. Anderson, E. Fermi, D. E. Nagle, and G. B. Yodh. Angular distribution of pions scattered by hydrogen. *Phys. Rev.*, 86:793–794, Jun 1952.

[10] H.L. Anderson, E. Fermi, E.A. Long, and D.E. Nagle. Total Cross-sections of Positive Pions in Hydrogen. *Phys.Rev.*, 85:936, 1952.

[11] P. W. Anderson. Plasmons, Gauge Invariance, and Mass. *Physical Review*, 130:439–442, April 1963.

[12] Sinya Aoki. 格子上の場の理論. Springer-Verlag Tokyo, 2005. (KOUSHI-JOUNOBANORIRON, literally: "Field theory on a lattice").

[13] Sinya Aoki, Yasumichi Aoki, Claude Bernard, Tom Blum, Gilberto Colangelo, et al. Review of lattice results concerning low energy particle physics. 2013.

[14] Bernard Aubert et al. Observation of a broad structure in the $\pi^+\pi^- \to J/\psi$ mass spectrum around 4.26-GeV/c^2. *Phys.Rev.Lett.*, 95:142001, 2005.

[15] Belal E. Baaquie. Gauge Fixing and Mass Renormalization in the Lattice Gauge Theory. *Phys.Rev.*, D16:2612, 1977.

[16] G. Bali. private communication.

[17] V. E. Barnes, P. L. Connolly, D. J. Crennell, B. B. Culwick, W. C. Delaney, W. B. Fowler, P. E. Hagerty, E. L. Hart, N. Horwitz, P. V. C. Hough, J. E. Jensen, J. K. Kopp, K. W. Lai, J. Leitner, J. L. Lloyd, G. W. London, T. W. Morris, Y. Oren, R. B. Palmer, A. G. Prodell, D. Radojičić, D. C. Rahm, C. R. Richardson, N. P. Samios, J. R. Sanford, R. P. Shutt, J. R. Smith, D. L. Stonehill, R. C. Strand, A. M. Thorndike, M. S. Webster, W. J. Willis, and S. S. Yamamoto. Observation of a hyperon with strangeness minus three. *Phys. Rev. Lett.*, 12:204–206, Feb 1964.

[18] Paulo F. Bedaque, Michael I. Buchoff, Brian C. Tiburzi, and Andre Walker-Loud. Broken Symmetries from Minimally Doubled Fermions. *Phys.Lett.*, B662:449–455, 2008.

[19] Paulo F. Bedaque, Michael I. Buchoff, Brian C. Tiburzi, and Andre Walker-Loud. Search for Fermion Actions on Hyperdiamond Lattices. *Phys.Rev.*, D78:017502, 2008.

[20] J. Beringer and others (Particle Data Group). The review of particle physics. *Phys. Rev.*, D86:010001, 2012.

[21] Claude W. Bernard and Maarten F.L. Golterman. Chiral perturbation theory for the quenched approximation of QCD. *Phys.Rev.*, D46:853–857, 1992.

[22] H. A. Bethe. The electromagnetic shift of energy levels. *Phys. Rev.*, 72:339–341, Aug 1947.

[23] J.D. Bjorken. Asymptotic Sum Rules at Infinite Momentum. *Phys.Rev.*, 179:1547–1553, 1969.

[24] Tom Blum, Carleton E. Detar, Steven A. Gottlieb, Kari Rummukainen, Urs M. Heller, et al. Improving flavor symmetry in the Kogut-Susskind hadron spectrum. *Phys.Rev.*, D55:1133–1137, 1997.

[25] Claudio Bonati and Massimo D'Elia. Comparison of the gradient flow with cooling in $SU(3)$ pure gauge theory. *Phys.Rev.*, D89:105005, 2014.

[26] Artan Borici. Creutz fermions on an orthogonal lattice. *Phys.Rev.*, D78:074504, 2008.

[27] Artan Borici. Minimally Doubled Fermion Revival. *PoS*, LATTICE2008:231, 2008.

[28] Keith A. Brueckner. Meson-nucleon scattering and nucleon isobars. *Phys. Rev.*, 86:106–109, Apr 1952.

[29] N. Cabibbo and E. Marinari. A New Method for Updating SU(N) Matrices in Computer Simulations of Gauge Theories. *Phys.Lett.*, B119:387–390, 1982.

[30] Nicola Cabibbo. Unitary Symmetry and Leptonic Decays. *Phys.Rev.Lett.*, 10:531–533, 1963.

[31] Stefano Capitani. Lattice perturbation theory. *Phys.Rept.*, 382:113–302, 2003.

[32] Stefano Capitani. New actions for minimally doubled fermions and their counterterms. 2013.

[33] Stefano Capitani. New chiral lattice actions of the Borici-Creutz type. 2013.

[34] Stefano Capitani. Reducing the number of counterterms with new minimally doubled actions. *Phys.Rev.*, D89:014501, 2014.

[35] Stefano Capitani, Michael Creutz, Johannes Weber, and Hartmut Wittig. Minimally doubled fermions and their renormalization. *PoS*, LATTICE2010:093, 2010.

[36] Stefano Capitani, Michael Creutz, Johannes Weber, and Hartmut Wittig. Renormalization of minimally doubled fermions. *JHEP*, 1009:027, 2010.

[37] Stefano Capitani, Johannes Weber, and Hartmut Wittig. Minimally doubled fermions at one loop. *Phys.Lett.*, B681:105–112, 2009.

[38] Stefano Capitani, Johannes Weber, and Hartmut Wittig. Minimally doubled fermions at one-loop level. *PoS*, LAT2009:075, 2009.

[39] Sergio Caracciolo, Pietro Menotti, and Andrea Pelissetto. One loop analytic computation of the energy momentum tensor for lattice gauge theories. *Nucl.Phys.*, B375:195–242, 1992.

[40] J. Chadwick. Possible Existence of a Neutron. *Nature*, 129:312, 1932.

[41] S.K. Choi et al. Observation of a narrow charmonium - like state in exclusive $B^{\pm} \to K^{\pm}\pi^{+}\pi^{-}J/\psi$ decays. *Phys.Rev.Lett.*, 91:262001, 2003.

[42] K. Cichy, J. Gonzalez Lopez, K. Jansen, A. Kujawa, and A. Shindler. Twisted Mass, Overlap and Creutz Fermions: Cut-off Effects at Tree-level of Perturbation Theory. *Nucl.Phys.*, B800:94–108, 2008.

[43] M. Creutz. Monte Carlo Study of Quantized SU(2) Gauge Theory. *Phys.Rev.*, D21:2308–2315, 1980.

[44] Michael Creutz. Comments on staggered fermions: Panel discussion. *PoS*, CON-FINEMENT8:016, 2008.

[45] Michael Creutz. Four-dimensional graphene and chiral fermions. *JHEP*, 0804:017, 2008.

[46] Michael Creutz. Local chiral fermions. *PoS*, LATTICE2008:080, 2008.

[47] Michael Creutz. Minimal doubling and point splitting. *PoS*, LATTICE2010:078, 2010.

[48] Michael Creutz, Taro Kimura, and Tatsuhiro Misumi. Index Theorem and Overlap Formalism with Naive and Minimally Doubled Fermions. *JHEP*, 1012:041, 2010.

[49] Thomas A. DeGrand and Pietro Rossi. Conditioning Techniques for Dynamical Fermions. *Comput.Phys.Commun.*, 60:211–214, 1990.

[50] P. A. M. Dirac. Quantised Singularities in the Electromagnetic Field. *Royal Society of London Proceedings Series A*, 133:60–72, September 1931.

[51] S. D. Drell and E. M. Henley. Pseudoscalar mesons with applications to meson-nucleon scattering and photoproduction. *Phys. Rev.*, 88:1053–1064, Dec 1952.

[52] S. Durr, Z. Fodor, J. Frison, C. Hoelbling, R. Hoffmann, et al. Ab-Initio Determination of Light Hadron Masses. *Science*, 322:1224–1227, 2008.

[53] F. J. Dyson. The radiation theories of tomonaga, schwinger, and feynman. *Phys. Rev.*, 75:486–502, Feb 1949.

[54] F. J. Dyson. The s matrix in quantum electrodynamics. *Phys. Rev.*, 75:1736–1755, Jun 1949.

[55] F. Englert and R. Brout. Broken Symmetry and the Mass of Gauge Vector Mesons. *Physical Review Letters*, 13:321–323, August 1964.

[56] L.D. Faddeev and V.N. Popov. Feynman Diagrams for the Yang-Mills Field. *Phys.Lett.*, B25:29–30, 1967.

[57] R. P. Feynman. Space-time approach to non-relativistic quantum mechanics. *Rev. Mod. Phys.*, 20:367–387, Apr 1948.

[58] R. P. Feynman. Space-time approach to quantum electrodynamics. *Phys. Rev.*, 76:769–789, Sep 1949.

[59] R. P. Feynman. The theory of positrons. *Phys. Rev.*, 76:749–759, Sep 1949.

[60] R. P. Feynman. Mathematical formulation of the quantum theory of electromagnetic interaction. *Phys. Rev.*, 80:440–457, Nov 1950.

[61] H. Fritzsch, Murray Gell-Mann, and H. Leutwyler. Advantages of the Color Octet Gluon Picture. *Phys.Lett.*, B47:365–368, 1973.

[62] M. et al. Galassi. GNU Scientific Library Reference Manual. 2009.

[63] J. Gasser and H. Leutwyler. Chiral Perturbation Theory to One Loop. *Annals Phys.*, 158:142, 1984.

[64] J. Gasser and H. Leutwyler. Chiral Perturbation Theory: Expansions in the Mass of the Strange Quark. *Nucl.Phys.*, B250:465, 1985.

[65] Christof Gattringer and Christian B. Lang. Quantum chromodynamics on the lattice. *Lect.Notes Phys.*, 788:1–343, 2010.

[66] Murray Gell-Mann. The Eightfold Way: A Theory of strong interaction symmetry. 1961.

[67] Murray Gell-Mann. Symmetries of baryons and mesons. *Phys. Rev.*, 125:1067–1084, Feb 1962.

[68] Murray Gell-Mann. A Schematic Model of Baryons and Mesons. *Phys.Lett.*, 8:214–215, 1964.

[69] Murray Gell-Mann. The Symmetry group of vector and axial vector currents. *Physics*, 1:63–75, 1964.

[70] Murray Gell-Mann and Yuval Neemam. The Eightfold way: a review with a collection of reprints. 1964.

[71] M. Geradin. The computational efficiency of a new minimization algorithm for eigenvalue analysis. *Journal of Sound and Vibration*, 19(3):319 – 331, 1971.

[72] Paul H. Ginsparg and Kenneth G. Wilson. A Remnant of Chiral Symmetry on the Lattice. *Phys.Rev.*, D25:2649, 1982.

[73] Leonardo Giusti, P. Hernandez, M. Laine, C. Pena, J. Wennekers, et al. On K → pi pi amplitudes with a light charm quark. *Phys.Rev.Lett.*, 98:082003, 2007.

[74] Leonardo Giusti, P. Hernandez, M. Laine, P. Weisz, and H. Wittig. Low-energy couplings of QCD from current correlators near the chiral limit. *JHEP*, 0404:013, 2004.

[75] Leonardo Giusti, C. Hoelbling, M. Luscher, and H. Wittig. Numerical techniques for lattice QCD in the epsilon regime. *Comput.Phys.Commun.*, 153:31–51, 2003.

[76] S.L. Glashow. Partial Symmetries of Weak Interactions. *Nucl.Phys.*, 22:579–588, 1961.

[77] M.L. Goldberger and S.B. Treiman. Decay of the pi meson. *Phys.Rev.*, 110:1178–1184, 1958.

[78] M.L. Goldberger and S.B. Treiman. Form-factors in Beta decay and muon capture. *Phys.Rev.*, 111:354–361, 1958.

[79] Jeffrey Goldstone, Abdus Salam, and Steven Weinberg. Broken symmetries. *Phys. Rev.*, 127:965–970, Aug 1962.

[80] Maarten F.L. Golterman and Jan Smit. Self-energy and Flavor Interpretation of Staggered Fermions. *Nucl.Phys.*, B245:61, 1984.

[81] David J. Gross and Frank Wilczek. Ultraviolet Behavior of Nonabelian Gauge Theories. *Phys.Rev.Lett.*, 30:1343–1346, 1973.

[82] D.J. Gross and Frank Wilczek. Asymptotically Free Gauge Theories. 1. *Phys.Rev.*, D8:3633–3652, 1973.

[83] D.J. Gross and Frank Wilczek. Asymptotically free gauge theories. 2. *Phys.Rev.*, D9:980–993, 1974.

[84] Marco Guagnelli, Rainer Sommer, and Hartmut Wittig. Precision computation of a low-energy reference scale in quenched lattice QCD. *Nucl.Phys.*, B535:389–402, 1998.

[85] Rajan Gupta and Tanmoy Bhattacharya. Light quark masses from lattice QCD. *Phys.Rev.*, D55:7203–7217, 1997.

[86] G. S. Guralnik, C. R. Hagen, and T. W. Kibble. Global Conservation Laws and Massless Particles. *Physical Review Letters*, 13:585–587, November 1964.

[87] S. Gusken, U. Low, K.H. Mutter, R. Sommer, A. Patel, et al. Nonsinglet Axial Vector Couplings of the Baryon Octet in Lattice QCD. *Phys.Lett.*, B227:266, 1989.

[88] Anna Hasenfratz and Francesco Knechtli. Flavor symmetry and the static potential with hypercubic blocking. *Phys.Rev.*, D64:034504, 2001.

[89] P. Hasenfratz and F. Niedermayer. Perfect lattice action for asymptotically free theories. *Nucl.Phys.*, B414:785–814, 1994.

[90] W. Heisenberg. On the structure of atomic nuclei. *Z.Phys.*, 77:1–11, 1932.

[91] Pilar Hernandez, Karl Jansen, and Martin Luscher. Locality properties of Neuberger's lattice Dirac operator. *Nucl.Phys.*, B552:363–378, 1999.

[92] P. W. Higgs. Broken Symmetries and the Masses of Gauge Bosons. *Physical Review Letters*, 13:508–509, October 1964.

[93] D. Holmgren. U.S. lattice clusters and the USQCD project. *PoS*, LAT2005:105, 2006.

[94] Jugoro Iizuka. Systematics and phenomenology of meson family. *Prog.Theor.Phys.Suppl.*, 37:21–34, 1966.

[95] K. S. Novoselov, A. K. Geim, S. V. Morozov, D. Jiang, Y. Zhang, S. V. Dubonos, I. V. Grigorieva, and A. A. Firsov. Electric Field Effect in Atomically Thin Carbon Films. *Science*, 306:666–669, October 2004.

[96] Thomas Kalkreuter and Hubert Simma. An Accelerated conjugate gradient algorithm to compute low lying eigenvalues: A Study for the Dirac operator in SU(2) lattice QCD. *Comput.Phys.Commun.*, 93:33–47, 1996.

[97] David B. Kaplan. A Method for simulating chiral fermions on the lattice. *Phys.Lett.*, B288:342–347, 1992.

[98] Luuk H. Karsten. Lattice Fermions in Euclidean Space-time. *Phys.Lett.*, B104:315, 1981.

[99] Luuk H. Karsten and Jan Smit. Lattice Fermions: Species Doubling, Chiral Invariance, and the Triangle Anomaly. *Nucl.Phys.*, B183:103, 1981.

[100] Hikaru Kawai, Ryuichi Nakayama, and Koichi Seo. Comparison of the Lattice Lambda Parameter with the Continuum Lambda Parameter in Massless QCD. *Nucl.Phys.*, B189:40, 1981.

[101] Taro Kimura, Shota Komatsu, Tatsuhiro Misumi, Toshifumi Noumi, Shingo Torii, et al. Revisiting symmetries of lattice fermions via spin-flavor representation. *JHEP*, 1201:048, 2012.

[102] Taro Kimura and Tatsuhiro Misumi. Characters of Lattice Fermions Based on the Hyperdiamond Lattice. *Prog.Theor.Phys.*, 124:415–432, 2010.

[103] Taro Kimura and Tatsuhiro Misumi. Lattice Fermions Based on Higher-Dimensional Hyperdiamond Lattices. *Prog.Theor.Phys.*, 123:63–78, 2010.

[104] H. Kluberg-Stern, A. Morel, O. Napoly, and B. Petersson. Flavors of Lagrangian Susskind Fermions. *Nucl.Phys.*, B220:447, 1983.

[105] Makoto Kobayashi and Toshihide Maskawa. CP Violation in the Renormalizable Theory of Weak Interaction. *Prog.Theor.Phys.*, 49:652–657, 1973.

[106] J. Kuipers, T. Ueda, J.A.M. Vermaseren, and J. Vollinga. FORM version 4.0. *Comput.Phys.Commun.*, 184:1453–1467, 2013.

[107] Willis E. Lamb and Robert C. Retherford. Fine structure of the hydrogen atom by a microwave method. *Phys. Rev.*, 72:241–243, Aug 1947.

[108] C.M.G. Lattes, H. Muirhead, G.P.S. Occhialini, and C.F. Powell. Processes involving charged mesons. *Nature*, 159:694–697, 1947.

[109] Weon-Jong Lee and Stephen R. Sharpe. Partial flavor symmetry restoration for chiral staggered fermions. *Phys.Rev.*, D60:114503, 1999.

[110] G. Peter Lepage and Paul B. Mackenzie. On the viability of lattice perturbation theory. *Phys.Rev.*, D48:2250–2264, 1993.

[111] M. Luscher and P. Weisz. Efficient Numerical Techniques for Perturbative Lattice Gauge Theory Computations. *Nucl.Phys.*, B266:309, 1986.

[112] Martin Luscher. Properties and uses of the Wilson flow in lattice QCD. *JHEP*, 1008:071, 2010.

[113] MILC collaboration. http://www.physics.utah.edu/ detar/milc/milc_qcd.html.

[114] Tatsuhiro Misumi. New fermion discretizations and their applications. *PoS*, LAT-TICE2012:005, 2012.

[115] Tatsuhiro Misumi. Phase structure for lattice fermions with flavored chemical potential terms. *JHEP*, 1208:068, 2012.

[116] Tatsuhiro Misumi, Michael Creutz, and Taro Kimura. Classification and Generalization of Minimal-doubling actions. *PoS*, LATTICE2010:260, 2010.

[117] Y. Nambu and G. Jona-Lasinio. Dynamical model of elementary particles based on an analogy with superconductivity. i. *Phys. Rev.*, 122:345–358, Apr 1961.

[118] Yuval Ne'eman. Derivation of strong interactions from a gauge invariance. *Nucl.Phys.*, 26:222–229, 1961.

[119] Herbert Neuberger. Exactly massless quarks on the lattice. *Phys.Lett.*, B417:141–144, 1998.

[120] Ferenc Niedermayer. Exact chiral symmetry, topological charge and related topics. *Nucl.Phys.Proc.Suppl.*, 73:105–119, 1999.

[121] Holger Bech Nielsen and M. Ninomiya. No Go Theorem for Regularizing Chiral Fermions. *Phys.Lett.*, B105:219, 1981.

[122] K.S. Novoselov, A.K. Geim, S.V. Morozov, D. Jiang, M.I. Katsnelson, et al. Two-dimensional gas of massless Dirac fermions in graphene. *Nature*, 438:197, 2005.

[123] S. Okubo. Phi meson and unitary symmetry model. *Phys.Lett.*, 5:165–168, 1963.

[124] K. Osterwalder and R. Schrader. Feynman-kac formula for euclidean fermi and bose fields. *Phys.Rev.Lett.*, 29:1423–1425, 1972.

[125] K. Osterwalder and E. Seiler. Gauge Field Theories on the Lattice. *Annals Phys.*, 110:440, 1978.

[126] Konrad Osterwalder and Robert Schrader. Axioms Foe Euclidean Green's functions. *Commun.Math.Phys.*, 31:83–112, 1973.

[127] A. Pais. Some remarks on the v-particles. *Phys. Rev.*, 86:663–672, Jun 1952.

185

[128] W. Pauli. Dear radioactive ladies and gentlemen. *Phys.Today*, 31N9:27, 1978.

[129] M. Pernici. Chiral invariance and lattice fermions with minimal doubling. *Phys.Lett.*, B346:99–105, 1995.

[130] Michael E. Peskin and Daniel V. Schroeder. An Introduction to quantum field theory. 1995.

[131] H. David Politzer. Asymptotic Freedom: An Approach to Strong Interactions. *Phys.Rept.*, 14:129–180, 1974.

[132] William H. et al. Press. Numerical Recipes: The Art of Scientific Computing. 2007.

[133] T. Reisz. A Convergence Theorem for Lattice Feynman Integrals With Massless Propagators. *Commun.Math.Phys.*, 116:573, 1988.

[134] T. Reisz. Renormalization of Feynman Integrals on the Lattice. *Commun.Math.Phys.*, 117:79, 1988.

[135] T. Reisz. Renormalization of Lattice Feynman Integrals With Massless Propagators. *Commun.Math.Phys.*, 117:639, 1988.

[136] Thomas Reisz. A Power Counting Theorem for Feynman Integrals on the Lattice. *Commun.Math.Phys.*, 116:81, 1988.

[137] G.D. Rochester and C.C. Butler. Evidence for the Existence of New Unstable Elementary Particles. *Nature*, 160:855–857, 1947.

[138] Abdus Salam. Weak and Electromagnetic Interactions. *Conf.Proc.*, C680519:367–377, 1968.

[139] Stefan Scherer. Introduction to chiral perturbation theory. *Adv.Nucl.Phys.*, 27:277, 2003.

[140] Julian Schwinger. On quantum-electrodynamics and the magnetic moment of the electron. *Phys. Rev.*, 73:416–417, Feb 1948.

[141] Julian Schwinger. Quantum electrodynamics. i. a covariant formulation. *Phys. Rev.*, 74:1439–1461, Nov 1948.

[142] Stephen R. Sharpe. Quenched chiral logarithms. *Phys.Rev.*, D46:3146–3168, 1992.

[143] R. Sommer. A New way to set the energy scale in lattice gauge theories and its applications to the static force and alpha-s in SU(2) Yang-Mills theory. *Nucl.Phys.*, B411:839–854, 1994.

[144] Leonard Susskind. Lattice Fermions. *Phys.Rev.*, D16:3031–3039, 1977.

[145] Brian C. Tiburzi. Chiral Lattice Fermions, Minimal Doubling, and the Axial Anomaly. *Phys.Rev.*, D82:034511, 2010.

[146] S. Tomonaga. On a relativistically invariant formulation of the quantum theory of wave fields. *Prog.Theor.Phys.*, 1:27–42, 1946.

[147] Cees van den Doel and Jan Smit. Dynamical Symmetry Breaking in Two Flavor SU(N) and SO(N) Lattice Gauge Theories. *Nucl.Phys.*, B228:122, 1983.

[148] Peter van Nieuwenhuizen and Andrew Waldron. A Continuous Wick rotation for spinor fields and supersymmetry in Euclidean space. pages 394–403, 1996.

[149] Peter van Nieuwenhuizen and Andrew Waldron. On Euclidean spinors and Wick rotations. *Phys.Lett.*, B389:29–36, 1996.

[150] G. Veneziano. U(1) Without Instantons. *Nucl.Phys.*, B159:213–224, 1979.

[151] J.A.M. Vermaseren. New features of FORM. 2000.

[152] Georg M. von Hippel, Benjamin Jäger, Thomas D. Rae, and Hartmut Wittig. The Shape of Covariantly Smeared Sources in Lattice QCD. *JHEP*, 1309:014, 2013.

[153] Andrew Waldron. A Wick rotation for spinor fields: The Canonical approach. *Phys.Lett.*, B433:369–376, 1998.

[154] Johannes Weber. Correlation functions with Karsten-Wilczek fermions. *PoS*, LAT2014:071, 2014.

[155] Johannes Heinrich Weber, Stefano Capitani, and Hartmut Wittig. Numerical studies of Minimally Doubled Fermions. 2013.

[156] Steven Weinberg. Dynamical approach to current algebra. *Phys. Rev. Lett.*, 18:188–191, Jan 1967.

[157] Steven Weinberg. A model of leptons. *Phys. Rev. Lett.*, 19:1264–1266, Nov 1967.

[158] C. Whitmer. Overrelaxation methods for Monte Carlo simulations of quadratic and multiquadratic actions. *Phys.Rev.*, D29:306–311, 1984.

[159] Frank Wilczek. On lattice fermions. *Phys.Rev.Lett.*, 59:2397, 1987.

[160] Kenneth G. Wilson. Confinement of Quarks. *Phys.Rev.*, D10:2445–2459, 1974.

[161] E. Witten. Current algebra theorems for the u(1) "goldstone boson". *Nuclear Physics B*, 156(2):269 – 283, 1979.

[162] Hartmut Wittig. Chiral effective Lagrangian and quark masses. *Nucl.Phys.Proc.Suppl.*, 119:59–70, 2003.

187

[163] Chen-Ning Yang and Robert L. Mills. Conservation of Isotopic Spin and Isotopic Gauge Invariance. *Phys.Rev.*, 96:191–195, 1954.

[164] Hideki Yukawa. On the interaction of elementary particles. *Proc.Phys.Math.Soc.Jap.*, 17:48–57, 1935.

[165] G. Zweig. An SU(3) model for strong interaction symmetry and its breaking. Version 2. pages 22–101, 1964.